Australian Government
Bureau of Meteorology

The Centre for Australian Weather and Climate Research
A partnership between the Bureau of Meteorology and CSIRO

CSIRO

Victorian Climate Initiative: Annual Report 2013–14

Murphy, B., Timbal, B., Hendon, H. and Ekström, M.

CAWCR Technical Report No. 076

November 2014

www.cawcr.gov.au

Victorian Climate Initiative: Annual Report 2013–14

Murphy, B., Timbal, B., Hendon, H. and Ekström, M.

The Centre for Australian Weather and Climate Research
—a partnership between CSIRO and the Bureau of Meteorology

CAWCR Technical Report No. 076

November 2014

ISSN: 1835-9884

Editors: Murphy, B., Timbal, B., Hendon, H. and Ekström, M.

Authors: Murphy, B., Timbal, B., Hendon (Bureau of Meteorology/CAWCR), H., Ekström, M. (CSIRO/CLW), Moran, R. (independent expert), Manton, M. (independent expert), Lucas, C., Nguyen, H., Rikus, L., Lim, E-P., Liu, G., Zhao, M., (Bureau of Meteorology/CAWCR), Fiddes S. (Melbourne University), Grosse, M., Bathols, J., Kirono D. (CSIRO/CAWCR) and Teng, J. (CSIRO/CLW)

Title: Victorian Climate Initiative: Annual Report 2013–14

ISBN: 978-1-4863-0469-1

Series: CAWCR technical report.

Notes: Includes bibliographical references and index.

Subjects: Hydro-climate
Climate variability and change
South-eastern Australia
Water availability

Contact details

Enquiries should be addressed to:

B.Timbal@bom.gov.au
Climate Information Services
Bureau of Meteorology
GPO Box 1289
Melbourne
VIC 3001

Copyright and disclaimer

Contents

List of figures

List of tables

ABSTRACT

Information about the future availability of water resources, on time scales from weeks to decades ahead, underpins the preparation of plans and strategies to ensure the provision of secure water supplies for Victorian urban and rural water users and the environment. At a time when changes in the global climate system are affecting regional climates around the world, it is important that forecasts and projections of future water availability in Victoria are based on the best understanding of the factors affecting Victorian climate, including how those factors are changing now and may change into the future. The uncertainties in these changes should also be quantified. The Victorian Climate Initiative (VicCI) was established in 2013 as a three-year programme to provide such information for Victoria, through improved understanding of the climate system and its impact on water availability. The VicCI programme is a partnership between the Victorian Department of Environment and Primary Industries (DEPI), the Bureau of Meteorology and CSIRO. It builds on the results of the South Eastern Australia Climate Initiative (SEACI), which ran from 2006 to 2012.

The VicCI programme is focused on some of the key challenges remaining after SEACI. Its research on climate variability, predictability and change will:

- inform drought response strategies for urban supplies and processes for determining seasonal allocations for rural supplies, through improved predictions of water availability on seasonal to inter-annual time scales; and

- underpin improved assessment of the risks to water resources from changes in climate over the medium to longer term, through improved understanding of the climate system and its representation in models.

The programme has seven projects under three themes:

1. improved seasonal climate predictions;

2. improved understanding of past climate variability and change; and

3. improved understanding of future climate and associated risks to water resources.

The initial science plan (www.cawcr.gov.au/projects/vicci/documents/Science_plan_final.pdf) identifies a number of key science questions, to provide guidance on the direction and nature of the research. This report documents progress in the first year of VicCI towards answering these science questions in each of the three themes. Moreover, it is shown that the research findings from this first year have direct implications for water resource management in Victoria (see Section 4).

In Theme 1 there has been progress in understanding the effects and impacts of the recent warming of the oceans to the north of Australia. It has been found that this warming significantly amplified the rainfall over eastern Australia during the 2010–11 La Niña event, which brought widespread flooding to Victoria. To the extent that the warming trend is due to anthropogenic climate change, the risk of extreme rainfall in eastern Australia during La Niña events is expected to increase into the future.

There is now better understanding of the interactions between the natural climate factors that drove the main contributions to the enhanced rainfall during the 2010–11 period. The climate of Victoria is influenced by three large-scale factors of the global climate system: the El Niño – Southern Oscillation (ENSO), which characterises atmosphere–ocean interactions across the Pacific Ocean; the Indian Ocean Dipole (IOD), which characterises atmosphere–ocean interactions in the Indian Ocean; and the Southern Annular Mode (SAM), which characterises the intensity and position of higher-latitude westerly winds and associated storm systems. Decadal-scale modulation of ENSO is represented by the Inter-decadal Pacific Oscillation (IPO). All of these factors were aligned in their 'wet' phases for the spring and summer rainfall in 2010–11. The alignment between ENSO and SAM not only promoted increased rainfall but also increased the predictability of the SAM, so that the extreme rainfall in spring 2010 was predictable beyond one season in advance by the Bureau's POAMA model, which feeds into the Bureau's operational streamflow forecasting system. The IPO, currently in its 'cold' phase, contributed to the recent trends in ocean temperatures to the north of Australia, and so enhanced the effect of global warming on the La Niña event. The cold phase of the IPO is a period of reduced predictability of ENSO, compared with the periods of warm phase such as the late 1970s to the late 1990s when ENSO could be predicted around nine months ahead. Nonetheless, the alignment of the key climate factors during the 2010–11 La Niña event extended the predictability of that extreme rainfall event so that actionable forecasts were produced with more than one season lead time.

From Theme 2 there is now further insight into the interactions between ENSO and SAM, and their interaction with the Hadley cell, which is the large-scale north–south (meridional) atmospheric circulation that transports the sun's energy from the tropics to higher latitudes. Using different approaches, it is confirmed that the Hadley cell has been expanding at a rate of about 50 km/decade around the globe since the late 1970s, and at about 65 km/decade in the Australian region. The expansion has not been steady, and abrupt jumps have occurred following the major El Niño event of 1997–98 and the major volcanic eruption of Mt Pinatubo of 1991. The expansion of the Hadley cell leads to changes in the subtropical ridge that are associated with the cool-season decline in rainfall in Victoria. Analysis of the output of global climate models shows that the expansion is at least partly due to anthropogenic climate change, and so the cool-season rainfall decline is expected to continue into the future. Moreover, because the climate models tend to underestimate the expansion of the Hadley cell, it is possible that the projected future decrease in Victorian rainfall from these models is underestimated.

There is a continuing trend, at least partly due to climate change, of the SAM to its positive phase, which is associated with decreased rainfall in winter but increased rainfall in spring and summer in Victoria. For example, the near-record high SAM in 2010 was found, through its interaction with ENSO, to have played a significant role in the extreme rainfall of that spring. The expected emerging upward trend of the SAM due to global warming, together with a continuing cool season rainfall deficit associated with the expansion of the Hadley cell, may make the traditional winter filling season for water supply systems even less reliable into the future. However, this may be at least partly offset by enhanced warm season rainfall as a result of the upward trend in the SAM.

A component of the work in Theme 3 in the first year of VicCI has supplemented the research of the Commonwealth's Climate Futures and NRM Climate Change programmes, by taking an overview of the latest climate projections for Victoria based on the output of 50 global climate models from around the world (which fed into the Fifth Assessment of the IPCC). It is found that the new rainfall projections are likely to be similar to those from the Fourth IPCC Assessment. In particular, projections for the first half of this century are not very dependent on the specific emissions scenario. Consequently it is considered not immediately necessary to revise existing strategic plans for future water resources in Victoria, as they have been designed to be robust to a wide range of future flow scenarios.

Analysis of the global climate models shows that many of the models could simulate the observed broad character of the subtropical ridge, but that not all models capture the observed relationship between Victorian rainfall and the subtropical ridge. Given the importance of this relationship to the observed trends in rainfall, it may be appropriate for studies of future projections of Victorian climate to only use models that capture this relationship reasonably well.

A simple statistical model has been developed to predict runoff based on antecedent rainfall for a number of Victorian catchments. It will be combined with rainfall projections from global climate models, downscaled using an analogue method, to estimate projected runoff for these Victorian catchments over future decades. These results will provide a benchmark for more sophisticated rainfall–runoff models and alternative downscaling methods—particularly dynamical downscaling using a regional climate model, which are being developed to provide future runoff projections. It is recognised that any nonstationarity of the rainfall–runoff relationship (which may arise in a changing climate) is a particular challenge for statistical approaches to linking climate model projections to runoff projections.

Overall, there has been good progress in the first year of VicCI towards answering the key science questions and in focusing the research on issues of direct relevance to water security in Victoria. Results to date confirm the relevance of the key science questions set out in the Science Plan. An ongoing programme of research across the three themes is being undertaken in 2014–15, which builds on results from Year 1 and further addresses the key science questions. For example, confidence in projections of Victorian rainfall of future expansion of the tropics and positive trends in the SAM will be improved by investigating past influences of the SAM and the contributions of various anthropogenic factors.

1. OVERVIEW

Strategies to ensure the sustainable management of water resources and the provision of secure water supplies for urban and rural water users and the environment are underpinned by assumptions about the current and likely future availability of water resources over a range of time scales (from weeks to decades ahead). The Victorian Climate Initiative (VicCI) was established in 2013 as a three-year programme of research to inform the preparation of such strategies for Victoria through improved prediction and understanding of the climate system and its representation by climate models, as well as the linkages between climate and water availability. This strategic knowledge provides the basis for improved projections of future climate and associated water availability in Victoria; in particular, it enhances knowledge of the uncertainties in future projections.

The VicCI programme is a partnership between the Victorian Department of Environment and Primary Industries (DEPI), the Bureau of Meteorology and CSIRO. It builds on the results of the South Eastern Australia Climate Initiative (SEACI), which ran from 2006 to 2012. A primary motivation for SEACI was the need to understand the causes of the Millennium Drought (1997–2009), which was the worst drought for south-eastern Australia for more than a hundred years. The Millennium Drought was unusual in its duration, severity and extent. It was unprecedented in being largely restricted to southern Australia, in having a large rainfall decline in autumn, and in having much reduced inter-annual rainfall variability. Moreover, the decline in rainfall led to a larger than anticipated decrease in runoff, which was challenging for water management and planning.

The rainfall decline in the Millennium Drought extended across the cool season (April–October), and it appeared to be related to changes in the Hadley cell—the large-scale north–south (meridional) atmospheric circulation that transports the sun's energy from equatorial regions to higher latitudes. There was evidence from SEACI that the Hadley cell is expanding at a rate of about 0.5° latitude (50 km) per decade. The extent of the Hadley cell is associated with both the intensity and the position of the subtropical ridge. Its expansion leads to an expanded subtropical dry zone, pushing mid-latitude storms further south to miss Victoria and resulting in reduced rainfall across southern Australia. The cool season rainfall deficits were shown to persist even when the drought was broken by spring–summer rainfall in 2010–11. There was also some evidence that the changes in the meridional circulation are at least partly attributable to human activities and so may be likely to continue, but the relative importance of global warming and Antarctic ozone depletion was not resolved.

Research in SEACI included support for the development of the Predictive Ocean Atmosphere Model for Australia (POAMA) modelling system for seasonal climate prediction in the Bureau of Meteorology, and the incorporation of POAMA output into the Bureau's operational seasonal streamflow forecast system. The POAMA model was used for studies on the nature and causes of seasonal and inter-annual variations in the climate of Victoria. From SEACI and related research, it is apparent that these variations are influenced by three large-scale features of the global climate system: the El Niño – Southern Oscillation (ENSO), which characterises atmosphere–ocean interactions across the Pacific Ocean; the Indian Ocean Dipole (IOD), which characterises atmosphere–ocean interactions in the Indian Ocean; and the Southern Annular Mode (SAM), which characterises the intensity and position of higher-latitude westerly winds and associated storm systems. While the influence of each feature is well understood individually, much is to be learned about the interactions between them—and between them and global warming.

Climate model simulations from SEACI and related programmes (using a worldwide set of models known as CMIP3, associated with the Fourth Assessment of the IPCC) indicate that, owing to global warming, both rainfall and runoff will decline over future decades in the southern part of south-eastern Australia. However, associated with the Fifth Assessment of the IPCC, a new set of global climate model projections (CMIP5) has been computed by the major modelling centres around the world. It is

therefore appropriate to determine whether these new projections will lead to substantial revision of hydro-climate projections for Victoria.

The VicCI programme aims to resolve some of the key challenges remaining after SEACI. Its focused research on climate variability, predictability and change will:

- improve predictions of water availability in the short term (seasonal to inter-annual time scales), which have the potential to inform drought response strategies and outlooks for urban supplies, and processes for determining seasonal allocations and risks of spill for irrigation systems; and
- underpin an improved assessment of the risks to water resources and supplies from changes in climate over the medium to longer term, based on improved understanding of the climate system and its representation by climate models.

The programme is composed of seven projects under three broad themes (see text box):

- improved seasonal climate predictions;
- improved understanding of past climate variability and change; and
- improved understanding of future climate and associated risks to water resources.

VicCI research programme structure

Theme 1: Improved seasonal prediction

Project 1: Understanding decadal variations of seasonal climate predictability and potential for multi-year predictions

Theme 2: Improved understanding of past climate variability and change

Project 2: Understanding the mean meridional circulation and its relevance to Victoria
Project 3: Understanding subtropical–extratropical interactions and their relevance to Victoria
Project 4: Exploration of the causes of tropical expansion

Theme 3: Improved understanding of future climate and associated risks to water resources

Project 5: Critical assessment of climate model projections from a rainfall perspective
Project 6: Convection-resolving dynamical downscaling
Project 7: Identification and application of improved methodologies for water availability projections

Project 1 aims to further improve seasonal climate prediction, to enhance understanding of decadal variations in seasonal predictability, and to investigate the potential for multi-year prediction. Projects 2, 3 and 4 aim to improve understanding of past climate variability and change in Victoria. There is a specific focus on the large-scale features of variability (ENSO, IOD and SAM), which provides a basis for the evaluation of the capability of global climate models for prediction and future projection. Project 5 makes use of the knowledge gained in Projects 1–4 to assess the utility of the latest climate model projections of future change. Projects 6 and 7 aim to develop methodologies for the next generation of runoff projections and associated risk assessments. Project 6 uses a high-resolution numerical model to simulate the current climate of Victoria, in order to assess the potential for high-resolution modelling to improve the representation of rainfall under future climate change conditions. Project 7 aims to determine the most appropriate methodologies for generating runoff projections out to 2040 and 2065, which will underpin the development of future long-term strategies to ensure reliable urban and rural water supplies for Victoria. It will draw on the knowledge gained from the other projects, especially Projects 5 and 6. A more complete science plan for VicCI research is provided at www.cawcr.gov.au/projects/vicci/documents/Science_plan_final.pdf.

The VicCI research programme is integrated across time scales and themes, so that the work to improve understanding of climate variability feeds directly into the work to assess seasonal to multi-

year predictability and into the work to assess climate model simulations, which in turn are used for projections of the future climate of Victoria. The research programme has strong connections with related programmes being undertaken in Australia and overseas. For example, in south-eastern Australia, results from VicCI complement other regional programmes such as NARClim, Goyder Institute Climate Change, and Climate Futures for Tasmania, which are focused on the development of specific regional climate change projections. Nationally, VicCI is working directly with CSIRO and the Bureau of Meteorology to connect the NRM climate change projections with water resource needs in Victoria. Internationally, the work of VicCI is linked with initiatives of the World Climate Research Programme and with development of modelling capability at the UK Meteorology Office.

This report provides a description of progress over the first year of VicCI. The Science Plan for VicCI lists a number of key science questions to guide each project. Section 2 of this report provides a summary of the progress towards answering these questions after one year of research and lists the direction of research in the second year. Section 3 summarises the key findings of the programme across projects and themes. Links across projects and themes are key for maximum leveraging of available research resources. Because the goal of the programme is to support water resource management and planning for Victoria, Section 4 describes the implications of the research findings for water resource management and planning. The final sections of the report give detailed descriptions of the research undertaken and results for each of the seven projects.

2. PROGRESS IN ANSWERING KEY SCIENCE QUESTIONS

The VicCI Science Plan gives detailed descriptions of each of the seven research projects that make up the overall programme. Within the descriptions, there are key science questions that aim to guide the research as results are gradually obtained. It is therefore appropriate to consider progress in each of the projects after one year in answering these questions. Given the evolutionary nature of research, not all the original questions are considered at this time.

Theme 1: Improved seasonal prediction

Project 1: Understanding decadal variations of seasonal climate predictability and potential for multi-year predictions

The climate of south-eastern Australia varies markedly on multi-year and decadal time scales, impacting the capability to make seasonal climate predictions but also obscuring the detection of anthropogenic climate change. Importantly, the capability to make seasonal climate predictions for south-eastern Australia primarily depends on the capability to predict ENSO because ENSO is the most predictable component of the climate system and the most important driver of rainfall variability in Victoria. Predictability therefore varies on decadal time scales: decades of high prediction skill are associated with high ENSO variability (i.e. when the signal-to-noise ratio is high), and decades of low skill occur during periods of quiescent ENSO variation (i.e. when the signal to noise is low). The relationship of these variations of ENSO predictability with recent warming trends in the tropical oceans and with varying phases of the Inter-decadal Pacific Oscillation (IPO), which characterises decadal-scale variations in interactions between the ocean and atmosphere across the wider Pacific basin, needs to be determined. This relationship is further complicated by the observed increase in mean sea-surface temperature (SST) in the tropical oceans. Understanding these relationships will provide more confidence in managing short-term climate variations in the future.

Why has ENSO prediction skill been low since 1999 compared to the previous 20 years (1980–1999)?

The decline in skill was attributed to a decline in ENSO activity as a result of a swing of the IPO to its 'cold' phase, which is characterised by relatively colder temperatures in the eastern Pacific Ocean and warmer temperatures in the western Pacific. This confirms that the slow variation in the background climate affected the activity and predictability of ENSO. Despite continued improvements in forecast systems, skill for prediction of ENSO can be expected to wax and wane decadally in the future as a result of natural variation of the background climate. Although impacts of ENSO on rainfall are expected to increase due to greenhouse warming, changes in predictability of ENSO are uncertain because they will depend crucially on the details of how the climate of the wider Pacific Ocean changes but as yet there is little consensus.

What has been the impact of the recent warming of ocean temperatures to the north of Australia on ENSO and ENSO's impacts on Australian climate?

The recent upward trend in ocean temperatures in the tropical Indian Ocean and western Pacific, due in part to the swing to the cold phase of the IPO, was found to have significantly amplified the springtime rainfall anomaly (10–30 per cent) over eastern Australia during the 2010–11 La Niña event as a result of enhanced promotion of high SAM. To the degree that the upward trend in SST in the tropical Indian and western Pacific is a result of anthropogenic climate change, the risk of extreme

rainfall in eastern Australia during La Niña events can be expected to increase in future events. However, some of the recent SST trend appears to be a result of a naturally occurring swing of the IPO, so we can also expect epochs of reduced impact of La Niña events in the future when the IPO is in a warm phase. Although swings in the IPO are not predictable, persistence of the IPO is long and therefore its impact (and other ongoing trends) are naturally captured in the Bureau's POAMA model because forecasts are initialised from observed the ocean state. As a consequence, the extreme rainfall in spring 2010 was largely predictable at least one season in advance.

Further science questions to be considered later in VicCI

While there has been some progress on the following questions, they will be considered in more detail in the future:

- What are the mechanisms of the observed multi-year variations of climate in south-eastern Australia? How predictable are they, especially the multi-year La Niña episodes that are the primary drivers of water resource management (e.g. mid 1970s, late 1980s, 2010–2012)?
- Why did the last two La Niñas (2010–11 and 2011–12) bring a lot of rainfall to Australia, but the 2007–09 La Niña did not?
- What role does global warming play in multi-year wet or dry periods?
- Can the drop in ENSO prediction skill be related to changes to changes in the global circulation associated with the expansion of the Hadley cell?
- What is the relationship between changes in ENSO activity and forecast skill due to the IPO and epochs of enhanced global warming and strengthening of the subtropical ridge?

During 2014–15, Project 1 will continue to further understanding of the causes of decadal variations in the capability to make seasonal climate predictions for Victoria by focusing on why the La Niña event in 2007–2009 did not bring above normal rainfall but the La Niñas during 2010–11 and 2011–12 did.

Theme 2: Improved understanding of past climate variability and change

Project 2: Understanding the mean meridional circulation and its relevance to Victoria

A key outcome of SEACI was the confirmation that the Hadley cell is expanding and this expansion could be playing a key role in the recent climate variability of south-eastern Australia. Projections of future climate indicate a continued expansion of the Hadley cell, so it is imperative to understand its impact on the climate of the region and the mechanism for, and likely limits to, the expansion. The results of SEACI indicated that the recent expansion of the Hadley cell has been relatively greater over Australia compared to the rest of the hemisphere. However, the seasonal variation of the expansion is complex: investigation of reanalysis data suggests that the expansion averaged around the hemisphere has a maximum in summer and autumn, but analysis of radiosonde data in the region of Australia and New Zealand shows little seasonal variation. The seasonality of the expansion bears on the issue of what is driving the expansion and on understanding the observed autumnal rainfall decline and how rainfall may respond to future changes.

Can we reconcile the seasonality of observed tropical expansion as given by different methodologies?

A critical comparison of metrics (or indicators) of tropical expansion reveals that the consensus expansion rate since 1979 is on the order of 0.5 degrees of latitude per decade (about 50 km/decade) in each hemisphere. In the southern hemisphere, statistically significant tropical expansion and associated changes to the subtropical ridge are detectable from the late 1960s. However, the expansion is not steady; for example, there were abrupt jumps following the major ENSO event of 1997–98 and the major volcanic eruption of Mt Pinatubo in 1991.

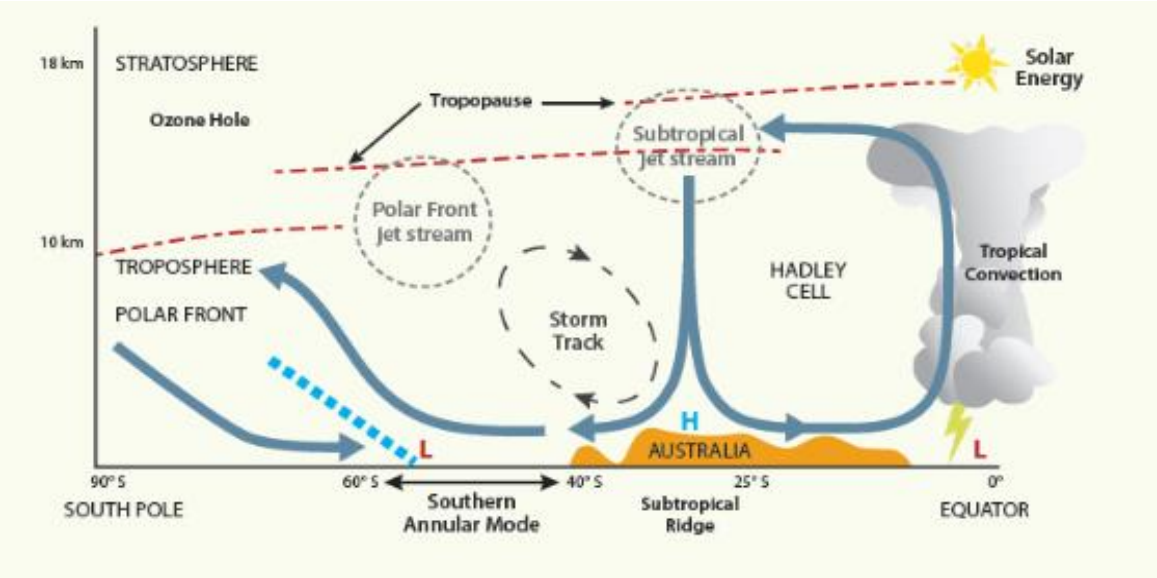

Fig. 2.1 Features of mean meridional circulation affecting Victoria

Analysis in the Australian region shows the regional expansion to be greater than the hemispheric average (about 65 km/decade). It is also found that the expansion and intensification of the Hadley cell is greatest in autumn, which is consistent with the earlier-observed local intensification and poleward shift in the subtropical ridge in autumn. The difference in conclusions on the local seasonality of the expansion between SEACI and VicCI is due to the improved analysis techniques that now provide a detailed picture of regional variations around the hemisphere.

Can new tools and methods be developed to assess regional expansion in the Australian sector?

A method to diagnose the regional Hadley cell in the Australian sector has been developed. A clear and significant expansion and intensification of the local Hadley cell is observed that is consistent with, but slightly larger (about 0.65 degrees per decade) than, the hemispheric-wide expansion. The expansion is most prominent in autumn (MAM) and is concomitant with the intensification and poleward shift of the subtropical ridge and decline in rainfall in south-eastern Australia. The larger regional expansion over the Australian sector may be the reason that Victorian climate has exhibited a stronger rainfall decline than that recorded at comparable latitudes around the hemisphere.
Software to compute the characteristics of the mean meridional circulation in isentropic coordinates (which essentially follow the trajectories of the air) has been developed. This isentropic analysis will be a potent tool to diagnose forced and naturally occurring interactions of the mid-latitude circulation with the low-latitude Hadley cell.

Further science questions to be considered later in VicCI

The following questions will also be considered in the future:

- What are the underlying factors that determine the seasonality of the expansion of the Hadley cell, and how are they affected by climate change?
- What role does the Australian land mass (including the maritime continent) play in the regional enhancement of the expansion of the Hadley cell, and why is the enhancement different over South America and South Africa? How will regional effects apply in a changing climate?
- What mechanism explains the relationship between the expansion of the Hadley cell and the intensification of the subtropical ridge? What is the role of extratropical dynamics compared with low-latitude forcing?
- How do relationships between the Hadley cell and the subtropical ridge vary on inter-annual and decadal time scales?

During 2014–15, Project 2 will aim to quantify the regional tropical expansion from all metrics and investigate their impacts on Australian climate variability. There will also be investigation of the causes of the zonal variations in changes in the Hadley Circulation.

Project 3: Understanding subtropical–extratropical interactions and their relevance to Victoria

Evidence is emerging that variations in extratropical circulations associated with the Southern Annular Mode (SAM) play a significant role in driving variations of the Hadley cell, and especially rainfall on the poleward edge of the Hadley cell: High SAM (i.e. a poleward shift in the polar front jet) is associated with a poleward-expanded Hadley cell (HC) and increased rainfall in subtropical latitudes in the warm season and deceased rainfall in the higher southern latitudes (i.e. across Victoria but especially along the Great Dividing Range) in the cool season. This relationship is captured in climate models to varying degrees. The shift to high SAM is especially promoted by ozone depletion, but increased carbon dioxide is also known to drive SAM to its high phase. Understanding the cause of this relationship between SAM and changes in the extent of the Hadley cell is crucial to understanding the behaviour of the Hadley cell in the future. It furthermore bears on the ability to predict regional climate seasonally. There is strong evidence that tropical SSTs during ENSO directly affect the Hadley cell, which then affects the SAM. These variations should be highly predictable. But, because SAM is primarily an internal mode of variability, predictability of Hadley cell variations will be limited by predictability of the SAM.

What is the nature and mechanism of the interaction of the SAM with the Hadley cell? What determines the seasonality of the interaction?

In winter, a high SAM phase was found to be associated with reduced rainfall in across the southern extremes of eastern Australia (i.e. across Victoria but especially along and south of the Great Dividing Range) due to a southward expansion of the subtropical dry zone and a concomitant poleward shift in the mid-latitude storm track. In contrast, in the warm seasons (especially spring and summer), a high SAM phase results in rainfall increases in subtropical Australia (including most of Victoria) because it causes the southern edge of the wet tropics to shift poleward. This contrasting response to high SAM in rainfall between winter and summer was shown to result from the development of the wintertime subtropical jet, which essentially acts to produce a barrier for interaction of the SAM with the Hadley cell.

What are the implications of the interaction of the SAM with the hemispheric mean meridional circulation (including the Hadley cell), especially the seasonality of the interaction, for predictability of subtropical rainfall?

Future forced upward trends of the SAM in response to increasing greenhouse gases and ozone depletion will be expected to result in drying across the southern-most portions of Australia during winter but moistening across subtropical eastern Australia during spring and summer. The near-record high SAM in 2010 was found to have played a primary role for the extremity of the wet conditions over south-eastern Australia during spring in 2010. This swing to high SAM and the occurrence of extreme rainfall was found to be largely predictable at least one season in advance because it was promoted by the strong La Niña conditions in the tropics that were acting on top of the recent upward trend in tropical SST.

Further science questions to be considered later in VicCI

While there has been some progress on the following questions, they will be considered in more detail in the future:

1. What role does ENSO or other tropical sea-surface temperature anomalies play in promoting the interactions between SAM and the Hadley cell? What is the best diagnostic to represent and understand these interactions?
2. Can the interaction of extratropical circulations and the mean meridional circulation explain the link between the Hadley cell expansion and the intensification of the subtropical ridge, associated with the deficit in cool season rainfall in south-eastern Australia?
3. How will these interactions change in future climates, and what is the implication for the future climate of Victoria?

During 2014–15, Project 3 will make use of the newly developed isentropic stream function code to explore tropical–extratropical interactions of relevance to Victorian climate. There will be continuing investigation of the linkage between the SAM and Australian climate in the present and future climate by investigating the causes of the severe drought in the spring of 2002 when the SAM was strongly negative. Such analysis will provide insight into the confidence of future climate projections for south-eastern Australia which strongly depend on the future behaviour of the SAM.

Project 4: Exploration of the causes of tropical expansion

Climate model simulations can best represent observed recent changes in the mean meridional circulation and the expansion of the tropics when ozone depletion and other anthropogenic external forcings are used, suggesting at least a partial human influence on recent changes. However, simulations of the tropical expansion are typically weaker than observed. It is thus critical to understand what is actually driving the changes and why the models are underestimating the change.

What are the relative roles of greenhouse gases, stratospheric ozone depletion, and anthropogenic aerosols in producing the observed expansion of the Hadley cell and the associated impact on subtropical rainfall?

Both observational and modelling studies suggest that the cause of the observed tropical expansion in the southern hemisphere has a significant anthropogenic component due to increasing greenhouse gases (acting year round) and the springtime Antarctic ozone hole. This forced expansion is directly related to changes in the subtropical ridge that has resulted in changed weather patterns over southern Australia. However, tropical expansion also results from naturally-occurring La Niña events and positive swings of the Southern Annular Mode in the spring–summer seasons. Climate models appear to underestimate the observed tropical expansion by a factor of two to four, and do not appear to capture the changes associated with natural modes of variability, especially the seasonality. These modes of variability may also themselves be changing in character due to climate change.

Further science questions to be considered later in VicCI

The following questions will also be considered in the future:

1. If ozone depletion is an important factor, what are the implications of the expected recovery of stratospheric ozone for projections at different time scales (e.g. 2020, 2050, etc.) and how well is this captured in existing projections?
2. If the Hadley cell expansion is driven primarily by carbon dioxide and other greenhouse gases, how will the expansion continue in the future?
3. If the Hadley cell expansion is primarily driven by variations in tropical sea surface temperatures (especially those associated with ENSO), how will the expansion vary in the future?
4. Why do current models underestimate the observed Hadley cell changes?
5. What are the implications of the possibility of attributing part of the observed changes to external factors for our best estimate of the current climate baseline?

During 2014–15, Project 4 will continue to dissect the contribution of various factors to the observed changes in the mean meridional circulation. A particular focus will be on the contribution from the stratospheric ozone changes compared to other anthropogenic factors. Quantification of the relative roles of these factors will help refine projections for future impacts of tropical expansion that are relevant to Victorian climate.

Theme 3: Improved understanding of future climate and associated risks to water resources

Project 5: Critical assessment of climate model projections from a rainfall perspective

Climate model projections from CMIP3 (those used in IPCC Fourth Assessment report in 2007 and SEACI) for the climate of south-eastern Australia show some consistent behaviour (e.g. drier to the south and wetter to the north) and some inconsistent behaviour (the magnitude of future rainfall change). Some of this uncertainty is linked to the models' ability to represent important links between climate variables at one location and those at another (i.e. teleconnections, such as the influence of the SAM on the Hadley cell), and key modes of variability that directly influence the climate of south-eastern Australia (e.g. stationary high pressure systems). In order to provide greater confidence for projections of future climate (with a particular focus on subsequent impacts on water availability), we need to assess models for the capability to simulate these key teleconnections and processes.

Is the relationship between the subtropical ridge (STR) and rainfall across south-eastern Australia, which underpins the secular changes in rainfall across the region but which was poorly represented in CMIP3 models, better represented in the CMIP5 models (those used in the IPCC Fifth Assessment report) in 2013. What are the reasons for the poor representation? What implication does the poor representation of the STR-rainfall relationship have for future projections?

Simulations of the Australian subtropical ridge (STR) in 50 latest-generation climate models were analysed. Many models were found to reproduce the broad character of the STR similar to that observed, but some models simulate the STR too far to the west, and some simulate it too wide. Some models also have a different relationship between the STR intensity and rainfall over Victoria, with either too broad an extent of the region of negative rainfall – STR intensity relationship over Victoria, or too restricted a region. These biases are an issue for making regional climate projections for

Victoria and hence a narrower and more reliable range of projections may be obtained by omitting some models.
Future projections of the STR and rainfall under a high emissions scenario were analysed. Most models showed an intensification of the STR over recent decades, but not all showed the observed southerly trend in its position. However, all models showed the STR to intensify and move south over this century. This confirms that changes to atmospheric circulation are generally projected to lead to reduced rainfall in Victoria in the cool season (April–October). Models with a poor simulation of the STR have a distinct rainfall projection for certain regions, suggesting that it may be possible to select models for future projections based on some constraints on their representation of the STR and its relationship to rainfall.

Further science questions to be considered later in VicCI

The following questions will also be considered in the future:

- How are model projections for either wet or dry tendencies related to the model's projections of tropical ocean warming (especially the relative warming between the Pacific and Indian Oceans)?
- Should the capability of models to simulate observed trends attributable to external forcings be used to confirm or invalidate future projections of these models? What is the best probabilistic approach to reconcile observed trends with model trends, and so to estimate future trends?

During 2014–15, Project 5 will prepare documentation on findings obtained through the NRM national projections specifically focused on Victoria. Additional work will aim to increase the confidence in the projections for rainfall by evaluating the uncertainties in the modelled relationship between rainfall and large-scale climate factors, with a particular focus on the effects of warming of the tropical ocean around Australia. Finally an investigation will be carried out to determine how the overall projected mean rainfall reduction may affect the potential for prolonged drought in the future (similar to what was experienced during the Millennium Drought).

Project 6: Convection-resolving dynamical downscaling

Statistical downscaling methodologies of varying complexity were investigated in SEACI in order to provide projections of future climate at the local scale. A key weakness in all methods used within SEACI was the underestimation of extreme rainfall events, which leads to underestimation of high runoff events, thereby also underestimating mean runoff. Improved spatial and temporal characteristics of rainfall can be obtained when using convection-resolving high-resolution regional climate models (RCMs) to downscale predictions and projections to regional scales.

What are the optimum physical parameterisation settings and grid resolution that best capture the key synoptic processes associated with heavy rainfall? Can a high-resolution RCM be configured for regional Victoria that provides faithful representation of key physical processes that drive extreme rainfall and runoff?

The Advanced Weather and Research Forecasting (WRF) modelling system was configured using three nested domains, with the innermost nest focused on a region of about 450 by 600 km along the Great Dividing Range. Three 15-day case study periods with contrasting synoptic conditions were identified during the 2010–11 La Niña event when south-eastern Australia experienced flooding events. Simulations for case study 1 were completed and the sensitivity to a range of model physics options is being assessed. Progress to date suggests that the properly-configured RCM will be able to well simulate key precipitation processes relevant to rainfall and runoff in Victoria.

During 2014–15, Project 6 will investigate and attempt to correct the spurious patterns appearing in the inner-most domains of the high-resolution dynamical downscaling simulation. Case study experiments will be completed and assessed to provide a skill-based assessment of what model configurations are most appropriate for subsequent downscaling experiments. Links will be developed with Project 7: rainfall data from the WRF model simulations will be provided to which bias-correction methods can be applied and the data will be used to drive hydrological models.

Project 7: Identification and application of improved methodologies for water availability projections

The aim of this project is to provide information about the behaviour of the latest generation of climate models and methodological choices that can improve the reliability and usefulness of runoff projections for mid- to long-term future time horizons (out to about 2065). In comparison with CMIP3, CMIP5 comprises a larger data set, with more models operating at higher resolution and with more complex physics.

Which existing bias-correction methods are best suited to adjust statistical characteristics of climate model output to observed data, in order to use model output directly in hydrological models?

A literature review was undertaken on regional climate model (RCM) bias correction methods. The best performing bias correction technique—distribution mapping—was assessed using daily precipitation series simulated by the Weather Research and Forecasting (WRF) model for eight Victorian catchments. The results confirmed the usefulness of distribution-based methods but also highlighted that, when the bias is nonstationary, none of the methods can lead to satisfactory results. Although bias correction does not seem to alter the change with time in RCM precipitation, it does introduce extra uncertainty in the change in runoff.

How can outputs from different CMIP5 models and subsequent downscaling methods be most appropriately merged into projections of future streamflow?

A simple statistical model, that uses a linear combination of the current month's precipitation, the previous month's precipitation and the previous 12 months of precipitation to reconstruct the monthly inflow of Melbourne's water catchments, was updated to include the previous ten years of rainfall as well, and applied across 27 Victorian catchments. The updated model was better able to capture the magnitude of streamflow reductions during the Millennium Drought, and it can be readily applied to provide initial estimates of projected streamflows given projected rainfalls. In future VicCI work the model will be applied across selected Victorian catchments to generate initial future inflow projections using daily rainfall derived from the analogue-based statistical downscaling of available CMIP5 models. The results will be compared with those from using different downscaling approaches and more sophisticated rainfall – runoff models.

Further science questions to be considered later in VicCI

The following questions will also be considered in the future:

- *Can statistical downscaling provide useful insight into the source and associated uncertainties of the wide range of projections from CMIP5 models?*
- *Which CMIP5 models show best skill in reproducing rainfall characteristics that define regional streamflow characteristics, accounting for the spatial and temporal behaviour of streamflow across different meteorological seasons and time frames?*
- *Which are the best methods for generating updated streamflow projections for periods around 2040 and 2065?*

During 2014–15, Project 7 will deliver streamflow projections for selected catchments across Victoria for the twenty-first century based on the latest IPCC science and the simple statistical method developed in the first year of VicCI for predicting streamflow from rainfall. In addition, a broader evaluation of some commonly used approaches that provide future climate projections for hydrological modelling (e.g. empirical scaling from global climate models, empirical scaling informed by regional climate models, bias correcting of regional climate model simulations, bias correcting of analogue downscaling) will be performed in order to compare the results with the simple method. The strengths and weaknesses of each method will be assessed, with a view to recommending methods for different applications.

3. KEY FINDINGS ACROSS THEMES

In Section 2 a summary of progress in answering the key science questions for each project raised at the start of VicCI was provided. However, the programme also requires an integration of results across the projects, and so here we highlight the key findings taking into account the linkages and dependencies across projects and themes.

3.1 Understanding the regional impacts and interactions of ENSO, the SAM, the IPO and tropical expansion

VicCI is aimed at improving information about the future availability of water resources on timescales from weeks to decades ahead. This requires improved understanding of the mechanisms and predictability of climate variability and change, and the limits of this predictability, in relation to Victoria. These issues are particularly addressed in Themes 1 (focus on seasonal prediction) and 2 (focus on past climate variability and future change).

An important issue is to understand the influence of the Inter-decadal Pacific Oscillation (IPO) on seasonal climate variability and prediction and to discriminate any contribution of this naturally occurring mode of variability from long-term trends in sea-surface temperature (SST) in response to anthropogenic climate change. There is a relationship between the IPO, which represents modulation of the frequency and magnitude of ENSO events, and the climate of eastern Australia during spring through to autumn. Work in Theme 1 has revealed that the observed swing of the Pacific climate to the cold phase of the IPO after 1999 has weakened the coupled variability at the heart of ENSO in the eastern Pacific, thereby resulting in weaker ENSO activity and therefore reduced seasonal predictability. However, at present there is little indication of any predictability of these decadal swings in variability, reflecting that the swings are indeed partly a result of random variations in ENSO activity. Further work is required to determine if we can identify in advance changes in epochs of the IPO that lead to changes from low to high variability and predictability.

A further consequence of the cold phase of the IPO is that it has contributed to some of the ocean surface warming to the north of Australia (with colder ocean temperatures in the eastern Pacific). It has been found that this SST warming acted in conjunction with the anomalous SSTs due to the La Niña in spring 2010 to promote the extreme rainfall experienced across south-eastern Australia. This occurred because the SST trend together with La Niña promoted a stronger positive SAM, much in the same way that global warming promotes high SAM in future climate projections with increasing greenhouse gases, thereby contributing to wetter conditions in subtropical eastern Australia during spring and summer. SAM's role is important as it places a strong constraint on predictability of subtropical rainfall even during highly predictable La Niña events. Furthermore, it is likely to be skewed to its positive phase in the future as indicated consistently by many climate models. Therefore, the work carried out in this part of the programme has important implications for predicting current and future climate in south-eastern Australia and for progressing our understanding of future climate projections for Victoria. In particular, the recent upward trend of the SAM mainly during late spring and summer has been promoted by ozone depletion. However, a robust finding of projected future

climate in response to increased greenhouse gases is a promotion of high SAM in all seasons. The emergence of this upward trend of the SAM in winter would in turn result in an expanded subtropical dry zone in winter, with an associated reduction in rainfall.

There remains a question about whether the seasonal climate impact of the interactions between the SAM and global warming would be additional to the impact of the expanding Hadley Circulation, discussed in Theme 2.

Research in the SEACI programme demonstrated the importance of the meridional circulation in understanding climate variability and change across Victoria. Starting from a hemispheric perspective, research in the first year of VicCI has strengthened the consensus on the rate of tropical expansion: since the late 1970s the expansion is of the order of 0.5 degree per decade in each hemisphere. However, this trend has not been steady, in part due to natural variability such as large volcanic eruptions and the influence of large-scale factors like ENSO. These factors may explain up to 30 per cent of the trend from 1979. In particular, there is essentially a jump in the expansion of the Hadley Circulation in the late 1990s, following the major ENSO event of 1997–98. This observation suggests that anthropogenic climate change can lead to abrupt changes in climate rather than gradual transitions.

On the whole, tropical expansion appears to be slightly larger in the southern hemisphere than in the northern hemisphere. It was also found that in the southern hemisphere significant expansion begins in the late 1960s. These findings are consistent with the hypothesis that, in the southern hemisphere over a long period, both the spring-time Antarctic stratospheric ozone depletion and the anthropogenic enhancement of greenhouse gases are the primary climate factors causing tropical expansion.

The work in Theme 2 has emphasised that tropical expansion is a globally complex phenomenon, with many regional differences. In particular, the expansion appears to be greatest over the longitudes of the Maritime Continent encompassing Asia and Australia. Less expansion is seen over North America and Africa, although the lack of quality data over the latter region lowers the confidence of this assessment. Investigation of the regional aspects of tropical expansion using various metrics applied to the different reanalysis datasets shows a robust expansion trend across all metrics, consistent with the global trend. Further work is required to confirm that enhanced expansion has occurred in the Australian region. Of particular interest is the newly developed method to diagnose the mean meridional circulation using an isentropic stream function, which essentially follows the trajectories of air parcels. This new approach will be a potent tool to diagnose extratropical–tropical interactions which occur around the latitudes of Victoria.

Progress has also been made in attributing the cause of these changes, but attribution relies on state-of-the-art climate models to compute the expected response to a given external forcing. Despite their overall usefulness, it is important to note that several shortcomings have been identified in historical simulations of the tropical expansion with these models, although the models do appear to reasonably reproduce the observed relationships between the Hadley Circulation and the subtropical ridge.

The robustness of global tropical expansion supports the hypothesis that a poleward shift of the subtropical zone leads to a drier climate at the surface during the cool season, and this is likely to be the main cause of the continuing cool season drying trend observed over Victoria. In addition, with larger tropical expansion over the Australian sector, it is expected that the Victorian climate is even more sensitive to changes in the meridional circulation, and this may explain the strong rainfall decline in the region compared to other subtropical longitudes. In south-eastern Australia, several changes in local climate were aligned with the 1997–98 jump in the extent of the Hadley Circulation, including the onset of the Millennium Drought.

3.2 Improved future projections of regional climate and associated risks to water resources

The recent release of the Fifth Assessment Report of the IPCC, coupled with the research undertaken over the last three years jointly by CSIRO and the Bureau of Meteorology to prepare state-of-the-art nationwide climate projections tailored to the needs of the Natural Resource Management (NRM) community, provides a unique opportunity to distil the latest science and its relevance to the state of Victoria. As summarised from work in Theme 3, the projections for Victoria include:

- warming will continue and the amount of warming after 2050 will primarily depend on the rate of emission of greenhouse gases;
- temperature increases of 0.5 °C to 1.3 °C are expected by 2030 in all future scenarios, with warming of up to 4.6 °C by 2090 for the highest emission scenario;
- the hydrological cycle will change and, although the main drivers of climate variability will continue to exert a strong influence, a rainfall reduction during the cool season is likely;
- extreme hot temperatures will increase and be more frequent, and heavy rainfall extremes are likely to increase.

Thus the observed warming trend over the past century will continue. While the pace of the warming during the second half of the century will depend primarily on the emissions pathway, uncertainties due to global climate model sensitivities and natural decadal variability will dominate during the first half of the century. Climate change will not be limited to warming trends but will affect the hydrological cycle through changes in rainfall and other climate variables, such as evapotranspiration. While these changes are less certain than those for temperature, a convergence is seen amongst models toward a reduction of rainfall during the cool period of the year, with no clear direction for the warm season. These results are similar to those found from models used in the IPCC Fourth Assessment Report, and so it is likely that updated projections of future streamflow will not be substantially different from those prepared from SEACI research.

A particularly important aspect is that confidence in projections arises not so much from the convergence amongst models, but more importantly from increased understanding of some key large-scale factors as investigated in Themes 1 and 2 and their role in the future projections of the climate across Victoria. Using the foundation developed in Themes 1 and 2, work in Theme 3 has found that some CMIP5 models capture the characteristics of the subtropical ridge (STR) for the longitude band of Victoria as well as the relationship between rainfall and changes in the latitude and intensity of the STR. These assessments can be used to increase the confidence in the projections; in particular, they can be used to identify the CMIP5 models that do not capture the observed behaviour of the STR and so should not be used for climate projections for south-eastern Australia.

In addition to the development of climate change projections, including downscaling techniques to provide high-resolution information, a two-pronged approach has been taken to translate these projections into impacts on runoff. A simple statistical method has been developed through analysis of the historical relationship between rainfall and runoff in several Victorian catchments. More complex methodologies using dynamical downscaling are also being developed.

Climate models inevitably have systematic biases in their simulations of local climate variables. A detailed literature review has identified the most accurate methods for bias correction. The knowledge gained from the review and testing of bias correction methods provides the basis for an improved methodology for future hydro-climate projections for Victoria.

For extreme rainfall events, even more complex numerical approaches at higher model resolution are required. This is frontier research not yet ready to be applied to produce future projections of extreme

rainfall event characteristics, but progress has been made in assessing the relative value of very fine resolution convection-resolving downscaling versus fine resolution downscaling with parameterised convection. The end goal of this research is to provide improved regional rainfall simulations and hence runoff projections for Victoria. Work has progressed on setting up the model experiment and testing appropriate physics combinations on selected case studies.

4. IMPLICATIONS OF FINDINGS FOR WATER RESOURCES MANAGEMENT AND PLANNING

Research conducted in Year 1 of VicCI has strengthened and refined some of the key findings from SEACI, and has provided additional insight into factors influencing the current and future climate of Victoria. This knowledge, together with the further research planned for Years 2 and 3 of VicCI, will contribute to improved forecasts and projections of future water availability which, in turn, will underpin a range of water management and planning processes.

4.1 Continuing cool-season rainfall deficit and enhanced summer rainfall

Findings from the first year of research in VicCI strengthen and refine a key conclusion drawn from SEACI regarding an expected continuing cool season (April–October) rainfall deficit. This is due to the changes in the global atmosphere–ocean system that are resulting in an expansion of the tropics (an expanding Hadley cell) and the associated intensification and movement southwards of the subtropical ridge and mid-latitude storm tracks. VicCI research has strengthened the consensus on the rate of this Hadley cell expansion (averaging ~50 km/decade in each hemisphere, since the late 1970s, and ~65 km/decade in the Australian region), although it has also established that the expansion is not continuous and can be subject to abrupt shifts, as occurred following a major El Niño event in 1997–98.

SEACI found that the Hadley cell expansion and changes in the subtropical ridge were at least partly attributable to global warming as they could be reproduced by global climate models (from the suite of CMIP3 models) only when human influences (in the form of greenhouse gases, aerosols, and stratospheric ozone depletion) were included. However, modelled trends were generally considerably smaller than observed. VicCI research using the CMIP5 suite of models has also found that modelled rates of tropical expansion are considerably lower (two to four times lower) than observed, although the models do appear to reasonably reproduce observed relationships between the Hadley Circulation and the subtropical ridge. While reasons for the lower modelled trends are to be further investigated, one possible implication is that current climate change projections may underestimate the impacts of increasing greenhouse gases on rainfall across southern Australia.

VicCI research has also shown that an expected upward trend in the Southern Annular Mode (SAM) towards its positive phase as a result of global warming is likely to result in a winter rainfall deficit and increased rainfall in the summer months for Victoria. Trends in SAM have been linked to increasing greenhouse gases (in all seasons) and stratospheric ozone depletion (in spring and summer). Given that to date there has not been a statistically significant trend in SAM in winter, the cool season rainfall deficit that is already occurring is expected to be largely attributable to the expansion of the Hadley cell and associated changes in the subtropical ridge. This means that an emerging positive trending SAM in winter would be likely to further intensify the rainfall decline during winter months.

It is important to note that, while there is a general expectation of a continuing cool-season rainfall deficit, in any year the deficit may be mitigated by climate influences affecting seasonal and inter-annual variability (ENSO, IOD and SAM). For example, a negative IOD in 2013 resulted in above average winter rainfall. This reinforces the need for improved seasonal climate predictions to support the effective management of Victoria's water resources.

In contrast to the impact on cool season rainfall, SEACI research pointed to the possibility that the expansion of tropical influences on climate could result in enhanced summer rainfall, thereby offsetting to some extent a reduction in cool season rainfall. Again, VicCI research supports this conclusion and also identifies that the trend in SAM towards its more positive phase is likely to result in enhanced spring and summer rainfall. Both these influences may therefore exert a mitigating effect on the expected rainfall deficit in the latter part of the cool season. As noted above, trends in SAM in spring and summer have been linked to both increasing greenhouse gases and stratospheric ozone depletion. While trends in greenhouse gases are expected to continue, the expected recovery of the ozone hole will offset the impact of greenhouse gases in spring and summer. Because the rate of trend in SAM will depend on both the rate of greenhouse gases emissions and ozone recovery, future trends in the SAM (and associated rainfall) in spring and summer will depend on the emissions trajectory into the future.

Overall, these results strengthen the conclusion from SEACI that the traditional filling season for water supply systems, which historically was considered to run from about May through to October, is not likely to be as reliable into the future. However, enhanced warm season rainfall is expected, and may to some extent offset cool season deficits. Methodologies for estimating risks of spill from major storages ideally should take this possibility of enhanced summer rainfall into account. In addition, there is likely to be an increased flooding risk in the warm season such as experienced in 2010–11.

4.2 Improved projections of future climate and streamflow

SEACI research underpinned the development of updated future streamflow scenarios across the State, which were used in 2012 for the purposes of developing long term strategic plans for Victoria (Water Supply Demand Strategies and Regional Sustainable Water Strategies). These future scenarios were based on results from 15 global climate models (GCMs) from the CMIP3 suite of models. All GCMs with available daily data were used in making these projections and a simple daily scaling approach was used to downscale data to a 5-km resolution. The range of uncertainty in the rainfall and runoff projections was large, and an evaluation of model performance (in terms of their ability to represent Victorian climate and key climate factors) did not suggest any obvious way of constraining the range of projections. In recognition of the likelihood of an ongoing cool-season rainfall decline, a ‘continuation of dry conditions’ (1997–2009) scenario was also considered in these planning processes. As a consequence of the wide range of future flow scenarios, it was necessary for water corporations to develop strategic plans that are robust to a wide range of climate futures and to include ongoing review mechanisms in these plans in the light of evolving climatic conditions.

VicCI research in Year 1 has built on work undertaken in SEACI, and complemented work being done as part of the Commonwealth’s Climate Futures and NRM climate change programs, to lay the foundation for developing methodologies for deriving improved updated projections of future climate and streamflow for Victoria based on the latest (CMIP5) global climate models. In particular:

1. An overview of the latest climate change projections for Victoria indicates that overall, the range in rainfall projections from CMIP5 is not likely to be very different from that derived from the CMIP3 models. It has also confirmed that (as was the case for CMIP3) during the first half of the century, projections are not very dependent on the chosen emissions scenario. As a consequence, it is suggested that it is not necessary to revise existing strategic plans in the short-term.

2. Progress has been made in examining how best to identify projections that adequately capture the rainfall characteristics that determine runoff. It has been suggested that global climate models should not be used for future projections in Victoria if they do not capture the observed behaviour of the subtropical ridge and the relationship between the intensity of the ridge and rainfall over Victoria.

3. The simple statistical model that has been developed (based on antecedent rainfalls) will use rainfall projections derived using the analogue statistical downscaling approach that has been utilised in developing projections for the various NRM regions across Australia. This has applications for estimating projected monthly streamflows for catchments in Victoria. Results from the simple model will be compared with results obtained using more sophisticated rainfall–runoff models and rainfall inputs derived using alternative bias-correction techniques and dynamical downscaling.

4. VicCI research in Year 1 has confirmed that no bias-correction technique can produce satisfactory results where there is nonstationary bias, which may be the case in the context of climate change. This problem will also affect runoff projections derived using the simple statistical model if rainfall–runoff processes change over time. The potential impacts of nonstationary bias are an important consideration when using bias-corrected downscaled data sets available through other initiatives, such as the Climate Futures programme.

4.3 Seasonal and inter-annual climate variability and predictability

Research conducted in SEACI led to an improved understanding of the key influences on the seasonal and inter-annual variability of Victoria's climate (ENSO, IOD and SAM). It highlighted the importance of the three oceans—Pacific, Indian and Southern—in influencing seasonal and inter-annual rainfall variability. The importance of these influences was evident during 2010–12 in particular. The spring and summer of 2010–11 saw one of the strongest La Niña events on record combined with a negative IOD and a positive SAM; i.e. all three key influences were in their wet phases in terms of expected spring–summer rainfall impacts on south-eastern Australia. These conditions, coupled with the warmest sea-surface temperatures on record to the north of Australia and in the eastern Indian Ocean, contributed to making 2010–11 Australia's wettest two-year period on record. The spring and summer of 2011–12 saw the re-emergence of another (weaker) La Niña, combined with a positive SAM, but this time the Indian Ocean played a smaller role. However, as noted earlier, the state of the Indian Ocean (a negative IOD) was key to producing above average winter rainfall in 2013.

SEACI research also contributed to the improvement of the Bureau of Meteorology's POAMA forecasting model and the development and implementation of operational seasonal streamflow forecasts on the Bureau's website. These forecasts are potentially useful for optimising short-term management strategies in relation to drought response, seasonal allocations and environmental flows, and in estimating risks of spill.

VicCI research in Year 1 has provided further insight into the behaviour and interaction of ENSO and SAM, and their predictability, the interactions between SAM and the Hadley cell, and the role of warming sea-surface temperatures to the north of Australia in enhancing the impacts of the La Niña event of 2010–11.

ENSO has long been recognised as a primary influence on Victorian rainfall, and the ability to predict seasonal rainfall primarily depends on the ability of forecast models to predict ENSO. VicCI research has confirmed that there has been a decline in ENSO prediction skill from around 1999 compared to the previous 20 years. During the earlier period, the Bureaus forecast model (POAMA) exhibited remarkable skill for lead times of at least nine months. In contrast, since 1999, good skill has barely been maintained for a one season lead.

VicCI research has established that this decline in skill is attributed to a decline in ENSO activity and an associated swing of the Interdecadal Pacific Oscillation (IPO) to its negative phase. The IPO characterises decadal scale variations in interactions between the ocean and the atmosphere across the wider Pacific Basin. While its swings in phase are not predictable, once established, the IPO does have considerable persistence (around two to three decades). Historically, the IPO negative phase tends to

be associated with more frequent and wetter La Niña events in eastern Australia (e.g. 1944–1977), resulting in an enhanced flood risk. The swing to an IPO negative phase is also associated with warming of sea-surface temperatures in the eastern Indian Ocean and western Pacific, with anthropogenic climate change expected to have made a contribution. VicCI research established that this warming of sea-surface temperatures significantly amplified the rainfall anomaly over eastern Australia (by 10 to 30 per cent) during the 2010 La Niña event.

To the extent that the upward trend in sea-surface temperatures is due to anthropogenic climate change, the risk of extreme rainfall in eastern Australia during La Niña events can be expected to increase into the future, and risks are likely to be further enhanced in the immediate future if the IPO remains in its negative phase. These impacts are naturally captured in the Bureau's POAMA forecasting model because forecasts are initialised from the observed ocean state that faithfully capture the recent observed trends. However, the reduction in ENSO prediction skill that has been evident since 1999, despite improvements in forecast models, means that useful forecasts beyond one season cannot be expected while the IPO remains in its negative phase.

Research completed during the early stages of VicCI established (using the Bureau's POAMA model) that the association between SAM and ENSO enables skilful predictions of SAM (which traditionally was considered to be predictable with lead times of only one to two weeks) to be made in early winter and early summer for at least one season in advance. Predictability of SAM in the cold season was found to stem from its association with warm-pool (Modoki or Central Pacific) ENSO, whereas predictability in the warm season was found to stem from the association of the SAM with cold-tongue (eastern Pacific) ENSO. Given that POAMA outputs are used as inputs to the Bureau's operational streamflow forecasting system, this predictive capacity is reflected in the streamflow forecasts. In particular, this means that the operational seasonal streamflow forecasts should capture situations where a positive phase of SAM might act to enhance the flood risk associated with a La Niña event in spring and summer and this could be well anticipated at least one season in advance.

5. ANNUAL PROGRESS REPORTS 2013–14

Project 1: Understanding decadal variation of seasonal climate predictability and the potential for multi-year predictions

Hendon, H.H., Lim, E-P., Liu, G. and Zhao, M.

CAWCR, Bureau of Meteorology

Key findings

Seasonal prediction hindcasts from the POAMA model were analysed and sensitivity experiments were carried out whereby the background initial states from 1985–95 and 2000–2010 were interchanged. It was found that predictability of the El Niño – Southern Oscillation (ENSO) has dropped dramatically since 1999 and is attributed to a swing of the Interdecadal Pacific Decadal Oscillation (IPO) to the cold phase. Although a consensus is emerging that impacts of ENSO will increase in a warming climate, predictability of ENSO can be expected to wax and wane as the climate continues to vary decadally. The swings in the IPO are not predictable, so it is not clear how much longer we will remain in this epoch of reduced predictability.

Carefully designed forecast sensitivity experiments were carried out with the POAMA model to assess the impact of the long-term trend in SSTs on the extreme wet conditions over Australia that developed during the 2010 La Niña The recent upward trend in ocean temperatures in the eastern Indian Ocean and western Pacific, due in part to the swing to the cold phase of the IPO, was shown to have amplified the rainfall anomaly over eastern Australia during the 2010 La Niña event.

Background

Climate in SEA varies markedly on multi-year and decadal time scales, impacting the capability to make seasonal climate predictions but also obscuring detection of anthropogenic climate change (ACC). Importantly, the capability to make predictions of seasonal climate variability in SEA varies decadally, with decades of high skill being associated with high ENSO variability and decades of low skill being periods of quiescent ENSO variations. Based on published findings, the epoch 1960–1979 exhibited relatively low ENSO variability, 1980–1998 exhibited high ENSO variability and since 1999 ENSO variability has been low. Together with these variations in ENSO variability, since 1999 ENSO activity has been observed to shift west in the Pacific. The relationship of these variations of ENSO variability and predictability with epochs of increased global warming and intensification of the subtropical ridge needs to be explored.

Furthermore, the epochs of high/low ENSO variability may be related to warm/cold phases of the Interdecadal Pacific Oscillation (IPO, noting that the IPO is not an oscillation in the true sense because its behaviour is more episodic without exhibiting a prominent periodicity). Furthermore, there is clear evidence that some specific ENSO events are predictable for one to two years but many are only predictable two to three seasons in advance. Further, ENSO variability today is acting on a warmer mean state and this warming may have played a role in changing both the behaviour of ENSO and the ENSO teleconnection to SEA. For example, there is some evidence to suggest that the La Niña pluvial phase may be more intense now than previously. Understanding these changes will provide more confidence for predictions of short term climate variations in the future.

Objectives

1. Diagnose decadal changes in the tropical ocean–atmosphere mean state and relate to decadal changes in behaviour and predictability of the El Niño – Southern Oscillation (ENSO).

2. Diagnose impact of recent SST warming associated with long-term trend for the atmospheric circulation and extreme rainfall during the La Niña event in 2010.

Activity 1: Decadal variation in ENSO predictability

El Niño – Southern Oscillation (ENSO) is the main source of predictable climate for eastern Australia (e.g. Risbey et al. 2009). The capability to reliably foresee a drought due to El Niño or pluvial due to La Niña two to three seasons in advance would greatly facilitate water resource management in south eastern Australia. Despite continued improvement in forecast systems (e.g. Hudson et al. 2011; Hudson et al. 2013; Yin et al. 2011; Zhao et al. 2014) and the advent of the ARGO profiling program that has provided unprecedented in situ observation of the tropical oceans for which initial conditions are generated (e.g. Balmaseda et al. 2007), forecast skill for predicting ENSO with dynamical coupled models has apparently degraded in the most recent decade (e.g. Barnston et al. 2011). Understanding why this has occurred will shed light on the expected skill and reliability of seasonal climate predictions in the future and will also guide forecast system development if we can pin the recent decline in skill to deficiencies in our forecast system.

Here we consider variation in forecast skill based on hindcasts made with the POAMA2 seasonal forecast system for the period 1980–2010. More details of the POAMA2 systems are provided in Activity 2. During this 31-year period, the climate of the Pacific varied interdecadally, whereby during 1980–99 the climate exhibited characteristics of the warm phase of the Interdecadal Pacific Oscillation (IPO), and after the massive El Niño event of 1997–98 the climate swung to the cold phase (McPhaden and Zhang 2004; L'Heureux et al. 2013). The key differences in background climate for these two epochs are captured by the simple decadal differences (2000–2010) minus (1985–1995) as shown in Fig. 5.1. The cold phase of the IPO, as experienced since 1999, was characterised by stronger easterly trade winds in the central Pacific along with increased upper ocean upwelling along the equator west of the dateline, colder surface temperatures in the eastern Pacific and warmer in the west, an elevated thermocline in the eastern Pacific, and enhanced rainfall in the far western Pacific (not shown). The opposite was experienced during the warm phase of the IPO during 1980–1999.

Importantly, variability of sea surface temperature (SST) in the key El Niño region of the equatorial eastern Pacific (Fig. 5.1a) was sharply decreased during the recent decade of the cold phase of the IPO (Hu et al. 2013). Furthermore, SST variability increased in the western Pacific, which reflects an increase in 'Modoki El Niño' since 1999 (McPhaden et al. 2011). The forecast skill for predicting SST in the Nino3 region using the POAMA2 model is displayed in Fig. 5.1d. During the earlier epoch, POAMA exhibited remarkable skill to lead times of at least 9 months. In contrast, in the recent epoch, forecast correlation of 0.6 was barely maintained for a one season lead. The implication is that the coupled model forecasts have provided very little useful long-range information about the upcoming behaviour of El Niño since 1999.

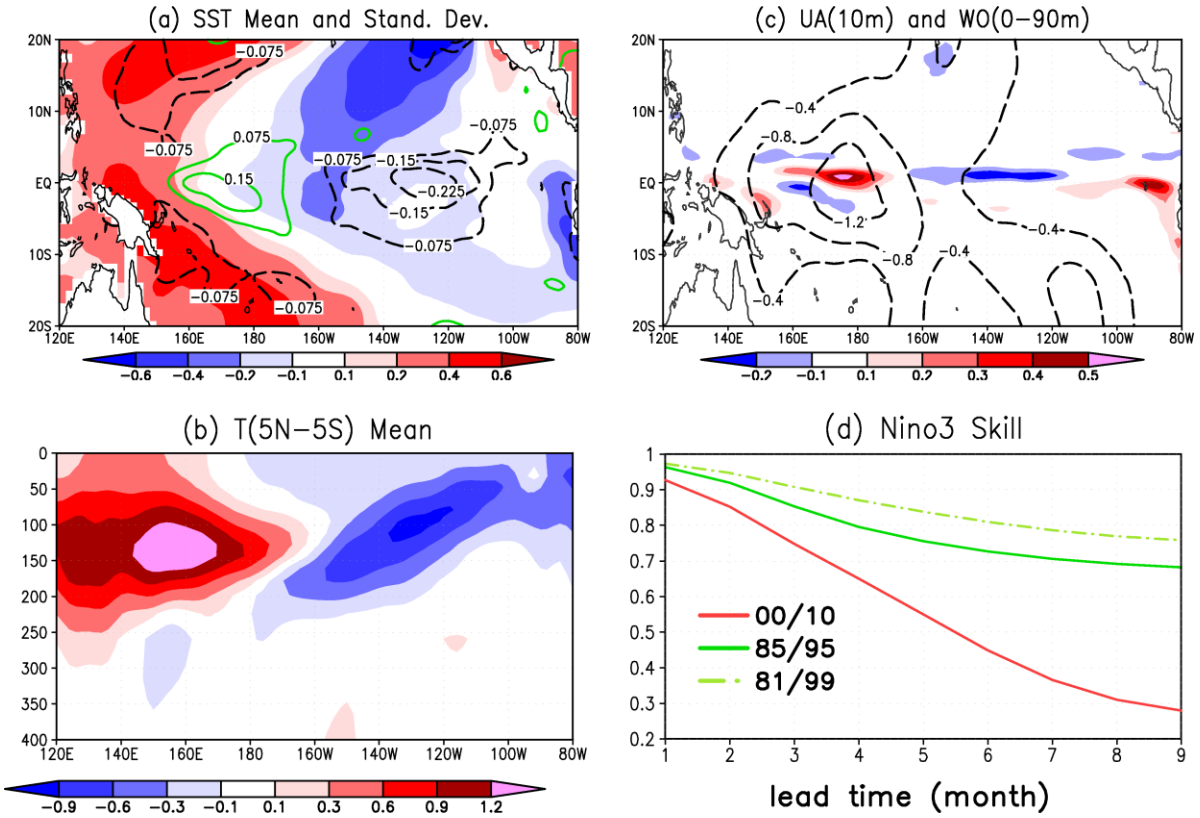

Fig. 5.1 Epochal mean state differences (2000–2010 minus 1985–1995)
a: SST (shaded °C) and its monthly standard deviation (contour interval 0.075 °C, solid green for positive differences and dashed black for negative differences);
b: temperature along equator (5°N–5°S) versus depth (shaded °C);
c: upwelling velocity averaged 0–90 m (shading at intervals of 0.1x10–4 m s^{-1}) and zonal wind at 10 m (contour 0.4 ms^{-1}, negative values dashed), and
d: prediction skill (correlation) of the Nino3 SST index based on POAMA control hindcasts (red curve 2000–2010; solid green curve 1985–1995; dot-dash green curve 1981–1999).

El Niño activity was reduced in this period (Fig. 5.1a) and so reduced forecast skill could simply stem from the stochastic variation of El Niño activity: enhanced predictability would occur during active epochs with high signal-to-noise ratio and reduced predictability would occur during quiet epochs with low signal (e.g. Kirtman and Schopf 1998). Furthermore, the stochastic nature of El Niño activity can then account for the apparent swings in the mean state climate, with the cold phase of the IPO in the recent epoch simply reflecting the absence of any strong El Niño events that would act to warm up the eastern Pacific (Rodgers et a. 2004; McPhaden et al. 2011). However, there are strong indications that the fundamental recharge–discharge mechanism at the heart of El Niño and which provides the predictability also weakened in the recent epoch (McPhaden 2012), indicating that the coupling of atmosphere and ocean has also weakened. This raises the possibility that the epochal mean state changes described in Fig. 5.1 are not just the result of stochastic variability of El Niño but stem from feedback of the mean state changes onto the behaviour of El Niño (e.g. coupling between atmosphere and ocean changed), hence predictability of El Niño changed.

We explore this possibility by conducting a simple re-forecast experiment with the POAMA system whereby we initialise the forecasts in the earlier epoch (1980–1999) using the mean state climate from the later period, and vice versa for the forecasts in the later period. We then compare these re-forecasts to the original POAMA hindcasts. The idea of this experiment is to explore how ‘real’ anomalies react to ‘observed’ changes in the mean state. Many previous studies have investigated how model simulated El Niño events react to model simulated changes in the mean state (e.g. Choi et al. 2009; DiNezio et al. 2012) and affect predictability (e.g. Wittenberg et al. 2014), but we feel our experiments

will give a more realistic impression of any impacts that the decadal variations in mean state have had on El Niño variability and predictability because the anomalies and mean state changes are based on observations.

We call the hindcasts from observed atmosphere and ocean initial states the 'control' forecasts. And, we call the re-forecasts with swapped mean states the 'experiment' forecasts. The mean state changes are applied to the full three-dimensional atmosphere and ocean initial conditions. Schematically, let Xc represent any observed (control) initial atmosphere–ocean state during the earlier epoch (1985–1995; note that we define the earlier epoch without inclusion of the massive El Niños of 1997 and 1982, although our results are similar if those years are included). Let Yc similarly describe any initial observed (control) state during the later epoch 2000–2010. With an overbar representing the time average over the respective epoch and a prime indicating a deviation from that mean, we can decompose any initial state used for the control forecasts during those two periods as:

$$Xc \quad X' + \bar{X}$$

and

$$Yc \quad Y' + \bar{Y}$$

The initial conditions for the experiments with the swapped basic states are then defined as:

$$Xe \quad X' + \bar{Y} \quad Xc + \Delta$$

and

$$Ye \quad Y + \bar{X} \quad Yc \quad \Delta$$

where

$$\Delta \quad \bar{Y} \quad \bar{X}$$

We then rerun the forecasts for the two periods and examine the difference between experiment and control, which should reveal the impact of the changed mean state on the coupled anomalies. There is no guarantee that the imposed mean state changes will be faithfully maintained during the forecast, so we concentrate on the differences in behaviour early on in the forecast (i.e. months 1–4) before the imposed mean state changes may have appreciably weakened.

The results from these reforecast experiments are summarised in Fig. 5.2, which shows the impact of the imposed mean state changes on the predicted amplitude of Nino3 SST index (Right) and on the predictability of the Nino3 SST index (Left). The impact on Nino3 amplitude is negative when we impose the later epoch mean state (i.e. the cold phase of the IPO) onto anomalies in the earlier epoch and positive when we make the later forecasts see the mean state of the earlier epoch (i.e. the warm phase of the IPO). The differences grow with lead time, peaking at about six-month lead time, at which point the percentage change in amplitude (~20 per cent) is comparable to the observed differences between the two epochs (not shown but as inferred from Fig. 5.1a). That is, the shift to the cold phase of the IPO has sufficient impact so as to largely account for the observed decreased of El Niño activity and vice versa for the shift to the warm phase of the IPO in the earlier period.

By computing a heat budget in the upper ocean, we have diagnosed the specific details of which shifts in the mean state have resulted in this changed coupled variability. Specifically, during the cold phase of the IPO we have found a roughly equal contribution from a weakened 'thermocline feedback' in the eastern Pacific, which results from a westward shift of the mean upwelling along the equator (Fig. 5.1b), and weakened 'zonal advective feedback' in the central Pacific, which results from weaker zonal current anomalies as a result of weaker coupling between atmosphere and ocean (i.e. in a cold basic state, a weaker wind anomaly is generated for a given SST anomaly). Thus weaker El Niño activity is favoured in the eastern Pacific. The opposite happens during the warm phase of the IPO.

The impact on predictability is summarised in Fig. 5.2 (Right), which shows the difference in explained total ensemble variance by the ensemble mean for the experiment and control. The weakened El Niño variability in the earlier epoch as a result of imposing the cold phase of the IPO results in an ensemble with more spread (i.e. lower signal to noise) and hence less predictability. The opposite happens in the later period when we impose the warm phase of the IPO.

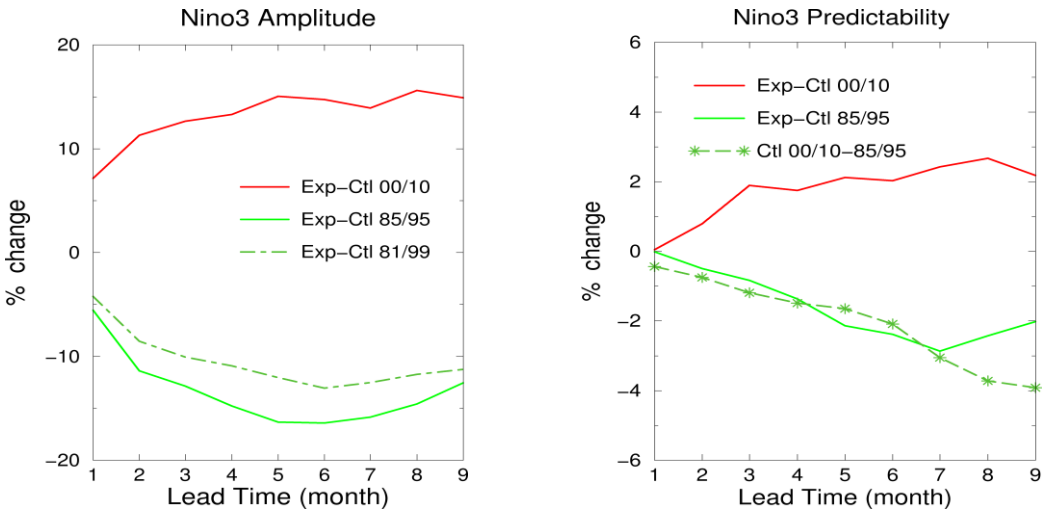

Fig. 5.2 Change in predicted Nino3 amplitude and predictability.
Left: Differences in predicted Nino3 amplitude are shown as the percentage change of the amplitude from the forecast experiment with swapped initial mean state compared to the control forecasts for 2000–2010 period (red curve), for 1985–1995 period (solid green curve), and for 1981–1999 period (dashed-dot green curve).
Right: Differences of potential predictability (experiment minus control) for 2000–2010 (red curve) and 1985–1995 (solid green curve). Dash-star green curve denotes the difference of potential predictability for control forecasts 2000–2010 minus 1985–1995.

Activity 2: Impact of SST trend on extreme rainfall during La Niña 2010

September–November 2010 was Australia's wettest spring since 1900. The climate of 2010–11 was marked by strong La Niña that was characterised by near record strength cold SST anomalies in the tropical eastern Pacific and warm SST anomalies in the tropical eastern Indian and western Pacific Oceans. Concurrently, a strong negative Indian Ocean Dipole Mode (IOD) developed in late winter–spring, which was characterised by warm SST anomalies in the tropical eastern Indian Ocean and cold SST anomalies in the tropical western Indian Ocean (Nicholls 2011, Hendon et al. 2014a; Fig. 5.3a). The statistical analysis of Hendon et al. (2014), who examined historical relationships of SST and rainfall, demonstrated that the strong La Niña and negative IOD explained about a half of the magnitude of the anomalous positive SST in the tropical eastern Indian/western Pacific in 2010, and the other half of the warming was accounted for by a long-term trend in that region, which is a part of the statistically significant warming trend in the entire Indian Ocean and the western Pacific (e.g. Deser et al. 2010; Fig. 5.3b,c).

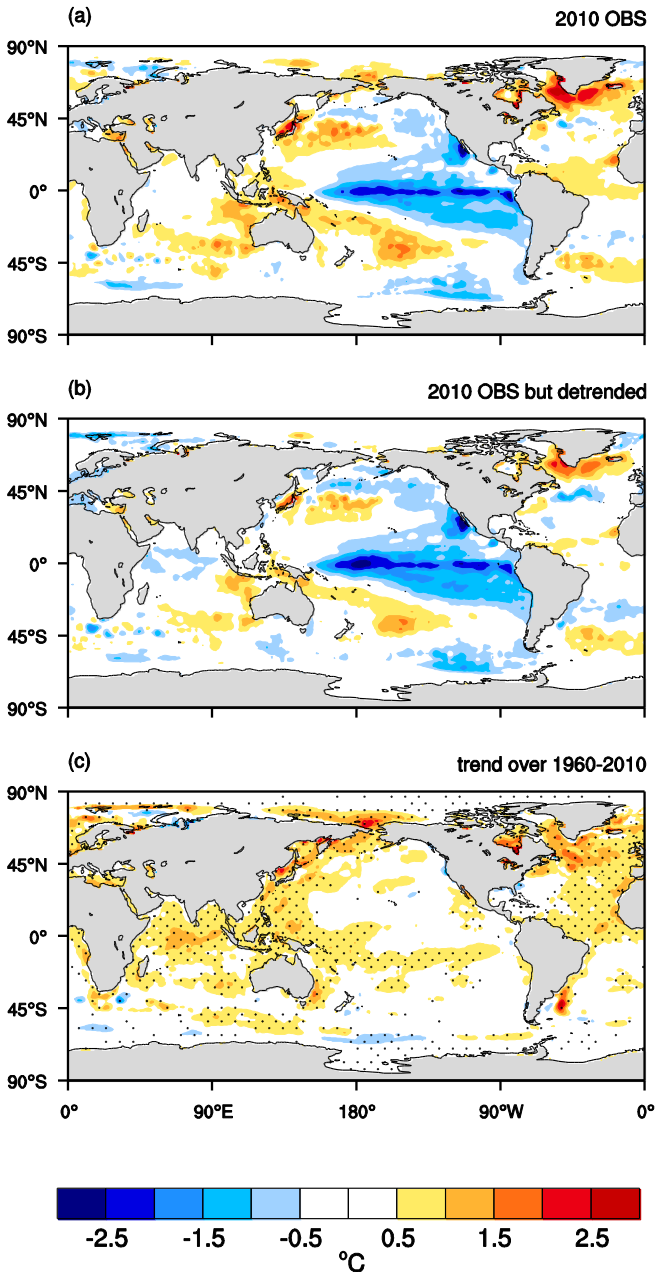

Fig. 5.3 SST anomalies
(a) September–November mean (SON) SST anomalies of 2010 computed relative to the climatological SSTs of 1980–2009, using Hurrell et al. (2008)'s SST product;
(b) as in (a) except linear trend over 1960–2010 at each grid point was removed; and
(c) SST trend over 1960–2010 (units are total temperature change over 1960–2010). Statistically significant trend at the 90 per cent confidence level (c.l.) is stippled, which is assessed by a Student t-test with 49 degrees of freedom.

Hendon et al. (2014) and Lim and Hendon (2014) suggested that much of the record rainfall in 2010 can be accounted for by the occurrence of the strong La Niña. La Niña directly promotes increased rainfall over Australia via a positive swing in the Southern Oscillation but also indirectly by promoting strong persistence of the positive phase of the Southern Annular Mode (SAM), which is characterised by anomalously high pressure in the mid-latitudes and low pressure in high latitudes with strong zonal symmetry (Fig. 5.4). Hendon et al. (2014) further inferred that the anomalously warm SSTs north of Australia due to the ongoing warming trend were another important player for causing the extreme wet Australian spring. Based on historical relationships between local SST to north of Australia and rainfall, they estimated that the trend in SST explained about 10 per cent of the eastern Australian areal mean rainfall anomaly in 2010, but the underlying mechanism has not been identified.

Therefore, this study is aimed at quantifying the role of the trend in the SSTs for promoting the anomalously wet conditions over Australia in 2010 spring and to identify the underlying physical mechanism. The approach is to conduct experiments with the Australian Bureau of Meteorology's seasonal prediction system, Predictive Ocean and Atmosphere Model for Australia (POAMA). The POAMA system, initialised with observed atmosphere and ocean states on 1 September 2010, made a

good forecast of the wet conditions during SON (Lim and Hendon 2014). We are therefore motivated to conduct a series of sensitivity experiments in order to diagnose the sources of the good forecast.

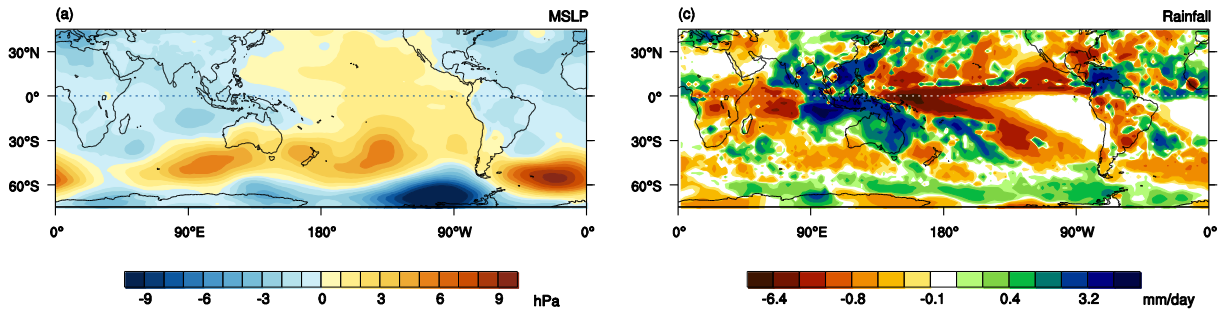

Fig. 5.4 Observed (a) mean sea level pressure (MSLP) and (b) rainfall anomalies of 2010 SON relative to the climatology over 1980–2009, using the ERA-Interim reanalysis (Dee et al. 2011) and the CMAP data (Xie and Arkins 1996), respectively.

POAMA is an atmosphere and ocean coupled-model forecast system (Wang et al. 2005). The atmospheric model of POAMA is the Bureau's Atmospheric Model version 3 (BAM3; Colman et al. 2005). The ocean component of POAMA is the Australian Community Ocean Model version 2 (ACOM2) (Schiller et al. 2002, Oke et al. 2005). The atmosphere and ocean component models are coupled by the Ocean Atmosphere Sea Ice Soil (OASIS) software (Valke et al. 2000).

In order to assess the sensitivity of 2010 austral spring climate to the trend in SSTs, we conducted the control ($CTRL_{2010}$), detrend (DTR_{2010}), trend (TR) and climatological ocean (CLIM) experiments. $CTRL_{2010}$ was initialised with the analysed ocean conditions of 1 September 2010 as provided by the POAMA ocean assimilation system, whereas DTR_{2010} was initialised with the same ocean conditions as the control experiment but the trend estimated for the period 1960–2010 was removed from the temperature field at each ocean grid point. CLIM was initialised with the climatological ocean conditions of 1 September based on 1980–2009. Finally, TR experiment was initialised with the ocean conditions consisting of the ocean temperature trend added to the climatological ocean conditions on 1 September at each grid point (Table 5.1). For all four experiments, the atmosphere and land component models were initialised from randomly selected conditions for 1 September chosen from 1980–2009. Because we use randomly chosen atmospheric initial conditions for all experiments, the experiments reveal the role of the boundary forcing provided by the ocean for producing the wet conditions. From these experiments, we will see if the trend in SSTs played a role in promoting the extreme wet conditions over Australia, as proposed by Hendon et al. (2014). We can also reveal any nonlinearity of the impact of the trend in SSTs when it operates in conjunction with the strong La Niña or solely with the climatological SSTs.

	Ocean Initial Conditions	Atmosphere/Land Initial Condition	Notes
$CTRL_{2010}$	Observed 1 Sep 2010	Randomly selected from 1 Sep 1980–2009	$CTRL_{2010}$–DTR_{2010} reveals impact of the trend acting on top of the strong La Niña of 2010
DTR_{2010}	Observed 1 Sep 2010 but temperature trend removed		DTR_{2010}–CLIM reveals impact of interannual (detrended) La Niña anomalies for 2010
TR	climatology ocean for 1 Sep (based on 1980–2009) plus observed trend ^{t}		TR-CLIM reveals impact of the trend acting on climatological ocean conditions
CLIM	Climatology ocean based on 1 Sep 1980–2009		

Table 5.1 Design of the four forecast sensitivity experiments

The comparison of DTR_{2010} to CLIM (Table 5.1) reveals the impact of the detrended interannual anomalies of SST (Fig. 5.5a) for producing the wet conditions in 2010. Fig. 5.5b and c reveal that most of the forecast wet anomaly and corresponding sea level pressure anomaly is captured from the detrended interannual SST anomalies. However, the role of the trend in the SST, as revealed by the comparison of $CTRL_{2010}$ to DTR_{2010}, was to significantly amplify the wet conditions over Australia and especially eastern Australia (Fig. 5.5f). The anomalies due to the trend account for upwards of one third of the total predicted anomaly, which is appreciably more than our previous estimate based on linear statistics (Hendon et al. 2014). The circulation response to the SST trend appears to be an increased local reduction of sea level pressure in tropical Australia due to the Southern Oscillation and an increased swing to positive SAM in the extratropics. The trend magnified the impact of La Niña because the warm-pool over the tropical eastern Indian and western Pacific Ocean became warmer by both La Niña/negative IOD and the SST trend (Fig. 5.5a,d) and so the warm SST in the western Pacific due to La Niña were operating on a warmer basic state. Therefore, diabatic heating of the atmosphere became greater and resulted in a larger response in tropospheric temperature and tropical/extratropical circulations (Fig. 5.6, Fig. 5.7).

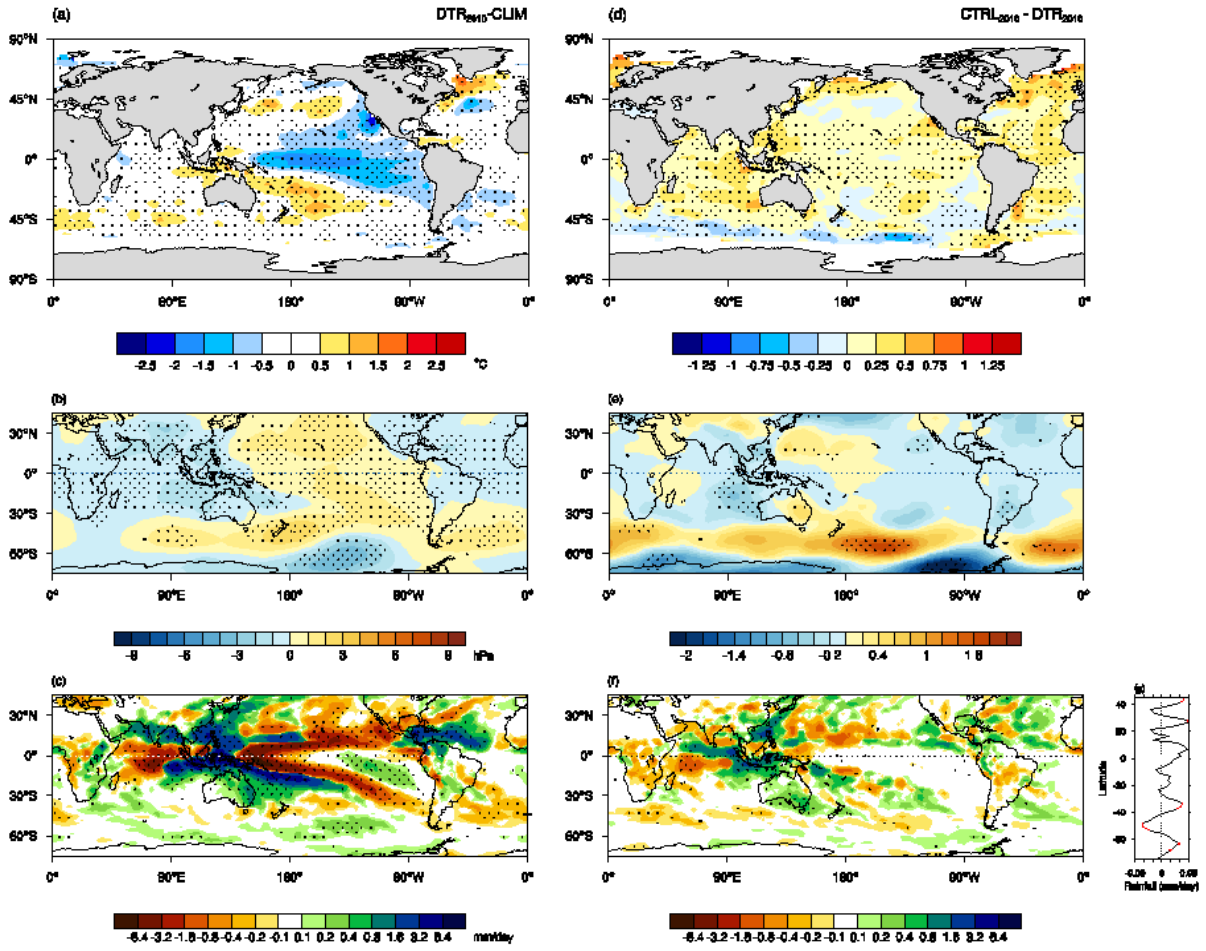

Fig. 5.5 Rainfall differences
(a) SST, (b) MSLP, and (c) rainfall difference of 2010 SON between the DTR_{2010} and the CLIM (DTR_{2010}–CLIM); (d)–(f) differences of SST, MSLP, and rainfall between the $CTRL_{2010}$ and DTR_{2010} ($CTRL_{2010}$–DTR_{2010}). Stippling indicates the statistical significance of the results at the 90 per cent c.l. tested by a Student t-test based on the two sets of 30 ensemble member forecasts of the experiments; (g) the latitudinal profile of zonal mean precipitation of the $CTRL_{2010}$–DTR_{2010}. Red lines indicate statistically significant differences at the 80 per cent c.l.

The impact of the trend on the extratropical circulation and eastern Australia rainfall is understood to have occurred because the trend-induced diabatic heating in the tropics acted as an important source for extratropical Rossby waves that propagated to the south and east, and ultimately shifted the eddy-driven jet over the south Pacific sector poleward and so positively contributed to the positive swing of the SAM (as evidenced by the sea level pressure pattern in Fig. 5.5e and circulation pattern in Fig. 5.6). Also, the strong upper tropospheric warming in the tropics–subtropics induced by the SST trend sharpened the meridional temperature gradient between the tropics and the SH extratropics (Fig. 5.7), which meant more energy available for generation of eddies in the SH higher latitudes. Consequently, more eddies with higher phase speeds were generated in the higher latitudes where the climatological jet has higher speed, and so induced a poleward shift of the eddy-driven jet in $CTRL_{2010}$ compared to DTR_{2010}. Therefore, the SST trend appears to have positively contributed to the strengthening of the positive SAM (Fig. 5.4), which we previously showed was promoted by atmospheric internal dynamics and strong La Niña (Lim and Hendon 2014). It is also worth noting that these changes in temperature and SH extratropical circulation as a result of the trend in tropical SSTs resemble those for future climate projections with increasing greenhouse gases as proposed in earlier studies (e.g. Chen et al. 2008).

In summary, the SST trend appears to have enhanced the wet condition over Australia because it acted in conjunction with the strong La Niña/negative IOD. In contrast, the trend added to the climatological SSTs produced a much weaker response in the atmosphere (weaker warming in the tropical upper troposphere and no shift to higher SAM) and consequently there was much weaker impact on Australian rainfall (not shown).

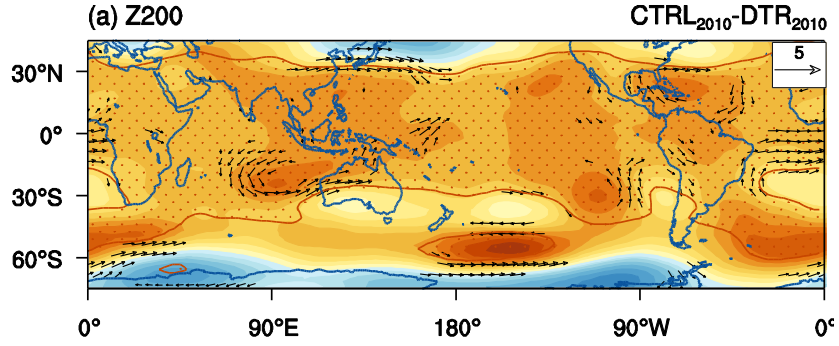

Fig. 5.6 200 hPa level geopotential height difference overlayed with horizontal wind vectors in $CTRL_{2010}$–DTR_{2010}. Only statistically significant difference of the winds at the 90 per cent c.l. was displayed, and the red contour and stippling indicate the statistically significant difference of the geopotential heights at the 90 per cent c.l.

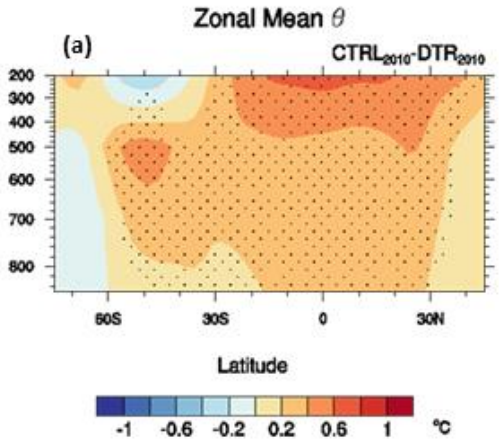

Fig. 5.7 Latitude-height cross section of potential temperature difference in the $CTRL_{2010}$–DTR_{2010}

Conclusions and future perspectives

In Activity 1, we showed that the observed swing of the Pacific climate to the cold phase of the IPO after 1999 appears to have weakened the coupled variability at the heart of ENSO in the eastern Pacific, thereby resulting in weaker El Niño activity and reduced predictability. The implications of this work are that we can expect predictability of ENSO to wax and wane due to natural decadal variations of the Pacific climate state. However, at present there is little indication of any predictability of these epochal swings in the mean state and variability (e.g. Wittenberg et al. 2014), reflecting in part that the swings are indeed a result of stochastic variations in ENSO activity (although we are arguing there is an important two way feedback). Nonetheless, these epochal mean state swings do have multi-year persistence, and because the POAMA model is initialised with observed states, the epochs of high predictability should naturally be captured. Further work is required to determine if we can flag in advance when we are in epochs of low variability/predictability.

In Activity 2, we investigated that the impact of the long-term trend in SSTs on the extreme wet conditions over Australia that developed during the 2010 La Niña. Carefully designed forecast sensitivity experiments demonstrate that SST warming due to the recent upward trend in the tropical Indian and western Pacific Oceans acted in conjunction with the anomalous SSTs due to La Niña and promoted a stronger positive SAM, much in the same way that greenhouse gas warming promotes high SAM, thereby contributing to wetter conditions in eastern Australia. To the degree that the upward trend in SST in the eastern Indian/western Pacific is a result of anthropogenic climate change, extreme rainfall in eastern Australia during La Niña events can be expected in future events. However, not all of this recent trend is due to forced climate change: the recent swing of the Pacific Decadal Oscillation to its cold phase since 1999 has contributed to some of the warming to the north of Australia. Although swings in the IPO are not predictable, persistence of the IPO is long and therefore its impacts (both positive during cold phases and negative during warm phases) are naturally captured in the POAMA model because it is initialised from observed ocean state.

Next year's plan is to continue to build understanding on causes of decadal variations in capability to make seasonal climate prediction for Victoria, This will focus on why the La Niña event in 2007–2009 did not bring above normal rainfall but the La Niña's during 2010–12 did. A hypothesis to explore is that the relationship between ENSO and the Indian Ocean Dipole (IOD) has recently weakened, perhaps due to the ongoing warming trend in the Indian and western Pacific Oceans, and this lack of tight coupling between the IOD and ENSO resulted in the occurrence of a positive IOD event (which typically acts to dry Victoria) during the 2007–2009 La Niña. Decadal variations in the historical relationship between IOD and ENSO will be assessed and related to the variations in the subtropical high and rainfall in Victoria. Forecast sensitivity experiments will be examined to see if the decadal variation in IOD–ENSO can be related to observed decadal variation of the mean state (i.e. the swing to the cold phase of the IPO after 1999).

Project 2: Understanding the Mean Meridional Circulation (MMC) and its relevance to Victoria

Nguyen, H., Lucas, C., Rikus, L., Timbal, B.

CAWCR, Bureau of Meteorology

Key findings

A critical comparison of tropical expansion metrics was carried out to assess whether the various metrics used in the literature are measuring the same thing and, if so, whether this can be used to reduce the uncertainty in estimates of tropical expansion. The main conclusion is that the consensus of various metrics suggests the rate of tropical expansion since 1979 is on the order of 0.5 degree of latitude (approx. 50 km) per decade in each hemisphere.

The regional Hadley circulation relevant to Australia was computed using decomposed meridional wind fields for all recent reanalysis products. Annual cycle and long term trends at annual and seasonal time scales were also computed and compared between the products in order to assess the robustness of the method. It was found that a clear and significant expansion and intensification of the Hadley cell relevant to Australia were observed consistent with the global mean. Preliminary analysis shows most prominent trends in autumn (MAM) concomitant with the local (South East Australia) subtropical ridge intensification and poleward shift for this season.

To further explore different metrics to diagnose the Hadley cell, we adapted the 'object identification of subtropical and extratropical jets' method and also applied a methodology involving computation of the isentropic streamfunction. Work on analysing the isentropic streamfunction is in progress at this stage. The object identification scheme applied to westerly winds averaged over all longitudes to extract all westerly jet streams was proven to be very robust and there is substantial agreement between results from all the available reanalyses for all jet properties.

Background

A wide range of metrics have been utilised to evaluate rates of tropical expansion, with varying results. The aim of this project was to quantify the amount of tropical expansion in both hemispheres by assessing all available metrics in the literature and comparing results to determine whether there is there any consensus about rates of tropical expansion and whether it is possible to reduce the uncertainty associated with these estimates. Further, given that the reported tropical expansion in the literature generally assumes zonal symmetry of the Hadley circulation (HC), which does not reflect the observed zonal dependence of tropical expansion reported in SEACI, we also investigate ways to evaluate the regional Hadley circulation over Australian longitudes. Reanalysis datasets were used to compute the various metrics of the HC and results were compared with estimates of tropical expansion inferred from radiosonde observations.

Objectives

1. Evaluate the relationships between HC metrics and other metrics (tropopause heights, subtropical and extratropical wind jets) using reanalyses.

2. Develop and adapt existing methods to evaluate the HC from a regional perspective and apply to reanalyses.

Activity 1: Tropical expansion metrics

A critical comparison of tropical expansion metrics

Previous work (SEACI) showed a clear link between the observed drought in South-East Australia and intensification and a poleward shift of the subtropical ridge (STR). Further, these changes were evidenced to be driven by global tropical expansion under global warming. However, to date there has been no consensus on the exact amount of tropical expansion. This seems to be data and method dependent, with results ranging from no expansion to expansion of up to two degrees latitude (note that one degree corresponds approximately to 111 km) per decade in recent decades. It is therefore crucial to accurately quantify this expansion and, by inference, accurately quantify its impact on the rainfall in the sub-tropics and in particular in Victoria.

Fig. 5.8 provides an overview of tropical expansion rates by both hemisphere and metric. Estimates from different metrics have particular, sometimes contradictory, characteristics; for example, satellite-based studies have the largest rates of expansion, and suggest a greater rate in the northern hemisphere (NH), while tropopause-based metrics show more expansion in the southern hemisphere (SH).

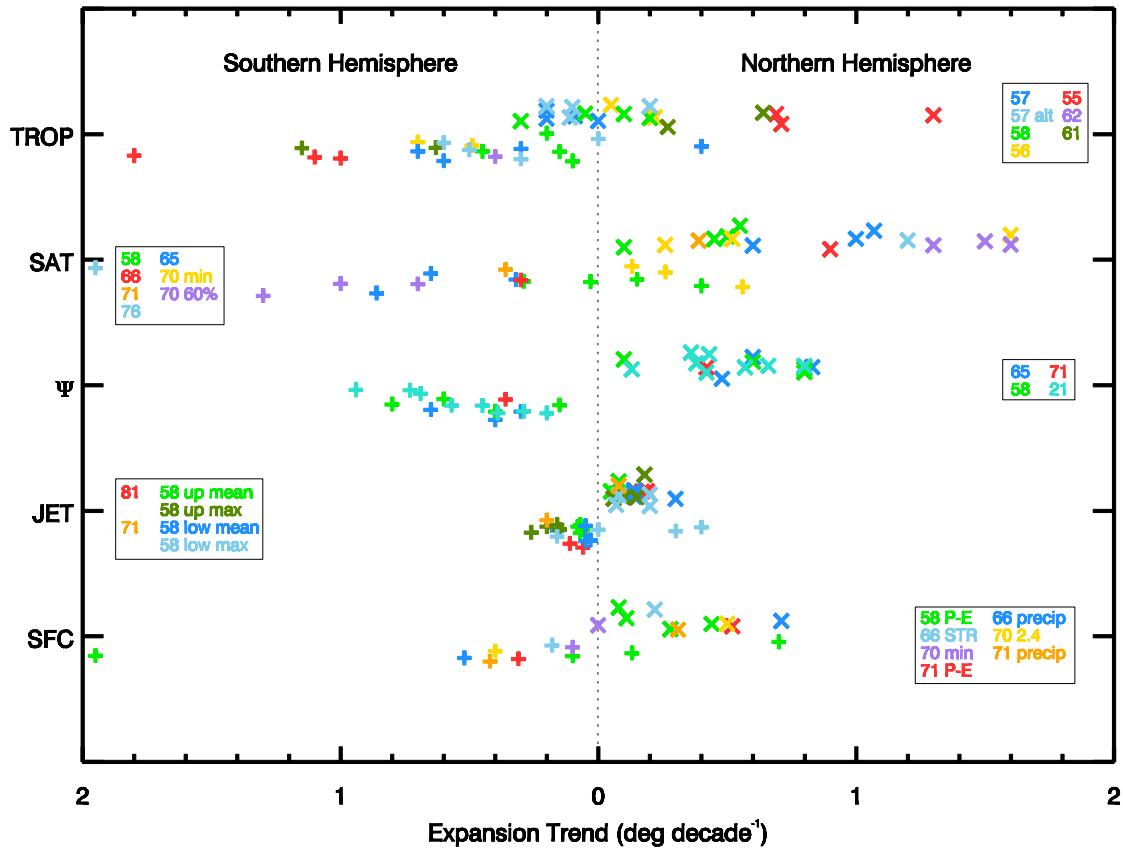

Fig. 5.8 Summary of result of observational tropical expansion studies, broken down by categories. Pluses (+) represent SH values, crosses (x) NH values of tropical expansion trend. Symbols in the corresponding hemisphere indicates expansion, symbols in the 'opposite' hemisphere indicate contraction. Within a particular methodology, the vertical position of each symbol is randomised to improve clarity of individual symbols; no other meaning is implied. Figure taken from Lucas et al. (2014).

These observations raise several questions relevant to the understanding of tropical expansion. Do the various metrics that have been used all measure the same phenomena? What effects do the myriad of

known data issues have on the results? Are potential inconsistencies in the widely used reanalysis products a significant factor? Can the identification of differences in the metrics be used to reduce the uncertainty in estimates of tropical expansion?

Here, we address these questions through close examination of multiple time series of the tropical edge (the basis of tropical expansion estimates) from different sources, including satellite outgoing longwave radiation (OLR), reanalysis-based Hadley cell and subtropical jet (STJ) measurements, radiosonde-based tropopause observations and data from the Global Precipitation Climatology Project (GPCP).

Satellite OLR

As seen in Fig. 5.8, satellite-based estimates of tropical expansion indicate the highest rates of expansion, particularly in the NH. Many of these studies based on the zonal, annual average OLR (e.g. Hu and Fu 2007; Hu et al. 2011). The historical record of OLR is derived from multiple polar-orbiting satellites. These satellites' orbits 'drift' result in a gradual change in the equatorial crossing time (ECT). The varying ECT creates biases in temperature measurements, particularly over land.

These biases can be removed, and their removal effectively eliminates the expansion trend from the OLR measurements. This is fully described in Lucas et al. (2014). The lack of trend in the corrected data better agrees with expectations of little change in OLR in future climate change scenarios. The applicability of this result for OLR to other satellite-derived metrics is unclear.

Subtropical jets

Characteristics of the subtropical jets (STJs) are defined with the object identification method applied to zonally averaged zonal winds as part of Activity 2 detailed below. Time series of the anomalies for the SH jets are displayed in Fig. 5.9. The position of the STJ is identified as the latitude of the centre of mass of a blob of local maximum zonal wind (Rikus 2014). Rikus (2014) reported that the multi-reanalyses ensemble-mean shift in the position of the STJs is largest in December–January–February (DJF) for both hemispheres, trending between 0.34 and 0.80 degrees per decade poleward in the northern and southern hemisphere, respectively, although only the southern hemisphere trend is statistically significant.

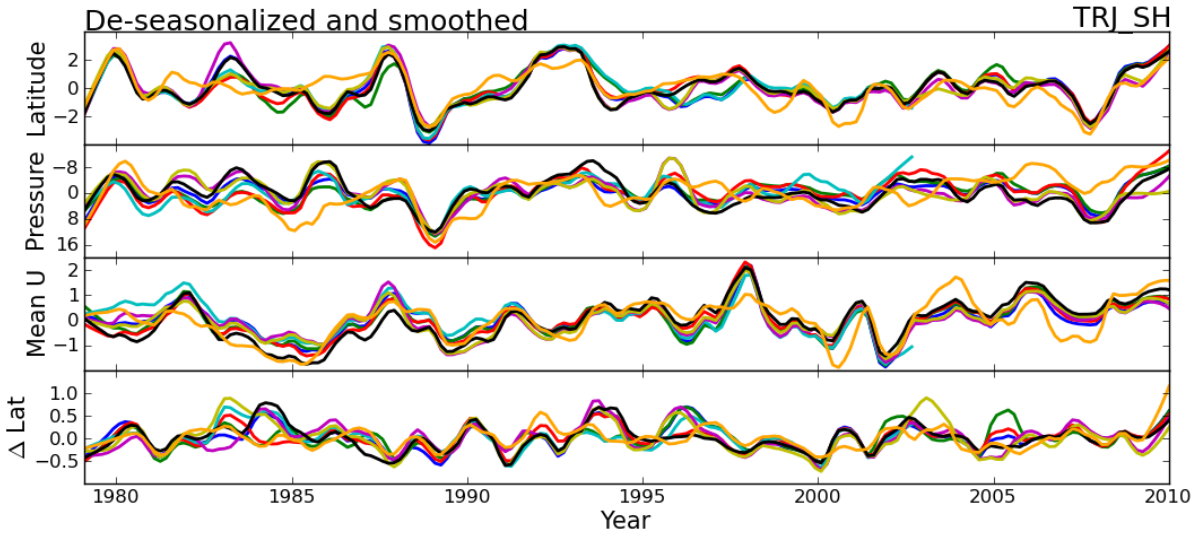

Fig. 5.9 Smoothed monthly time series of the latitude and pressure (hPa) of the zonal mean zonal wind (m/s) centre of mass and of the subtropical jet in the southern hemisphere from 8 reanalysis datasets.

ΔLat is the measure of the latitude of all the points in the identified blob (method described in Activity 2). The seasonal means have been removed and a loess filter applied.

Hadley cell

Characteristics of the Hadley cell (HC) are determined with the isobaric meridional mass streamfunction (ψ), a vertical integral of the zonally averaged meridional wind. The position of the tropical edge is identified as the subtropical 'zero crossing' of ψ (e.g. Nguyen et al. 2013). Across the reanalyses, the average expansion trends are around 0.5 degrees per decade in each hemisphere.

The computed trends vary depending on the reanalysis chosen, and the behaviour of the tropical edge displays some abrupt changes in many cases. This is particularly evident in the SH, where marked breakpoints are identified in all reanalyses except the 20CR in 1990 and 1998. Are these abrupt changes (e.g. 1998) the result of data artefacts or does it represent a real phenomenon? These changes are later observed in the tropical tropopause days described below. Therefore we speculate that they do represent a real phenomenon.

Tropopause Height

Global radiosonde data are used to compute the height of the (lapse-rate) tropopause (Z_T). The tropical edge is defined based on the annual number of tropical tropopause days (TTD), defined as $Z_T > 14.5$ km. Here, the edge criterion is TTD=200 days. Using this metric, expansion rates of 0.45 and 0.29 degrees per decade are reported in the SH (Lucas et al. 2012) and NH (see Project 4), respectively.

Lucas et al. (2012) compared the observed results with those calculated using several reanalysis products, including the state-of-the-art ERA-Interim. Significant differences between the ERA-Interim and the radiosondes are noted before 1985 and after 2001. After 2001, we speculate that this is due the introduction of advanced instrumentation into the satellite observing system. A similar tendency is also noted over the NH, focused in particular around the North American region. The apparent discontinuity is limited to the 200- and 300-day contours in the NH (see Project 4).

GPCP Precipitation

Zhou et al. (2011) and Allen et al. (2012) have used metrics derived from the GPCP precipitation data to characterise the tropical edge. These two studies produced contradictory results, differing particularly on the magnitude of the expansion.

Here, we use zonally and annually averaged GPCP precipitation data and identify the latitude of the observed subtropical minimum in precipitation as a measure of the tropical edge. The location of the tropical edge as determined by this metric is around 20° in each hemisphere, notably equatorward compared to other metrics. Here, we identify expansion trends of 0.32 and 0.18 degrees per decade in SH and NH, respectively, in closer agreement with Allen et al. (2012).

Fig. 5.10 presents the various measures of the tropical edge time series (except for OLR and STJ) described above for the NH (top) and SH (bottom). Interannually, the individual time series are poorly correlated with each other. However, the different metrics identify a consistent envelope that defines movement of the tropical edge over the past 30 or more years. This suggests that at some fundamental level, the different metrics broadly reflect the position and variation of some 'tropical edge'. However, the specific details vary because of the 'different physics' of the metrics.

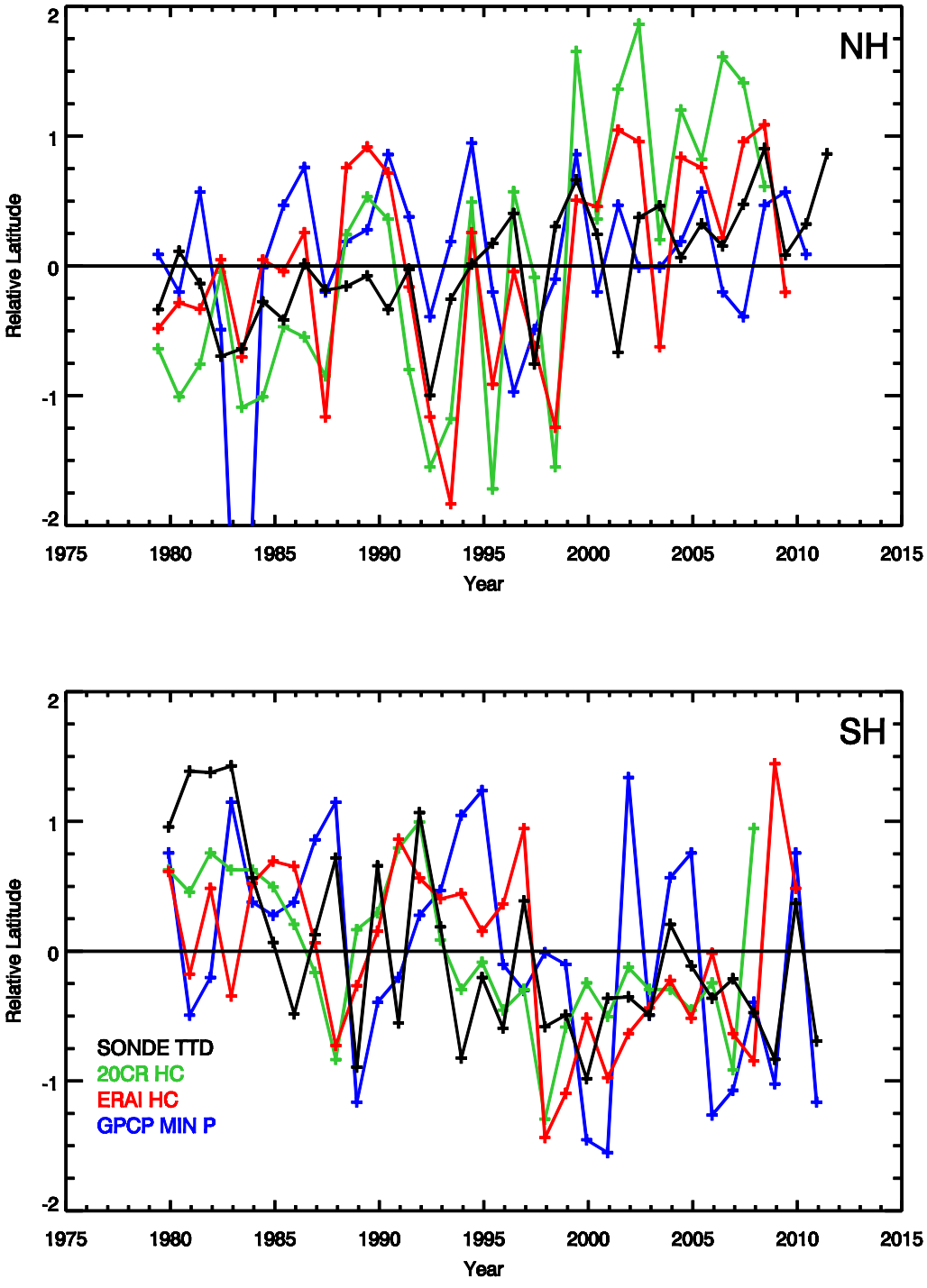

Fig. 5.10 Tropical edge time series for the NH (top) and SH (bottom) from the tropopause-based data from radiosonde (black), the GPCP edge (blue) and two HC-defined estimates: one from the ERA-I (red) and the other from the satellite-free 20CR (green). An OLR-based time series is not shown. Relative positions are shown, with the mean removed from each series.

Conclusions

The analysis of Lucas et al. (2012) indicates that OLR-based metrics require significant correction before they can be reliably used in the analysis of tropical expansion. Hence, we can discount these observations, which are generally higher than others. Eliminating these estimates, the consensus of remaining observations suggests that the most likely rate of tropical expansion, since 1979, is of the order of 0.5 degrees per decade in each hemisphere. However, this trend is not continuous, in part due to natural variability caused by large volcanic eruptions (e.g. Mt. Pinatubo 1991) and ENSO.

In both hemispheres, there qualitatively appears to be a shift in the position of the tropical edge in the late 1990s across all the metrics analysed here. This is similar to what is observed in the HC time series for the SH, and suggests that this abrupt change to the circulation identified in the HC of most reanalyses is at least partially real.

This research suggests that abrupt changes to global circulation and, in turn, climate, as opposed to a gradual transition, are possible as a result of anthropogenic climate change. More work is required to verify this finding. Understanding the physical processes driving a strong shift, if it proves real, and the subsequent climate effects on both global and regional scales is important for adapting to future climate change. This is particularly relevant in Victoria and Southeast Australia. In these regions many broad changes to local climate were coincident with this 1997–98 shift, including the onset of the Millennium Drought (e.g. CSIRO 2012).

Activity 2: Regional Hadley cell expansion

Evaluation of the Hadley cell from the regional perspective relevant to Australia

The tropical expansion previously reported was estimated assuming zonal symmetry. In reality the tropical edge is marked by longitude dependence (SEACI results, and Lucas et al. 2012). In particular Lucas et al. (2012) reported marked variability in tropical expansion for the three southern hemisphere continental longitudes, with the Australian sector exhibiting the largest expansionary trend. This result, combined with conclusions from Activity 1, lead us to the question how the Hadley circulation can be defined regionally and how it impacts the different regions beneath it. This can be key to explaining how the Victorian rainfall decline differs from other subtropical regions. Further this will enable a direct and more relevant comparison between the regional Hadley cell and the local subtropical ridge, which is evidenced to have strong longitudinal variability. Here we explore four methods to evaluate the regional Hadley cell over Australia:

Decomposition of vertical velocity

This method decomposed the vertical velocity into the meridional component then computed the regional vertical structure of the circulation. This work was carried out and led by Julian Schwendike and co-authors from Monash University. Details of the methodology can be found in their recent paper (Schwendike et al. 2014). The decomposition of the vertical motion into zonal and meridional planes is based on the Ψ-vector method of Keyser et al. (1989). The upward mass flux derived from the meridional part of the vertical velocity defines the local Hadley circulation. An example of meridional mass flux at 500hPa is shown in Fig. 5.11 for DJF and JJA. The ascent near the equator in both seasons coincides with the Intertropical Convergence Zone (ITCZ) associated with the maximum rainband. In contrast the subsidences poleward of this maximum at around 30° is concomitant with the subtropics. The global and regional Hadley circulation over the Australian sector obtained from this method is illustrated in Fig. 5.12. The same features as for the global Hadley circulation are observed over the Australian sector in DJF, with a clear double cell structure associated with ascent at the

equator and descent poleward around 30° in each hemisphere. By contrast, in JJA the circulation is dominated by a single cell structure, characterised by ascent in the NH around 10ºN and descent in the SH sub-tropics; only very weak descent aloft is evident in the NH subtropics. The differences between the global and the Australia-centred Hadley circulation are only in their intensities, with the regional circulation being generally the stronger.

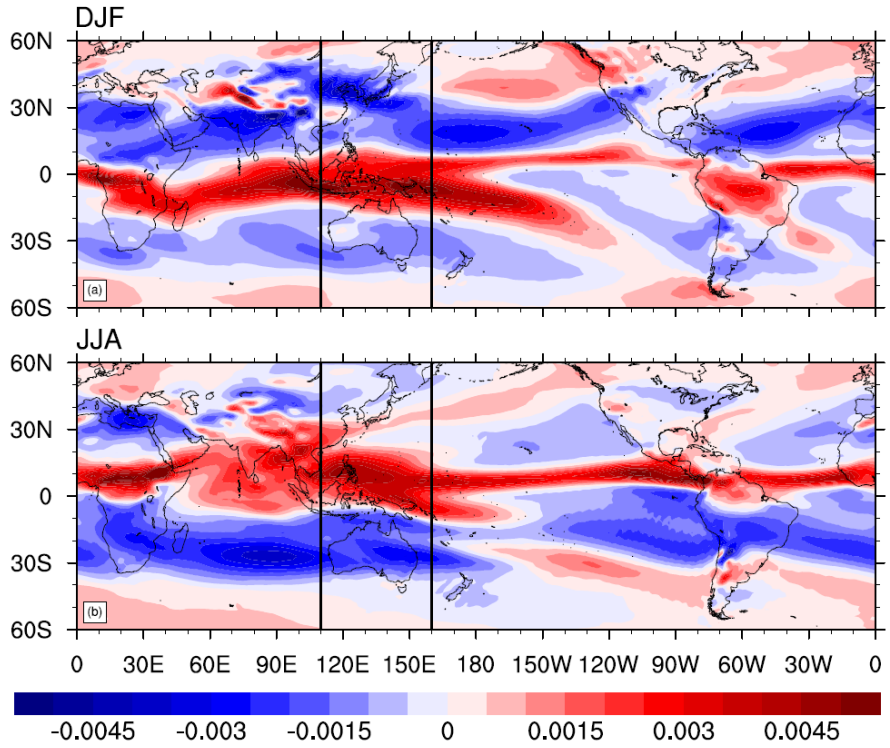

Fig. 5.11 Seasonal mean meridional mass flux at 500hPa for December–January–February (DJF) and June–July–August (JJA) from the ERA-Interim reanalysis dataset
(taken from Schwendike et al. 2014)

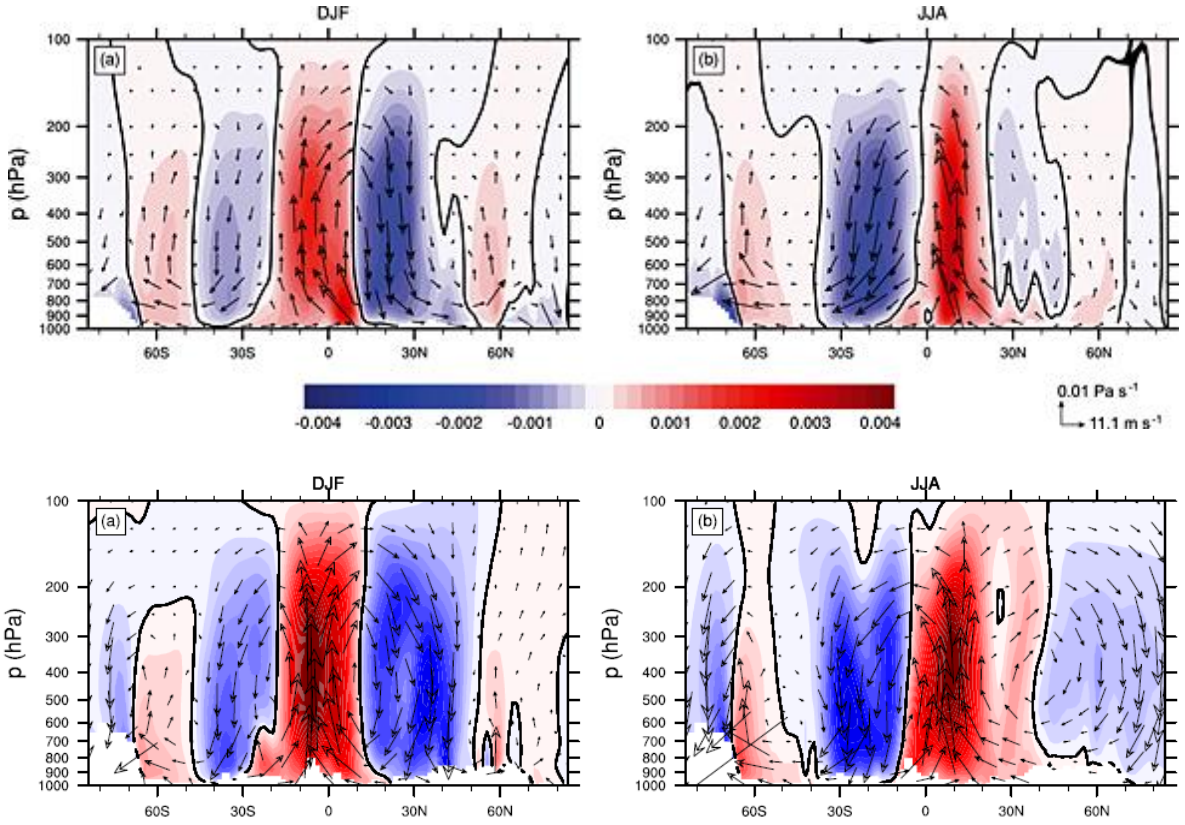

Fig. 5.12 Seasonal mean global (top) and regional over Australia (bottom) vertical meridional mass flux (shading) and associated mean meridional circulation (vectors) for DJF and JJA from the ERA-Interim reanalysis dataset (taken from Schwendike et al. 2014).

Object identification of the subtropical jet streams

A simple closed object identification scheme (or blob algorithm) has been applied to the zonal mean monthly mean zonal wind fields to identify objects corresponding to westerly jet streams. This work was led by Lawrie Rikus who summarised the method and its robustness in a paper submitted to Climate Dynamics (Rikus 2014). Fig. 5.13 is a snapshot of the blob analysis method. First local maxima are identified by applying a mean field filter and saving a list of the points with values more than 0.4m/s larger than the surrounding area within a radius of 5 grid points. The list of local maxima is sorted in order of peak mean zonal wind (U) value and this forms the first guess for the jet objects. For each object in the list a local area blob is defined by finding all connected points with U values within 10 per cent of the local maximum. If a blob intersects a previously defined blob it is removed from the list as it is then encompassed by an already identified blob with greater maximum U. The latitude and pressure of the jet corresponding to each of the remaining blobs are defined by calculating the U-weighted centre of mass of the blob. The zonal mean jet zonal wind speed is calculated as the mean U over the blob area. The standard deviation of the latitudes of all the points in the blob is also calculated to quantify the latitudinal variation of the blob. Fig. 5.13, three jets are identified: the two subtropical jets and the polar front jet in the northern hemisphere. We are interested in the subtropical jets that can be related to the tropical edges. Fig. 5.14 shows smoothed time series of the characteristics for the southern hemisphere subtropical jet for the Australia region (90°–180°E) from all eight available reanalysis datasets. Marked interannual variability is seen in all variables. The spread between the different reanalyses is largest for the pressure and mean U. The trends computed from the latitude time series for the multi-reanalysis mean shows a poleward shift of 0.5 and 0.3 degrees per decade in DJF and JJA, respectively.

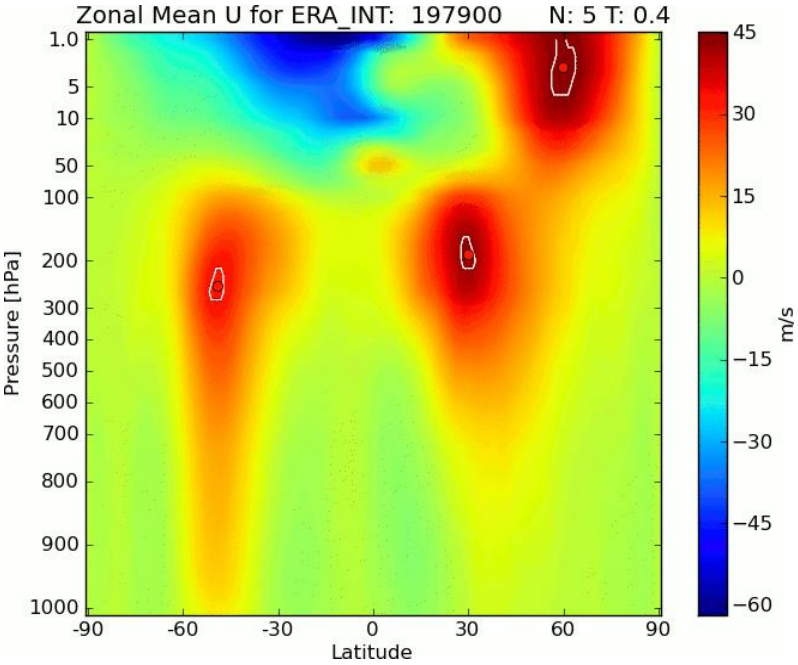

Fig. 5.13 Example showing the results of the blob algorithm for ERA-Interim with blob extent defined by 10 per cent of the local maximum of zonal mean U.
The red dots denote the centre of mass and the white contours the extents ΔLat of the remaining blobs at the end of each algorithm.

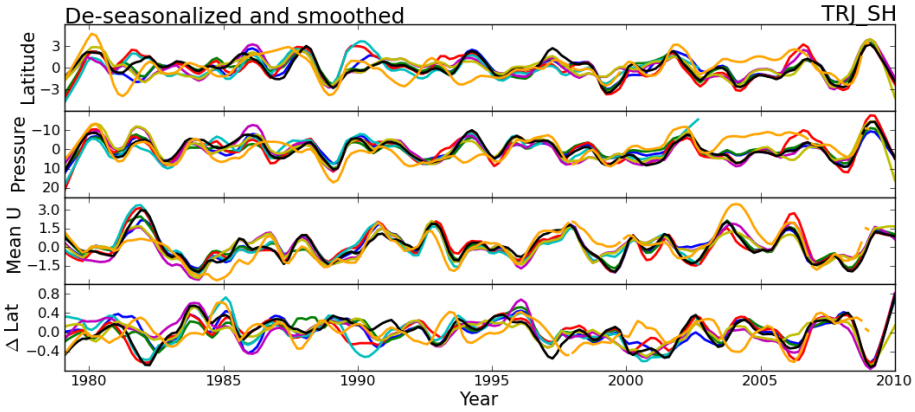

Fig. 5.14 Smoothed monthly anomaly time series of the latitude and pressure (hPa) of the zonal mean zonal wind (m/s) centre of mass of the subtropical jet over the longitude sector 90°–180°E in the southern hemisphere from eight reanalysis datasets.
ΔLat is the measure of the latitude of all the points in the identified blob as indicated in Fig. 5.13. The seasonal means have been removed and a loess filter applied.

Decomposition of horizontal winds

The velocity potential and divergent meridional wind are decomposed from horizontal wind fields. These variables represent the irrotational part of the total wind field that contributes to the meridional circulation. Fig. 5.15 shows these variables at the tropopause (200hPa) where the ascending branch of the mean meridional circulation diverges and deviates poleward. This is particularly apparent over the maritime continent north of Australia, characterised by the negative peak in velocity potential about the equator associated with poleward meridional wind on each hemisphere. Note that the opposite behaviour can be seen near the surface to describe the bottom end of the mean meridional circulation. The annual trends of these variables computed for the last three decades (Fig. 5.16) show an intensification of the velocity potential of the poleward wind in the southern hemisphere. This

indicates an intensification at least of the southern hemisphere Hadley cell for Australia and Indian Ocean.

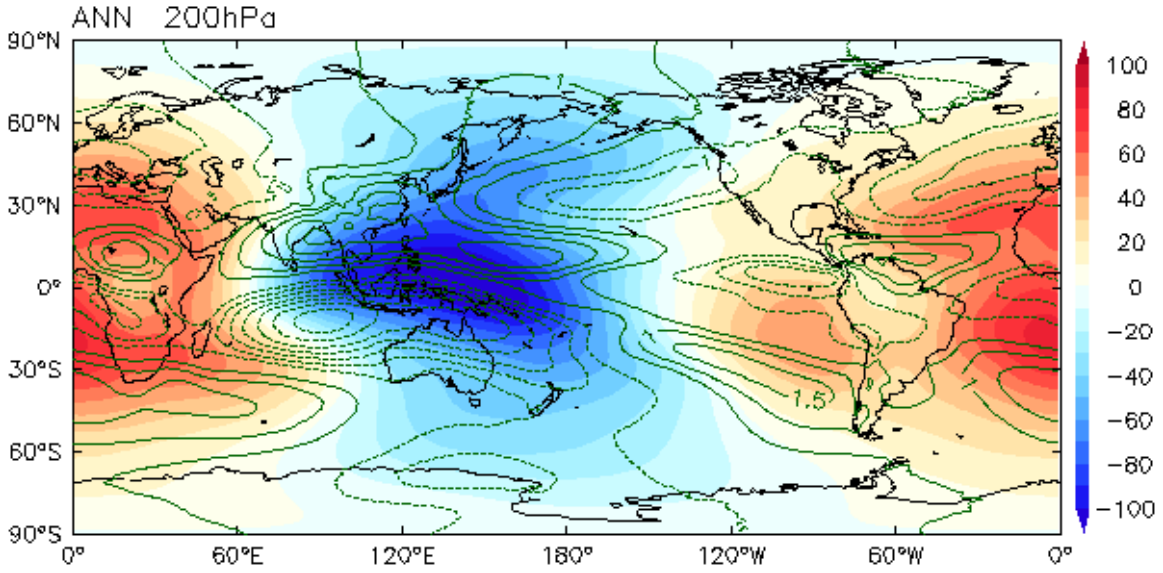

Fig. 5.15 Annual mean velocity potential (shading, m²/s) and meridional divergent wind (contours, m/s) at 200 hPa from ERA-Interim.

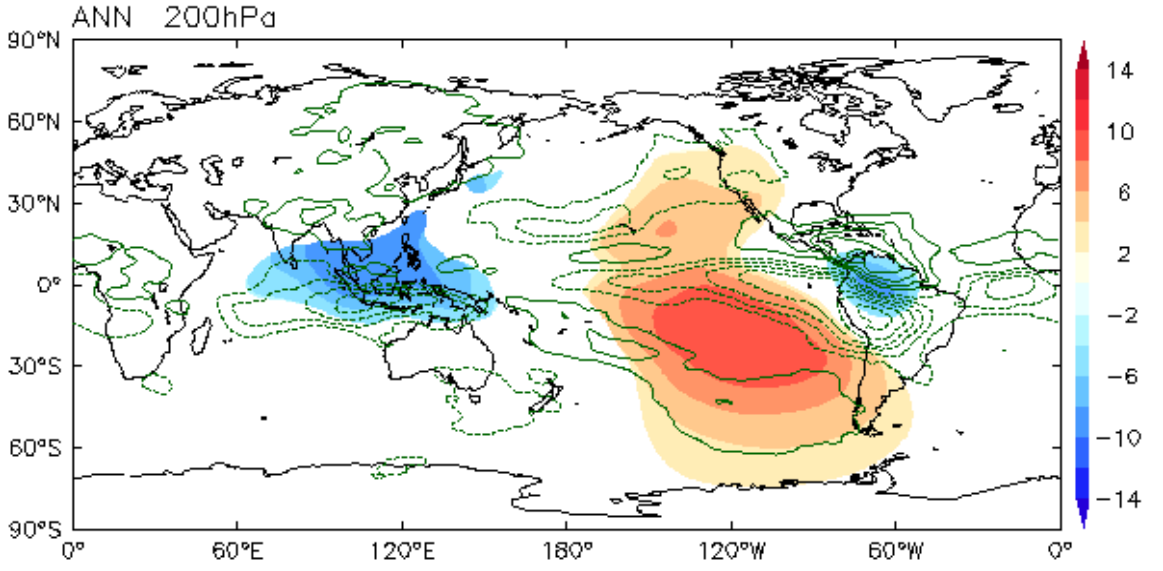

Fig. 5.16 Annual trends of velocity potential (shading, m²/s) and meridional divergent wind (contours, m/s) at 200 hPa from ERA-Interim over the last three decades.

Estimate of regional streamfunction

The regional streamfunction is derived from the irrotational part of the meridional wind (as indicated above) averaged over a range of longitudes. By definition only this part of the meridional wind contributes to the meridional circulation, without any zonal mass transport in and out of a limited domain. The resulting annual mean streamfunction calculated for the Australian sector is shown in Fig. 5.17 using the ERA-Interim dataset. This regional view differs from the global view in the way that the overturning cells do not change sign on their poleward edges. Therefore it is not possible to determine the edge of Hadley cells the same way as for the global mean. The annual trend of this regional streamfunction in the last three decades shown in Fig. 5.18 clearly indicates a statistically

significant expansion of both cells throughout the troposphere. Preliminary results show that the expansion is most prominent in autumn (not shown here), concomitant with the largest poleward shift and intensification of the local subtropical ridge (STR) observed for the same season (SEACI). This work will be completed next year in terms of quantifying the amount of regional expansion of the HC. The method which is currently under investigation is to integrate vertically the streamfunction (Fig. 5.17) through the height of the overturning circulation (900–200hPa) then identify local minima and maxima. The edges of the Hadley cells can then easily be identified and the intensities of the cells can be estimated.

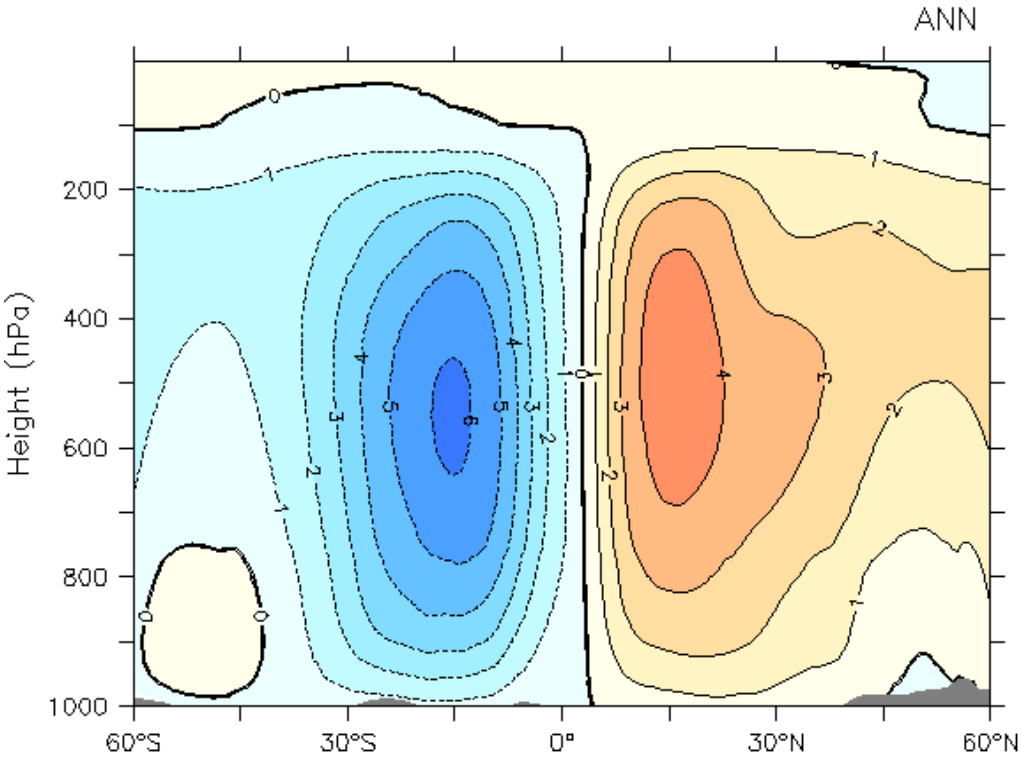

Fig. 5.17 Annual mean regional streamfunction for the Australian sector (110°–175°E) from ERA-Interim.

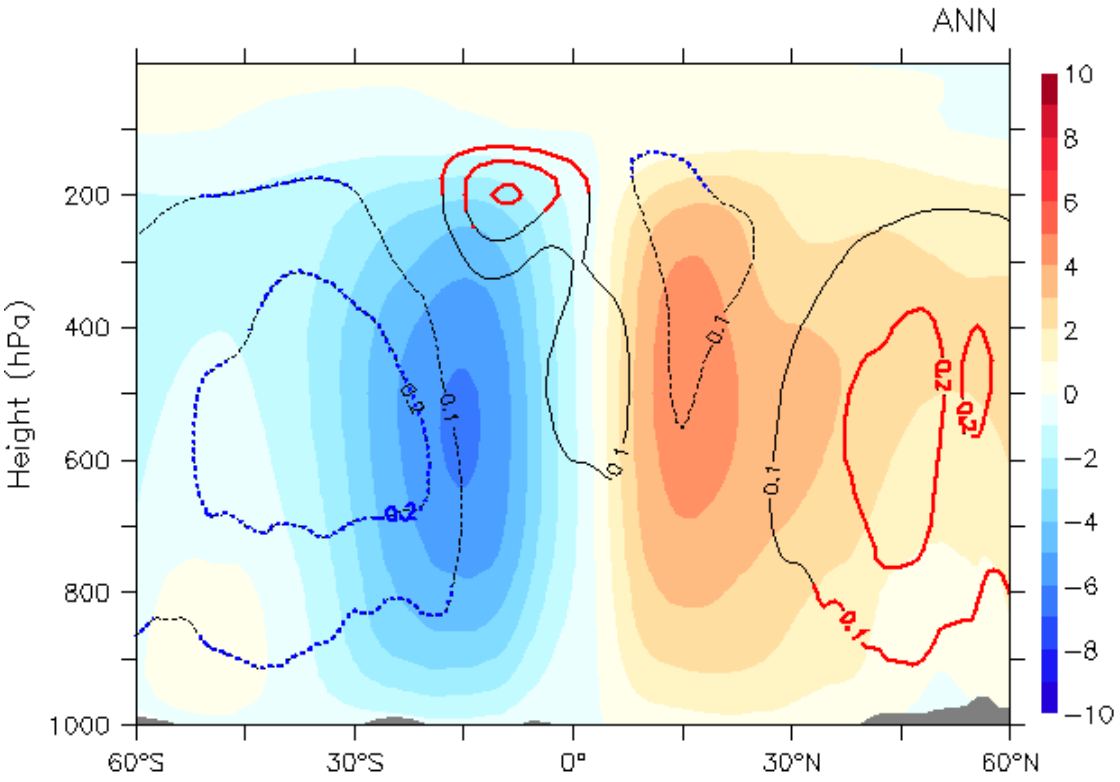

Fig. 5.18 Annual mean regional streamfunction (shading) and trend (contours) over the last three decades of the for the Australia sector (110°–175°E) from ERA-Interim.
Trend values statistically significant at the 95 per cent level are coloured (blue for negative and red for positive).

Estimate of tropopause height frequency from radiosonde data

Historical radiosonde data are analysed using the tropopause height frequency method to determine the tropical edge over the Australia – New Zealand sector. This is the only study utilizing observations independently of reanalysis-derived or satellite-derived data to date. This study was led by Chris Lucas and methods and results were described in Lucas et al. (2012) as part of SEACI. This allows an assessment to be made of the various methods described above utilizing exclusively reanalysis data. The method, described in Activity 2 above for the global perspective, is based on the frequency of tropical tropopause days (TTD) per year, which is a normalised count of the number of days with the reported geopotential height greater than some height threshold representative of the tropopause values. Fig. 5.19 shows the contours of the TTD time–latitude array for the Australia – New Zealand region. The tropical edge is assimilated to the 200 TTD contour. Following this hypothesis, a 90 per cent level statistically significant expansion trend of 0.62 degrees per decade was found for the region for the past three decades.

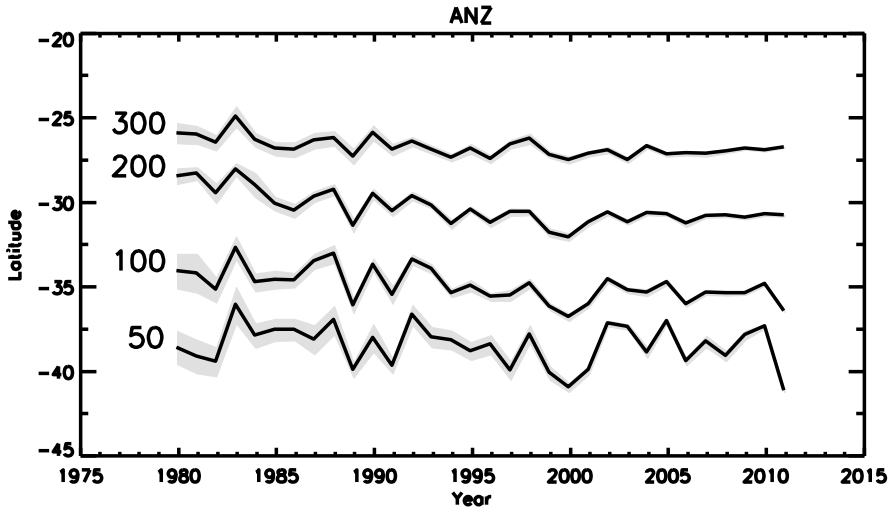

Fig. 5.19 Contours of the annual tropical tropopause days (TTD) time latitude array for the Australia – New Zealand sector. The grey shading represents the uncertainty in the location of the contours.

Conclusions and future perspectives

Many studies have shown that the tropics have expanded over recent decades, but the different metrics used mean there is uncertainty in the rate of expansion and whether they measure the same phenomena. A critical comparison was carried out across various metrics and led to the conclusion that at some degree the different metrics do reflect the position and variation of the tropical edge. There is a consensus in terms of tropical expansion that can confidently be estimated at the rate of 0.5 degrees per decade in each hemisphere (from 1979). This expansion appears to be not continuous but caused mainly by an abrupt shift around 1998, seen in all metrics.

Investigation of the regional aspects of tropical expansion using various metrics applied to the different reanalysis datasets shows a robust expansion trend across all metrics, consistent with the global trend. Further work is required to quantify the expansion in the Australian region from all these metrics. A slightly larger expansion trend than the global perspective is expected for Australia longitudes, with 0.62 degrees per decade inferred from the Tropical Tropopause Days-based metric. Consistent with this, preliminary analysis of the regional streamfunction methods also indicates not only expansion of the regional Hadley cell of 0.67 degrees per decade but also an intensification of it with a 99 per cent confidence level for Australia longitudes. This larger regional expansion compared to the global trends confirms the zonal dependence in the observed tropical expansion highlighted in observations by Lucas and Nguyen (2014, Project 4). Both global and regional results here can further be compared with the isentropic meridional circulation method developed by Lucas and Murphy (described in Project 3).

The robustness of global tropical expansion evidenced here validates the hypothesis that a poleward shift of the subtropical zone leads to a drier climate at the surface and this might be the main cause of the continuous drought observed over Victoria from 1997–2009 and an ongoing cool season rainfall decline. While some rainfall deficits are driven by hemispheric-scale or global-scale modes of variability and hence extend to other parts of the southern hemisphere (Vernon-Kidd et al. 2014), the larger regional tropical expansion over the Australian sector suggests Victoria's climate is even more sensitive to changes in the meridional circulation. This may explain the strong rainfall decline for the region compared to other subtropical longitudes.

Next year's plan is to complete Activity 2 in terms of quantifying the regional tropical expansion from all metrics, summarise the findings in a paper to submit to *Journal of Climate* and investigate the impacts of regional tropical expansion on Australian climate variability. We also aim to investigate causes of zonal dependence in the Hadley Circulation changes.

Project 3: Understanding subtropical–extratropical interactions and their relevance to Victoria

Lim, E-P., Hendon, H.H., Lucas, C., Murphy, B. and Nguyen, H.

CAWCR, Bureau of Meteorology

Key findings

The positive phase of the Southern Annular Mode (high SAM) is associated with a poleward shifted mid-latitude storm track in all seasons. In winter when the mid-latitude storm track plays an important role in the climate of the southern part of Australia, the poleward shift of the storm track results in drier conditions across south eastern Australia. In contrast, during spring–summer, the high phase of the SAM increases rainfall in south eastern Australia because it causes the poleward edge of the tropics to shift poleward to the latitudes of Victoria. Forced upward trends of the SAM in response to increasing GHGs and ozone depletion are thus expected to act to dry southern portions of Australia during winter but moisten subtropical latitudes during spring–summer.

A near record strength of high SAM was diagnosed to have played a primary role in the extremity of the wet conditions over eastern Australia during 2010 spring. This swing to high SAM and its impact on rainfall was found to be largely predictable at least one season in advance because it was promoted by the strong La Niña conditions in the tropics that were acting on top of the recent upward trend in tropical SSTs.

Software to compute the characteristics of the mean meridional circulation in isentropic coordinates has been developed. This will be used in future studies of tropical/extratropical interactions. This alternate method for investigating the mean meridional circulation will provide added insight into the possible links between the tropical expansion and the intensification of the subtropical ridge, and also into the observed south-eastern Australia cool season rainfall deficit.

Background

Evidence is emerging that variations in extratropical circulation associated with the Southern Annular Mode (SAM) play a significant role in driving variations in lower latitude circulation (e.g. the Hadley circulation), and especially rainfall on the poleward edge of the Hadley circulation: High SAM (i.e. a poleward shifted mid-latitude jet) is associated with an expanded Hadley cell (HC) that results in increased rainfall in subtropical latitudes during summer.

This relationship during summer is captured in climate models to varying degrees. It is especially promoted by ozone depletion, but increased CO_2 is also known to drive SAM to its high phase. Understanding the cause of this relationship between SAM and the HC is crucial to understanding the behaviour of the HC in the future. It furthermore bears on the ability to predict regional climate seasonally.

In addition to forcing by greenhouse gases and ozone depletion, there is strong evidence that tropical SSTs during ENSO directly affect the HC, which then affects the SAM (e.g. the HC contracts toward the equator during El Niño thereby resulting in a shift toward low SAM). These variations should be highly predictable. But, SAM is primarily an internal mode of variability. So, the limits of predictability of HC variations will be set by the degree that the internal variations of the SAM determine the poleward extent of the HC.

Objectives

1. Develop new software to calculate isentropic mass stream function
2. Investigate seasonal variations of subtropical precipitation associated with the Southern Annular Mode (SAM)
3. Investigate relationship between SAM variability and the El Niño – Southern Oscillation (ENSO).

Activity 1: Isentropic stream function

Calculation of an isentropic mean meridional circulation

The mean meridional circulation (MMC) acts to transfer excess heat from warm, moist tropical regions to cooler, drier regions nears the pole. Evaluation of this circulation and its response to natural variability and anthropogenic climate change is important for exploring the impacts of climate change.

A common method of measuring the MMC is through the use of the isobaric mass stream function, a transformation of the zonal mean meridional mass flux in the pressure–latitude plane into a circulation pattern. With use of the hydrostatic equation, this calculation reduces to a vertical integral of the meridional wind component in pressure. This yields the familiar three-cell model of the MMC, as can be seen in numerous papers (e.g. Nguyen et al. 2013).

An alternate picture of the MMC can be created by performing the calculation in an isentropic coordinate system, using potential temperature (θ) as its vertical coordinate. On a latitude-θ cross-section, vertical displacements are directly linked to diabatic heating; horizontal displacements represent adiabatic flow. However, the spatial variability of the isentropes can be problematic; near the surface the isentropes can disappear below ground level. Layers that have constant θ with height or pressure are also difficult to interpret; in this case, a given θ-level can represent some depth in physical space.

The isentropic mass stream function is computed analogously to the isobaric example [e.g. Townsend and Johnson 1985]. The zonal mean meridional mass flux in the latitude-θ plane is computed and vertically integrated with the appropriate constants to produce streamlines describing the MMC. This isentropic view of the MMC shows important differences from the isobaric version (e.g. Schneider 2006). The circulation shows linkages between the tropics and extratropics. The Hadley cell is present as in the isobaric view, but linked in the near surface with an extratropical cell, analogous to the polar cells of the isobaric view, but often stronger. This isentropic view suggests a more dynamic MMC that is a continuous hemispheric circulation where tropical–extratropical interactions are important, rather than three largely independent cells.

In the next section, some details of the software code that has been produced to make this calculation will be provided, followed by some basic climatological information based on the isentropic MMC computed from the software.

Isentropic MMC calculation

This section provides some details of the algorithm used to calculate the isentropic stream function (ISF) that has been developed. In general, we follow the calculation methodologies that have been previously published, so far as they can be determined from the literature. In particular, Haagenson and Shapiro (1979), Townsend and Johnson (1985) and Schneider et al. (2006) were useful resources. This code is written using the Interactive Data Language (IDL).

The algorithm requires the full three dimensional fields of temperature (T), zonal and meridional wind (u, v) on vertical levels where the pressure (p) is known. Surface values of these fields are also required. The surface reanalysis is done independently of the free troposphere; this occasionally results in superadiabatic layers, where θ decreases with height, between the surface and the first grid point above the surface. As this is non-physical, especially at monthly or longer time scales, the surface point is adjusted to match the θ at the first grid point. These adjustments are typically small, less than 0.5 K. We use the standard ERA Interim reanalysis (Dee et al. 2011) interpolated to pressure levels as the main data source, but data from any reanalysis should be acceptable. Potential temperature (θ) is computed at each point using the standard formula, providing the basis for the transformation to the θ-based coordinate systems.

A three-dimensional grid is created in isentropic space, replacing p with θ. Following Schenider et al. (2006), the grid in θ varies with $-1/\kappa$, where $\kappa = R/c_p = 2/7$, the ratio of the gas constant for dry air and the specific heat of air at constant pressure. The isentropic grid has 125 points, evenly spaced in $\theta^{-1/\kappa}$ from θ=210 K to θ=450 K. This upper limit is typically found in the lower stratosphere, but well above the tropical tropopause. The resulting vertical coordinate is staggered in θ, with smallest spacing (~1 K) near the surface and wider spacing in the stratosphere.

For each point in isentropic space, T and p are computed using the formulae found in Appendix A of Haagenson and Shapiro (1979). Temperature on a θ-level is estimated from the nearest values above and below in p-space through linear interpolation over θ. The pressure is backed out using the potential temperature equation. To get the wind on θ-levels, a vertical profile of wind at each horizontal grid point (i.e. for each latitude–longitude pair) in p-space is created; points below the surface are removed. Where isentropic layers exist, wind components are averaged on all points in the layer to produce a single value. For this profile, a cubic spline interpolation is used to put the profile onto the θ-grid.

The next step is to compute the mass flux on the θ-grid. For this step, a computation of the isentropic density is required. The isentropic density is defined as $\rho_\theta = -\frac{1}{g}\frac{\partial p}{\partial \theta}$, where g is the acceleration due to gravity. This calculation involves the numerical computation of the derivative, which is done using a centred finite difference except at the first point above the surface, where a forward difference is used instead. The ρ_θ is multiplied by the meridional velocity to obtain the meridional isentropic mass flux at each point on the θ-grid. All mass flux values below the local surface are set to zero.

This meridional mass flux is zonally averaged at each level, resulting in a latitude-θ plane. To calculate the stream function, the following integral is evaluated bottom-up at each point in the θ-grid

$$ISF = 2\pi \cos\varphi R_E \int^{\theta} \overline{\rho_\theta v}\, d\theta$$

where R_E is the radius of the Earth and ϕ is the latitude.

Test Results

To demonstrate that the scheme works, a simple analysis is performed using monthly-mean ERA-Interim reanalysis data from 1979–2010. These data are used to calculate ISF for each month in the period. From these monthly calculations, seasonal climatologies are calculated, as well as composites for ENSO phases.

Fig. 5.20 shows the mean ISF for each of the four calendar seasons. The isentropic representation clearly displays a strong annual cycle of the stream function. The Hadley cell is strongest in the winter hemisphere while in the transition seasons the cells are of comparable strength in the two hemispheres. The figure also displays evidence of linking of the Hadley and polar cells in the DJF in the northern

hemisphere and in JJA in the southern hemisphere (SH), with the cells being linked in both hemispheres in MAM and SON. This linkage is seen near the surface, where a thin 'thread' of the stream function connects the Hadley and polar cells. This linkage occurs at potential temperatures colder than the median surface temperature, indicating that it is the result of cold air near the poles being transported towards the equator.

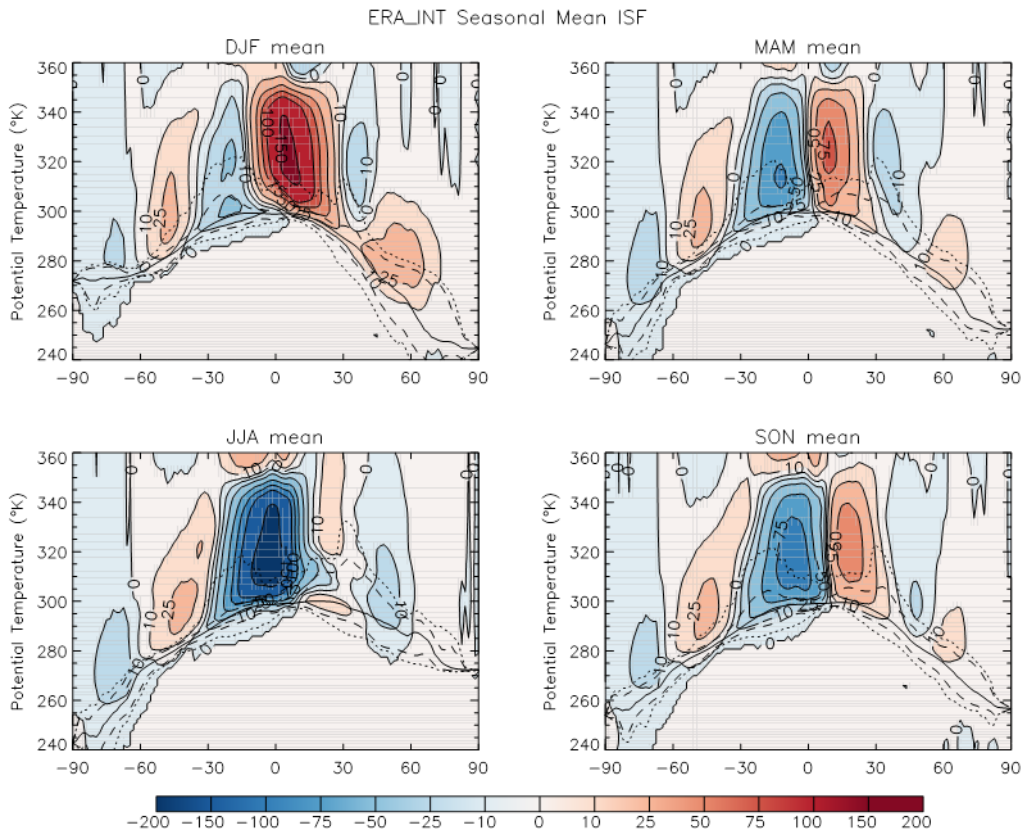

Fig. 5.20 Climatological mean isentropic stream function for the four calendar seasons, using ERA-Interim reanalysis data from 1979–2011.

Composite ISF patterns were calculated for El Niño (1982–83, 1986–87, 1987–88, 1991–92, 1994–95, 1997–98, 2002–03, 2004–05, 2009–10), La Niña (1988–89, 1998–99, 1999–2000, 2000–01, 2007–08) and neutral (all other) years for the DJF season, when ENSO is at its peak. Anomalies from the seasonal mean pattern for El Niño and La Niña are shown in Fig. 5.21. Robust changes in the stream function are seen in both ENSO phases and for most of the meridional circulation cells. When the anomalies are compared with the mean pattern in Fig. 5.20 (top left) it is clear that the Hadley cell contacts and strengthens in El Niño years and expands and weakens in La Niña years. The extratropical response is more significant in La Niña than for El Niño, with significant changes indicating poleward shifts in the circulation cells in the SH.

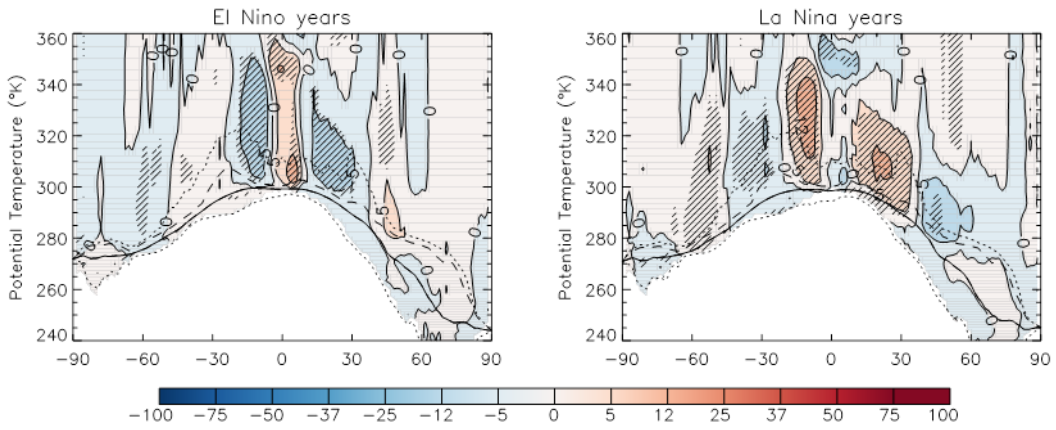

Fig. 5.21 Anomalies from the long-term mean of December–February isentropic stream function (ISF) from (left) El Niño years and (right) La Niña years. Hatching indicates anomalies are significantly different from zero at the 90 per cent confidence level.

Activity 2: Understanding tropical–extratropical interactions over the southern hemisphere

Seasonal variations of subtropical precipitation associated with the Southern Annular Mode

The Southern Annular Mode (SAM) is the leading mode of the variability of the SH extratropical circulations at time scales beyond one week. Although the SAM is understood to originate as an internal mode of extratropical variability, variations of the SAM are promoted by El Niño – La Niña and by increasing greenhouse gases and ozone depletion. In its high-polarity phase, the mid-latitude westerlies associated with the polar front jet are shifted poleward, and surface pressure is anomalously low over the polar region and high in the mid-latitudes (Fig. 5.22). The associated latitudinal shift of the mid-latitude storm tracks results in changes in rainfall, air and sea surface temperatures, and ocean surface currents throughout the extratropics of the SH. Specifically, high-polarity SAM is associated with decreased rainfall across southern latitudes of Australia in winter but increased rainfall across subtropical Australia during austral spring and summer (e.g. Hendon et al. 2007, Risbey et al. 2009).

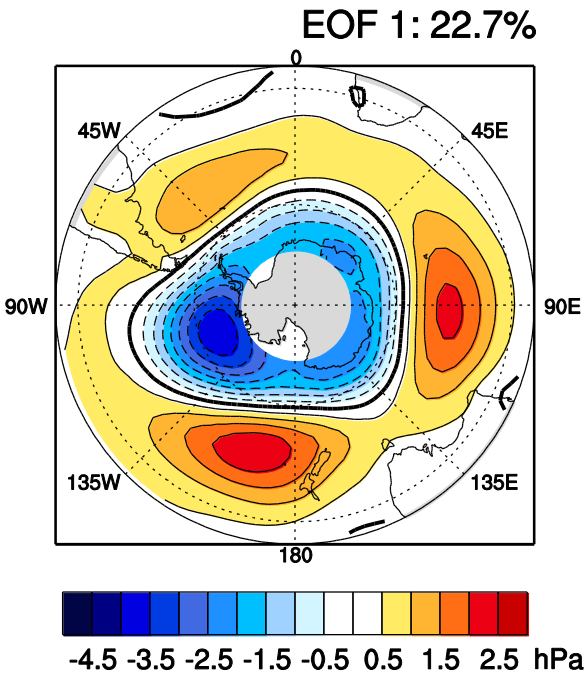

Fig. 5.22 ERAI monthly MSLP anomalies regressed onto the standardised time series of the 1st mode of the EOF analysis of monthly mean MSLP (the SAM index). The EOF analysis was performed on the MSLP weighted by cosine latitude over the domain of 20–75°S in the period 1980–2009. The positive phase (high SAM) is displayed, and the explained variance by this mode is shown in the top right corner of the figure.

Kang et al. (2011) showed that high SAM during austral summer promotes hemisphere-wide upward motion in the SH subtropics, therefore resulting in increased precipitation in the subtropics. This suggests that the increased precipitation in the Australian subtropics associated with high SAM during spring–summer–autumn is likely to be a part of the induced change in the mean-meridional circulation (i.e. poleward expansion of the Hadley circulation). However, the lack of positive rainfall response in the subtropics during winter is unexplained. This study is aimed to understand this seasonality in the response of subtropical circulation/rainfall to the SAM. The intent is to provide more insight into the role of the SAM for seasonal variation of Australian rainfall, to provide increased insight into seasonal predictability of rainfall for which SAM variations play a prominent role, and to better understand the impacts on rainfall of forced changes of the SAM due to increasing GHGs and ozone depletion/recovery. In this report, we limit our interest to the contrast between the summer and winter responses.

We base our analysis primarily on observed behaviour of SAM/circulation/rainfall during 1979–2011. We diagnose the SAM using the index available from the US National Weather Service Climate Prediction Center (CPC), which represents the temporal variations of the 700 hPa level geopotential height anomaly pattern describing the SAM phenomenon (similar to Fig. 5.22). To focus on internal variations of the SAM, we linearly remove the relationship to El Niño and the Southern Oscillation (ENSO) as represented by the variation of NINO3.4 SSTs and we remove the long-term trend in the SAM index. Circulation changes are diagnosed with zonal (u) and meridional (v) wind data from the ERA-Interim reanalysis (Dee et al. 2011). Precipitation changes are diagnosed with the Global Precipitation Climate Project version 2 analyses (GPCP; Adler et al. 2003) and the ERA-Interim reanalysis. Because the SAM is understood as a zonally symmetric variation of the mid-latitude jet, our analysis uses zonally averaged variables.

Our key analysis technique is to regress monthly anomalies of precipitation, winds, and convergence of eddy momentum fluxes onto the monthly standardised time series of the SAM index. To elucidate the seasonality of the anomalies associated with the SAM, we form the regressions using monthly data in summer (December–January–February, or DJF) and winter (June–July–August, or JJA) (sample size of 99 per season, i.e. three months x 33 years). Fig. 5.23 shows the regression of zonally symmetric precipitation onto the SAM index for the four seasons. The anomalies are shown for a positive one standard deviation anomaly of the SAM index. High SAM is clearly associated with a poleward shift of the rainfall in the mid-latitude storm track (i.e. increases centred on 60ºS and decreases centred on 45ºS). However, in summer (and spring and autumn) a positive increase of rainfall in the subtropics (centred on 25ºS) is also seen. This anomaly in the subtropics is clearly absent in winter (heavy boxes in Fig. 5.23 highlight this subtropical region).

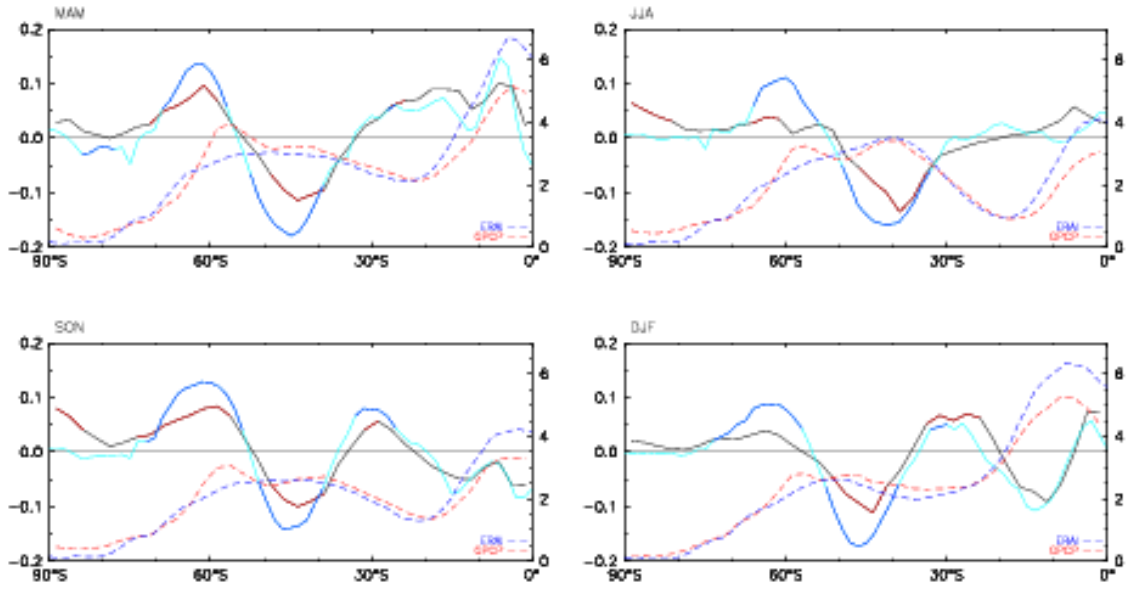

Fig. 5.23 Regression of zonal mean GPCP precipitation (solid black curve with red for significant anomalies at the 90 per cent confidence level) and ERA-Interim precipitation (solid light blue curves with dark blue for significant anomalies) onto the monthly detrended and ENSO-removed Southern Annular Mode (SAM) index for March–April–May (upper left), June–July–August (upper right), September–October–November (lower left), and December–January–February (lower right). Dashed curves are climatological means (red from GPCP and blue from ERA-Interim). Scale for anomalies is on the left (mm d^{-1}) and for mean is on the right (mm d^{-1}). Heavy solid boxes highlight the key subtropical region discussed in text and emphasise the absence of a positive subtropical rainfall anomaly in winter.

We subsequently show that the positive anomalies of subtropical rainfall during high SAM are associated with anomalous upward motion in the subtropics, thereby extending poleward the domain of the upward branch of the SH Hadley circulation. Based on the continuity of mass, the zonal-mean upward motion is induced by the divergence of zonal-mean meridional winds in the upper troposphere. The meridional wind associated with the SAM is understood to develop to balance the eddy momentum fluxes that are the cause of the poleward shift of the jet during high SAM. We deduce the dynamically induced (i.e. eddy driven) meridional wind due to the eddies that are driving the SAM from the simplified zonal-mean zonal momentum budget:

$$\bar{v}_{eddy} = \frac{1}{(f+\bar{\varsigma}_c)}\left\{\underbrace{\frac{1}{a_e \cos^2\phi}\frac{\partial}{\partial\phi}\left[\cos^2\phi\left\{\overline{(u'v')}_a + \overline{(u^*v^*)}_a\right\}\right]}_{(1)} + \underbrace{\frac{\partial}{\partial p}\left[\overline{(u'\omega')}_a\right]}_{(2)}\right\} \qquad \text{(Eq. 1)}$$

where overbar indicates monthly mean, $f + \overline{\varsigma_c}$ is the absolute vorticity, a_e is the earth's radius, ϕ is latitude on spherical coordinates. Term (1) is the meridional divergence of transient and stationary eddy momentum flux, respectively, and term (2) is the vertical divergence of transient eddy momentum flux. Subscript c indicates the climatological monthly average over all years and subscript a indicates the SAM covariant anomaly.

Eq.1 expresses that divergence of westerly momentum flux by transient and stationary eddies (term 1), which acts as easterly forcing, is balanced by poleward flow (negative V_{eddy}), and vice versa for

convergence of eddy momentum flux. The divergence of transient eddy momentum flux (first part of term 1) is the most dominant term for variations of the SAM.

Dynamically-induced vertical motion at the mid-troposphere (600 hPa) due to the divergence of the eddy-driven meridional winds (V_{eddy}) is obtained by vertically integrating the zonal-mean continuity equation downward from 100hPa using monthly mean V_{eddy} at each pressure level and assuming that the vertical motion at 100 hPa is zero:

(Eq. 2)

$$\overline{\omega}_{eddy}(600) = -\frac{1}{a_e \cos\phi}\int_{100}^{600} \frac{\partial \overline{v}_{eddy} \cos\phi(p)}{\partial\phi}\, dp$$

We refer to $\overline{\omega}_{eddy}$ as the eddy-induced vertical velocity. We compare these eddy-induced V and ω to the direct regression of V and ω from the reanalyses onto the SAM index in Fig. 5.24 in order to see whether our derivation of vertical velocity is a good approximation of the observed vertical velocity during high SAM, and therefore, to confirm that the SAM related vertical motion is dynamically induced. Fig. 5.24a shows that the meridional wind deduced from the eddy momentum balance accounts well for the actual variation of meridional wind during the SAM, indicating that the SAM-induced changes in the meridional circulation are dynamically driven even in the SH subtropics. Although the behaviour of meridional winds during high SAM is grossly similar in winter and summer in the mid and high latitudes, there is a substantial difference in the subtropical latitudes: In summer there is a rapid shift of V from southward flow (negative anomaly) to northward flow (positive anomaly) between 40°S and 20°S (Fig. 5.24a red lines). Hence, there is strong divergence of meridional winds in the 20–40°S latitude band, which induces upward motion (Fig. 5.24b red lines), and therefore, promotes rainfall at these latitudes (Fig. 5.23 bottom right). However, in winter, the meridional winds tail off slowly into low latitudes (Fig. 5.24a blue lines), and therefore, there is no divergence of meridional winds in the low latitudes. Thus, no upward motion and associated rainfall is promoted in the subtropics (Fig. 5.24b blue lines, Fig. 5.23 upper right).

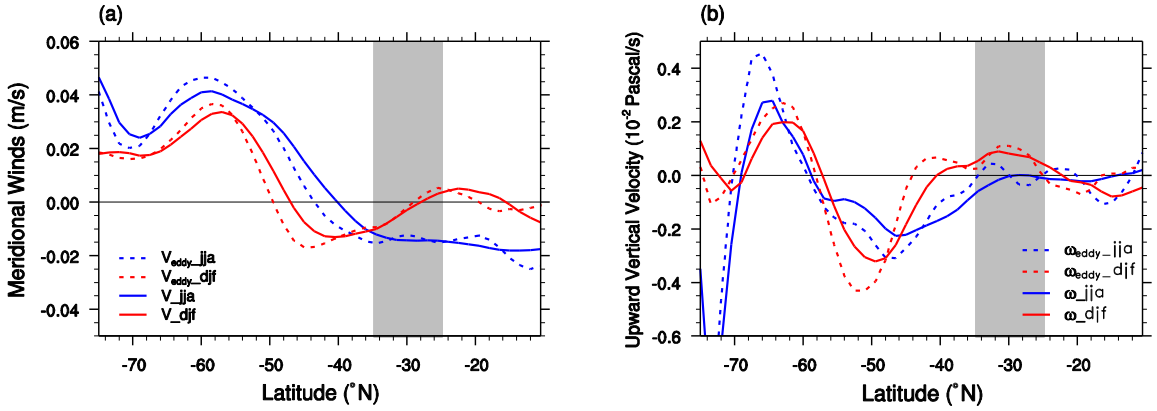

Fig. 5.24 (a) Vertically integrated (100–600 hPa) meridional wind from direct regression onto SAMI (solid curves, red for summer months and blue for winter months) and derived from the SAMI covariant momentum budget Eq. 1 (dashed curves). (b) Vertical velocity at 600 hPa (positive is upward motion) from direct regression onto SAMI (solid curves) and from vertically integrating the continuity equation using the meridional wind anomalies from the SAMI covariant momentum budget (Eq. 2; dashed curves) (positive values indicate upward motion).

So, why are the SAM-induced meridional winds in the subtropics divergent in summer and not divergent in winter? The answer comes from understanding why the eddy momentum flux divergence abruptly goes to zero in summer but tails off gently at low latitudes in winter. We understand the distribution of eddy fluxes by considering where the eddies are generated, how they propagate and where they break (or are absorbed by the mean flow). Climatologically, in summer there is only one jet, centred at 40–50°S (Fig. 5.25), which is maintained by the eddy-mean flow interaction (i.e. eddies develop in the jet and propagate to low latitudes thereby converging westerly momentum into the jet) and outflow from the Asian summer monsoon. We refer to this jet as the eddy-driven jet, and it is characterised as having the maximum winds aloft overlaying the maximum westerlies at the surface. However, in winter, there are two jets—the subtropical jet centred at ~30ºS and the eddy-driven jet centred at ~50ºS. The subtropical jet is maintained by the strong winter Hadley circulation and is characterised by the maximum wind aloft (near 200 hPa) overlaying the zero-line in wind at the surface. The eddy-driven jet, also referred to as the polar front jet, is distinct from the subtropical jet and is defined by the local maximum in westerly wind that extends from the surface to the upper troposphere (Fig. 5.25 upper panels).

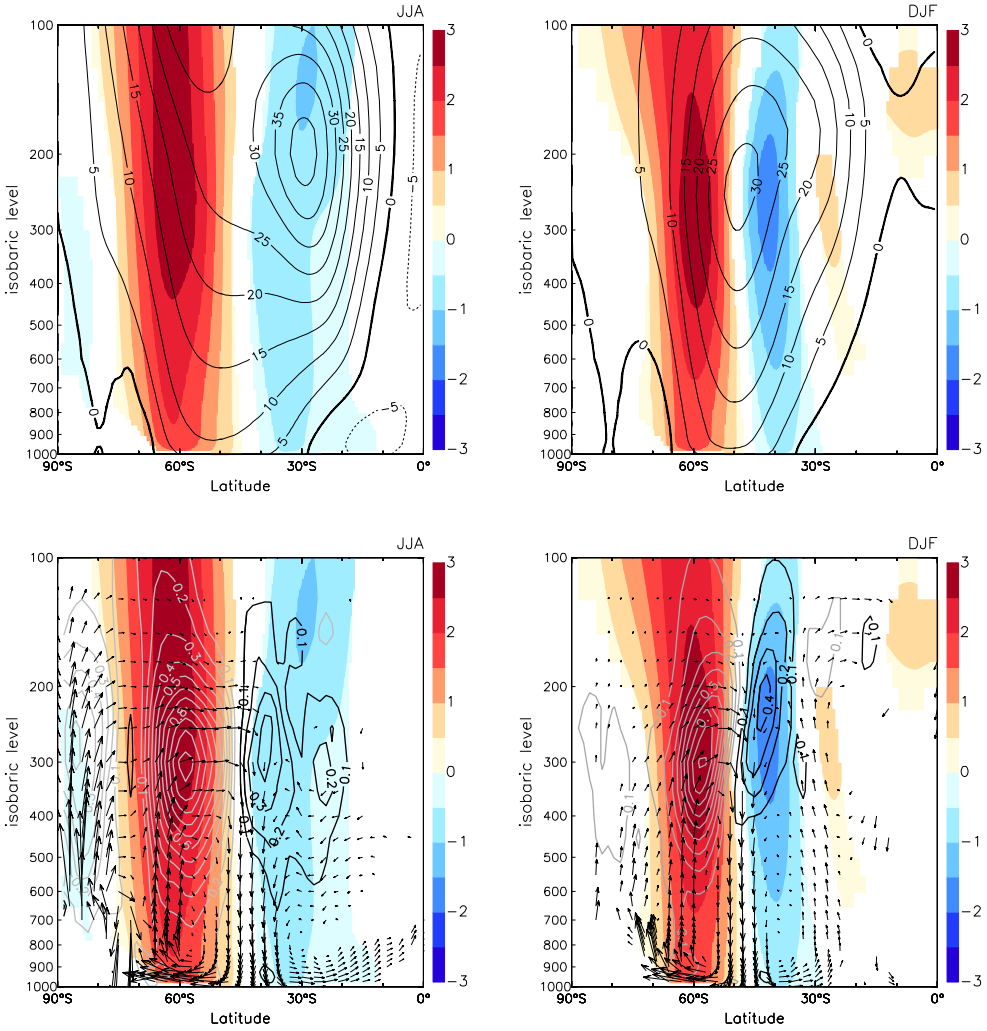

Fig. 5.25 Top: regression of ERA–Interim zonal mean zonal wind (shading, scale on right in ms^{-1}) onto the monthly detrended and ENSO-removed SAMI for June–August (left) and December–February (right). The climatological mean zonal wind is contoured (contour interval 5 ms^{-1}). Bottom: regression of ERA–Interim transient eddy momentum flux convergence (contours interval 0.1 m s^{-1} d^{-1}; convergence is light grey, divergence is black), and mean meridional circulation (vectors). The horizontal component of the meridional circulation vector (m s^{-1}) is meridional wind and vertical component is pressure–vertical velocity (multiplied by –100 Pa s^{-1}, so that

upward/downward motion is indicated by upward/downward pointing vectors). The maximum horizontal vector has magnitude 0.3 ms^{-1}. The regressed zonal wind anomaly is repeated from top panels. Only regressed values significant at the 90 per cent confidence level are shown and vectors are thinned to every other vertical level for clarity.

High SAM is characterised by a poleward shift of the eddy-driven (polar front) jet, and the related positive and negative westerly anomalies are consistent with the pattern of anomalous convergence and divergence of transient eddy momentum flux, respectively (Fig. 5.25 bottom panels). The pattern of convergence and divergence of momentum flux can be understood as resulting from the generation and decay of transient eddies, respectively. In summer during high SAM, anomalous eddies generated in the higher latitudes act to converge westerly momentum into the eddy-driven jet, and these eddies propagate away from the jet to towards the equator where they decay (and cause easterly acceleration) at their critical latitude centred on the equatorward flank of the single jet at ~40°S. In comparison, in winter the anomalous eddies generated in the higher latitudes during high SAM decay in a much broader latitude band of 15–45°S, with peak divergence (easterly acceleration) occurring at 40ºS, which is on the equatorward flank of the eddy-driven jet and well poleward of the subtropical jet. However, there is a secondary peak at 25°S, which is on the equatorward flank of the subtropical jet. This double peak structure of the eddy momentum flux divergence results from the presence of the winter-time subtropical jet and this means that the eddy-induced meridional wind is broader in latitude, hence less divergent at low latitudes in winter during high SAM compared to summer. Consequently, the latitudinal gradient of induced meridional wind is too flat to promote subtropical upward motion during high SAM in winter.

To summarise, in this project, we have attempted to improve our understanding of what causes the distinctive seasonality in the impact of SAM on subtropical rainfall. Our analyses have revealed that i) the subtropical rainfall induced by high SAM is driven by the eddy-driven circulation change, and ii) the absence of the subtropical rainfall response in winter is due to the presence of the strong subtropical jet that causes the decay of eddies and resultant poleward flowing winds to be broadly spread out in latitudes, and therefore, results in little divergence of meridional winds and associated upward motion and rainfall.

These results well explain why the state of Victoria would experience significantly dry conditions in winter but significantly wet conditions in summer during high SAM as shown in Hendon et al (2007): High SAM is associated with a poleward shift of mid-latitude storm tracks in all seasons and a shift of rainfall away from the mid-latitudes to higher latitudes. This results in decreased rainfall from 40–50ºS but extending in winter as far north as ~35ºS, and therefore drying across Victoria in winter. Besides, the promotion of subtropical rainfall during high SAM is missing in winter. Therefore, the net impact of high SAM in winter is best described as a poleward *expansion* of the subtropical dry zone and therefore Victoria dries during high SAM. During spring and summer, high SAM induces increased rainfall in the subtropics (22–35ºS) and so makes Victoria wetter. During summer the net impact of high SAM is best described as a poleward *shift* of the subtropical dry zone (the mid-latitude storm track moves further away to the south from Victoria but the wet tropics to the north move further south). Fig. 3.7 shows these changes schematically.

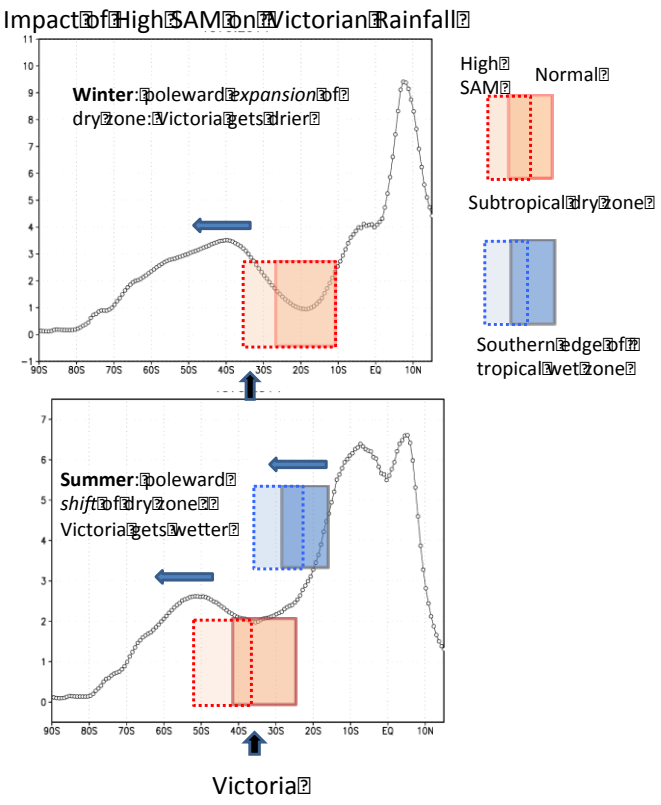

Fig. 5.26 Impact of high SAM on Victorian rainfall:
High SAM causes a poleward shift of mid-latitude storm track in both winter and summer, thereby shifting the mid-latitude wet zone southward away from Victoria. During winter, the net result is an expanded subtropical dry zone and Victoria becomes drier. But in summer, the wet edge of tropics also shifts poleward, so the net effect is a poleward shift of the dry zone, and Victoria becomes wetter. Dotted curve is climatological precipitation from ERA–Interim. Boxed red regions are subtropical dry zones (solid for climatology; dotted during high SAM) and blue region is the southern edge of the tropical wet zone. Black arrow indicates approximate location of Victoria. Blue arrows indicate poleward shift of storm track and southern edge of tropical wet zone during high SAM.

Understanding and predicting the strong Southern Annular Mode and its impact on the record wet east Australian spring 2010

In 2010 eastern Australia experienced its wettest spring on record, which has been largely attributed to the occurrence of a strong La Niña event. However, we also identify a primary role for an extraordinary positive excursion of the Southern Annular Mode (SAM). The impacts of La Niña on Australian rainfall would be expected to have been predictable months in advance due to the predictability of La Niña, but because the predictability of the occurrence of the strong SAM is less known, the strong influence of the SAM on eastern Australian rainfall would have been a limiting factor for a long-lead prediction for Australian rainfall of 2010 spring.

Nonetheless, Hendon et al. (2014) speculated that the extraordinary high SAM may have been predictable due to the largeness of the La Niña in spring 2010, given the historical relationship between La Niña and high SAM during austral spring–summer (e.g. L'Heureux and Thompson 2006; Lim et al. 2013). The purpose of this study is to determine the degree to which the near-record high SAM was predictable and to explore the role of the extraordinarily strong high SAM in the record high rainfall over eastern Australia in spring 2010. To tackle these research problems, we firstly assess the forecast skill of the Australian Bureau of Meteorology's dynamical seasonal forecast system, Predictive Ocean and Atmosphere Model for Australia (POAMA) for September, October, and November (SON) 2010 and conduct two forecast sensitivity experiments.

The POAMA is an atmosphere and ocean fully coupled forecast system. The atmospheric model of POAMA is the Bureau's Atmospheric Model version 3 (BAM3; Colman et al. 2005). The ocean component of POAMA is the Australian Community Ocean Model version 2 (ACOM2) (Schiller et al. 2002, Oke et al. 2005). The atmosphere and ocean component models are coupled by the Ocean Atmosphere Sea Ice Soil (OASIS) software (Valke et al. 2000). In producing POAMA forecasts, the atmosphere model is initialised with realistic atmospheric and land conditions generated from our nudging scheme called ALI, and the ocean model is initialised with high quality realistic ocean conditions generated from our ocean data assimilation system called PEODAS. Control forecasts consist of a 30 member ensemble that were initialised on 1 September 2010 and are of three months

duration. In order to investigate if the 2010 high SAM was forced by the strong La Niña, we generated the second set of forecasts by initialising the ocean with the realistic conditions of 1 September 2010 but initialised the atmosphere with randomly chosen initial conditions drawn from 1 September from the years 1980–2009 (hereafter, referred to as randomAexp). Then, for the third set of forecasts, we initialised the atmosphere with the realistic conditions of 1 September 2010 but initialised the ocean with randomly chosen states from 1 September for the previous 30 years (referred to as randomOexp).

If the high SAM in 2010 was forced by the La Niña, randomAexp will show a positive amplitude of the SAM despite unrealistic atmospheric initial conditions because the atmosphere will see the initial La Niña state in the ocean that will be maintained at least for the three months of the forecast. But, we would not expect to see a positive amplitude of the SAM from randomOexp because La Niña conditions will not be present in the forecasts. If the 2010 high SAM was not forced by the La Niña but was the outcome of the strong atmospheric persistence from late winter, randomAexp will not predict the positive SAM, but randomOexp should produce high SAM at least in the first month of the forecasts.

Conditions of La Niña and SAM in 2010 spring were diagnosed by the 2010 SON amplitudes of the NINO3.4 SST index and the time series of the 1st EOF of monthly mean sea level pressure anomalies, respectively. The forecast amplitudes of these indices were verified against the observed NINO3.4 SST index obtained using Hurrell et al. (2008)'s SST data and the observed SAM index, using the ERA interim MSLP data (Dee et al. 2011). The rainfall forecasts were verified against the observed data of the Australian Water Availability Project analyses (Jones et al. 2009).

Fig. 5.27 displays the standardised amplitudes of the NINO3.4 SST, Southern Oscillation Index (SOI), SAM and eastern Australia areal mean rainfall in 2010 September, October and November. The observed amplitudes are shown with yellow bars and the control POAMA forecasts are shown with blue bars. The yellow bars confirm the strong La Niña of 2010 spring by displaying largely negative NINO3.4 SST and largely positive SOI in all three months. SAM was weakly positive in 2010 September (Fig. 5.27a) but it became much stronger in October and November (Fig. 5.27b,c). Eastern Australia received extreme amount of rainfall in September 2010, reaching 4 standard deviations. Rainfall was less intense in October and November but still exceeded 2 standard deviations. POAMA forecasts demonstrate high skill in predicting the 2010 SON climate. Not only the strong La Niña and positive SOI were well predicted but also the strong positive SAM and extremely wet eastern Australia were skilfully predicted for the three months of the forecasts. However, POAMA somewhat over-predicted the amplitudes of the atmospheric indices in October and November 2010.

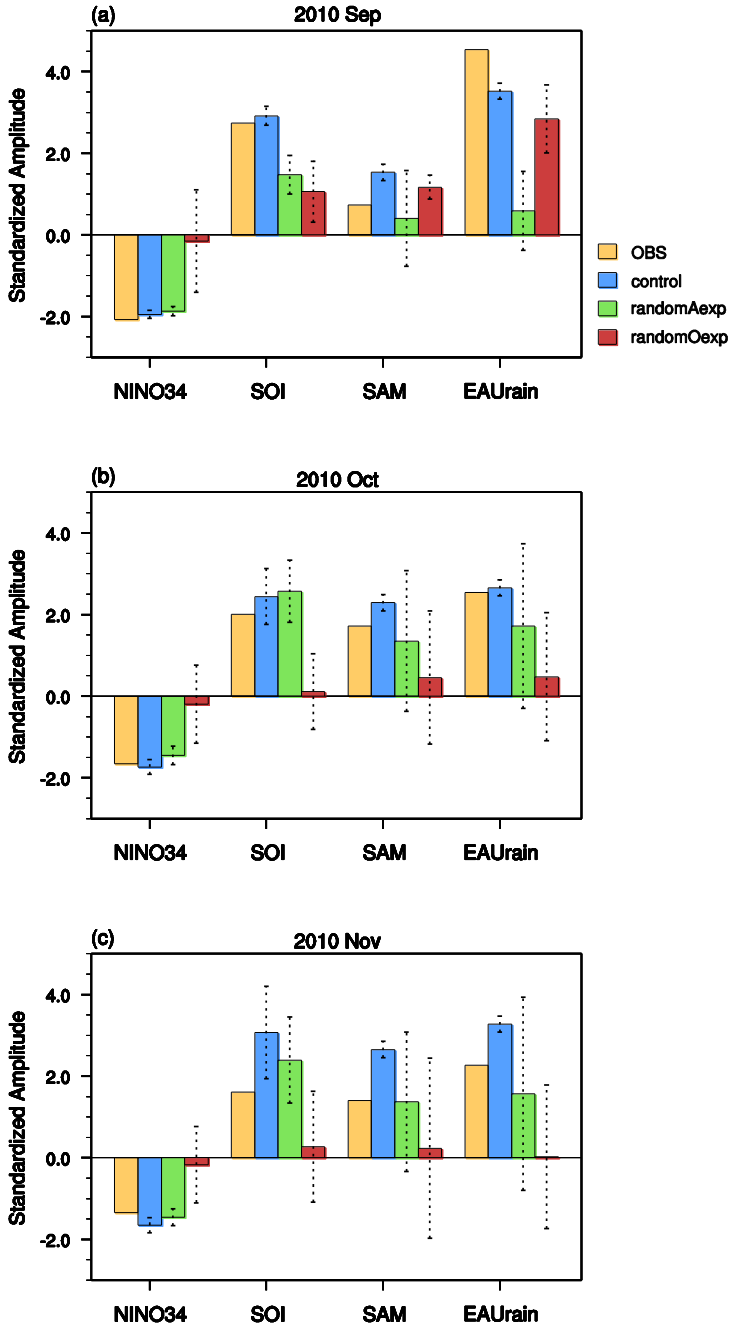

Fig. 5.27 Anomalous amplitudes of the Nino3.4 index, SOI, SAM and eastern Australia area-mean rainfall in 2010 in (a) September, (b) October and (c) November in the observations (i.e. ERA–Interim reanalysis; yellow) and the forecasts from the control run (POAMA2; blue), randomAexp (green) and randomOexp (red) at 0 lead time. The forecast anomalies were created and standardised, using the climatology and standard deviation of the ensemble mean forecasts of p24c over the base period 1980–2009. One standard deviation of ensemble spread is indicated with vertical dotted lines.

When forecasts were initialised with random atmospheric conditions but with the realistic ocean initial state of 1 September 2010 (randomAexp), the NINO3.4 SST was still skilfully predicted in all three months, but the atmospheric indices, especially eastern Australian rainfall, were significantly under-predicted in the first month of the forecasts (Fig. 5.27a). However, once the model atmosphere adjusted to the forecast La Niña SST, the forecast amplitudes of the positive SOI and SAM and eastern Australian rainfall became realistic in October and November (Fig. 5.27b,c). Therefore, it is understood that positive SAM could be predicted in October and November 2010 given the ocean initial conditions on 1 September. The third set of forecasts (randomOexp) confirms the association of the positive SAM and the La Niña in late spring 2010. In randomOexp, the SAM and eastern Australian rainfall forecasts were not significantly affected by random ocean initial conditions in the first month of the forecasts, indicating that their first month forecasts were dominated by the atmospheric processes. But the SOI was predicted to be much weaker in this experiment as the SST was not the La Niña state. However, in October and November after the model atmosphere has had

time to fully adjust to SSTs that do not have a La Niña signal, (as indicated by near zero amplitudes of NINO3.4 index), randomOexp failed to predict the strong positive SAM and high rainfall over eastern Australia. Therefore, both randomAexp and randomOexp suggest that La Niña was the necessary condition for the positive SAM and excessive eastern Australian rainfall in October and November of 2010. Finally, forecasts of the positive SAM in POAMA control in October and November is predicted to be significantly larger than from randomAexp, which implies a long lasting impact of the realistic atmospheric initial conditions on the prediction of the SAM.

Forecasts that predict the high SAM and the wet condition over Australia in 2010 spring can also give us some insight on whether the strongly positive SAM would have brought additional rainfall to eastern Australia beyond what the La Niña promoted, thereby contributing to the extremity of the wet conditions. To address this question, we have examined the scatter of the predicted eastern Australian rainfall against the predicted SAM for SON 2010. We look at the scatter of the 30 member ensemble forecasts from the POAMA control (Fig. 3.9b) and randomAexp (Fig. 3.9d). We also plot the scatter of predicted rainfall versus predicted SOI (Figures 3.9a,c) in order to understand the relative contribution of the variation of the predicted SOI and SAM for driving the variation of predicted rainfall over eastern Australia. For both the POAMA control and the randomAexp, there is a positive relationship between rainfall amount and strength of the SAM in the 30 forecasts.

The same is true for rainfall–SOI, but the spread is larger for the SOI (~10 per cent explained variance) than for the SAM (~20 per cent explained variance). These results confirm the important role of the SAM for driving eastern Australian spring rainfall variability (e.g. Hendon et al. 2007 and Min et al. 2013) and support the contention that the extraordinarily strong high SAM played a key role for the extraordinary wet conditions in 2010 spring. However, the large spread of the SAM seen in Fig. 3.9d (i.e. large atmospheric internal variability) emphasises the limiting role for predictability of rainfall, even though high SAM tends to be promoted by La Niña (e.g. Lim et al. 2013).

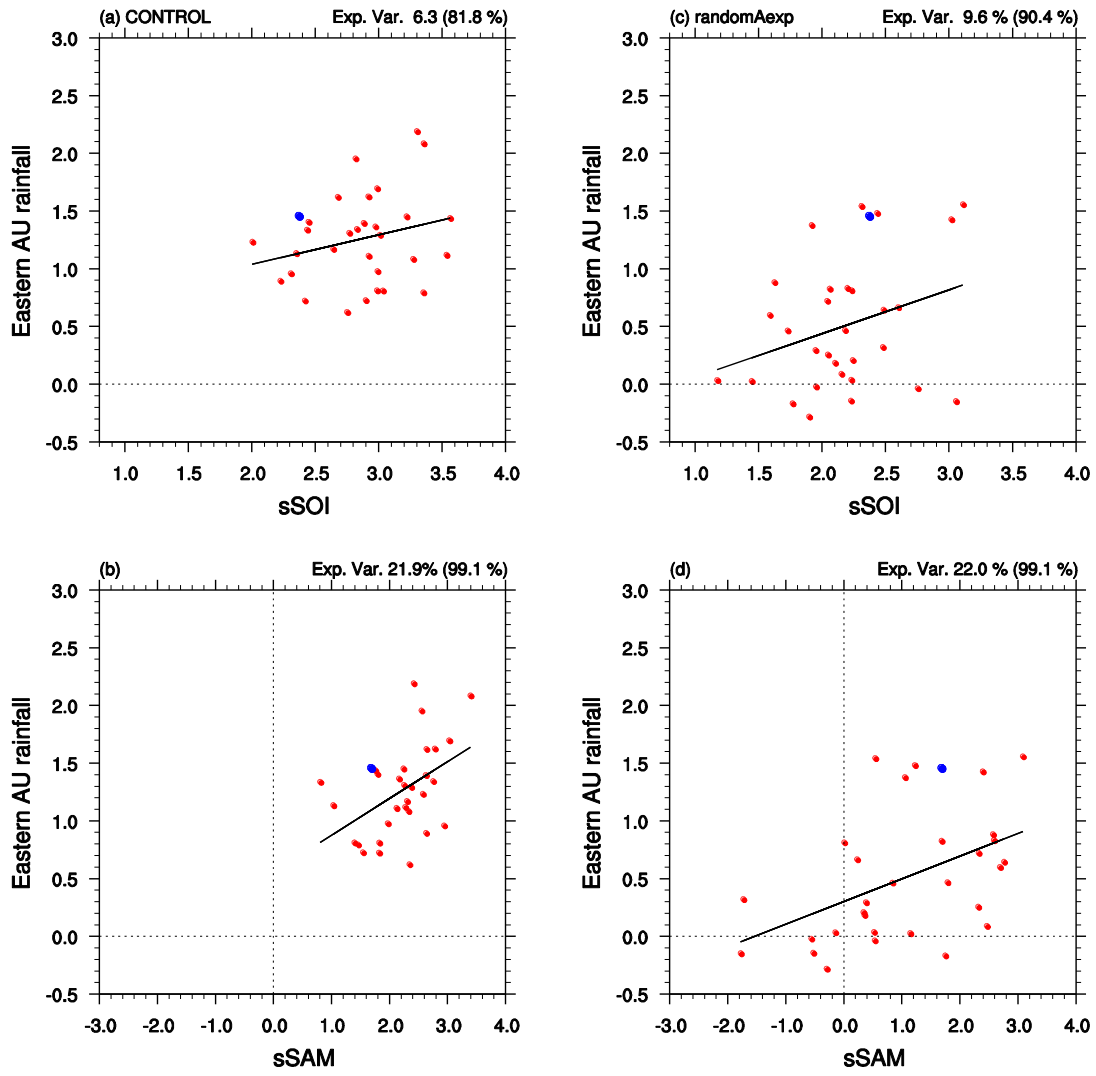

Fig. 5.28 Scatter plots of forecasts of eastern Australian area-averaged rainfall in 2010 SON as a function of the predicted magnitudes of standardised (top) SOI and (bottom) SAM index in the control forecasts (left panels) and randomAexp (right panels).
The observed values are indicated with the blue dots and forecasts are indicated with the red dots.

To summarise, seasonal forecasts from the POAMA system are shown to have been skilful in predicting the wet condition over eastern Australia as a result of a good prediction of the response to La Niña and the strong positive excursion of the SAM. Good forecasts were provided up to two seasons in advance. Forecast sensitivity experiments demonstrate that:

i) the strong positive phase of the SAM was an important factor for the extremity of the 2010 spring rainfall;

ii) the strong La Niña was the necessary condition for promoting the positive phase of SAM and the anomalous wet conditions over eastern Australia during October to November 2010; but

iii) internal atmospheric processes were important for producing the moderate strength of the positive SAM in September 2010 and for the amplification of the positive SAM forced by La Niña in October to November 2010.

Conclusions and future perspectives

Activity 1 has developed new software to diagnose the Isentropic Stream Function, which will be a potent tool to diagnose extratropical–tropical interactions as highlighted in Activity 2 and 3. The software appears to function largely as anticipated, showing the expected response to ENSO (contracting/expanding and strengthening/weakening of the December–January Hadley cell during El Niño/La Niña years, respectively) and connections between the Hadley cell and the extratropical cell. The connections are present in the seasonal composites, although they do not appear as consistently in monthly data. Ferrel Cell equivalents are also more prominent than expected based on our understanding of the literature. The code has been thoroughly reviewed, and no obvious errors identified, so the differences may be the result of particular approach taken here; several possible paths could have been taken to arrive at the final solution. In the second year of the project, the ISF code will be used to explore tropical–extratropical interactions of relevance to SEA, including diagnosing the seasonality of the SAM – Hadley cell interaction and the promotion of the SAM by ENSO and greenhouse gas warming/ozone depletion.

In Activity 2 the link between the Southern Annular Mode (SAM) and subtropical rainfall via atmospheric circulation was analysed. It was found that high SAM in spring and summer acts to increase rainfall in the subtropics by effectively causing the wet-tropics to the north to move south and therefore bring above normal rainfall to Victoria. However, in winter high SAM does not influence subtropical rainfall and so the poleward shift of mid-latitude storm track associated with high SAM results in a southward expansion of the subtropical dry zone and hence drier than normal conditions in Victoria. These findings shed light on why the rainfall response over Victoria to high SAM is opposite in winter versus summer. Experiments were also conducted with the POAMA seasonal prediction model to investigate the role of ENSO and SAM for the high south eastern Australia rainfall during spring 2010. It was found that the strong positive SAM phase was important factor in the high rainfall, and also that the strong La Niña conditions promoted the high SAM.

The outcomes of Activity 2 have important implications for predicting current and future climate. The strong influence of the SAM on south eastern Australian rainfall means that limited predictability of the SAM on a seasonal timescale (e.g. Lim et al. 2013) places a strong constraint on predictability of rainfall even during highly predictable La Niña. Based on the past 50 year record, high SAM during summer has been promoted by ozone depletion (e.g. Arblaster and Meehl 2006; Gillet et al. 2013). Hence, a primary impact of the recent upward trend in the SAM has been an upward trend in summertime subtropical precipitation (Kang et al. 2011), which can be viewed as a poleward shift of the subtropical dry zone and a poleward shift of the tropical wet zone. On the other hand, there is no statistically significant trend in SAM in winter, and therefore any current winter rainfall trend over Victoria is unlikely to be a result of secular changes of the SAM.

From a climate change perspective, a robust finding of projected future climate in response to increased greenhouse gases is a promotion of high SAM in all seasons (e.g. Yin 2005; Gillet et al. 2013). The emergence of this upward trend of the SAM in winter in the future climate would then result in an expanded subtropical dry zone in winter and so a drier Victoria in winter (e.g. Scheff and Frierson 2012). The emergence of high SAM thus would mean a further contribution to any ongoing drying trend for south eastern Australia, such as that resulting from a local poleward expansion of the subtropics and associated intensification of the subtropical ridge. By contrast, the upward trend of the SAM in summer would result in a poleward shift of subtropical dry zone away from Victoria with a poleward shift of the wet-tropics into Victoria and so we can expect increased warm season (spring–summer–autumn) rainfall in the future climate.

Following on these implications, we will continue to investigate the linkage between the SAM and Australian climate in the present and future climate by assessing the CMIP5 models for their capability to simulate the seasonality of the response of the SAM to ENSO (strong in summer and

weak in winter). We will focus on the capability to maintain separate eddy driven and subtropical jets in winter but a single jet in summer, because if separate jets are not maintained in winter, then any apparent sensitivity of rainfall to secular changes in the SAM will be erroneous. Such analysis will provide insight into the confidence of future climate projections for south eastern Australia, which strongly depend on the future behaviour of the SAM.

Finally, the results of Activity 2 bear on the results from Project 1 Activity 2, which investigated the role of the recent trend in SST for contributing to the extreme rainfall during the 2010 La Niña event. The SST trend appears to have positively contributed to the driving the positive SAM and associated springtime rainfall over eastern Australia. The SST trend appears to have promoted high SAM by driving changes in tropical temperatures and therefore SH extratropical circulation. Interestingly, these SST-trend forced temperature and circulation changes resemble those for future climate projections with increasing greenhouse gases (e.g. Chen et al. 2008) and so could be magnifying impacts from ongoing GHG forcing. The results in Projects 1 and 3 thus help to paint a more complete picture of what happened in spring 2010 in regard to tropical SSTs–SAM–Australian rainfall: the extreme rainfall resulted from the strong La Niña operating on top of the long-term trend of tropical SSTs which promoted high SAM.

Project 4: Exploration of the causes of tropical expansion

Lucas, C., Nguyen, H. and Timbal, B.

CAWCR, Bureau of Meteorology

Key findings

Both observational and modelling studies support the idea that the cause of tropical expansion in the southern hemisphere has a significant anthropogenic component—the result of increasing greenhouse gases and the springtime Antarctic ozone hole. This expansion is directly related to changes in the subtropical ridge that, for instance, can lead to changing weather patterns over southern Australia.

In the southern hemisphere, statistically significant tropical expansion and associated changes to the subtropical ridge are detectable from the late 1960s.

However, tropical expansion is complex phenomenon that displays considerable regional variability, driven to some degree by natural modes of variability like the El Niño – Southern Oscillation (ENSO) and the Southern Annular Mode (SAM).

Climate models appear to underestimate observed tropical expansion, and do not appear to capture the changes associated with natural modes of variability. These modes of variability may themselves be altering due to climate change.

To understand the impacts that tropical expansion may have in areas like Victoria, these regional factors will need to be fully considered.

Background

The philosophical approach here is ‘knowledge of the past is the key to understanding the future’. As such, the purpose of this project is to document the history of past tropical expansion and to understand the physical causes behind changes to the mean meridional circulation (MMC). What factors lie behind changes to the MMC? Are they globally uniform as suggested in some hypotheses, or do they vary regionally? How do larger changes to the MMC affect the known weather drivers, such as the subtropical ridge, on both regional and global scales? Answers to these questions will help provide a solid physical basis for understanding the present and future impacts of tropical expansion.

The work in Project 4 is based on both observational studies and on simulations using state-of-the-art climate models. The aim of these studies is to tease out the natural factors that influence the edge of the tropics, such as the El Niño – Southern Oscillation (ENSO), as well understanding of the anthropogenic forcings that are important. In the southern hemisphere, these are believed to be the increase in greenhouse gases and stratospheric ozone depletion.

Objectives

1. Documentation of the regional characteristics of tropical expansion around the globe.

   This activity is based on the application of the methodology developed in SEACI-2 for characterising tropical expansion using radiosonde data (Lucas et al. 2012) to the northern hemisphere (NH). Similar to the approach for the southern hemisphere (SH), this is done over three broad regions. The current results are combined with those from the SH to estimate the regional and global variability and trends in tropical expansion between the hemispheres. This is important to document as it expected that the different external forcings should not have the same signature in both hemispheres. This aims to improve understanding of the relative roles of the various processes that influence the edge of the tropics on regional and global scales in both hemispheres.

2. Attribute the relative roles of individual climate forcings in the observed tropical expansion in the southern hemisphere (SH).

   A two-pronged approach is to be used: i) a regression analysis relating hypothesised climate drivers, such as greenhouse gases, stratospheric ozone and aerosols, and observed tropical expansion and ii) a verification of the observations based results using 'single forcing' GCM experiments with the CCSM4 global climate model (ongoing collaboration with CAWCR colleagues who have close links with the CCSM4 modelling group).
   This is an extensive analysis difficult to apply across many models and hence the focus has been put on a single model from which an extensive dataset is available: three member ensembles with either greenhouses gases or stratospheric ozone or aerosols or natural forcings alone as well as from a three-member ensemble with all forcings combined (15 simulations in total). It will be possible in subsequent years to extend that work, if warranted, to other models, in particular the ACCESS model, although the data are not available at this stage.
   The outcome will be a quantification of the relative roles of the factors that are hypothesised to drive tropical expansion. This knowledge will help refine projections for future impacts of tropical expansion that are relevant to Victorian climate.

3. Analyse Hadley circulation changes in a large set of simulations of current climate with anthropogenic and natural external forcings with as many as possible model simulations from the CMIP5 dataset.

   Apply the stream function approach to compute the zonal mean hemispheric Hadley circulation (HC) intensity and extend this analysis across a large number of state-of-the-art models to complement the SEACI2 findings which were based on only two models (CCSM3 from the CMIP3 dataset and the CSIRO-Mk3.6 from the CMIP5 dataset) for which model results were inconclusive and appear problematic.
   The analysis of a larger number of models will provide a more robust perspective on the degree to which changes in the large-scale hemispheric HC can be attributed to anthropogenic forcings.

Activity 1: Regional tropical expansion

Regional characteristics of tropical expansion

A robust expansion of the tropics has been observed in both the northern and southern hemispheres, as summarised in the recent review of Lucas et al (2014) (see also Project 2). Many of the studies undertaken to date have focused on the zonal average view. The specific impacts of this expansion remain unclear, beyond the broad indication that tropical expansion is expected to lead to a shift of the subtropical dry zone and increasing the frequency of drought on the poleward edges of the subtropics.

Comparison of the rates of expansion between the NH and the SH can lead to insight into the mechanisms of expansion. In the SH, stratospheric ozone depletion is believed to play a role in the expansion, in addition to anthropogenic greenhouse gas forcing present globally. With an additional forcing in the SH, a greater rate of expansion would be expected there. This is observed in some studies, but not in others.

A further complication is the impact of natural teleconnections that may impact the interpretation of the trends. For example, Grassi et al. (2012) and Allen et al. (2014) have recently suggested that the NH expansion may be driven in part by the Pacific Decadal Oscillation (PDO), and in particular its interaction with anthropogenic aerosols. The PDO is a mode of natural climate variability that operates on decadal time scales. It is related to the Interdecadal Pacific Oscillation (IPO, see Project 1) but the PDO is focused in the north Pacific region. Variations in the PDO and IPO are highly correlated on interannual timescales and hence relationships with one will generally apply to the other.

Recent studies indicate that there are regional variations in tropical expansion. For example, Choi et al. (2014) showed longitudinal variation in SH expansion rates using the subtropical ridge as a metric.

The aim of this project is to investigate the characteristics of tropical expansion over broad regions of the globe, both the northern and southern hemispheres and within subregions of each hemisphere. How does tropical expansion vary across hemispheres and regionally? What natural teleconnection factors influence the position of the tropical edge in different places?

This study uses the methodology of Lucas et al (2012) to produce estimates of radiosonde-based tropical expansion over the NH based on the number of tropical troposphere days (TTD), an annual count of days where the tropopause height exceeds 14.5 km. This technique has the advantage of being purely defined from observational sources, so is presumably free from some of the artificial discontinuities that may be introduced within model/observation hybrid reanalysis datasets. The results of this study are combined with those from Lucas et al (2012) for the SH to produce the inter-hemispheric comparison, as well as providing the basis for the regional picture of tropical expansion. The role of teleconnections is investigated using partial correlation/regression methodologies, relating the global and regional contour positions to seven common teleconnection patterns. This is done on both an annual and seasonal basis. The period 1979–2010 (2011 in NH) is considered here.

Inter-hemispheric comparison

Fig. 5.29 shows times series of the hemispheric-average TTD latitudes for the NH and SH. Four time series are shown, with TTD = 300, 200, 100 and 50 days. Here, the region between the 300-day and 50-day contours is defined as the subtropics, a transition zone between the tropical- and extratropical-dominated circulations. The 200-days contour is loosely coincident with the edge of the Hadley Cell as defined from mass stream function calculations (e.g. Nguyen et al. 2013), and in the SH represents the most reliable estimate due to data considerations (see Lucas et al. 2012). For reference, the 300 and 200 day contours are collectively called the tropical (TR) contours, while the 100 and 50-day contours are the extratropical (ET) contours.

Fig. 5.29 shows that in the mean, the subtropics are more meridionally extensive in the NH as evidenced by the ET contours being displaced more poleward in the NH. One possible explanation for this is the distribution of land in the regions. In the SH, little land is found poleward of 40° latitude (excepting Antarctica, which isn't included in this study), while the continents extend poleward of 60° in the NH. The greater extent of land has also been shown to play an important role in the differences of the HC between hemispheres (Cook 2003).

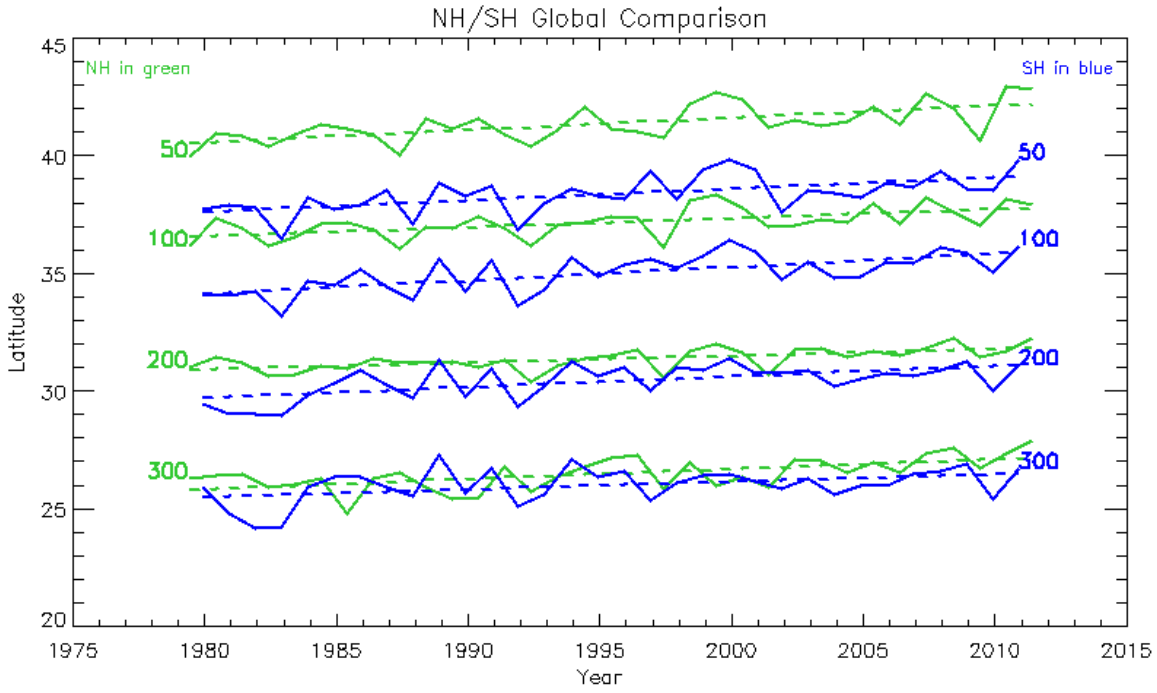

Fig. 5.29 Hemispheric-average TTD contours for the NH (green) and SH (blue)

Table 5.2 compares values of the trends for each of the hemispheric-average contours in the NH and SH. Trend lines are shown in Fig. 5.29. In both hemispheres, statistically significant expansionary trends are identified on all TTD contours. In all cases these trends are less than 0.6 degrees per decade. Some caution must be taken for the trend values on the SH ET contours in particular, due to issues with the sparseness and quality of the data in South America and Africa regions. See Lucas et al. (2012) for more detail. For the 200- and 100-day contours, again roughly coinciding with the traditionally-defined edge of the tropics, SH trend values are notably larger. However, following the procedure of Lanzante (2005), these differences are not statistically different, being approximately one standard deviation apart. While not significant, the larger SH trends on these key contours support the idea of stratospheric ozone depletion playing a role SH tropical expansion.

Contour	NH	SH
300	0.42 ± 0.20	–0.32 ± 0.29
200	0.29 ± 0.15	–0.45 ± 0.23
100	0.38 ± 0.20	–0.57 ± 0.26
50	0.52 ± 0.22	–0.49 ± 0.28

Table 5.2 Trend values and 2-σ confidence intervals for the hemispheric-average TTD contours. Note that expansion trends are negative in the SH.

Regional differences in expansion

Fig. 5.30 indicates the six regions considered for regional differences in tropical expansion using the data and techniques noted in Lucas et al. (2012). These regions are defined by the availability of radiosonde data and focus largely on land areas. For the NH, the regions are North America (NA), Europe and North Africa (EUR) and Asia (ASIA). The dividing line between EUR and ASIA is 60°W and is chosen to ensure sufficient data is available over EUR. In the SH, the regions are Australia – New Zealand (ANZ), Africa (AFR) and South America (SA).

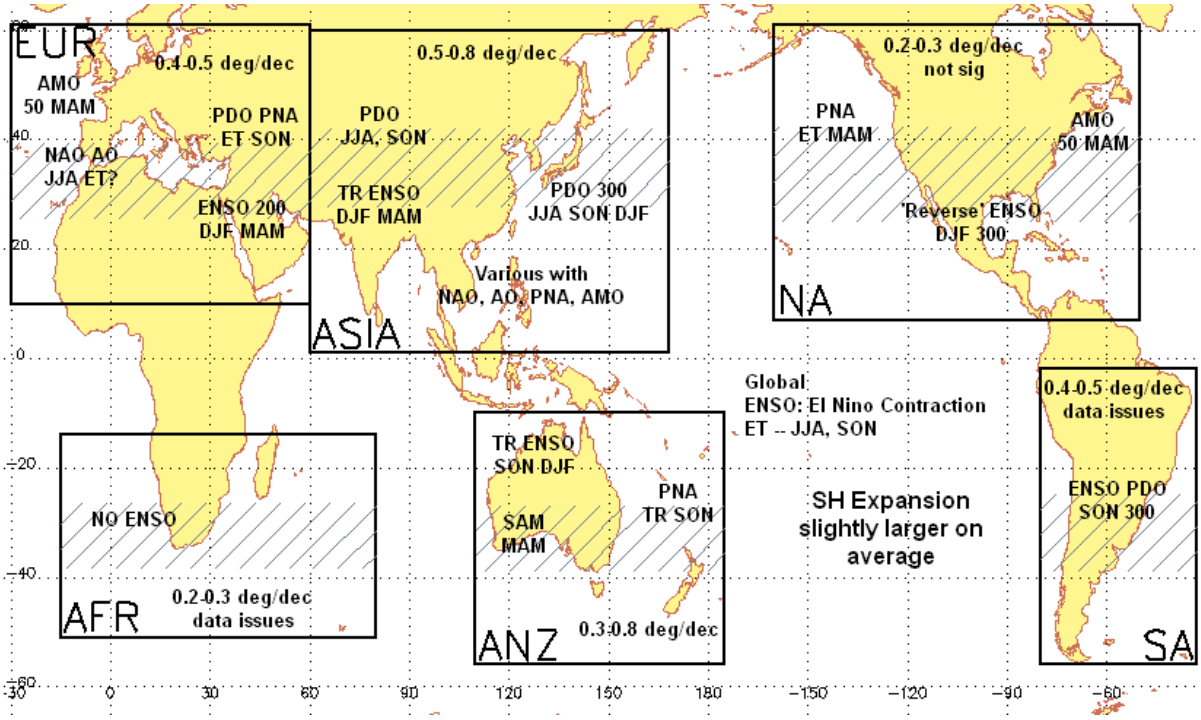

Fig. 5.30 Summary of regional and hemispheric characteristics of tropical expansion.
The hatching indicates the mean position of the subtropics identified in each region. Ranges for tropical expansion rates are summarised for each region. Also noted are significant relationships with various teleconnection patterns, the contours on which they identified by their value, ET (100 and 50 contours), TR (300 and 200 contours) and the seasons in which a correlation occurs.

In the SH, the identified subtropics (hatched areas on Fig. 5.30) are relatively uniform over the regions examined. The largest expansion rates are found over the ANZ region (0.3–0.8 degrees per decade), while AFR has the lowest rates (0.2–0.3 degrees per decade). SA shows trends of 0.4–0.5 degrees per decade. Both AFR and SA have data issues that make the trend values on the ET contours, in particular, unreliable, although the interannual variability appears to be unaffected.

Considerably more variability is noted in the NH. Over EUR, the extent of the subtropics is similar to that in the SH. In ASIA, the entire subtropics are shifted relatively poleward. The subtropics are most extensive in NA; the TR contours lie comparatively equatorward, while the ET contours are positioned similarly to those in ASIA.

Expansion rates are also more variable in the NH. The expansion is strongest over ASIA, ranging from 0.5–0.8 degrees per decade. Over EUR, expansion rates are 0.4–0.5 degrees per decade. Observed rates of expansion are lowest over NA; an expansion of 0.2–0.3 degrees per decade is noted, but the trends are not statistically significant. On the 300-day contour in particular for this region (not shown), there is a considerable variability with strong equatorward ‘dips’ of 2–3° latitude lasting for 1–3 years.

Teleconnections

To explore the effects of natural factors that may influence tropical expansion, seven teleconnection patterns are considered. ENSO (Wolter and Timlin 1998) and the PDO (Mantua and Hare 2002) were noted earlier. Also examined are the Pacific North America pattern (PNA; Leathers et al 1991), the Southern Annular Mode (SAM, Marshall 2003), the North Atlantic Oscillation (NAO; Hurrell 2009) and the Arctic Oscillation (aka Northern Annular Mode; Thompson and Wallace 1998). The multi-decadal Atlantic Meridional Oscillation (AMO; Enfield et al. 2001) is also examined.

The relationship of these modes of variability to tropical expansion is explored using partial correlation and partial regression analyses, relating the positions of regional contours to time series of indices reflecting the state of these modes of variability. All contours/indices are detrended before performing the calculation to isolate only the interannual variability. Several approaches are taken. First, annual time series of the indices are related to the hemispheric-average contours, yielding a global view that is comparable to earlier studies. Secondly, annual contours in each individual region are related to the annually averaged indices, providing a view as to what factors are important on a regional basis. Finally, seasonally averaged indices are related the annual contour positions, identifying the particular season when a mode of variability influences the annual number of TTDs. The results are graphically reported in Fig. 5.30 and summarised below.

Globally, ENSO is the most significant teleconnection that has an impact on the TTD contours. In all regions except AFR, ENSO affects the ET contours particularly during JJA and SON, resulting in an expansion during La Niña and contraction during El Niño (Oort and Yienger 1996). Between the two extreme phases, the contours may change by 2–3° latitude. Over ASIA and ANZ in particular, ENSO also impacts the TR contours, centred on DJF. This is about half of the magnitude of the ET effect. ENSO also impacts the 300-day contour over NA, but has a ‘reverse’ effect in that the contour expands during El Niño. This is linked to the ‘dips’ in this contour noted earlier.

The PDO shows significant correlations primarily in the NH. This effect is most prevalent over ASIA, occurring in all seasons except MAM and on most contours. A correlation is also noted in EUR during SON; no significant relationships are noted in NA. When the Central Pacific is warm (i.e. a negative PDO), the tropics in this region are further poleward. There is also a significant effect of PDO observed in SA, and at the 90 per cent level in ANZ. Here, the effects are on the 300-day contour and they are opposite to the effects in the NH; the contour is further equatorward during a negative PDO. This suggests that the PDO shifts the entire tropical zone by ~1° towards the North Pole in its negative phase.

The SAM has a highly significant impact on tropical expansion over the ANZ region during MAM. A positive SAM during this season results in greater expansion across all contours. The size of the effect is up to 0.5 degrees per index unit. Project 3 discussed the impact of SAM on the SH subtropical circulation and precipitation. More investigation is required to link the SAM–subtropical circulation to the TTD variability measured in this project. There are also hints of an effect in the NH, with the 300-day contour in EUR showing significance during DJF. Also during DJF, the NA 300-day contour and the annual NH hemispheric-average TR contours show correlation at the lower 90 per cent level. The regressions suggest a small expansion during positive SAM.

The PNA primarily affects the NA ET contours during MAM. The correlation is positive, so expansion over NA is expected during the positive phase, which coincides with greater geopotential height anomalies over the USA/Canada border regions. A positive correlation is also found with ANZ TR contours during SON, indicating a contraction of those contours. The PNA pattern has been shown to be linked to the tropical circulation through the phase of the MJO (e.g. Moore et al. 2010)

The remaining teleconnection patterns only show weak or inconsistent relationships with the TTD contours. During MAM, the AMO has significant correlations with the 50-day contour in EUR and NA. Significant relationships are also noted with the ASIA 100-day contour during SON and the

annual NH hemispheric-average. The regression coefficients are large here, typically on the order of 1.5–3.0 degrees per unit. However, the AMO index is typically considerably smaller than 1 and changes very slowly.

Most confusing are the results with the NAO and AO time series. These two time series are highly correlated (~0.8 at annual time scales). When significant correlations are found, this pair of variables generally offset one another, acting in nearly equal and opposite senses. It is suspected that this is an artefact of the partial correlation technique applied here and the results are not real. The most physically plausible correlation identified occurs over EUR on the ET contours during JJA. More research is required to understand any linkage of these variables and tropical expansion.

Activity 2: Single forcing attribution

What drives southern hemisphere tropical expansion?

Since 1979, an expansion of tropics has been observed using multiple methods and observational platforms. A synthesis across the observations suggests that the expansion rate is on the order of 0.5 degrees per decade in each hemisphere. Anthropogenic climate forcings have been proposed as drivers of the expansion. These include:

1) greenhouse gases;

2) stratospheric ozone depletion; and

3) direct and indirect aerosol effects.

Natural factors, like volcanic eruptions and ENSO, also affect variability of the position of the tropical edge on shorter time scales (Lucas et al. 2014).

Here, the relative contribution of these forcing factors to the tropical expansion in the SH is investigated. Two approaches are used:

1) the statistical analysis of observations of tropical expansion; and

2) 'single forcing' experiments with a state-of-the-art coupled general circulation model.

A particular interest (at this stage) is the partition between ozone and greenhouse gas forcings.

Statistical analysis of observations

Observations of the tropical edge in the SH are derived from radiosonde observations over three broad regions using the tropopause height frequency methodology (Lucas et al 2012) (see also Project 2). Here, the tropical edge is taken as the annual position of the 200 tropical tropopause days (TTD) per year contour. Results from the three individual SH regions are averaged to produce a global composite. The observed trend in the global composite is about 0.45 degrees latitude per decade, a trend that is significant at the 95 per cent level.

These results are related to observable proxy variables representative of the forcing factors. These variables are:

- Multivariate ENSO Index (Wolter and Timlin 1998);
- NASA Ozone Hole Area (proxy for ozone (O_3) forcing);

- global or SH temperature anomaly (GISS, proxy for GHG and aerosol, Hansen et al. 2010); and
- stratospheric aerosol optical depth (proxy for volcanoes, Sato et al. 1993).

These proxy variables are used as multiple linear regression predictors of TTD-based tropical edge. As the proxies are cross-correlated, linear effects are removed from them in the following order:

1) stratospheric aerosol;
2) MEI; then
3) temperature.

Ozone hole area and global temperature are the most highly correlated. After this removal process, the correlation between all variables is zero.

Two versions of regression are performed using either the global or SH temperature series. The regression (Fig. 5.31) captures 58.7 per cent of the variance for the global time series (59.4 per cent; for the SH) – the RMS error of the regressions is 0.4 degrees. The trend for both regressions is about 0.37 degrees per decade, close to the observed value.

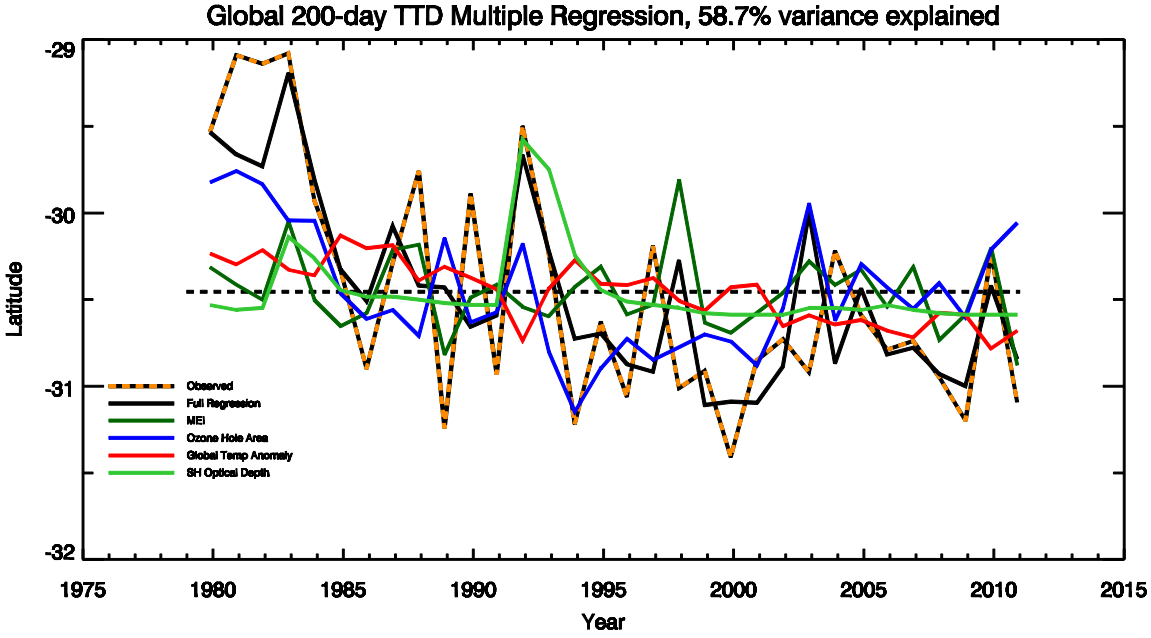

Fig. 5.31 Observed SH tropical edge time series and results of full regression and individual components. Refer to plot legend to distinguish lines.

Of this trend approximately 10 per cent is due to MEI and 20 per cent due to volcanoes (optical depth). This is simply a matter of the timing over which the trend is computed. Neither of these effects is expected to lead to a long term change. There are more La Niña events at end of record than early, producing an apparent expansion. Similarly, the significant volcanic eruptions occur earlier in the record (1982, 1991). These natural factors are not a forcing, but do impact the observed value of the trend, depending on the ultimately arbitrary choice of start date for the trend calculation.

The remaining 70 per cent of the trend is due to anthropogenic forcing: ozone depletion and rising temperatures (presumably due to greenhouse gas increase). The exact partition between the influence of these two variables is unclear in the statistical analysis, due to the strong correlation between the

two variables. We can use the two realizations of the regression to assign a range: 10–40 per cent of total trend is due to global temperature (i.e. GHG increase), while the remainder (60–30 per cent) is due to ozone depletion.

Single forcing simulations

To further investigate the attribution of SH tropical expansion, simulations with the Community Climate System Model 4 (CCSM4; Gent et al. 2011) using the CMIP5 historical scenarios are analysed between 1960 and 2005. Five sets of simulations are examined including four 'single forcing' scenarios where only one set of climate forcings is applied while the other variables are kept at pre-industrial levels. The five sets of simulations are: ALL (all forcings included), NAT (volcanoes and solar only), O3 (ozone only), GHG (greenhouse gas only) and AER (anthropogenic aerosol only). Three-member ensembles are used for each scenario, a total of 15 model runs.

The tropospheric height frequency methodology is adapted for use with the monthly model output. A parameterization of the number of monthly TTD based on the zonal mean tropopause height is derived from a single realization of the ALL run. This parameterization is then applied to all the model runs. Tests indicate that this adequately captures the expansion signal and the interannual variability present in the run with daily data. For this analysis, the 200-day TTD contour is used as with the observations. Fig. 5.32 shows the annual tropical edge positions for the five ensembles.

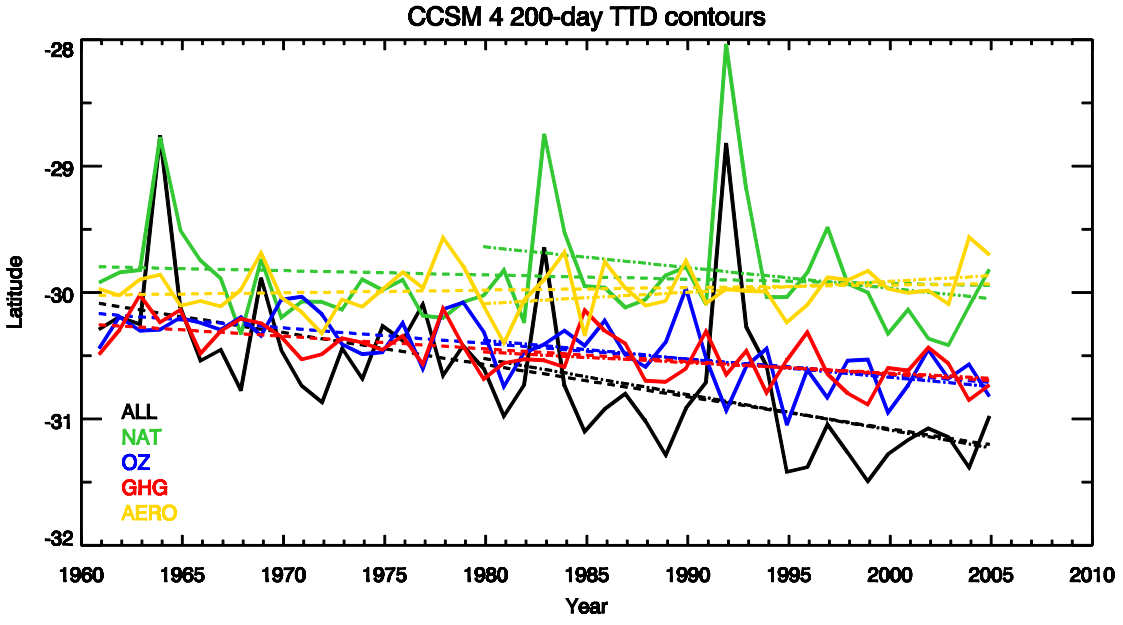

Fig. 5.32 Single-forcing ensemble averages of SH tropical edge position, as defined by the TTD=200 day contour. Individual ensembles are distinguished by line colour following the plot legend. Linear regression fits from 1960 and 1979 are shown as dashed and solid lines, respectively.

To perform the attribution, trends on the 200-day TTD contour are examined over the whole period (1960–2005) and from 1979. The first estimates the total expansion from the pre-ozone hole and over a longer period, providing a more robust estimate of the expansion. The second period is over approximately the same period as the observational record.

Table 5.3 shows the trends from the five ensembles. Trend lines are plotted on Fig. 5.32. The trend over the shorter period is slightly larger than the longer period; however, both are little more than half of the observed value. The trend in the longer period is statistically significant; while those in the shorter period are not. Trends from the individual single forcings approximately add up to that in the ALL experiments, indicating a quasi-linear response to the forcings (Table 5.3). From 1960, the results

show that O3 and GHG are the dominant forcings. NAT and AER show only small trends over this time frame. From 1979, the picture is quite different, with NAT producing the largest trend. This is largely due to the strong contraction associated with the El Chicon and Mt Pinatubo eruptions in 1982 and 1991, respectively. This contraction is considerably stronger than what is seen in the observed record. The only significant trend identified from 1979 is in the O3 experiments. A Southern Oscillation Index was derived from the model surface data; no relationship between tropical expansion and ENSO was identified.

Run	Trend (1960–2005)	Trend (1979–2005)
ALL	**–0.25 ± 0.14**	–0.28 ± 0.40
NAT	–0.03 ± 0.12	–0.16 ± 0.31
O3	**–0.12 ± 0.05**	**–0.15 ± 0.12**
GHG	**–0.10 ± 0.04**	–0.08 ± 0.11
AER	+0.02 ± 0.05	+0.09 ± 0.11

Table 5.3 Trends and 2-σ confidence intervals for each ensemble of models from 1960 and 1979.

Conclusions

The simulations do not fully capture the magnitude of the observed tropical expansion nor do they reproduce the known relationship between ENSO and the tropical edge. Clearly, the volcanic response of the models is too large. However, the simulations do appear to be generally encapsulating the fundamental physics of the situation as it is currently understood. The observations may also have shortcomings. Much of the strong correlation with ozone is due to the strong movement in the tropical edge during 1979–1985. The metric used here, based on observed radiosonde data, is the only one known to capture such a sharp change in the tropical edge; the same metric based on reanalysis data does not show this sharp change (see Lucas et al. 2012). Whether this is a problem with radiosonde data or the reanalysis products is unclear. It is also unclear as to why other metrics do not capture such a sharp change. More investigation is required to understand this, such as that undertaken in Project 2, Activity 1. Despite these shortcomings, the observational and modelling results broadly agree on the partition of forcing factors of SH tropical expansion.

Combining results from the two approaches, the best estimate is that *since 1979*, the partition of forcing factors for SH tropical expansion is 30 per cent resulting from natural factors (volcanoes and ENSO), 40 per cent resulting from stratospheric ozone depletion and 30 per cent resulting from increasing greenhouse gases, with an error range *roughly* estimated at ± 10 per cent. The strong role of natural factors is largely the result of the choice of staring point of the analysis. The longer analysis suggests that natural variability plays a smaller role. The role of aerosol remains unclear. The CCSM4 simulations suggest that aerosols are unimportant for SH tropical expansion, but this may be the result of the type of aerosols specified in the CCSM4 and requires further investigation to determine if this is a robust result. While our results suggest that O_3 has been dominant in the recent past, its role is expected to diminish as the ozone hole recovers; GHG is expected to be more dominant in the future. How exactly the tropical edge will evolve over the next 20–30 years is unclear. Will the SH tropical edge contract until greenhouse gas forcing ‘catches up’?

Activity 3: Tropical expansion and the subtropical ridge

Unprecedented expansion of the southern hemisphere Hadley cell

Qualitatively, studies using a range of metrics, methodologies and data sources point towards a consensus that the 'tropical edge' (however defined) has been moving poleward since (at least) the late 1970s (Lucas et al. 2014) (see also Project 2). However, the rate at which this expansion is

proceeding remains uncertain. Recent work with the Ψ methodology shows an average expansion of 0.55 degrees per decade in each hemisphere across eight widely used reanalysis products (Nguyen et al. 2013), although the range of estimates varies considerably. This variability in the expansion rate is due to differences in the reanalysis models, as well as the different factors influencing the general circulation in the northern and southern hemisphere. While multiple studies suggest the cause of HC expansion is largely anthropogenic in origin, none of the simulations fully reproduces the observed change.

Here, we use the 20th Century Reanalysis (20CR) and historical simulations from phase 5 of the Coupled Model Intercomparison Project (CMIP5), to show that anthropogenic global mean surface temperature increase is linked to the expansion of southern hemisphere (SH) Hadley Cell and intensification of the zonal mean subtropical ridge (STR) since the late 1960s.

Trends of the SH Hadley Cell and Subtropical Ridge

Fig. 5.33 shows time series of annual mean global surface temperature (GT), southern hemisphere Hadley cell edge (HCE) and intensity (HCI), and subtropical ridge position (STRP) and intensity (STRI) derived from the 20CR. The increase in global surface temperature (consistent with the observations) over the entire period of 1880–2008 here is in stark contrast with the other variables. Prior to the early 1950s, 20CR global temperature remains too cool and there is no coherent variation between the other variables. The year 1952 is where the number of station reports on monthly mean surface temperature showed a dramatic increase (Fan and Van den Dool 2008), which is likely to constrain the 20CR ensemble and improve the reanalysed temperature in the model. Applying the method used by Lund and Reeves (2002) to monthly time series of the HCE, a breakpoint is identified in July 1951. Based on this, we suggest that the period in the 20CR prior to the early 1950s in the SH is unreliable because of data issues and hence limit the study hereafter to 1952 onward.

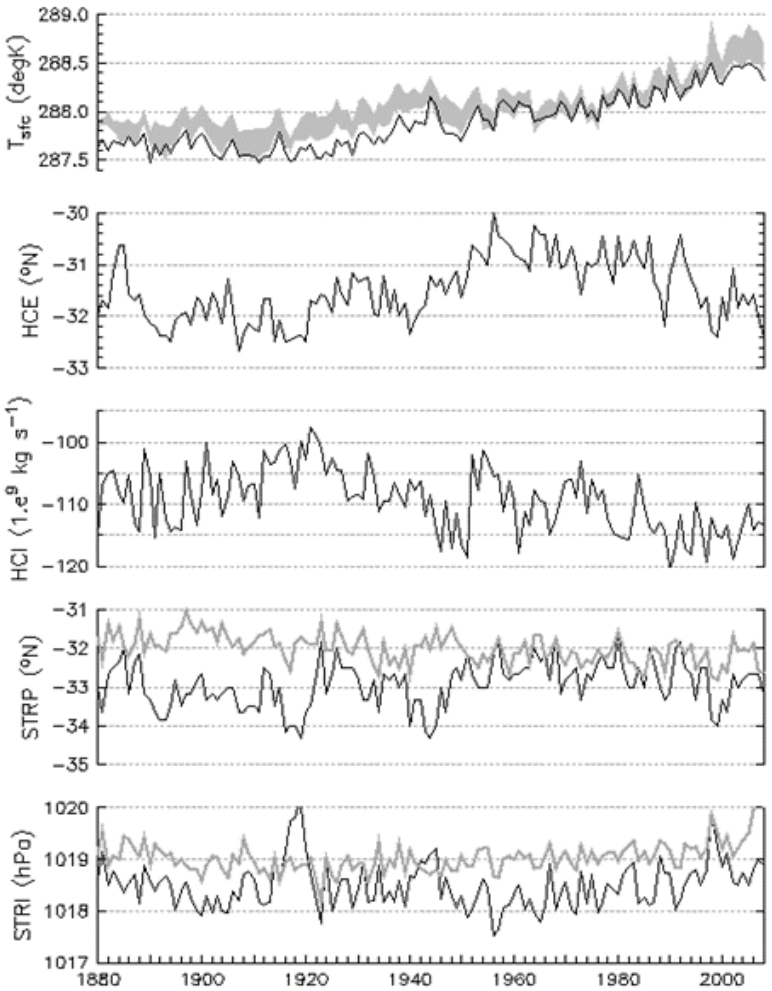

Fig. 5.33 Annual mean indices from 20CR.
From top to bottom: global surface temperature, southern hemisphere HCE, HCI, STRP and STRI. The grey curves are anomalies derived from observations.

To examine how unusual this trend is in the historical context, we compute linear trends of the annual mean standardised anomalies to allow a direct comparison of trend size across variables over a yearly-running window of 30 years in length. This is computed over the period 1950–2008 which represents 30 windows in total. Fig. 5.34 shows the resulting linear trends as a time series, where the indicated year corresponds to the first year of the window. The trends in 20CR global temperature are below those from observations in all windows from 1958. Despite the weaker values, the 20CR trends follow the observed tendency, increasing in amplitude with time and remaining statistically significant at the 95 per cent level throughout.

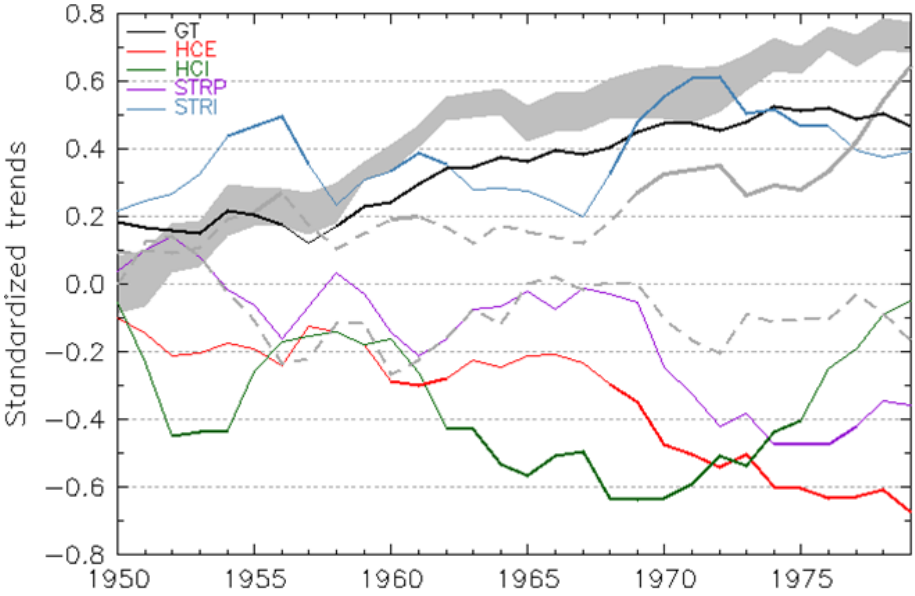

Fig. 5.34 Linear trends over a 30-year running window derived from 20CR and observations when available of: GT (black for 20CR and grey spread for observations), HCE (red), HCI (green), STRP (blue for 20CR and positive grey line for observation) and STRI (purple for 20CR and negative grey line for observation) computed from the standardised anomalies (sigma/decade). The year on the x-axis corresponds to the first year of the window. Values statistically significant at the 95 per cent level are bold. All values have been standardised to enable them to be compared.

Three other indices also exhibit trends that tend to increase with time; the HCE, STRP and to a lesser extent STRI. The HCE trend remains statistically significant from 1968 and reaches its maximum (standardised value of 0.7 per decade) in the last window (1979–2008). The STRP trend time series is concomitant with HCE trends, but reaches the statistical significance only between 1974 and 1977. Trends in the STRI increase from the late 1950s until the early 1970s, after which they begin to decrease. These trends are significant in windows from 1962 until 1975. There are many differences in the detail between the 20CR and observed STR metrics, perhaps related to the coarseness of the observed dataset (consistent with the 0.22 degrees per decade expansion inferred from observed STR by Choi et al. 2014).

To identify possible relationships between the above variables and global warming, linear fits of the trends against GT and HCE and the variance explained (r^2) are calculated (not shown). There is no strong relationship between GT increase and HCI intensification (r^2=0.14) or STRI intensification (r^2=0.24). In contrast, HCE and STRP are aligned in the same way with GT, explaining approximately two thirds of the total variance. This suggests that the HC expansion and the STR poleward shift are both strongly related to global warming. The relationship between HCE and STRP trends confirms their covariance, with r^2 =0.85. Further, linear fits of HCE and STRI trends show an r^2 =0.41. The physical processes driving these relationships remain unclear at this time. No relation is obtained between HCE and HCI, confirming the previous findings of Nguyen et al. (2013).

CMIP5 model assessment

Ten CMIP5 models with either anthropogenic GHG, natural or both external forcings applied were selected in order to provide an explicit attribution of the observed results. The same 30-year window running trend calculation is performed to assess the models' ability to replicate the trends and the strong linear relationships between global warming and HC expansion, and the implications for the STR.

Strong linear relationships between different HC indices are obtained in CMIP5 comparable to 20CR. The scatter plot between trends in GT and HCE (Fig. 5.35a) in CMIP5 confirms the clustering of the response according to the forcing applied, and a linear response of HCE to GT with r^2=0.6. Global warming associated with HC expansion seen in the anthropogenic GHG-induced simulations contrasts with the natural-induced simulations. However, the slope of the relationship differs from 20CR. For a comparable amount of global warming, HC expansion is weaker in CMIP5 by a factor of 4. This difference highlights the CMIP5 models' inability to correctly simulate the observed HC expansion in response to global warming.

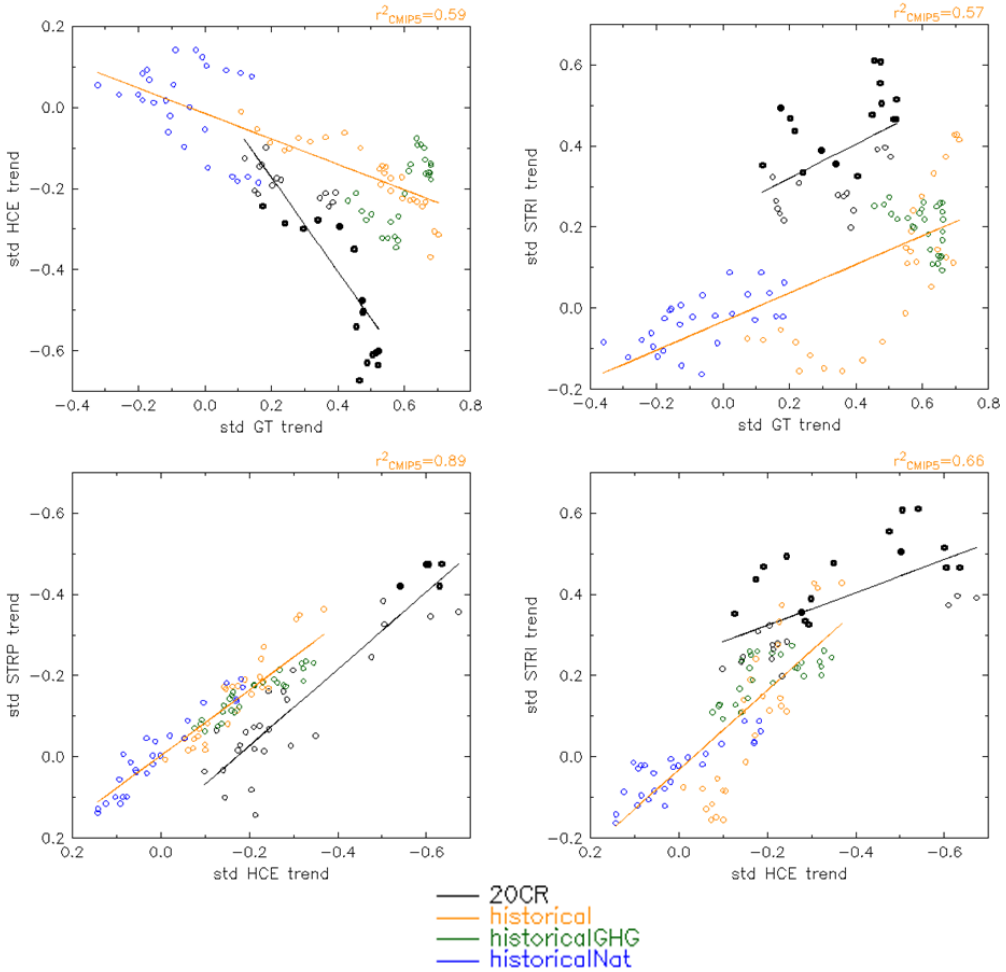

Fig. 5.35 Scatter plot between standardised trends of (top left) global surface temperature and HCE; (top right) global surface temperature and STRI, (bottom left) HCE and STRP and (bottom right) HCE and STRI together with their linear best fits from 20CR (black line) and the CMIP5 model average (orange line). Values statistically significant at the 95 per cent level are marked by a thick dot and the linear fit variance is indicated.

A strong relationship can also be inferred between GT and STRI (Fig. 5.35b). While the CMIP5 slope matches the one from 20CR, it is shifted, indicating that the models underestimate the amount of STR intensification in relation to global warming. There is a marked separation between the natural and anthropogenic GHG-induced clustering. The variance explained in the CMIP5 simulations (r^2 = 0.57)

is higher than for 20CR, but that high value is mostly driven by the forcing-based clustering rather than an increased sensitivity to global warming in the CMIP5 models. It is suspected that the difference in sampling of the GT parameter space—greater in the simulations—accounts for the lower amount of variance explained in the observations.

For the relationships internal to the mean meridional circulation (MMC), linear relationships are similar to those in the 20CR. For HCE and STRP (Fig. 5.35c), r^2 =0.89 and the slopes are nearly identical. A strong linear relationship is also obtained from the multi-model average scatter plot between HCE and STRI, explaining two thirds of the total variance (Fig. 5.35d). The results suggest that the CMIP5 models produce somewhat realistic changes in the properties of the STR in response to HC expansion.

Conclusions

This study confirms the 20CR data from 1952 to the present can be used to infer the southern hemisphere mean meridional circulation expansion since 1979 reported in the literature, and to further demonstrate that statistically significant trends are identifiable from 1968. This HC expansion is concomitant with increasing global warming and intensification of the zonal-mean STR. Examination of these trends in CMIP5 historical simulations using natural and GHG forcings confirms earlier findings that anthropogenic GHG forcing is required for HC expansion. The expansion appears to be underestimated in the models for a given amount of global warming, perhaps by a factor of four. However, the CMIP5 models appear to capture the internal characteristics of the MMC, correctly predicting trends in the STR characteristics in response to changes in the Hadley Cell edge.

Ultimately, these changes in STR will impact the rainfall in the sub-tropics; in particular, a rainfall decline is expected in association with STR intensification. If STRI change is underestimated due to the incorrect simulation of the Hadley Cell changes by the models, then the possibility exists that future projections of rainfall declines may also be underestimated.

Conclusions and future perspectives

The aim of the research undertaken as part of this project was to explore the factors driving tropical expansion. Understanding the causes behind the observed expansion in the past can provide a greater insight into the future evolution of the expansion and a better understanding of potential societal impacts.

This research shows that tropical expansion is a globally complex phenomenon, with many regional differences. The evidence presented here shows that the expansion appears to be greatest over the longitudes of the Indo-Pacific and Maritime Continent, encompassing Asia and Australia. Less expansion is seen over North America and Africa, although the lack of quality data over the latter region lowers the confidence of this assessment.

In the southern hemisphere, significant expansionary trends have been detected beginning in 1968. On the whole, tropical expansion appears to be slightly larger in the southern hemisphere, although the difference in expansion rates between hemispheres is not statistically significant. These findings are consistent with the hypothesis that, in the southern hemisphere over a long period, both the springtime Antarctic stratospheric ozone hole and the anthropogenic enhancement of greenhouse gases are the primary climate forcings behind tropical expansion. However, on shorter time scales, natural variability such as large volcanic eruptions and/or interaction with teleconnection patterns like ENSO significantly alter the observed expansion rate; these factors may explain up 30 per cent of the trend from 1979.

These attributions are based on state-of-the-art climate model simulations. Despite their overall usefulness, several shortcomings were identified in the prediction of the tropical expansion from historical simulations with these models. Foremost is the model's inability to simulate the observed

rates of expansion; as shown in the studies here, modelled expansion rates were 2–4 times lower than observed. Models also failed to adequately capture the effects of natural variability; the volcanic response of tropical expansion was too strong, while the well-known relationship between ENSO and the tropical edge was not detected. On the positive side, climate models did appear to reasonably reproduce the observed relationships between the Hadley cell edge and the subtropical ridge.

The inability of climate models to simulate teleconnection effects on tropical expansion may be related to the apparent underestimate of tropical expansion by climate models. In this project, multiple teleconnections are shown to influence the location of the tropical edge on interannual and decadal time scales. A well-known ENSO relationship has a nearly global reach, particularly on the extratropical edge of the subtropics. In North America, this ENSO effect acts contrary to the expected pattern. Decadal patterns such as the Pacific Decadal Oscillation and the Atlantic Meridional Oscillation also play a role, particularly in the northern hemisphere. The Southern Annular Mode was shown the strongly impact tropical expansion in the Australia New Zealand region during Austral Autumn.

If these teleconnection phenomena are subject to secular trends as a result of climate change, the effects will likely not be reflected in the future projections of tropical expansion. Some phenomena, for example the Southern Annular Mode, are known to be undergoing such trends; the current and future status of others is unclear. The global and regional effects of such phenomena need to be accounted for when evaluating tropical expansion in climate models as the effects are potentially significant. This could be particularly important for identifying regional trends that may significantly differ from the expected global tendencies.

This work is related to other projects within VicCI, Project 2 seeks to understand the differences between tropical expansion metrics and regional variations in the expansion. The results of this Project, highlighting teleconnection patterns and their regional influence, provide insight into the natural factors driving regional impacts of expansion. Extending the record of tropical expansion further back in time is also important for understanding differences in metrics and the factors behind tropical expansion. There are also links with Project 3 which examines the role of tropical–extratropical interactions. As the stratospheric ozone hole, a polar phenomenon, appears to be a driver of tropical expansion in the SH, there must be a link between the two regions. The teleconnection links with tropical expansion also shed light on these interactions. Future work with this project will focus on applying the knowledge gained to better identify likely impacts of specific regions such as Victoria and southeast Australia.

Project 5: Critical assessment of climate model projections from a rainfall perspective

Murphy, B. and Timbal, B.
CAWCR, Bureau of Meteorology

Grose, M., Bathols, J. and Kirono, D.
CAWCR, CSIRO

Key findings

State-of-the-art, nationwide climate change projections being delivered jointly by the CSIRO and the Bureau of Meteorology for the needs of Natural Resource management groups have been analysed to provide a summary of climate projections for the state of Victoria. Also, information in the IPCC Fifth Assessment report and recent research have been summarised for climate model performance and the projected future of the main drivers of Victorian climate.

The most robust and important projections for Victoria are: warming will continue and the amount of warming after 2050 will primarily depend on the rate of emissions; the hydrological cycle will change, the main drivers of climate variability will continue to exert a strong influence; a rainfall reduction during the cool season is likely due to a continued southward shift in the extratropical storm track; extreme hot temperatures will increase and be more frequent and heavy rainfall extremes will increase.

Simulations of the Australian Subtropical Ridge (STR) in 50 latest generation climate models were analysed. Many models were found to reproduce the broad character of the STR similar to observed, but some models simulate the STR too far to the west, and some simulate it as too wide. Some models also have a different relationship between the STR intensity and rainfall over Victoria compared to observations, with either too broad an extent of the region of negative rainfall – STR intensity relationship over Victoria, or too restricted a region. These biases present an issue in making regional climate projections for Victoria.

Future projections of the STR and rainfall under a high emissions scenario were analysed. Most models showed an intensification of the STR over recent decades, but not all showed the observed southerly trend. However, all models show the STR to intensify and move south over the century. This confirms that changes to atmospheric circulation are generally projected to lead to reduced rainfall in Victoria in the cooler seasons. Models with a poor simulation of the STR have a distinct rainfall projection for certain regions, suggesting it may be possible to reject some models and quantify a narrower and more reliable range of projected changed for the STR and rainfall.

Background

Climate projections from climate models are showing some consistent behaviour (e.g. dry to the south and wet to the north across SEA) and some inconsistent behaviour (the degree of future rainfall change). Some of this uncertainty is linked to the models' ability to represent important teleconnections (e.g. the impact of the SAM on the HC) and key modes of climate variability (e.g. the tropical influences of the Pacific vs. Indian oceans) identified through SEACI research as being important for SEA rainfall. In order to provide guidance as to which models to use for projecting future climate (with a particular focus on subsequent impacts on water availability), we need to assess individual models for the capability to simulate these key teleconnections and modes of climate variability.

Objectives

1. Compile CMIP5 model projections for key modes of variability relevant to Victoria's climate.

2. Evaluate CMIP5 models projections of the changes in the subtropical ridge (STR) and its relationship to the projected global warming.

Activity 1: Climate projections for Victoria

Introduction

Victoria is particularly vulnerable to climate change on a number of fronts due to its highly variable rainfall, exacerbation of extreme temperatures and changes to the coastal environment. Many changes to the climate of Victoria have already been observed and the latest scientific findings conclude that these are set to continue and, in some cases, accelerate. Up-to-date information on the latest science of climate change will support adaptation planning to the risks posed by the impacts of these changes.

This report summarises the most current climate projections for Victoria. A summary is given on climate model performance and projections of the climate drivers of relevance to Victoria and projections of the main climate variables. The evaluation and projection information is based on the Fifth Assessment Report of the Intergovernmental Panel on Climate Change (IPCC) and climate change projection reports from the Natural Resource Management for the regions encompassing Victoria.

Observed Climate Variability and Change in Victoria

Victoria has warmed at 0.05–0.15 °C per decade since 1911 with accelerated warming since the 1960s (Fig. 5.36 Maps of trends in mean temperature [°C per decade]Fig. 5.36), in line with the Australia-wide and global rates of warming. The mean warming and the acceleration are all well captured by the CMIP5 climate simulations of the past climate from 1850 to 2005.

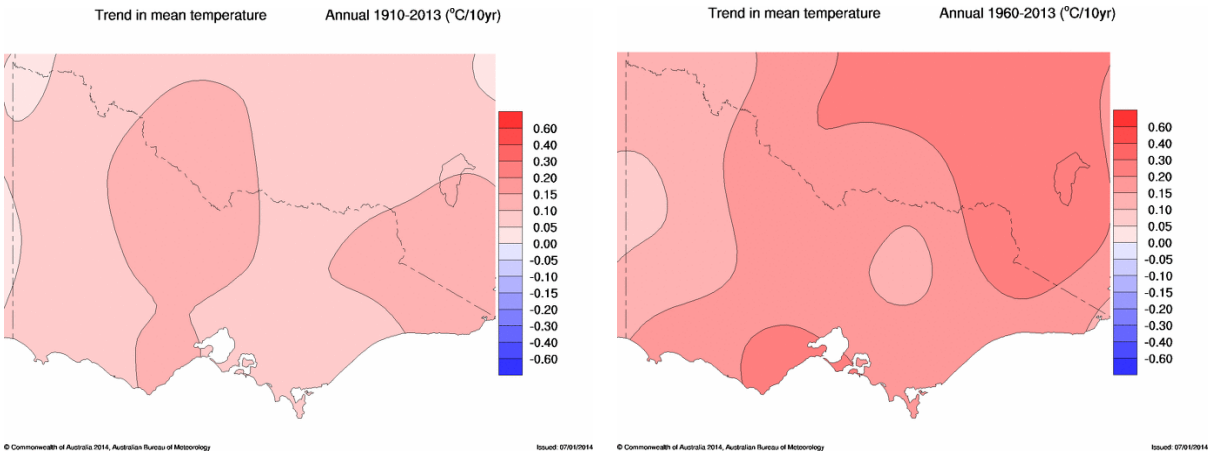

Fig. 5.36 Maps of trends in mean temperature [°C per decade]
a) 1910–2012 and b) 1960–2012
(source: Bureau of Meteorology ACORN)

Victoria experienced prolonged periods of extensive drying in the early twentieth century and the record breaking Millennium Drought from 1997–2009 (Fig. 5.37). However, annual rainfall shows no long term trend throughout the twentieth century, while the difference between warm and cool season rainfall shows a significant long-term trend. Since 1960 autumn rainfall has shown the largest decline, but winter and spring rainfall have also declined. Timbal and Drosdowsky (2013) reported that about

70 per cent of the rainfall deficit of the cool season was consistent with the expected rainfall response to the observed strengthening that has been observed in the subtropical ridge (STR).

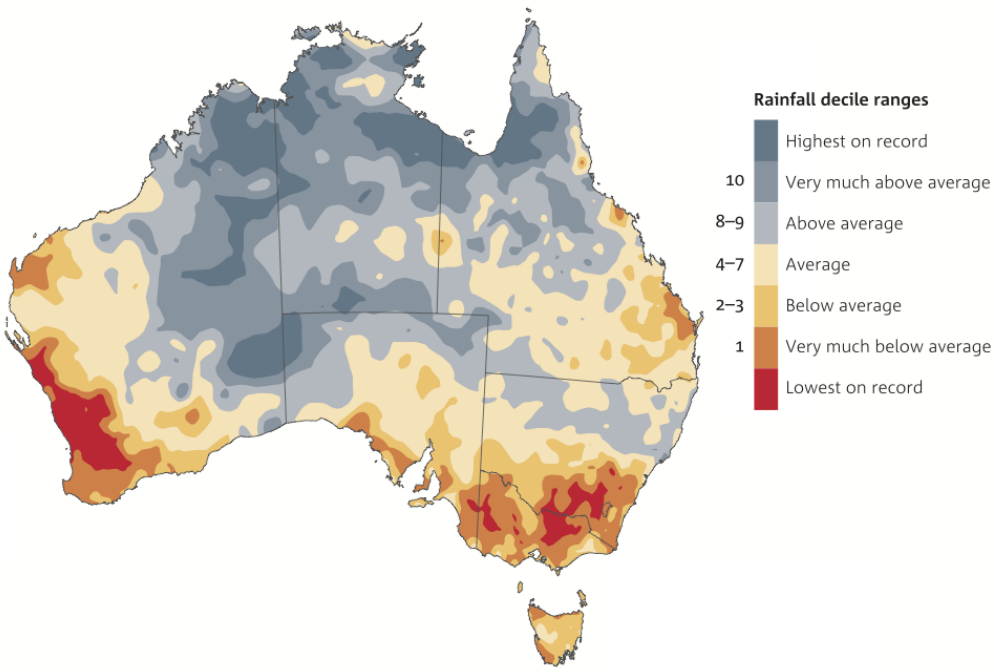

Fig. 5.37 Rainfall deciles for the cool season (April–October) from 1997–2012 (source: Bureau of Meteorology AWAP)

The Millennium Drought was broken spectacularly by record rainfall in 2010–12. This record rainfall fell mostly in spring and summer, but rainfall deficits in autumn and winter, which were one of the main characteristics of the drought, continued. The rains in 2010–12 resulted from the very strong La Niña event. They were found (see Projects 1 and 3) to be amplified by warm sea surface temperatures (SST) in the eastern Indian and western Pacific Ocean that are partly due to global warming trends and partly to the negative phase of the Interdecadal Pacific Oscillation, as well as the positive phase of the Southern Annular Mode (SAM). There is no indication that the southward shift and intensification of the subtropical ridge has been reversed, as evidenced by no significant rainfall surpluses in late autumn to early winter from 2010–12.

Simulating Climate Change

- **Climate Models**

Extrapolation from historical climate trends is not a reliable method of estimating future climate change due to the complexity of the climate system and the many non-linear responses to changes in external climate forcings. Climate models are the only reliable tools for dealing with these complexities as they are founded on the accepted principles of physics. They are closely related to numerical models used for day-to-day weather forecasting and have been developed and used by many different modelling groups around the world to produce simulations of past, near-future and longer-term projections of climate.

The latest generation of global climate models (GCMs), analysed for the Fifth Assessment Report of the Intergovernmental Panel on Climate Change (IPCC 2013), have been run with a set of standard simulations for past and future climate. Simulations from about 50 models have been contributed to the archive of the Coupled Model Intercomparison Project Phase 5 (CMIP5, Taylor et al. 2012), the analysis of which by the international climate science community is still underway. The number of

models has more than doubled since CMIP3 (24 models) and models now generally have higher spatial resolution. The experimental design and the scenarios of future climate projections have changed from CMIP3 to CMIP5, and many CMIP5 models are more sophisticated, with added components such as biogeochemistry models and interactive aerosols. The projections for the twenty-first century are not directly comparable due to the changes in future scenarios but the results are broadly the same, although the skill in reproducing past climate and observed trends has improved somewhat.

• Emissions scenarios and CMIP5 experiments

It is not possible to know the trajectory of future emissions of greenhouse gases (GHG) and aerosols that will drive changes in *external forcing* to which the climate will respond (as opposed to *internal forcing* which is intrinsic to the climate system and drives climate variability). In order to represent the uncertainty in the emissions based on a range of plausible assumptions about population and economic growth, technological developments and transfer, and political and social changes trajectories, several different *emissions scenarios* are used to force global climate models. These provide a wide sample of possible outcomes for future climate.

For CMIP5 a set of 'representative concentration pathways' (RCPs) (Moss et al. 2010, van Vuuren et al. 2011) are used that provide concentrations of greenhouse gases and aerosols, as well as land use changes. The RCPs are named by the overall change in radiative forcing estimated from their emissions. The RCPs differ from the SRES scenarios used in CMIP3 and they represent a wider set of scenarios that SRES. No one RCP is considered more likely than others and they are used to provide a range of possible climate outcomes

RCP8.5 (the highest emissions scenario) represents a future with little curbing of emissions. RCP6 represents lower emissions, while RCP4.5 concentrations are slightly above those of RCP6 until after mid-century, but emissions peak earlier and are stabilised late in the century at below current emission levels. RCP2.6 is the most ambitious mitigation scenario, with emissions peaking early in the century (around 2020), then rapidly declining. For further details on these RCPs see IPCC (2013) and the NRM Technical Report (Box 4.2) (NRM, 2014a). For comparison between CMIP3 and CMIP5 projections, some RCPs and SRES scenarios are comparable: RCP8.5 most closely matches A1FI and RCP4.5 mimics B1; there was no SRES scenario equivalent to RCP2.6.

Climate projections are generally presented as changes from the recent mean climate for 1986–2005. The current climate is estimated from the *historical* CMIP5 experiment, wherein GHG and aerosol concentrations mimic those observed from 1861–2005. Projected changes from the 1986–2005 mean are presented for different 20-year periods of the twenty-first century.

• Model evaluation

While the skill of future climate projections cannot be determined, a good simulation of the key aspects of global and regional climate provides a basis for placing some confidence in the regional projections of the models. The skill of GCMs can be assessed by comparing their simulations of the past and current climate to observations. One source of imperfection in GCMs is that they perform their calculations on a discrete grid with around 200 km between grid cells. In CMIP5 GCMs have between 2 and 10 grids cells covering Victoria and so their results represent a spatial average. Models are designed to simulate large-scale processes well, so the spatial and temporal details of these processes on regional scales are simulated with much more varying capacity. Current and future climate simulations should be interpreted as representing a large region including areas adjacent to the state.

The performance of GCMs in simulating mean climate seasonal cycles was assessed in the projections for the Murray Darling basin (NRM, 2014c), and the results will generally apply to Victoria as a

whole (Fig. 5.38). Models reproduce well the timing and magnitude of the seasonal cycle of temperature and mean sea level pressure. However, the spread in mean sea level pressure amongst models is large, but this is more a systematic bias (a systematic shift all year around) and the critical movement of the annual cycle is well captured. For rainfall, climate models show a very large scatter around the observations (right panel in Fig. 5.38), and the largest errors are found for the warm season rainfall. Globally, the distribution of temperature extremes are well represented in GCMs and CMIP5 models simulate more realistic extreme rainfall and aspects of large-scale drought than CMIP3 models. Over Victoria CMIP5 models underestimate some extreme rainfall events.

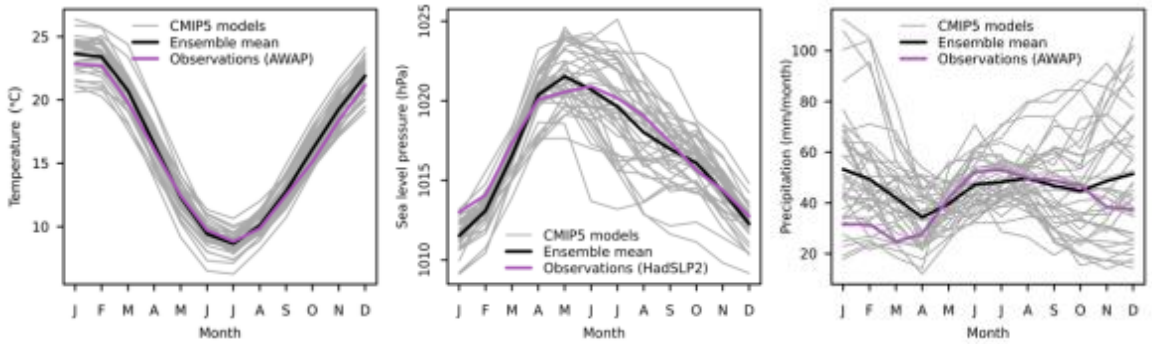

Fig. 5.38 Annual cycle of Murray Basin Cluster mean temperature (left), sea level pressure (middle) and rainfall (right) showing relevant observations (colour line), the CMIP5 individual models (grey lines) and ensemble mean (black line).

Analysis of CMIP5 models is ongoing, but much evaluation of their skill in reproducing the main climate features of relevance to Victoria has already been carried out. Overall, the CMIP5 models show some improvement over CMIP3 models, but no major breakthroughs have been made. GCMs now represent the main modes of variability with some veracity, although interpretations of projections need to carefully consider the biases that still exist. Most of the following information is collated from IPCC (2013).

- **El Niño – Southern Oscillation**

CMIP3 GCMS were able to simulate the main features of ENSO with considerable similarity to observations and this skill has improved in CMIP5 models. However, this is mostly due to their being fewer poorer performing models rather than there having been significant breakthroughs. The range of magnitude of ENSO variability has narrowed significantly and the time scale of largest variability now better matches observations, as does the timing of ENSO in the seasonal cycle. However, there are still errors in the mean background climate and processes that are important for ENSO variability, such as cloud feedbacks and trade wind strength that mean improvements in many models' results may result from compensating errors. The simulation of rainfall teleconnections of ENSO to Australia, such as the reduction in rainfall associated with El Niño events, have biases in many models, but the multi-model mean pattern is reasonably well simulated in spring, The relatively short length of the historical climate record makes it difficult to determine whether the observed shift of the dominant El Niño events from east Pacific to central Pacific events, and other changes in ENSO behaviour in the past two decades, are due to anthropogenic climate change or simply reflect the range of naturally occurring ENSO regimes.

- **Indian Ocean Dipole**

The general features of the IOD, such as the timing of events in the annual cycle (in winter and spring) and its correlation with ENSO, are simulated by many models. However, there are biases in the amplitude of IOD events and in the patterns of sea surface temperature (SST), with many models overestimating the intensity of the IOD. As with ENSO, the simulations of IOD rainfall teleconnections over Australia are reasonably well simulated in spring.

- **Southern Annular Mode and subtropical ridge**

CMIP3 GCMs were able to reproduce the broad characteristics of the SAM, but spatial patterns of the associated shift in the jet and resultant rainfall anomalies cover a wide range. GCMs are now able to better reproduce observed SAM variability and trends, but biases still exist in the position of the eddy-driven mid-latitude jet (see Project 3), which is important for correctly simulating the correct position of the SAM.

Project 5 examined model performance in 50 CMIP5 models in simulating the STR. It was found that most models faithfully simulate the broad characteristics of the observed STR, but four models had a STR situated too far to the west and three had the STR being too broad. Also, as in CMIP3 models, the relationship between the intensity of the STR and Victorian rainfall was different to observed in many models. These model biases will affect rainfall projections for Victoria and so need to be taken into account.

Project 4 found that tropical expansion in GCMs is two to four times smaller than observed and the effects of natural variability are not adequately captured. For example, the effect of ENSO is underestimated in most models. These will affect models' projections of future changes, although most models do simulate the observed relationship between the STR and the southern Hadley cell. As tropical expansion has been greater in Australian longitudes, making Victorian rainfall apparently more sensitive to changes in the mean meridional circulation (MMC), model biases are potentially more of an issue in Victoria than elsewhere.

Climate projections

- **Global climate projections**

Global-scale and large-scale CMIP5 projections are comparable to those in CMIP3. It was stated in IPCC (2013) that had CMIP5 models been used in the Fourth Assessment Report the projected mean temperatures and ranges would not have been substantially different; differences in temperature projection were due mostly to different emissions scenarios. While the different sets of emissions scenarios cannot be directly compared, when changes are scaled per degree of global-mean warming the patterns of mean temperature and rainfall changes around the world are very similar.

Warming will be greater over land than over oceans and generally largest at high northern latitudes. The changes in rainfall patterns in the Australian region are indicative of a southward shift in the extratropical storm track. This is one of the most consistent projections amongst models although the magnitude of the shift varies.

- **Projected changes in climate drivers**

- **ENSO**

There is still no consensus amongst models as to whether ENSO variability will become weaker or stronger, but there is high confidence that it will remain the dominant mode of natural interannual climate variability and its global impacts will intensify. Future changes in ENSO activity are uncertain because the changes in the mean climate state of the Pacific vary from model to model. Any change in ENSO intensity is therefore uncertain, although recent research shows the frequency of extreme El Niño events may double due to climate change, from once in 20 years to once per decade (Cai et al. 2014). The impact of these events in Australia is highly variable, with the 1982–83 event leading to widespread drought while the 1997–98 had much more moderate impacts. Some of the impacts of ENSO (e.g. floods) may intensify as the world warms due to the increased moisture capacity of warmer air (Seager et al., 2012) and this may lead to more extreme rainfall. It is also expected that average rainfall along the equator will be enhanced. New research suggests global warming will also

enhance El Niño-driven drying in the west tropical Pacific (Power et al., 2013). This may affect ENSO rainfall impacts in Australia.

Project 1 found that the wet conditions in spring in Victoria during the strong La Niña event of 2010–11 were amplified by the warming SSTs in the eastern Indian and western Pacific oceans, as well as the negative phase of the Interdecadal Pacific Oscillation, through enhancement of the positive phase of SAM. As the warming of these SSTs is partly due to global warming, extreme rainfall under La Niña conditions may be enhanced in the future.

- **IOD**

While the overall frequency of IOD events (positive and negative) is not projected to change, the difference in amplitude between positive and negative events – currently positive events have larger amplitude – is projected to decrease (Cai et al. 2013). Also, the SST pattern of the IOD is projected to change in ways characteristic of a positive IOD event – cooler temperatures across the eastern Indian Ocean and warmer in the western Indian Ocean during spring. However, these results need to be taken with caution because many models have a systematically too-strong IOD for the current climate.

- **SAM**

Future trends in the SAM are likely to be driven by stratospheric ozone and GHG concentrations. Both have pushed the SAM toward a positive phase in spring and summer over recent decades, but as the ozone layer recovers the influence of ozone on the direction of SAM will reverse. Ozone and GHG will therefore push the SAM in opposite directions. Because the rate of trend depends on the rate of GHG emissions and ozone recovery, the future trends in the SAM depend on the emissions scenario. By mid-century the observed positive trend will weaken under RCP4.5, while GHG forcing will dominate for higher emissions scenarios and the eddy-forced jet will move further south in all seasons.

Project 3 has shown that the positive phase of the SAM has different impacts in Victoria during winter to the other seasons—drying in winter and wetter conditions in spring–summer–autumn. A positive trend in SAM in would lead to a drier Victoria in winter, adding to that due to an intensification of the STR. The positive SAM trend would also lead to more rainfall in summer as the wet tropics expand southward. The results of Project 1 showing the intensification of rainfall during the spring 2010 La Niña event was enhanced by the positive phase of the SAM. This would suggest La Niña conditions would be wetter in spring–summer under projected trends towards positive SAM.

- **Subtropical ridge (STR)**

VicCI projects 2, 4 and 5 have examined projections of the STR. They have shown that the observed shift and intensification of the STR and associated tropical expansion are driven by GHG and stratospheric ozone changes. Future projections indicate a consensus amongst models toward a further broadening of the MMC (IPCC, 2013). The STR would be expected to respond in future in the same sense as the MMC and the SAM, so that the rate of southward shift will depend on the emissions scenario; ozone recovery will oppose the GHG driven southward shift but at higher emission rates GHG forcing will dominate.

The examination of projections in Project 5 found that all 37 models available projected both intensification and a southward shift of the STR under RCP8.5. It was also found that biases in simulations of the STR in the current climate affect future rainfall projections. Models rejected for poor STR simulation show different rainfall projections in spring and summer to accepted models. However, in the cool season, of most relevance to Victoria, there is no clear distinction between rainfall projections from the different sets of models.

- **Temperature projections for Victoria**

There is high confidence in projections of continued substantial warming in Victoria for mean, maximum and minimum temperature, taking into consideration the strong agreement on direction and magnitude of change amongst GCMs, downscaling results and the robust understanding of the driving mechanisms of warming. For the near future (2030), the mean projected warming shows only minor differences between scenarios, with warming of around 0.5–1.3 °C (relative to 1986–2005). Under RCP8.5, the mean temperature change for Victoria for mid-twenty-first Century (2046–2065 relative to 1986–2005) is 2.0 ºC and by the end of the twenty-first Century (2081–2100) 3.7 ºC, which are very similar values to the global means.

Changes to temperature extremes are projected to follow the increases in mean temperature. A substantial increase in the temperature reached on the hottest days, the frequency of hot days and the duration of warm spells are projected with high confidence, based on model results and physical understanding. Correspondingly, a decrease in the frequency of frost days is projected with high confidence. For example, in Melbourne the average number of days above 35 °C in a year is projected to more than double by late in the century under the RCP8.5 and median model ensemble warming.

- **Weather systems, winds and storms**

Overall small changes are projected for surface winds following all RCPs, particularly in the near future (2030) period (high confidence). Decreases in winter are projected for northern Victoria for later in the century (2090) with medium confidence based on model results and physical understanding (southward movement of storm track and strengthening of the subtropical ridge). For the same physical reasons wind speeds may increase along coastal areas of Victoria (medium confidence). Literature suggests a decline in the number, but an increase in the intensity of east coast lows, which would have an effect on both mean rainfall and heavy rain events especially in the eastern districts.

- **Rainfall projections for Victoria**

Natural climate variability will likely remain the major driver of rainfall changes in Victoria for at least next few decades. Projected changes in mean rainfall for 2020–2039 are –10 to +5 per cent for annual, around –15 to +7 per cent in winter, and –15 to +15 per cent in summer. Therefore short-term changes are small relative to variability.

The projected changes in the main climate drivers in section 4.2 support GCM results showing projections for a cool season rainfall decline and a rainfall increase in the warm season in Victoria. This result is also supported by downscaling simulations. However the magnitude of these changes is quite uncertain. By 2090 the mean seasonal changes from the GCMs in winter are –5 per cent under RCP4.5 and –12 per cent under RCP8.5, and those in summer are –2 per cent under RCP4.5 and +2.5 per cent under RCP8.5, but range about +/–10 per cent around these mean values for RCP4.5 and about +/–20 per cent for RCP8.5. It should also be noted that although future mean rainfall projections have similarities with the observed trends during the last 30 years, the magnitude of the observed deficit during the Millennium Drought (1996 to 2009) is equivalent to the worst case scenario by the end of the twenty-first century. CMIP5 models do project a range of possible outcomes, so although overall drying is most likely, projections for increased rainfall over Victoria are plausible (Fig. 5.39).

Understanding of physical processes and high model agreement gives us a high confidence that the intensity of heavy rainfall extremes will increase. This increase will be larger and more significant during the warm season when largest rainfall events are currently being observed. The magnitude of change, and the time when any change may be evident against natural fluctuations, however, cannot be confidently projected. On the other hand, the time spent in drought will increase over the course of century under RCP8.5 in line with changes to mean rainfall, and the frequency and duration of extreme droughts will increase (medium confidence).

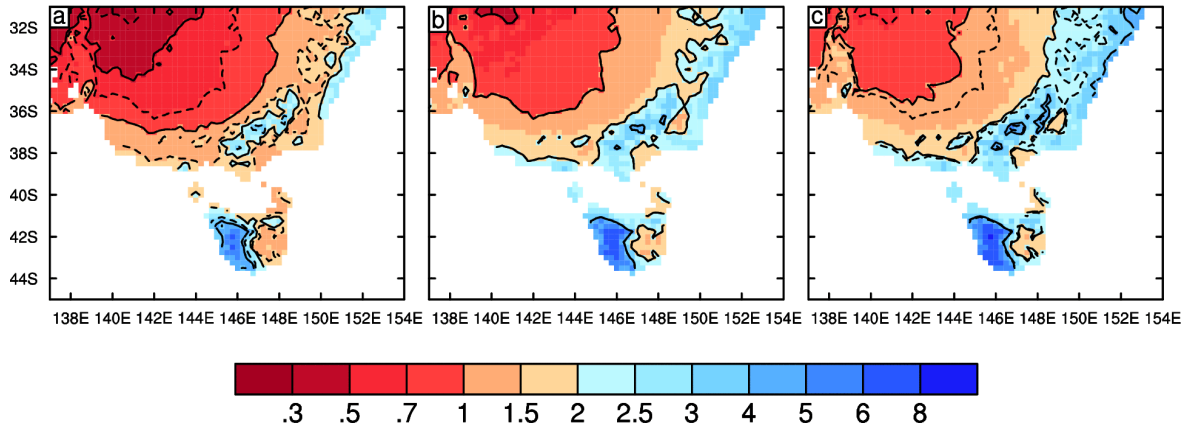

Fig. 5.39 Annual mean rainfall (as a rate in mm per day), for (b) the present climate, and (a) the drier end of the projected model range and (c) wetter end of the projected range.
The present climate uses AWAP for 1986–2005, on a 0.25º grid. The drier/wetter classification uses the 10th and 90th percentiles amongst models for percentage change at 2090, under the high emission scenario (under a global warming of 3.7 °C case). For clarity, the 0.5 mm/d, 1 mm/d, 2 mm/d and 4 mm/d contours are plotted with solid black lines. In (a) and (c) the same contours from the original climate (b) are plotted as dotted lines. From NRM Regional Projections Report: Southern Slopes (NRM, 2014b).

Snowfall and maximum snow depth has been observed to decline significantly during the last 50 years. Snowfall is projected to experience a further reduction, increasing with time, with magnitude dependent on the emission scenarios and the altitude. Offline snow modelling (Bhend et al. 2012) highlights a likely reduction in the area covered by snow due to an increase of the average snow line and a reduction of the snow accumulation and the length of the snow season affecting all the snow pack. Taking these studies into account, there is high confidence in substantial reductions in snow, particularly under RCP8.5.

- **Projections of other phenomena**

There is high confidence that climate change will result in a harsher fire weather climate in the future. However, there is less only medium confidence in the magnitude of the change to fire weather. Increased temperature combined with lower rainfall results in a higher drought factor, which indicates the fuel's readiness to burn. The number of days with a 'severe' fire danger rating, periods when bushfires potentially have greater human impacts (e.g. Blanchi et al., 2010), increases by up to 35 per cent by 2030 and from 40–110 per cent by 2090.

Projections for potential evapotranspiration indicate increases with global warming in all seasons with largest absolute rates in summer. However, despite high model agreement we have only medium confidence in these projections due to shortcomings in model's simulation of observed historical changes.

Soil moisture projections suggest overall seasonal decreases for later in the century (medium confidence). These changes in soil moisture are strongly influenced by those in rainfall, but tend to be more negative due to the increase in potential evapotranspiration. For similar reasons, runoff is projected to decrease, but only with low confidence.

Continued increase in Victorian sea levels is projected with very high confidence. For the near future (2030), the projected range of sea level rise for the Victorian coastline is 0.07 to 0.19 m above the 1986–2005 level, with only minor differences between RCPs. For the far future (2090) the sea level rise is in the range 0.27 to 0.66 m for RCP 4.5 and 0.39 to 0.89 m for RCP 8.5. Taking into account the nature of extreme sea levels along, structures (e.g. sea walls) would need to be raised by up to 17 cm

by 2030 for all RCPs and by up to 85 cm by 2090 for RCP4.5 and up to 125 cm for RCP8.5 to maintain the current frequency of extreme sea level exceedences.

- **CMIP5 projections compared with CMIP3**

There has been no profound change in the climate projections for Victoria in the latest generation CMIP5 model simulations compared to those from CMIP3 that were reported in SEACI. The simulations conducted under the two experiments and the emissions scenarios used are different so it is not possible to compare them directly. The analysis of CMIP5 results is still ongoing. However, overall the projected changes in rainfall and temperature are quite similar, and consequently the existing strategic plans for future water resources in Victoria are still relevant as they have been designed to be robust to a wide range of future flow scenarios.

Analysis of the CMIP5 model simulations will nevertheless provide further insight and reduce uncertainty in future climate projections. The CMIP5 database contains many times more data than CMIP3 and the models are now have higher spatial resolution and are more sophisticated, including new components such as biogeochemistry models and interactive aerosols. The proportion of poor performing models is also now much reduced, meaning that CMIP5 simulations potentially provide more detailed information with increased mean-model skill.

Applying regional projections

Information has been provided on how Victoria's climate may respond to increasing greenhouse gas concentrations. This section provides some guidance on how future climate impacts can be framed in the context of climate scenarios for adaptation planning the Climate Futures web tool, available on the Climate Change in Australia website. An example of its use is presented to illustrate what can be done with the tool.

Since climate models can vary greatly in their simulated climate response to increasing greenhouse gas emissions, it can be useful to organise models according to their simulated climate response. For example, sorting according to rainfall and temperature would give an immediate feel for how models fall into a set of discrete climate scenarios framed in terms such as: much drier/slightly warmer, much wetter/slightly warmer, much drier/much hotter and much wetter/much hotter, etc. As an example of how this information can be presented for adaptation planning,

Fig. 5.40 shows how the change simulated by CMIP5 models to the winter climate in the Southern Slopes West Victoria and Murray Basin clusters for 2090 (years 2080–2099) under the RCP8.5 scenario can be organised with regard to temperature and rainfall. The table organises CMIP5 models into groupings according to their simulated changes to winter rainfall (rows) and winter temperatures (columns), and shows that models fall in a large range. When considering the two variables together, we see that the most commonly simulated climate for the 2090 under RCP8.5 in both regions is a 'Much Hotter' and 'Much Drier' climate (7 and 16 of 34 models), but many model simulations fall in other categories.

In viewing the projection data in this way, the user can gain an overview of what responses are possible when considering the CMIP5 model archive for a given set of constraints. In a risk assessment context, a user may want to consider not only the maximum consensus climate, as simulated by models, but also the 'best case' and 'worst case' scenario. What these are will depend on the application, and outcomes may in fact eventuate that are 'better' or 'worse' than these scenarios, but as an example we can imagine that we are viewing

Fig. 5.40 from the point of view of a water resources manager. Then the best case scenario would be a 'Much Wetter and Much Warmer' climate (for which one climate model can be chosen to represent this climate future) and the worst case the 'Much Hotter and Much Drier' scenario, which in this case coincides with the maximum consensus climate. Overall the projections are similar for the two regions with drier conditions by far the most likely.

		June - August (JJA) Surface Temperature (C)			
		Slightly Warmer < 0.50	Warmer 0.50 to 1.50	Hotter 1.50 to 3.00	Much Hotter > 3.00
June - August (JJA) Rainfall (mm)	Much Drier < -15.00			+ 5 of 33 models (15%)	+ 7 of 33 models (21%)
	Drier -15.00 to -5.00			+ 5 of 33 models (15%)	+ 6 of 33 models (18%)
	Little Change -5.00 to 5.00			+ 5 of 33 models (15%)	+ 2 of 33 models (6%)
	Wetter 5.00 to 15.00			+ 2 of 33 models (6%)	
	Much Wetter > 15.00			+ 1 of 33 models (3%)	

		June - August (JJA) Surface Temperature (C)			
		Slightly Warmer < 0.50	Warmer 0.50 to 1.50	Hotter 1.50 to 3.00	Much Hotter > 3.00
June - August (JJA) Rainfall (mm)	Much Drier < -15.00			+ 2 of 33 models (6%)	+ 16 of 33 models (48%)
	Drier -15.00 to -5.00			+ 2 of 33 models (6%)	+ 5 of 33 models (15%)
	Little Change -5.00 to 5.00			+ 2 of 33 models (6%)	+ 3 of 33 models (9%)
	Wetter 5.00 to 15.00			+ 2 of 33 models (6%)	
	Much Wetter > 15.00			+ 1 of 33 models (3%)	

Likelihood	Proportion of models
Not projected	No models
Very Low	< 10%
Low	10% - 33%
Moderate	33% - 66%
High	66% - 90%
Very High	> 90%

Fig. 5.40 Climate Futures web tool output showing results for (top) Southern Slopes West Victoria and (bottom) Murray Basin NRM regions when assessing plausible climate futures for 2090 under RCP8.5. Output is organised into futures linking coherent mean winter (JJA) temperature and rainfall as defined by GCM simulations. Colours indicate likelihood, with pale yellow indicating very low likelihood and yellow low likelihood.

Assuming that the user has identified what futures are likely to be of most concern for the system of interest, Climate Futures allows the user to explore the numerical values for each of the models that populate those climate futures. Further, it provides a tool for choosing a single model to represent each of their selected climate futures, based on the closest fit to changes in climate that that climate future

represents, but also taking into account models that have been identified as sub-optimal for particular regions based on model evaluation. Through this approach users can select a small set of models to provide scenarios for their application, taking into consideration model spread and the sensitivity of their application to climate change.

Summary

The performance of the latest generation of climate model simulations from around the world (CMIP5), their ability to simulate the main drivers of Victoria's climate and projections for the twenty-first century have been summarised, taking information from the latest IPCC assessment report and reports for each of the NRM clusters covering Victoria. This report brings together the information relevant for the future climate of Victoria.

CMIP5 models are able to simulate the main climate drivers and their impacts on Victoria's climate, although some biases exist that need to be taken into account. Changes in the main modes of climate variability affecting Victoria are generally not clear or robust, but some signals have emerged:

El Niño Southern Oscillation will continue to be the dominate source of interannual climate variability, but increased atmospheric moisture with global warming will see intensified extreme rainfall events.

Trends in the Southern Annular Mode and subtropical ridge have been driven by ozone depletion and greenhouse gas increases, with the former dominating. These will continue to force changes in the SAM during the twenty-first century, but will have opposing effects as stratospheric ozone is replenished. The southward shift and intensification of the STR will continue, more so for higher emissions scenarios where GHG forcing will dominate.

The frequency of Indian Ocean Dipole events is not projected to change, but some characteristics of the events may change.

Increasing greenhouse gas concentrations and changing aerosol concentrations will lead to continued changes to Victoria's climate, with the magnitude of many of changes depending on future emissions. There is high confidence that:

Temperatures will continue to increase. For Victoria, mean warming of 0.5–1.3 °C is projected for 2030 in all future scenarios, with mean warming of 3.7 ºC by 2090 for the highest emissions scenario. Extreme hot temperatures will increase and be more frequent.

Natural variability of rainfall will remain high and cool season rainfall will decline. The intensity of heavy rainfall extremes will increase. Snow cover will be reduced.

The subtropical ridge will intensify and shift southward in the cool season, which is expected to reduce rainfall in Victoria during winter but may increase rainfall in summer.

Harsher fire weather will occur, with the number of severe fire days increasing.

Sea levels will continue to rise by up to 0.89 m for the highest emissions scenario.

Projections also point to other changes, but with lower confidence: the frequency and duration of extreme droughts will increase, wind speeds will decrease in the north of state but increase along the coast, potential evapotranspiration will increase which, along with lower cool season rainfall, will reduce soil moisture and runoff.

Activity 2: Model projections of changes to the Australian subtropical ridge in CMIP5

Introduction

New work on the primary atmospheric feature relevant to Victoria in the newest generation of climate models is confirming previous findings and revealing new insights.

The subtropical ridge (STR) is the high pressure belt that marks the climatological centre of the descending arm of the Hadley circulation. Over Australia the STR indicates the northerly boundary of the winter-dominated rainfall region of southern Australia and the boundary of the dominantly westerly winds. The STR of a particular climate is usually defined by the latitude and magnitude of the peak of mean sea level pressure (MSLP) in the long term average, illustrated on the left in Fig. 5.41. There is an annual cycle in the intensity (STR-I) and position (STR-P) of the subtropical ridge, where it is weakest and lies over Victoria in summer and is stronger and lies to the north in winter (Fig. 5.41, right). Different observed datasets show some differences in these indices, illustrated by the cycles of two datasets on the plot. The position, intensity and character of the ridge influences rainfall in Victoria in the entire cool season (here we use the window of March to October) by affecting the frequency and strength of weather systems that cross southern Australia to the south of the STR. In the cool seasons the STR is immediately to the north of Victoria, and a stronger or more southerly STR steers weather systems further south so they deliver less rainfall over Victoria. Systematic shifts to the STR position or intensity imply a marked influence on southern Australian rainfall.

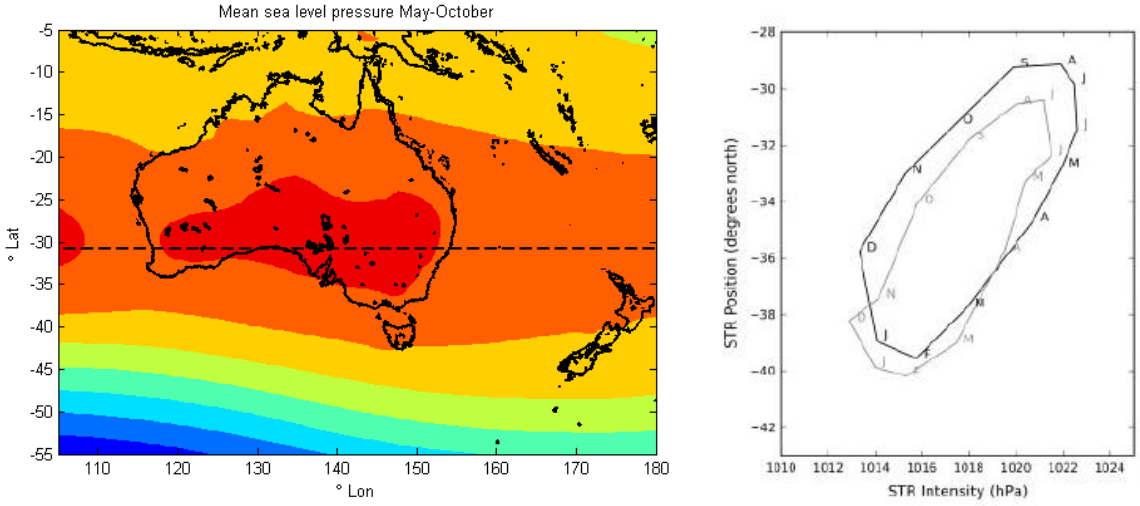

Fig. 5.41 Mean sea level pressure in May–October from ERA Interim Reanalysis in 1980–1999 (left), with the dashed line showing the approximate position of the Australian subtropical ridge; The mean annual cycle of STR intensity and latitude over southeast Australia in Bureau observations (1900 and 2008, black line) and NCEP Reanalysis (1948–2002, grey line) (right). Months of the year are marked as letters (right panel taken from Kent et al. 2013).

A warming climate is expected to cause the Australian STR to intensify and move south in the cool season, as part of a global-scale expansion of the Hadley circulation and expansion of the subtropical dry zone. This is broadly associated with a decrease in Victorian rainfall in these seasons. There is good evidence that the STR has intensified in recent decades and this has contributed to the cool season rainfall long-term decline in Victoria in recent decades and to the 1997–2009 drought (Larsen and Nicholls 2009; Timbal and Drosdowsky 2013; Whan et al. 2013). There is also some evidence that the STR has moved south in recent decades. The previous set of Global Climate Models (GCMs) run

for the Coupled Model Intercomparison Phase 3 project (CMIP3) released in 2007 (Meehl et al. 2007) are a useful tool to examine the future of the STR. Kent et al. (2013) found that CMIP3 projects a further intensification and a southerly movement of the STR with a median of rate of 0.21 hPa and 0.25° latitude per degree of global warming. However, there are complicating factors in getting a clear picture of the effect of changes in STR and resulting rainfall in the future for Victoria. These factors come from model biases in the simulation of the STR itself as well as biases in the relationship between the STR and rainfall. The new CMIP5 set of models offer new opportunities to explore projected changes in the STR and resulting rainfall change, and in this project we evaluate the STR in all the CMIP5 models available, and take a look at the latest projections.

Evaluation

We analysed the simulation of the Australian STR in the fifty CMIP5 models currently available. We compared the models to data based on observations, the NCEP/NCAR Reanalysis 1 (Kalnay et al. 1996). We used similar methods to Kent et al. (2013), including interpolation and a curve-fitting routine of monthly mean MSLP in 140–150 °E for each model. MSLP at various longitude bands were examined in models, to evaluate the character of the STR. We find that many models simulate the broad character of the STR similar to observed, but four models simulate an STR that matches the southeast STR character in observations but place it too far to the west, and three models simulate the ridge that matches the southeast Australian in observations but produce it across a region that is too wide. We suggest that these models could be excluded from further analysis. However, more subtle biases present in other models still also present an issue in making regional climate projections for Victoria.

Many of the CMIP5 models have a different relationship between the STR-I and rainfall over Victoria, just as there was in CMIP3 models. Some example models are shown in Fig. 5.42, showing the correlation between the annual STR-I and annual rainfall anomaly in observations (top left). An example model shows a similar extent of the region of negative correlation with STR-I over Victoria (top right, MRI-CGCM3). Some other models show this region to be broader than observed (bottom left, CSIRO-Mk3.6) or too restricted (bottom right, MPI-ESM-LR). These biases affect the interpretation of the regional rainfall projections, since it lowers the confidence in which a change in the STR will be expressed correctly in Victorian rainfall.

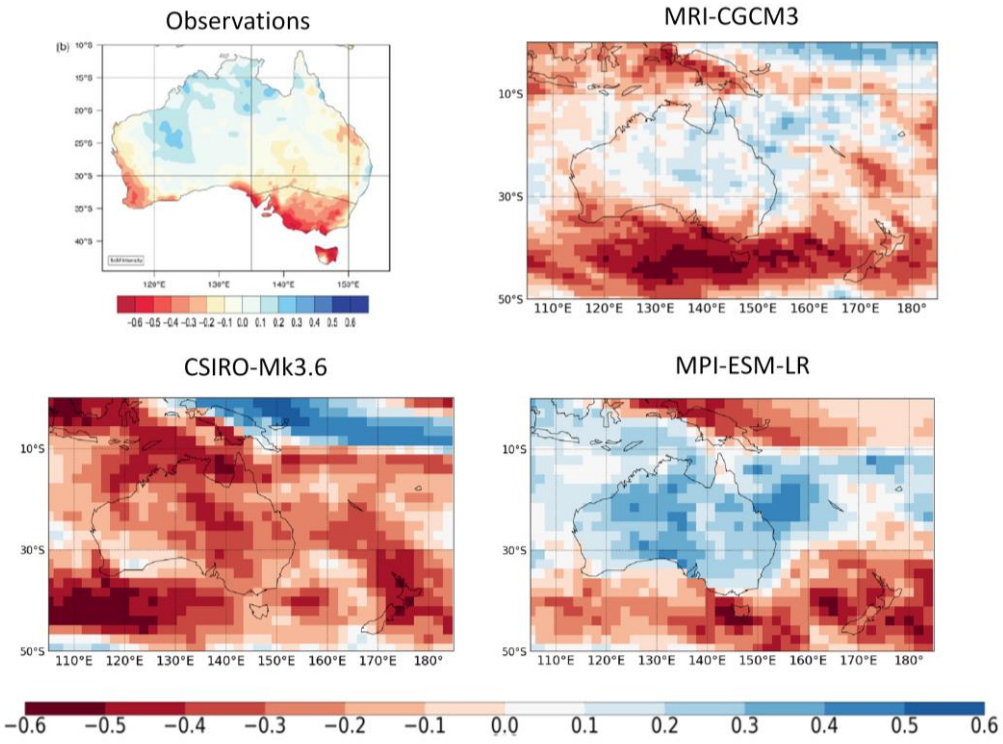

Fig. 5.42 The correlation of annual STR-I and annual rainfall anomaly in 1948–2002 in observations (top left, taken from Kent et al. 2013) and three example models.

Projections

We examined the future projections over the twenty-first century of the STR and rainfall in the 37 models currently available for the high emission scenario, RCP8.5 (van Vuuren et al. 2011). We aim to include as many models as possible in the final analysis. Past trends and projected changes in STR-I and STR-P are shown for the 37 models in Fig. 5.43. Most models showed an intensification of the STR over recent decades, but all models show it to intensify over the century under this RCP, with a shift of over 1 hPa over the century in the model mean annual index. Similarly, almost but not all models showed a southerly trend of the STR in past decades, but all models show a projected southerly movement in future, with an increase of over 1° of latitude over the century in the model mean annual index. Once the difference in warming between scenarios is accounted for, these changes appear to be broadly consistent with CMIP3 models presented by Kent et al. (2013). We find that there is no strong relationship between past trends and projected future change across models. This means that the models aren't simply divided into those that respond strongly and those that respond weakly in the past and the future, but points towards complicating factors. The bias in the current climate, and different cycles of natural variability in each model are likely to make a difference, and this is under further investigation. Project 4 found that most underestimate the rate of tropical expansion and this may be linked to their failure to adequately capture the effects of natural variability. The effect of any future trends in these modes will therefore not be well simulated by models, affecting projections of Victoria's future climate.

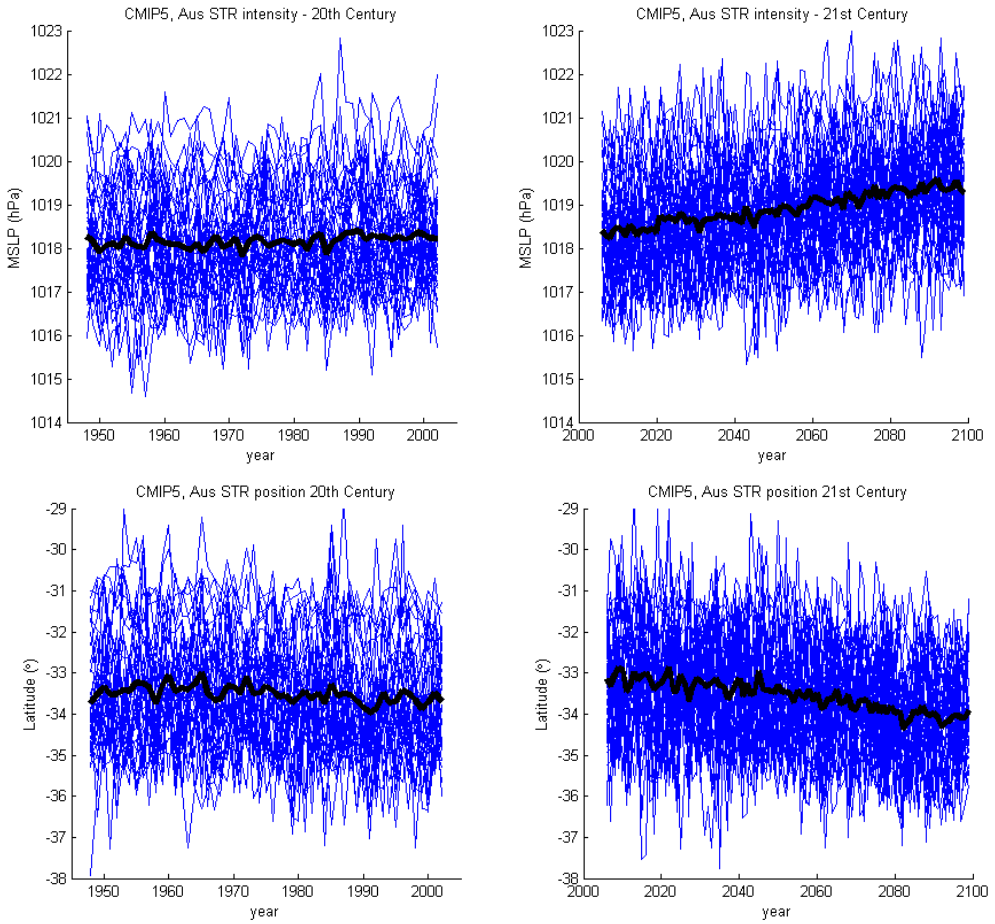

Fig. 5.43 Time series of STR-I (top) and STR-P (bottom) for recent decades (left) and the twenty-first century (right) in all models (blue lines) and the multi model mean (black line), based on 37 CMIP5 models.

In certain regions and seasons, the models rejected by this study (see above) give a different regional rainfall projection for the 'clusters' used in the Natural Resource Management (NRM) national projections project, compared to those accepted (Fig. 5.44). Examining the range of models used in the NRM project (see caption), we find that the models rejected for STR width show a distinctly drier rainfall projection than the rest of the ensemble for spring and summer in regions including Central Slopes (CS), Murray Basin (MB) and Rangelands North (RN) (Fig. 5.44). In summer the STR in observations and models is generally south of 36 °S, so these regions lie to the north of the STR in this season. In contrast, models rejected for simulating the southeast Australian STR too far to the west show a wetter rainfall projection than the rest of the ensemble in spring and summer in the central eastern regions of Central Slopes and East Coast South (ECS). These findings suggest that the bias in the STR in the current climate has an effect on the projection of change in the future. The exact link between the two is under investigation. There is no clear distinction between the rainfall projections in the rejected models compared to the accepted models south of the STR in the cool season, where the STR is of most relevance to Victoria (e.g. the Southern Slopes (SS) clusters in autumn and winter).

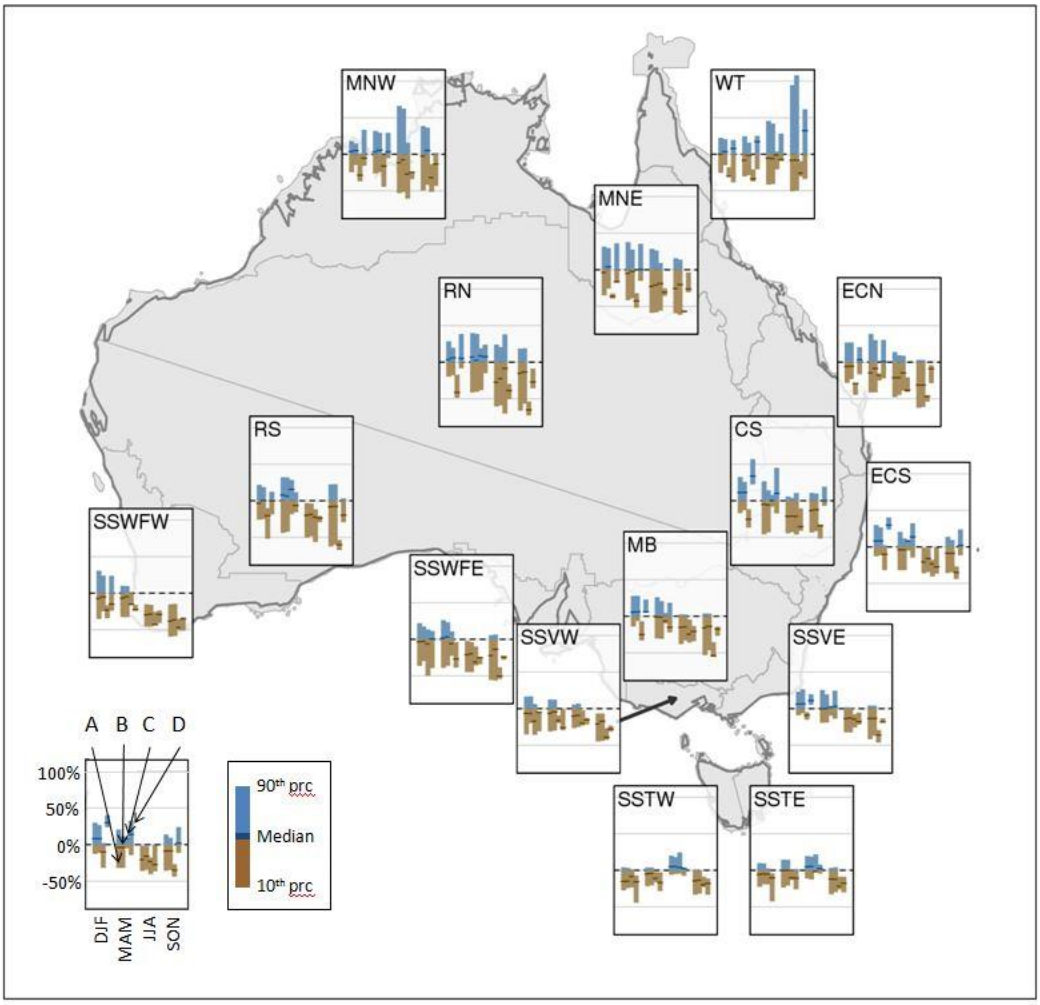

Fig. 5.44 Rainfall projections (percentage change) for 1986–2005 to 2080–2099 for RCP8 for the NRM national projections 'cluster' regions, showing the median, 10th and 90th percentile of the model range.
Plots show calendar seasons (DJF summer, MAM autumn, JJA winter, SON spring). In order, the bars show (A) all 39 models used in NRM projections, (B) 33 models in NRM not rejected, (C) Three models rejected for STR width and (D) Three models rejected for STR location (one rejected model was not considered in the NRM project).. Cluster regions are: MNW Monsoonal North (West), MNE Monsoonal North (East), WT Wet Tropics, RN Rangelands North, ECN East Coast North, RS Rangelands South, MB Murray Basin, CS Central Slopes, ECS East Coast South, SSFWF South and South Western Flatlands (West), SSFWE South and South Western Flatlands (East), SSVW Southern Slopes Victoria West, SSVE Southern Slopes Victoria East, SSTW Southern Slopes Tasmania West, SSTE Southern Slopes Tasmania East.

Summary

The new set of CMIP5 models provides further evidence of the influence of climate change in forcing the Australian Subtropical ridge (STR) to intensify and move further south. In the cooler months the STR lies to the north of Victoria, so a stronger or more southerly STR leads to reduced rainfall by reducing the average strength and frequency of weather systems that bring rain. Therefore, this new work confirms that changes to atmospheric circulation are generally projected to lead to reduced rainfall in Victoria in the cooler seasons. However, the biases in the simulation of the STR and the connection between the STR and rainfall remain a barrier to reliable regional rainfall projections.

The new set of models also provides the opportunity to examine the range between models. While we do not find a relationship across all models in terms of past trends and future change in the indices

themselves, we do find that models with a poor simulation of the STR have a distinct rainfall projection for certain regions and seasons. This suggests that it may be possible to reject some models and quantify a narrower and more reliable range of projected change for the STR and rainfall than the entire CMIP5 ensemble indicates.

Conclusions and future perspectives

Research undertaken over the last three years jointly by CSIRO and the Bureau of Meteorology to deliver state-of-the-art nationwide projections tailored to the needs of the Natural Resource management (NRM) groups nationwide is almost complete and will be made publicly available in mid-2014. This will be a valuable resource for climate change impact studies across the state of Victoria.

The key findings for this work is that the state of Victoria will experience further warming continuing the trend observed over the past century across the State. The pace of the warming will depend primarily of the emissions scenarios during the twenty-first century, at least in the second half of the twenty-first century. During the first half, uncertainties due to global climate model sensitivities and decadal natural variability will dominate. Climate change will not be limited to warming trends but will affect the hydrological cycle through rainfall changes and other parameters. While these changes are less certain, a convergence is seen amongst models toward a reduction of rainfall during the cool period of the year (March– October) with no clear direction for the warm time of the year.

Confidence in the climate change projections emerge from consistency of the signal across models as well as understanding of the models' ability to reproduce the large-scale modes of variability and weather phenomena which are known to be important for the local climate across Victoria. Evaluating the latest set of climate models (the CMIP5 database) in that regard has been part of the effort undertaken in developing the climate change projections for NRM planning. In particular, effort has been made in understanding how the CMIP5 models capture the subtropical ridge (STR) for the longitude band of Victoria and how within these climate models the STR changes in latitude and intensity relates to rainfall. Many models were found to broadly reproduce the observed STR character although some biases exist in its position and extent and its relationship with rainfall. The model mean reproduced the observed intensification of the STR and observed southward shift, but there is a spread between individual models and not all models simulated these trends. However, all models show the STR to intensify and move south over the twenty-first century. The assessment is helping in evaluating the confidence in the projections and identify the poorly performing CMIP5 models that it may be useful to reject.

Work performed this year has helped highlight the relevance of the NRM work for Victoria and potential climate impact studies across the state. Several publications will be coming out of the NRM work and will inform users about details available within these projections as well as datasets made available to perform impact studies. However, no documentation will be specifically about the state of Victoria as the publications are aiming at clusters of NRM regions that do not correspond to state boundaries. Therefore the continuation of this project will deliver Victoria-specific documentation of the climate change projections across the state as a central source of information on this important body of work. Additional work will aim to increase the confidence in the projections, in particular for rainfall, by evaluating the range of uncertainties on how it relates to known mechanisms of the climate system and in particular how the tropical oceans surrounding of Australia will warm. Finally an evaluation will be undertaken to determine how the overall projected mean rainfall reduction may affect the future potential for prolonged drought (similar to what was experienced during the Millennium Drought).

Project 6: Convection-resolving dynamical downscaling

Ekström, M.

CSIRO

Key findings

Work in the first year has focused on setting up the model experiment and testing appropriate physics combinations on selected case studies for dynamical downscaling at 10 and 2 km resolution—the purpose being to assess the relative merits of finer resolution downscaling for hydrological impact modelling.

Based on user guidance and peer-review literature, ten configurations of WRF were identified, focusing on the sensitivity of rainfall to the microphysics schemes (that generates the grid scale rainfall), in combination with two different planetary boundary schemes.

Through a process of discussion with stakeholders, visual examination of synoptic mean sea level pressure charts and daily rainfall maps, and consideration of recorded flooding events, three case study periods of 14 days each were identified for testing the WRF physics ensemble: 8–21 August 2010, 6–19 October 2010, and 31 January – 13 February 2011.

Model simulations were completed for the first case study period for both 2 and 10 km resolutions. An evaluation of daily rainfall patterns against observed gridded rainfall data showed that for both domains, a somewhat better performance (as judged by skill metrics) was given by simulations using microphysics scheme WDM6 in combination with the planetary boundary layer scheme MYNN.

The results are promising, but the fine resolution set-up is resource intensive, implying that with limited computing resources, important choices are required with regard to simulation period and extent of spatial domain.

Background

Within the Victorian Climate Initiative (VicCI), we are interested in understanding future impacts on runoff, as changes in runoff are directly relevant to management of water supply in the state of Victoria.

Simulations of future climate are generated by global climate models (GCMs) that typically operate on scales of 100–250 km. This scale is considered much too coarse for most hydrological applications (Fowler et al. 2007); hence there is a need to translate the climate change signal in the GCM output to a finer resolved regional signal. Numerous methods exist that attempt to bridge this scale-gap and they are all referred to as ‘downscaling’ methods.

In Project 6, we are assessing the value of fine resolution dynamical downscaling for the purpose of downscaling rainfall to provide input to hydrological impact models. The term ‘dynamical downscaling’ denotes methods that use a numerical model to simulate the dynamical response at a finer resolution than the GCM (Laprise 2008). There are several different approaches to dynamical downscaling, the most common is the use of a Limited Area Model (LAM), which is given input from a ‘host’ GCM along its lateral and lower model domain boundaries.

Output from dynamical downscaling is attractive to users of downscaled data, as it gives a dynamical response to a wide range of variables for a defined spatial and temporal domain. There are however a

number of drawbacks with the method, such as their heavy usage of computation and data storage resources. This means that dynamical downscaling is usually run only for a selection of host GCMs and emission scenarios, which limits their ability to represent uncertainty in these components. Further, the models themselves are not perfect so will contain a model-bias relative to the observed real climate (Foley 2010).

In Project 6, we are interested in quantifying the value of dynamical downscaling conducted on a fine resolution (10–12 km) versus operating the LAM at a very fine resolution (<3 km). These resolutions relate to the spatial scales where a dynamical model is able to resolve convective motions in the atmosphere (<3 km) and the finest resolution whereby it is advisable to use parameterised convection (>10 km). Operating the model at the finer scale is much more expensive in computing terms, hence there needs to be good justification for conducting downscaling at very fine resolutions. This is especially true in a climate change context as downscaling output are typically of the order of multiple decades. The motivation to use fine resolution convection-resolving models for downscaling across Victoria is based on reported improved skill by these types of experiments to represent the spatial and temporal characteristics of rainfall events (Kendon et al. 2012); a characteristic that could improve projections of future runoff.

The potential added value of using very fine resolution downscaling across Victoria is assessed through a hind-cast study, where a LAM is configured to produce output at the two scales of interest using input data from a re-analysis data set (based on observations) rather than output from a GCM. The use of re-analysis data as input means that it is possible to evaluate the skill of the LAM against historical observed data. This study will provide guidance on whether output from fine resolution simulations leads to significantly different (and improved) runoff projections relative to somewhat less computationally expensive model resolutions.

Objectives

1. Model configuration: Install and configure the LAM, identify model domain, elevation data in model and prepare input data.

2. Identification of test cases: Select spatial and temporal domains.

3. Selection of model physics: From amongst available options, select the most appropriate parameterisation schemes to be assessed in the test cases.

4. Assess skill in simulation of daily rainfall by the selected physics configurations.

Activity 1: Model configuration

Input data

When WRF is run in hind-cast mode (i.e. simulation of past climate) it uses observed data to ‘force’ the model simulation. Observed climate information is fed into WRF via its lateral (atmospheric variables) and bottom (surface variables) boundaries. Further, to give the model a starting image, the model’s initial conditions are also provided by the observed data set.

Here, the observed data fields are extracted from the ERA interim re-analysis (Dee et al. 2011). For surface, subsurface levels (4 levels) and pressure levels (37 levels), data are 6 hourly at: 00, 06, 12 and 18 hrs UTC. Required variables on pressure levels are: height (m), temperature (K), U and V wind (m/s) and relative humidity (%). At surface level the model requires U and V surface winds (m/s), temperature (K), relative humidity (%), surface pressure (Pa), sea level pressure (Pa), sea surface

temperature (K) and sea-ice fraction (fraction). Ground level variables are: soil moisture (m^3/m^3) and soil temperature (K).

The WRF pre-processor (WPS) re-grids the re-analysis data onto the projected model domain levels. Some of the routines to interpolate observed input fields were modified to better handle the large discrepancy in scale between the re-analysis data and the model domains (primarily soil and other surface variables that have more heterogeneous fields compared to most atmospheric variables).

Model configuration

The downscaling experiment is conducted using the Weather and Research Forecasting (WRF) system version 3.5.1 (Skamarock and Klemp 2008). WRF is a community model system that supports two different dynamical cores, the Advanced Research WRF (ARW—www.mmm.ucar.edu/wrf/users) hosted by the Mesoscale and Microscale Meteorology Division of the U.S. based National Center of Atmospheric Research (NCAR), and the WRF-NMM hosted by the Developmental Testbed Centre (DTC—www.dtcenter.org/wrf-nmm/users). The ARW core is commonly the choice for regional climate downscaling applications and was the choice for VicCI.

The model resolutions that we are interested in are 10–12 km and less than 3 km. This could be achieved by running WRF twice at each respective resolution. However, this would be inappropriate due to the very large discrepancy between the resolution of the input data (around 125 km) and the target resolution. Further, the model domain would have to cover much of the Australian continent extending south and east into the Australian Bight and Tasman Sea in order to resolve processes relevant for rainfall in Victoria. This would make the experiment extremely resource hungry and computationally slow if run at 3 or 10 km resolution.

From a computing resource point of view, a more sustainable solution is to nest model runs within WRF itself. This means that a model domain (parent domain) receives input from an external host model (in this case ERA Interim), and within this domain a second smaller model domain is nested (child domain) and run at a higher resolution to the parent domain. The child domain, receives forcing from the parent domain along its lateral and lower boundaries. Further nests can subsequently be constructed within the first child domain to achieve finer model resolutions. When nesting model domains, it is crucial to think about the placement of the boundaries as one would want to locate this blend of nests in an area where it will cause least disturbance to circulation patterns that influence the case study region and away from major topographical features.

In Project 6 a three nested structure was used to achieve the fine resolution needed to resolve convective motions in the atmosphere with resolutions of 50 km, 10 km and 2 km respectively; we denote these as d01, d02 and d03 (Fig. 5.45). The parent domain (~50 km grid, d01) covers the entire Australian continent, with somewhat larger extension into oceans in the east and south. The first child nest at 10 km (d02) resolution is focused on southeast Australia covering the coastal border in the south and east. The second nest (2 km, d03) is focused on an inland area, where the central low lands of Victoria rise towards the Alps in the eastern part of the state (Fig. 5.46). The location of the innermost nest was decided upon following discussions with DEPI (see Section Activity 2).

The highest resolution digital elevation model (DEM) provided with the WRF package has a 2 minute resolution (~1.8 km), this is not sufficiently fine for the inner nest and may have local errors that can influence the simulation at 2 km resolution. Hence, for the nests d02 and d03 a 9s DEM (~270m), developed by the CSIRO and Geoscience Australia, was obtained to improve the digital terrain information. During initial testing of WRF, it was noted that many physics combinations became unstable and investigation suggested that it was due to the steep relief in the DEM. For this reason a strong smoother was used to reduced gradients in the 9s DEM.

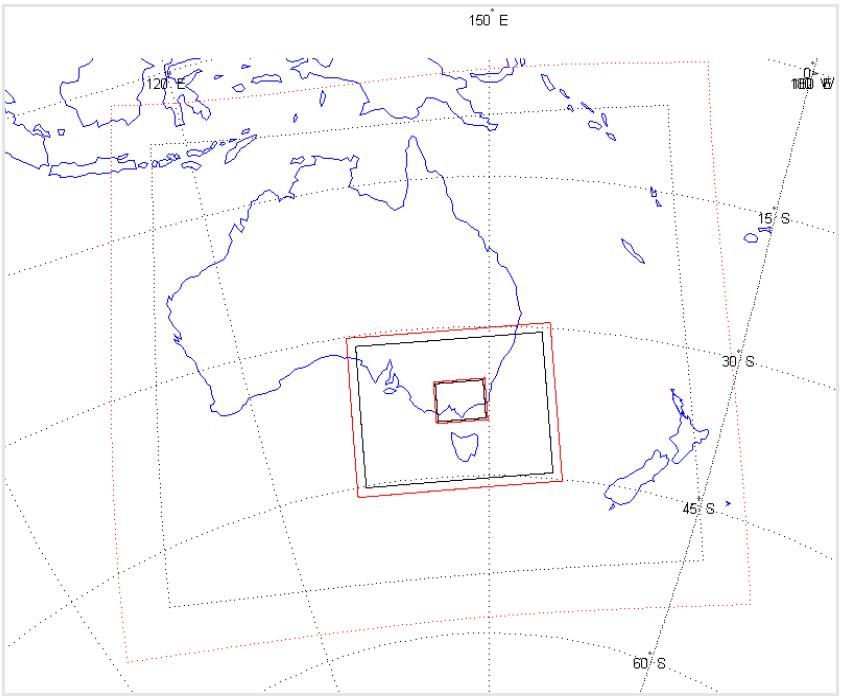

Fig. 5.45 Spatial extent of the three model domains: d01, d02 and d03 (in decreasing size).
The red dots denote the outer boundary and the black dots outline the domain excluding the relaxation zone where information from bordering nests is blended.

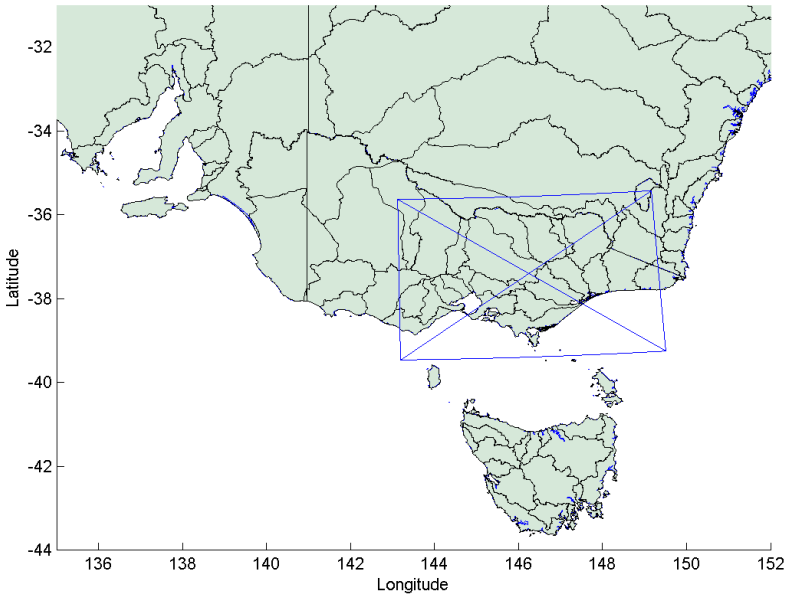

Fig. 5.46 Spatial extent of the innermost domain (d03) with relaxation boundary removed.

Activity 2: Identification of test cases

Broad-scale characteristics around the spatial domain of interest and what type of events to focus on were discussed amongst researchers and DEPI. Time wise, the winter–spring–summer floods of 2010–2011 were noted as interesting events to focus on. Space-wise, the region north of Melbourne, encompassing the southernmost part of the Dividing Range and its western slopes was proposed as that most relevant from a water supply perspective. It was also noted that an overlap with regions covered by radar products could be a relevant constraint.

Based on a visual assessment of rainfall maps and synoptic charts for the 2010–2011 period and a consideration of flood events as noted in the Victorian Government review of the 2010–11 Flood Warnings and Response, three time periods were selected as case study events. Each case study is 14 days (15 days simulation time, with first day removed as model spin-up) and includes at least one major rainfall event. These are described below.

The first study represents a winter (or cold season, i.e. April–October) case—8–21 August 2010. During this period, rainfall was triggered by an upper level trough, and low level cold front associated with a low-pressure system developing on 10 August over Victoria, which moved westward over the next few days. Further passages of cold fronts occurred during the period 15–17 August (Fig. 6.3a), and again on the 19–20 August. Rainfall was associated with these passages.

The second study represents the shoulder season between the cold and warm (November–March) season and includes the heavy rainfall noted for mid-October (6–19 October 2010). Notable rainfall events during this period occurred in conjunction with a cold front passage on 7 October, an upper level trough on 13 October followed intense rainfall associated with a deep low centred over Victoria on 15–16 October (Fig. 6.3b).

The third study represents the summer (or warm season) and encompasses the early February flooding events noted above: 31 January – 13 February 2011. This period included the passage of tropical cyclone *Yasi*, north of the study region; the passage enabling advection of a moist tropical air mass ahead of the prefrontal westerly trough approaching from the west (Fig. 6.3c).

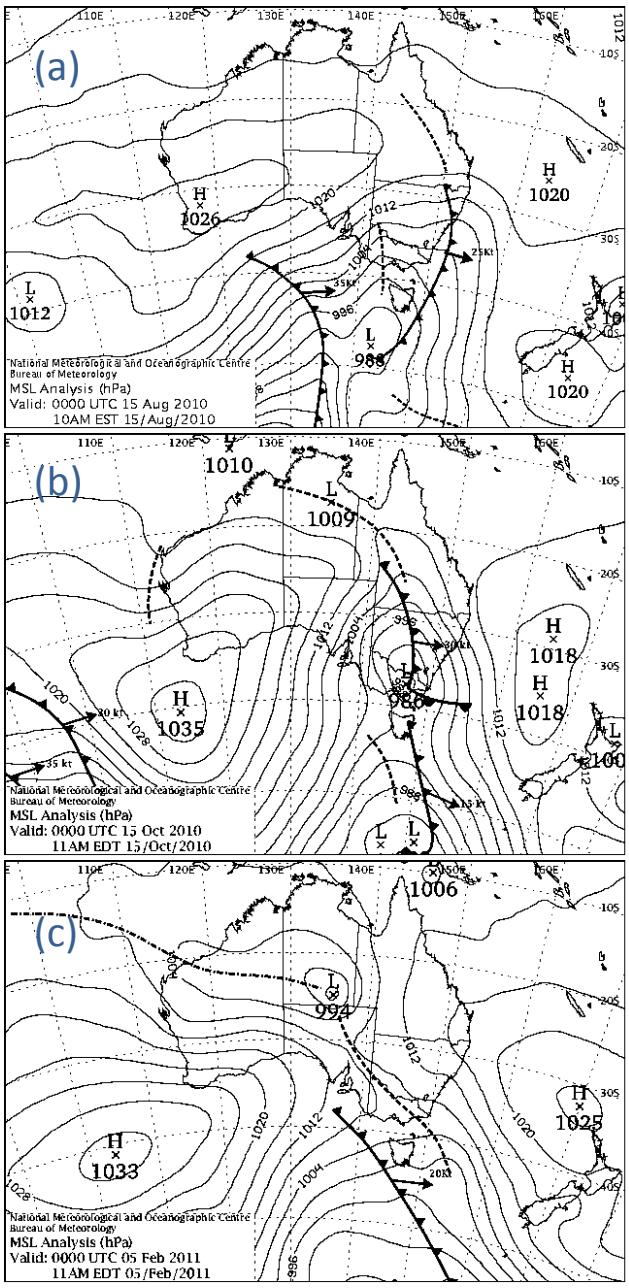

Fig. 5.47 Mean sea level pressure analysis (00 UTC) from the a) 15 August 2010, b) 15 October 2010 and c) 5 February 2011.

Source: Maps generated using the Bureau of Meteorology online Analysis Chart Archive

Activity 3: Selection of model physics schemes

WRF can be configured using a variety of combinations of physics options, reflecting the diverse nature of WRF's application. Further, because it is a community supported model, user groups can introduce new physics schemes that after robust testing are included as viable options in the WRF modelling system. Consequently, for most physics parameter schemes, there are multiple options to choose from.

The multitude of options can be a challenge to users because many options appear on their theoretical merits more or less equal; suggesting that sometimes there is no obvious 'right' choice. In these instances, it is prudent to conduct preliminary tests to see what configuration works best for the intended application and geographical region.

Selecting physics schemes for WRF was made with the requirements for the high-resolution innermost domain at focus. Guidance was sought from WRF support material and peer-review literature relevant for the VicCI case study in terms of its geographical location and application, e.g. Evans et al. (2012). The reasoning and justification for each selected scheme is reported in the Water for a Healthy Country report 'Test of WRF physics schemes for Project 6 of the Victorian Climate Initiative' (Ekström 2014). A short summary of pertinent details is given below.

For WRF simulations, users have to select physics schemes that are responsible for convective processes (cu scheme), microphysics (grid scale rain processes, mp scheme), planetary boundary layer processes (pbl scheme), radiative processes (short and long wave radiation, ra schemes), surface schemes (fluxes between the surface and the atmosphere, surf_phys) and a land surface model (lsm).

For Project 6, in most instances it was possible to select an appropriate scheme given the requirements of the innermost nest. For example, the rapid radiative transfer model for GCMs for long and short wave radiation (RRTMG; Iacono et al. (2008)), the Noah Land surface model (Chen et al. 2007), the Betts–Miller–Janjic (BMJ) cumulus scheme for d01 and d02 (Janjic 1994, 2000) and the fifth generation Penn State/NCAR Mesoscale Model (MM5) surface physics scheme (Zhang and Anthes 1982). For the selection of mp scheme and pbl scheme, however, it was believed that these two schemes would be important for the skill of the simulation and it was not clear what scheme would be most appropriate.

For this reason, a physics ensemble was created where five mp schemes were tested—the five schemes that enabled simulation of five hydrometeors (cloud water, rain drops, ice crystals, snow and graupel (and hail for some), using so-called 'double moment' schemes (where mass as well as concentration of species are predicted rather than using single moment schemes where particle size distribution is derived from fixed parameters), i.e. the WRF double moment 6-class (WDM6) scheme (Lim and Hong 2010), the Thompson scheme (Thompson et al. 2008), the Milbrandt scheme (Milbrandt and Yau 2005), the Morrison scheme (Hong and Pan 1996) and the National Oceanic and Atmospheric Administration (NOAA) National Severe Storms Laboratory (NSSL) scheme (Mansell et al. 2010). Further, two different pbl schemes were selected where each represent one of the two different ways by which WRF pbl schemes distribute surface fluxes within the boundary layer, i.e. local closure scheme Mellor-Yamada Nakanishi and Niino Level 2.5 scheme (MYNN; Nakanishi and Niino (2006)) or the non-local closure scheme Yonsei University scheme (YSU; Hong et al. (2006)). Thus, in total, the physics ensemble comprised ten model configurations (Table 5.4).

NB	PBL	MP	SURF_PHYS	RA SW/LW	LSM	CU D01/D02
1	MYNN	WDM6	MM5	RRTMG	Noah	BMJ
2	MYNN	Thompson	MM5	RRTMG	Noah	BMJ
3	MYNN	Milbrandt	MM5	RRTMG	Noah	BMJ
4	MYNN	Morrison	MM5	RRTMG	Noah	BMJ
5	MYNN	NSSL	MM5	RRTMG	Noah	BMJ
6	YSU	WDM6	MM5	RRTMG	Noah	BMJ
7	YSU	Thompson	MM5	RRTMG	Noah	BMJ
8	YSU	Milbrandt	MM5	RRTMG	Noah	BMJ
9	YSU	Morrison	MM5	RRTMG	Noah	BMJ
10	YSU	NSSL	MM5	RRTMG	Noah	BMJ

Table 5.4 List of physics options associated with each ensemble member N1–N10.
Acronyms and references are provided in the text above.

Activity 4: Assessing skill in simulation of daily rainfall by the selected physics configurations

In the first year, one of the three case study periods was completed for the specified physics ensemble. During this experiment only eight of ten ensemble members proved stable under the chosen configurations; runs using the mp scheme NSSL (N5 and N10) became unstable and terminated.

An initial evaluation of WRF performance focused on the simulation of daily rainfall totals, where WRF rainfall output was assessed against the daily gridded observed rainfall from the Australian Water Availability (AWAP) project (Jones et al. 2009) available on a 5 by 5 km resolution grid.

The evaluation was conducted on the native grid of the model; hence the AWAP data was re-gridded to the model domains d02 and d03. Further, model output was aggregated to daily totals matching the local time (model output is hourly UTC in domain d02 and d03 following the timestamp of the input data).

Model skill in simulating rainfall was assessed using skill measures (or scores) adapted for deterministic categorical forecasts, i.e. for variables that are event-based. Five measures were considered, four simple scores (bias, simple accuracy, false alarm ratio and threat score as described by Wilks (2006), see Appendix 5.1 for details on how to calculate the simple skill scores) and one the more complex Fractions Skill Score (FSS) (Roberts 2008, Roberts and Lean 2008, Mittermaier et al. 2013).

A detailed description of results is provided in Ekström (2014). Here we note that in both domains, all ensemble members gave a good representation of the timing of events (see Fig. 5.48 for d02 and Fig. 5.49 for d03). Further analysis will be carried out to investigate the varying skill in simulating the magnitude of the high rainfall events.

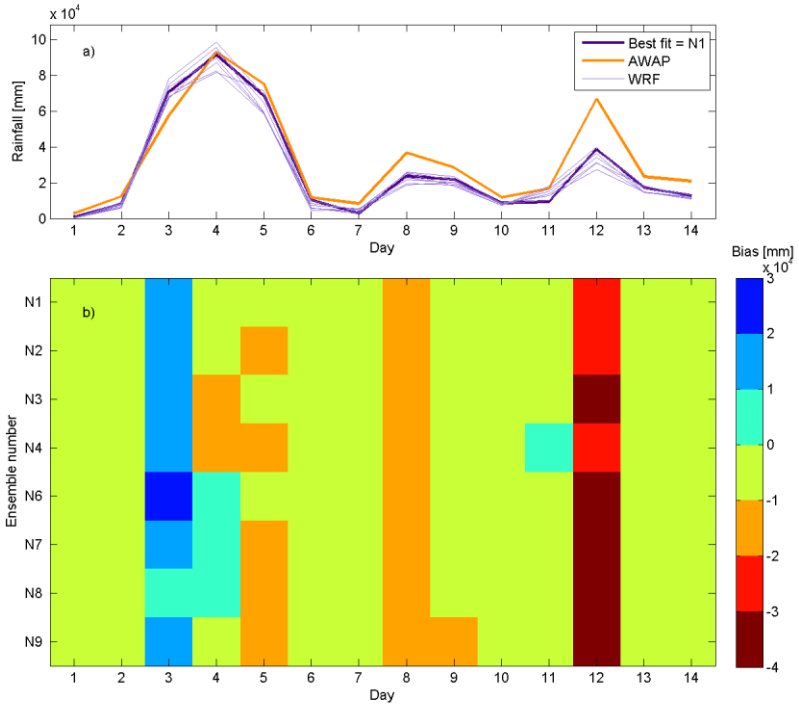

Fig. 5.48 Temporal evolution of rainfall in domain d02 (case study 1)

a) grid total rainfall (mm) for WRF members (blue) and AWAP (orange);
b) bias (difference in grid total rainfall, WRF-AWAP).

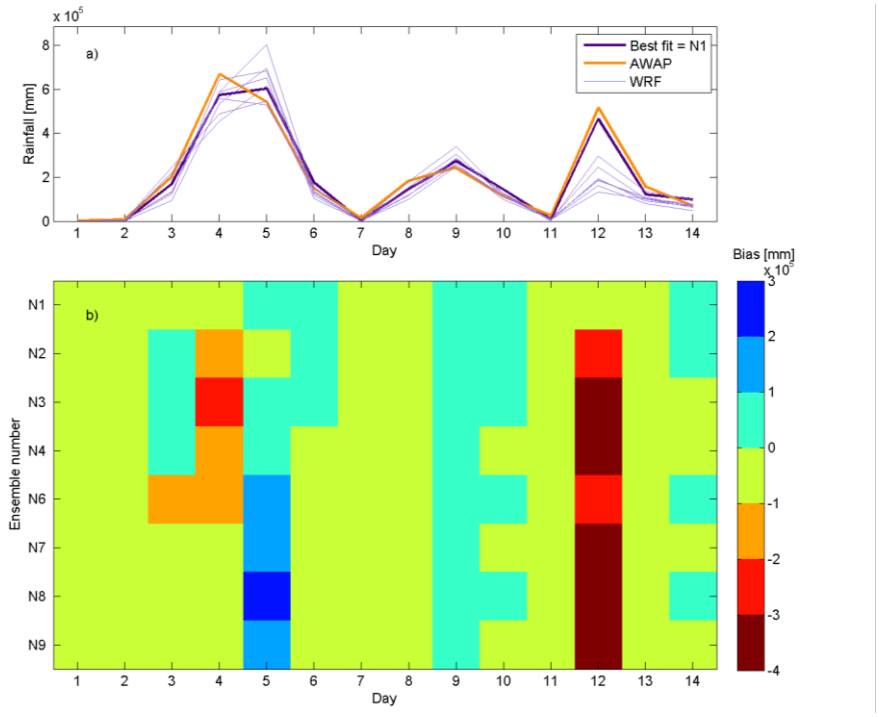

Fig. 5.49 Temporal evolution of rainfall in domain d03 (case study 1)

a) grid total rainfall (mm) for WRF members (blue) and AWAP (orange);

b) bias (difference in grid total rainfall, WRF-AWAP).

Somewhat better performance (as judged by the used metrics) was gained by simulations using mp scheme WRF double-moment six-class scheme (WDM6) in combination with pbl scheme Mellor-Yamada Nakanishi and Niino Level 2.5 (MYNN). Overall, simulation of rainfall in the 10 km domain appeared to have good skill, as judged by a number of skill scores (results from simple skill metrics are given in Fig. 5.50 for d02 and Fig. 5.51 for d03). However, model performance in the innermost domain (2 km) proved worse, and a visual assessment of rainfall patterns indicate spurious striation in the rainfall pattern, which may be corrected by different choices of dampening or movement of the lateral boundaries away from complex topography.

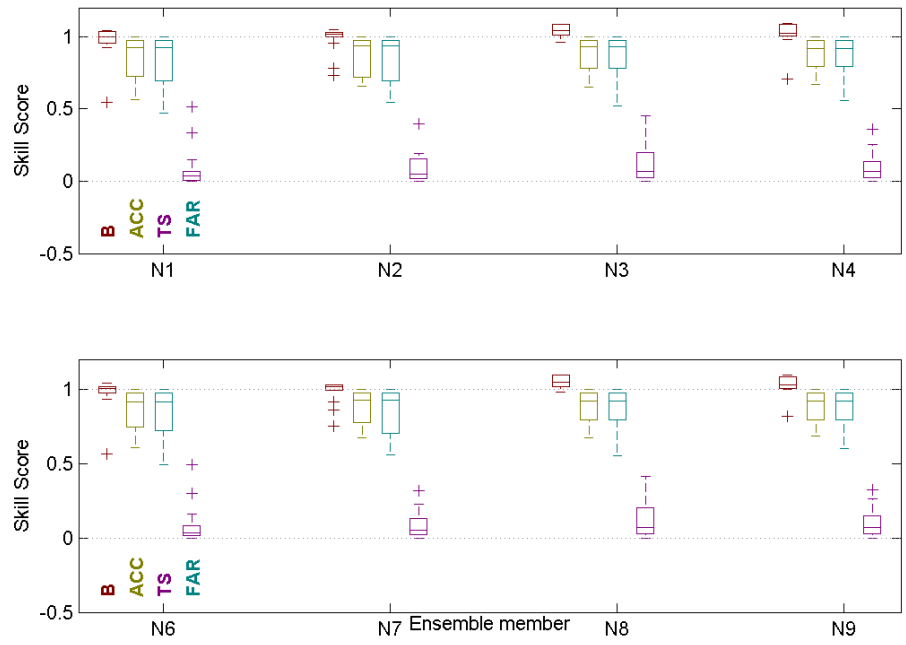

Fig. 5.50 Simple skill scores for domain d02.
Upper panel shows ensemble members N1–N4 (using pbl scheme MYNN) and lower panel shows ensemble members N6–N9 (using pbl scheme YSU). B = Bias, ACC = simple accuracy score, FAR = false alarm ratio, and TS = threat score (see Appendix 5.1 for definitions).

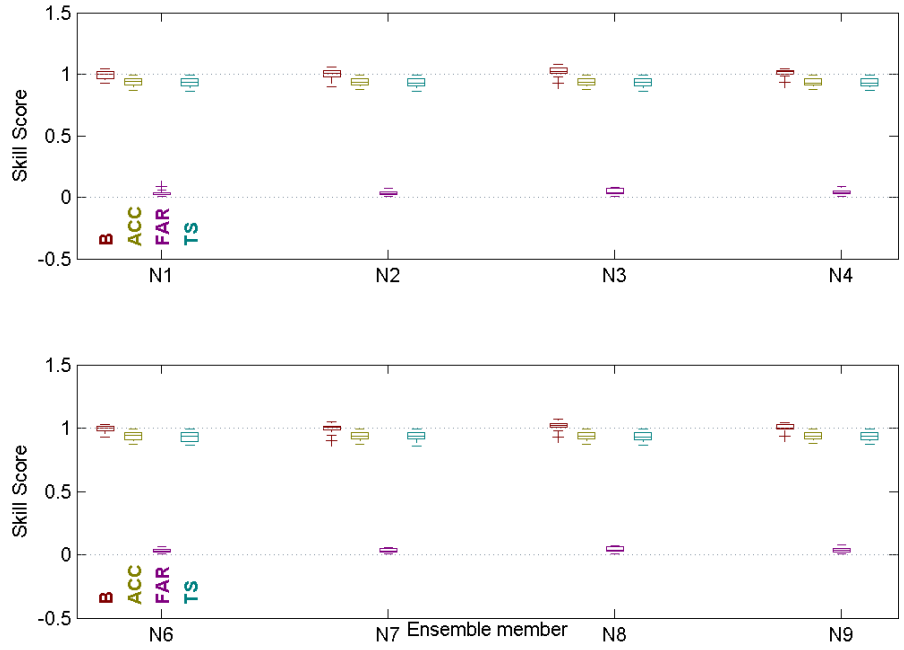

Fig. 5.51 Simple skill scores for domain d03.
Upper panel shows ensemble members N1–N4 (using pbl scheme MYNN) and lower panel shows ensemble members N6–N9 (using pbl scheme YSU). B = Bias, ACC = simple accuracy score, FAR = false alarm ratio, and TS = threat score (see Appendix 5.1 for definitions).

Conclusions and future perspectives

In Project 6 the relative value of very fine resolution convective-resolving downscaling versus fine resolution downscaling with parameterised convection is assessed. This work is expected to lead to the provision of improved regional rainfall simulations and hence runoff projections for Victoria.
In its first year, work in Project 6 focused on setting up the model experiment and testing appropriate physics combinations on selected case studies. Three case study periods were identified focusing on catchments to the west and south of the Great Dividing Range. The three case study periods were identified in a two stage process involving consultation with stakeholders at DEPI and the Bureau of Meteorology and a visual assessment of rainfall events and synoptic circulation during the identified period of interest. In total three study periods of two weeks each were selected: 8–21 August 2010, 6–19 October 2010 and 31 January 2011 – 13 February 2011.
Guided by peer-review literature and WRF user support material, an ensemble of 10 different physics configurations was identified for further testing, focusing in particular on more complex microphysics schemes in combination with two different pbl schemes. Using a three nested configuration (50 km/10 km/2 km), the WRF physics ensemble was applied to the first case study period. During this experiment only 8 of 10 ensemble members proved stable; runs using the mp scheme NSSL became unstable and terminated.
Using a set of skill metrics and visual evaluation, rainfall magnitudes and patterns were assessed for domain d02 (10 km) and d03 (2 km) against observed data set AWAP. For both domains, a somewhat better performance (as judged by the used metrics) was gained by simulations using mp scheme WDM6 in combination with pbl scheme MYNN. To separate skill amongst WRF configurations, further evaluation is required, e.g. looking at other variables and assessing why rainfall patterns differ amongst the ensemble members.

Using fine resolved dynamical downscaling shows promise as it has the capacity to better resolve the spatial and temporal characteristics of rainfall events. However, operating models at this high resolution is resource intensive, both in terms of computing but also in terms of storage of the output. Further, the duration of simulations is much longer for fine resolution experiments due to their much larger number of calculations needed to complete an experiment. This means that for the same amount of computing resources, a finer resolution experiment would have to simulate for either a shorter period or for a smaller spatial domain in comparison to a coarser resolution set-up of the same model. These are considerations that need to be held in mind, when evaluating the relative merits of fine resolution downscaling.

In year 2, work in Project 6 will investigate and attempt to correct the spurious patterns appearing in the innermost domain. Case study experiments will be completed and assessed so to provide a skill based assessment on what model configuration(s) are most appropriate for subsequent GCM downscaling experiments. In the third year, links will be developed with Project 7: Rainfall data from the WRF simulations will be provided, to which bias-correction methods can be applied and the data will be used to drive hydrological models. This will allow an evaluation of whether the finer resolution rainfall data obtained using the WRF simulations produces improved runoff simulations.

Appendix 5.1: Definition of simple skill scores

Please find below a definition of the simple skill scores used to assess skill in simulating daily rainfall, as presented in Fig. 6.6 and 6.7 of this report.

- Bias score (a measure of over-/under-simulation of rainfall; Table A and Equation 1)
    - *A value of 1= unbiased forecast, whilst values smaller than one indicate under-forecast and values above one indicate over-forecast.*

- Simple accuracy score (fraction correct; Table A and Equation 2)
    - *This score takes values between 0 and 1, where the best score is 1*

- False alarm ratio (fraction of simulated events that were false; Table A and Equation 3)
    - *This score takes values between 0 and 1, where the best score is 0*

- Threat score (fraction of hits, relative to all forecasted or observed events; Table A and Equation 4)
    - *This score takes values between 0 and 1, where the best score is 1*

		Observation		Marginal of simulation ↓
		Yes	No	
Simulation	Yes	a (hits)	b (false alarm)	(a+b) total 'yes' for sim
	No	c (misses)	d (correct rejects)	(c+d) total 'no' for sim
Marginal of obs →		(a+c) total 'yes' for obs	(b+d) total 'no' for obs	

Table 5.5 Contingency table for simple skill metrics

$$B \quad \frac{a+b}{a+c} \quad \frac{\text{forecasted events}}{\text{observed events}} \tag{1}$$

$$ACC \quad \frac{a+d}{N} \quad \frac{\text{correct simulation}}{\text{all simulations}} \tag{2}$$

$$FAR \quad \frac{b}{a+b} \quad \frac{\text{false alarm}}{\text{simulated events}} \tag{3}$$

$$TS \quad \frac{a}{a+b+c} \quad \frac{\text{hits}}{\text{all forecasted or observed events}} \tag{4}$$

Project 7: Identification of improved methodologies for water availability projections

Teng, J.
CSIRO Land and Water

Timbal, B.
CAWCR, Bureau of Meteorology

Fiddes, S.
Melbourne University

Key findings

Two areas of modelling were explored this year: 1) relating monthly streamflow directly with rainfall and temperature using linear regression; and 2) assessing the effect of bias correction on future hydro-climate projections. The work undertaken during this initial year of the program will allow delivering a range of water availability projections of various methodological complexities and ensuring a robust understanding of impacts of climate change on water availability across Victoria.

A simple method to describe monthly streamflow based on linear regression of rainfall and temperature (Griffiths et al., 2014, submitted) was applied to 27 catchments across Victoria. Most catchments showed satisfactory results (explained variance in excess of 80 per cent) with some catchments (mostly located in Gippsland) showing less skill. This simple approach has proven its worth and will be applied across the 26 Victorian catchments to generate future streamflow projections using the daily meteorological analogue-based statistical downscaling of available CMIP5 models.

A thorough literature review was undertaken on the regional climate model (RCM) bias correction methods and the recent comparison studies. The best performing bias correction technique—distribution mapping—was assessed using daily precipitation series simulated by the Weather Research and Forecasting (WRF) model for eight Victorian catchments. The results confirmed the usefulness of distribution-based methods but also highlighted that when the bias is nonstationary, none of the methods can lead to satisfactory results. We also found that although bias correction does not seem to alter the change signals in RCM precipitation, it does introduce extra uncertainty in the change signals in runoff (Teng et al., 2014, drafted).

Background

The aim of this project is to provide information about model behaviour and methodological choices that can improve the reliability and usefulness of runoff projections for mid- to long-term future time horizons (2030 and 2090), which are needed for the next round of strategic planning for urban water supplies in 2016. Two research activities were planned for this year to explore the different aspects of modelling techniques.

Objectives

1. Investigate simple methods to relate gridded rainfall to streamflow observations for high-yield catchments and their applicability to future climate simulations;

2. Conduct a literature study of bias-correction techniques applied to climate change data. Test bias-correction methodologies using available climate change data sets in order to investigate the effect of bias correction on hydro-climate projections.

Activity 1: Reconstructing streamflow using rainfall and temperature

Introduction

The trends and variability of Victoria's water catchments are of upmost importance for governments and agencies to understand. Over the last 50 years significant declines in rainfall and streamflow in the Murray Darling Basin (MDB) have been observed and the occurrence of one of the biggest droughts in the MDB history was experienced. During the Millennium Drought (MD), Timbal (2009) showed that the rainfall deficits experienced from 1997–2009 were the most severe on record with similar surface water records set across the entire MDB (Leblanc et al. 2011). The specificities of the MD for the high rainfall, high streamflow area of the Great Dividing Range across Victoria, such as the greater Melbourne water catchment area, have not been fully detailed. Previous studies or relevance include an analysis up to 2007 of selected rain gauges across the State (Murphy et al., 2010) as well as analysis of the impact of the MD on the hydrology across South Eastern Australia as part of the SEACI program (e.g. Potter and Chiew, 2009; Potter et al., 2010) and other research initiative (Kiem and Verdon-Kidd, 2010). It is noted that declines runoff or streamflow are generally two to three times the magnitude of the respective decline seen in the precipitation for the MDB region (Post and Moran 2013) although this number, called elasticity (see Chiew, 2006 for a definition), can grow in excess of seven for catchment with very low annual streamflow as there is a marked nonlinear relationship between the elasticity and the annual streamflow (Murphy et al., 2010). In addition to the examination of the intensity and impact of the MD, research conducted to support the development of operational streamflow forecast for South Eastern Australia has investigated in details the importance of various climate drivers on Victorian streamflow (Wang et al., 2009; Kiem and Verdon-Kidd, 2009)

The objectives of this activity are:

- analyse trends and variability of 27 regional catchment streamflows across Victoria including Melbourne Water catchment area, with a particular focus on long term trends and the magnitude of the anomalies during the MD; and

- reconstruct the streamflow using an updated version of a simple statistical model, based on rainfall and temperature parameters, and assess its performance to capture variability of streamflow as well as long-term trends and the magnitude of the reduced streamflows during the MD.

27 catchments across Victoria were chosen for analysis, based on their streamflow, size and location relative to the Great Dividing Range (GDR). All 27 catchments show an overall declining trend from 1977–2012, with the catchments in the far west and east of the state showing the largest declines whilst those in the alps, or in close proximity to, show considerably lesser decline. The same is true when the average streamflow of the Millennium Drought (MD) is analysed compared to that of the 1977–2012 mean, which shows that the catchments most removed from the GRD experienced the biggest streamflow deficit. Beside the long term trends and decadal variability, interannual variability in rainfall and subsequent streamflow is looked at and related to well know modes of tropical sea surface temperature (SST) variability.

In order to reconstruct streamflow, a simple statistical model was used, based on rainfall and temperature parameters. A high correlation was found between the observed and reconstructed streamflow (average R=0.93) and whilst it was able to reconstruct the overall mean of the streamflow extremely well, it could only reconstruct about 79 per cent of the variance. In terms of the 1977–2012 trends observed in the streamflows, the reconstructions were on average able to capture the right magnitude whilst in most cases the MD deficits were underestimated.

Study area, data and method

- **The catchment data and locations**

Following discussions between the Department of Environment and Primary Industries (DEPI) and the Bureau of Meteorology, 24 catchments were chosen for their yield, size and location, aiming to represent a range of water regimes across the state of Victoria. These catchments were complemented by three catchments based on Melbourne's water resources and used in the preliminary study (Griffiths et al., 2014). The locations of these 27 catchments are seen in the topographic map in Fig. 5.52.

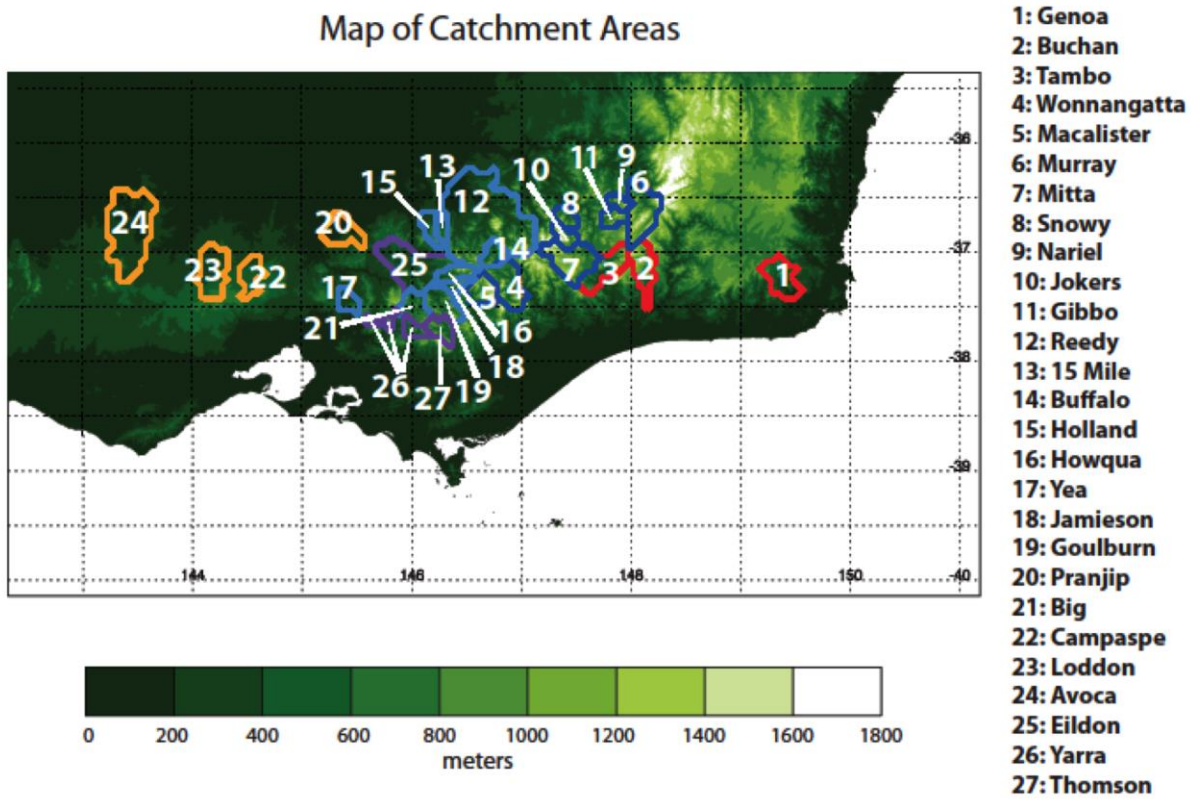

Fig. 5.52 Topographical map of the catchment boundaries.
Red boundaries signify the east subregion, the alps are shown in dark blue, the western slopes light blue, the far west in yellow and the Melbourne water catchments previously analysed in purple.

These 27 catchments have been divided into subregions based on location and the streamflow regime for ease of analysis, which are also displayed on the map; full characteristics of these catchments are provided in Appendix 5.2. The catchment streamflow data is a monthly data set and was provided by the DEPI and made available by the Bureau of Meteorology Extended Hydrological Predictions (EHP) section as part of the Hydrologic Reference Stations (HRS) network. The catchments do not have a common start period; for this study the bulk of the analysis is done considering the common time period for all catchments: 1977–2012. These catchments were selected in order to 'spread across contrasting hydro-climatic regions; the network includes unregulated streamflow stations in catchments with minimal effects of water resource development and land use change' (see full description at www.bom.gov.au/water/hrs/about.shtml).

- **The statistical model**

Griffiths et al. (2014) developed a statistical model that uses a linear combination of the current month's precipitation, the previous month's precipitation and the previous 12 months of precipitation to reconstruct the monthly streamflow of Melbourne's water catchments. It was found that without the

previous year's rainfall, which provided 'memory', the reconstructed streamflow was unable to capture the significant trends seen in the latter part of the time series thus confirming findings from other work which underpin the current Bureau operational streamflow forecast (Wang et al., 2009). The monthly average maximum temperature was also included in the linear model, however it was found to only improve the results marginally.

Results showed that the model could replicate the magnitude of the streamflow across the Melbourne catchments to a high degree, as well as the longer term declining trends; however, the trends and magnitude of the MD were less well captured. In this study, a further reconstruction has been added, where the 120-month (ten-year) rainfall memory is included in order to address the issue of capturing the MD. This model was then applied to the 24 regional catchments and the three Melbourne water catchments.

The streamflow calculated over the six different reconstructions is as follows: Rec1 uses just the current month's precipitation, Rec2 includes the previous month's precipitation, Rec3 then includes the current month's temperature, Rec4 includes the previous 12 months precipitation, Rec5 excludes the temperature parameter and Rec6 includes all parameters as well as the previous 10 years of rainfall. Griffiths et al. (2014) showed that Rec4 performed the best for the Melbourne catchments and whilst all reconstructions have been initially analysed in this study, the results of only best reconstructions, Rec4, Rec5 and Rec6 will be shown and discussed. The rainfall and temperature data used in this study is the Australian Water Availability Project (AWAP) data, where high quality station data is interpolated over a 0.05°x0.05° grid (Jones et al. 2009).

	Explained variance (R^2 %)			**Reconstructed variance (%)**		
Catchment	*Rec4*	*Rec5*	*Rec6*	*Rec4*	*Rec5*	*Rec6*
East	82.9	82.9	83.9	67.9	45.9	69.6
Alps	87.8	87.3	88.1	75.8	51.3	76.1
West Slopes	88.2	87.1	88.4	82.9	62.6	83.5
Far West	83.8	81.5	85.5	85.2	67.3	88.4
Melbourne	84.1	83.6	84.5	77.0	54.6	77.0
Average	**86.4**	**85.5**	**86.9**	**78.8**	**57.2**	**79.8**

Table 5.6 The explained variance (R^2) of the observed streamflow compared to the reconstructed streamflow and the percentage of observed streamflow variance reconstructed by the models for each catchment subregion (see Fig. 5.52).

Results and analysis

- **Reconstructing the streamflow**

Looking firstly to the subregional correlations of model to observed streamflow for the top three reconstructions, shown in Table 5.6, we can see that like the results previously found for the Melbourne region, the difference between Rec4 (current month's rain, previous month's rain, current month's temperature and previous year's rain) and Rec5 (same as Rec4 but without the temperature) change very marginally, with Rec4 generally performing better. Rec6 (same as Rec4 but with a ten year rainfall memory added), performs the best as a whole, with an overall average of R = 0.93 and an explained variance R^2 = 0.86. The catchment that performs the worst, Thomson, still has a high correlation of R = 0.88, whilst the best, Big, has a value of R = 0.96. These results indicate that this reconstruction performs substantially well across the state of Victoria. The time series of Rec6 for four representative catchments can be seen by the dashed grey line in Fig. 5.53. When the reconstructed mean is analysed compared to the observed mean, it is found that every reconstruction does a near perfect job of capturing the magnitude for each catchment (results not shown). The ability of the statistical model to reconstruct the variance however, while high is not perfect. Shown in Table 5.6,

the most complex reconstruction, Rec6, again performs the best with an overall ability to replicate 80 per cent of the streamflow variance. Overall, results show some differences according to the regional cluster identified earlier. On the western side of the Alps, most catchments do generally well, whilst in the Alps and to the east the reconstruction does less well. Interestingly, there is a negative correlation of R = –0.56 (significant at the 99 per cent level) between the elevation of the catchment and the ability for the model to reconstruct the variance. That finding may be indicative of a potential limitation of the reliability of the gridded data at high elevation where stations are few and far apart. It may also be indicative of complex hydrological process due to heterogeneous terrain. No attempt was made in the project this year to better understand the lower performance of the model for higher elevation catchments.

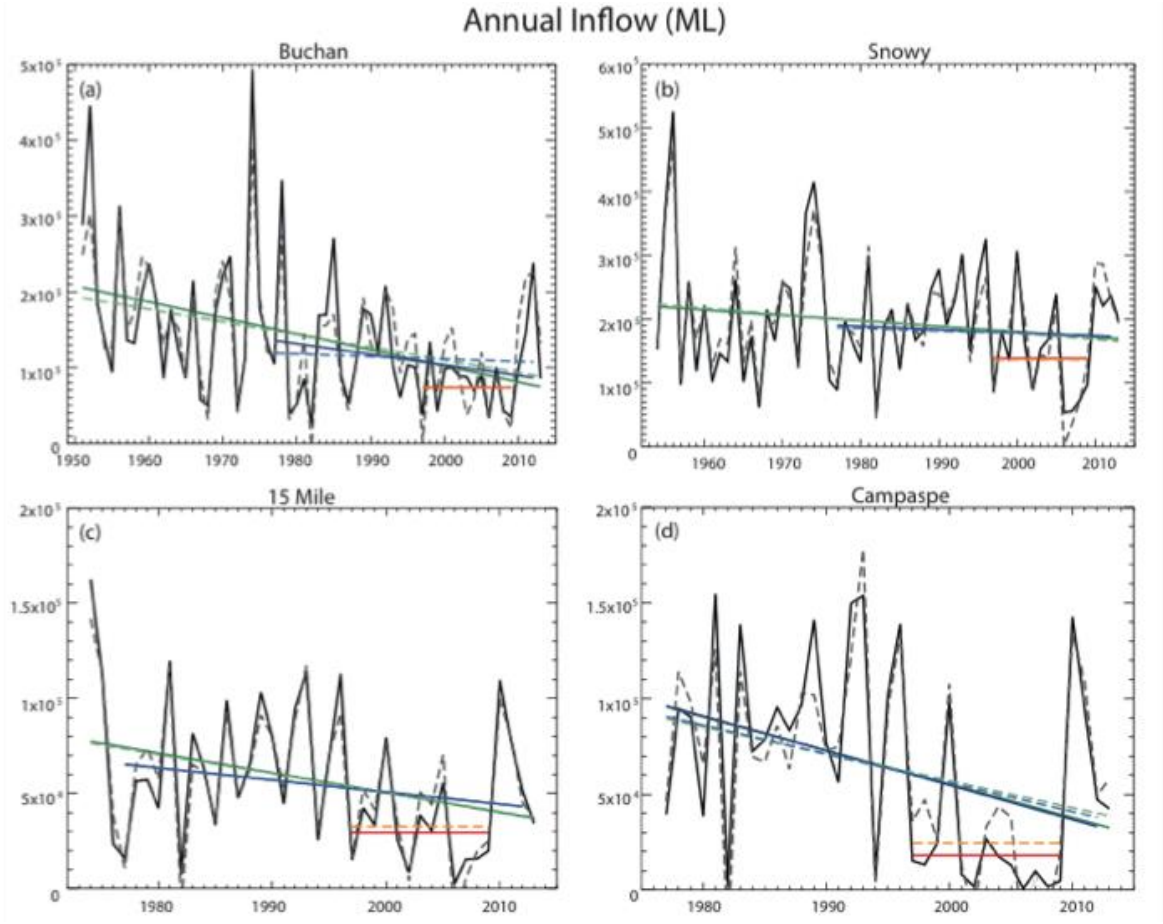

Fig. 5.53 The time series of a chosen catchment from each subregion for the entire available time period for (a) Buchan representing the east subregion, (b) Snowy representing the alps, (c) 15 Mile representing the western slopes, and (d) Campaspe representing the far west.
Solid lines indicate the observed streamflow and dashed lines represent the Rec6 streamflow. Trends for both the observed and reconstructed streamflow over the entire time period available are shown in dark/light green, the 1977–2012 trends are shown in dark/light blue and the 1997–2009 average is shown in red/orange respectively. Note different time and streamflow scales.

- **Observed catchment streamflow**

Fig. 5.53 shows the annual time series of the four representative subregions. Firstly, a declining trend (green solid line) can be seen across the entire time series and from 1977–2012 (blue solid line) for the four catchments shown. It is noteworthy that this is true of all 27 catchments bar one. Secondly, a significant drop in the magnitude and variability is observed in the Campaspe and Buchan streamflows during the MD, whilst in the 15 Mile catchment the reduction of streamflow is less obvious, and even

more so in the Snowy catchment. Significant recovery can be seen after the MD, where streamflows return to generally average values.

The 1977–2012 linear trends (ML/decade as a percentage of the mean), are shown across all catchments (Fig. 5.54a) and are averaged over subregions in Table 5.7. The catchments that experience little influence from the GDR show the biggest declining trends over this period, with Avoca and Genoa catchments experiencing trends of –31.6 per cent and –29.7 per cent respectively. Areas that experience higher rainfall due to orographic enhancement, such as those in the alpine subregion and to the west of the alps have experienced a far less dramatic reduction in streamflow, with the Jokers catchment even experiencing a change of +1 per cent. These results confirmed the dependence of elasticity on mean streamflow (Murphy et al., 2010). It is worth noting however that some numbers in percentage terms may be large but small in absolute terms such as changes during the dry season.

Annual						
	MD anomalies (%)			**1977–2012 decadal trends (%)**		
Catchment	**Obs**	**Rec4**	**Rec6**	**Obs**	**Rec4**	**Rec6**
East	–48.3	–36.6	–42.1	–16.7	–2.1	–8.9
Alps	–21.8	–23.5	–23.6	–2.0	–4.2	–4.3
West Slopes	–37.5	–34.5	–35.1	–8.8	–10.5	–11.2
Far West	–73.0	–56.1	–62.1	–27.6	–16.5	–24.4
Melbourne	–33.0	–25.5	–25.8	–8.7	–9.6	–9.3
Average	**–38.8**	**–33.7**	**–35.4**	**–10.4**	**–8.5**	**–10.6**

Seasonal												
	MD anomalies (%)						**1977–2012 decadal trends (%)**					
	WET			**DRY**			**WET**			**DRY**		
Catchment	**Obs**	**Rec4**	**Rec6**	**Obs**	**Rec4**	**Rec6**	**Obs**	**Rec4**	**Rec6**	**Obs**	**Rec4**	**Rec6**
East	–39.7	–33.2	–39.3	–49.1	–44.7	–47.6	–21.7	–4.2	–11.6	–0.4	4.7	0.6
Alps	–19.6	–22.1	–22.5	–27.0	–29.0	–28.1	–5.6	–6.9	–7.4	15.8	9.2	10.7
West Slopes	–36.2	–33.6	–34.7	–44.4	–40.9	–37.9	–13.0	–13.5	–15.1	27.6	16.1	22.1
Far West	–74.3	–56.0	–63.3	–77.4	–65.1	–56.2	–36.1	–22.0	–32.8	66.3	47.6	71.2
Melbourne	–26.6	–25.3	–25.5	–29.6	–24.8	–24.7	–10.3	–11.3	–11.1	0.0	–2.3	–1.8
Average	**–36.3**	**–32.5**	**–34.8**	**–43.0**	**–39.6**	**–37.3**	**–14.9**	**–11.5**	**–14.6**	**23.7**	**15.4**	**21.0**

Table 5.7 MD anomalies from 1977–2012 mean and the 1977–2012 decadal trends (both shown as a percentage of the 1977–2012 mean) for the annual, wet (May–November) and dry (December–April) seasons of the observed streamflow and the reconstructed (Rec6) streamflow for each catchment.

Fig. 5.54b shows the magnitude of the 1977–2012 decadal trends as calculated by Rec6. Comparing it to Fig. 5.54a we can see that generally, the reconstructions do quite well. More specifically, in the alpine region, the trend is often over estimated (by about 5 per cent), whilst in the far west and particularly the east it is underestimated (by 5–30 per cent), this can be seen in Table 5.7. The catchments in the western slopes tend to have trends the closest to those of the observations. As noted earlier, Griffiths et al. (2014) found that Rec4, whilst able to capture the long term trends satisfactorily, was unable to capture the full extent of the MD anomalies. In this work, although using a different time period, the added reconstruction with the long term memory (Rec6) was able to do a better job, whereby both the 1977–2012 trend and the MD anomaly were better simulated by Rec6 than Rec4 (see Table 5.7).

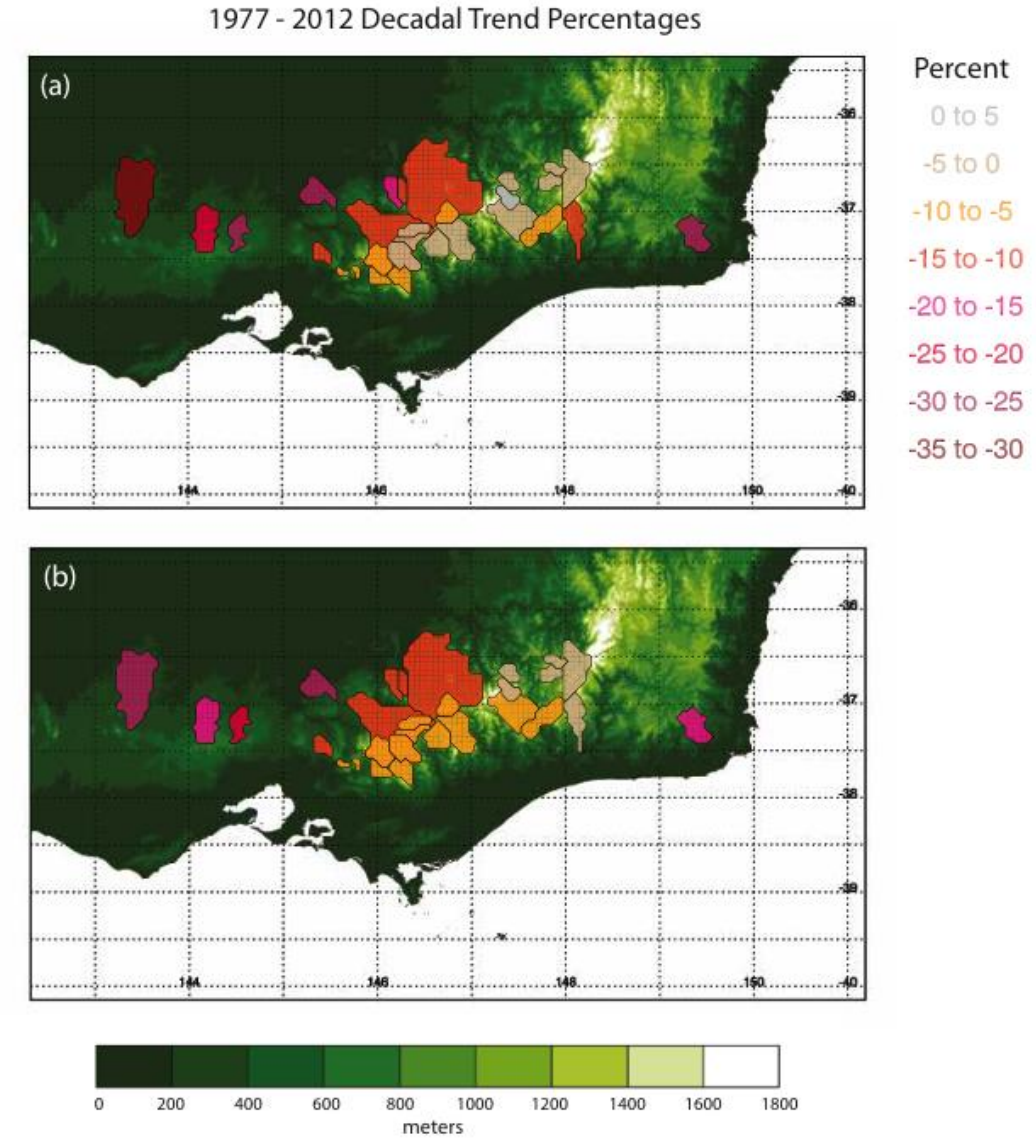

Fig. 5.54 The 1977–2012 trends (ML/decade) as a percentage of the 1977–2012 mean for (a) the observed catchment streamflow and (b) Rec6 catchment streamflow.

Previous work as part of SEACI identified that ongoing rainfall trends across south-eastern Australia have a marked seasonal cycle being only observed during the cool season (Timbal, 2009; CSIRO, 2012) due to the relationship with strengthening belt of high pressure being important at this time of the year (Timbal and Drosdowsky, 2013). This is evaluated here using the streamflow season during the cool time of the year (May–November) and dry part of the year (December–April). It is a shift of 1 month compared to the cool and warm seasons used for rainfall which reflect the time lag response of streamflow to rainfall.

The wet seasons show declining trends spatially similar to the annual trends; however for the dry season, the majority of catchments have actually experienced an increase in the amount of streamflow received each year, with catchments in the far west reporting the biggest increases and only the catchments south-east of the GDR (including Melbourne catchments) not experiencing increased dry season streamflows (Table 5.7). However, it must be noted that trends are calculated as a percentage of the 1977–2012 mean and for all catchments the dry season mean streamflow is far less than that of the wet season. Subsequently, increases in the dry season, whilst still experienced, are generally

insignificant relative to the annual trends. Nevertheless, these differences in sign are an indication that what is causing strong declines in the wet season has little influence on the dry season. The relationship of rainfall to STR intensity has been documented to behave in this way (Timbal and Drosdowsky 2013, Griffiths et al. 2014).

Beyond the linear trends, the observed magnitude of the MD reduced streamflow and the ability of the reconstructed series to match it is of interest (Fig. 5.55). As per the long-term trend, catchments in, or in close vicinity to the GDR experienced a far less dramatic drop in annual streamflow over this 12-year time period than those in the east and far west of Victoria (see Table 5.7). Once again the Avoca catchment has experienced the biggest deficit, with an 87 per cent decline in the average streamflow, whist the Mitta and Jokers catchments have experienced less than a 20 per cent decline over the same period. Whilst the seasonal MD anomalies are larger in the dry season than the wet percentage-wise (see Table 5.7), again, due to the wet season receiving climatologically far more streamflow, changes in the wet season are what predominantly drove the MD.

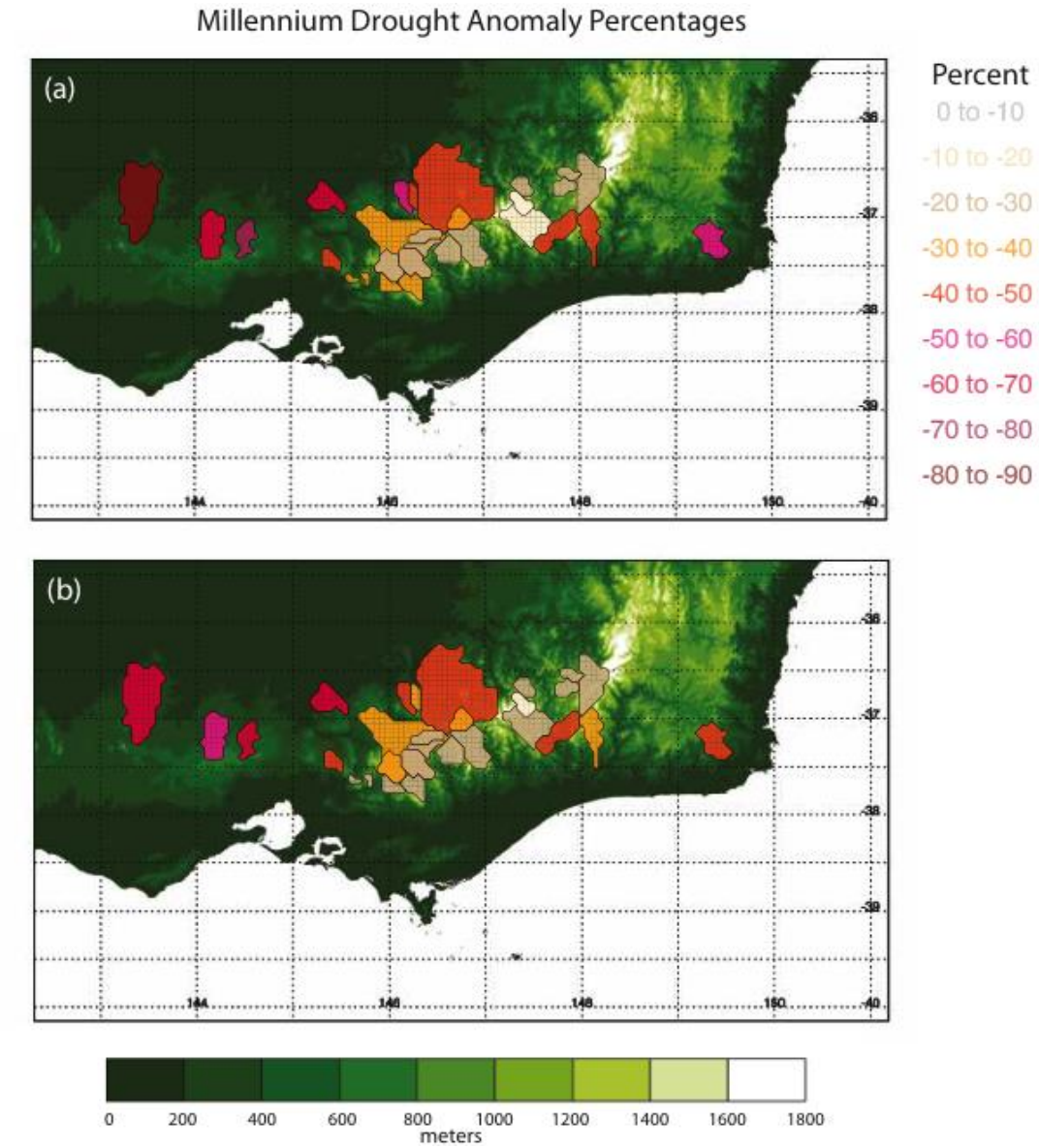

Fig. 5.55 The 1997–2009 MD anomalies as a percentage of the 1977–2009 mean for (a) the observed catchment streamflow and (b) Rec6 catchment streamflow.

The MD anomalies calculated by Rec6, shown in Fig. 5.55b and Table 5.7, show similar patterns of performance to that of the decadal trends. Those in the far west are underestimating trends by about 10–20 per cent whilst the catchments in the Alps, the western slopes and the east perform rather well although still generally underestimating by up to about 10 per cent. As far as the wet and dry seasonal trends go, the far east and west are again less well simulated than those of the western slopes and alps, for both the 1977–2012 trend (see dashed lines in Fig. 5.56) and the MD anomalies (Table 5.7); however, as a whole Rec6 performs well.

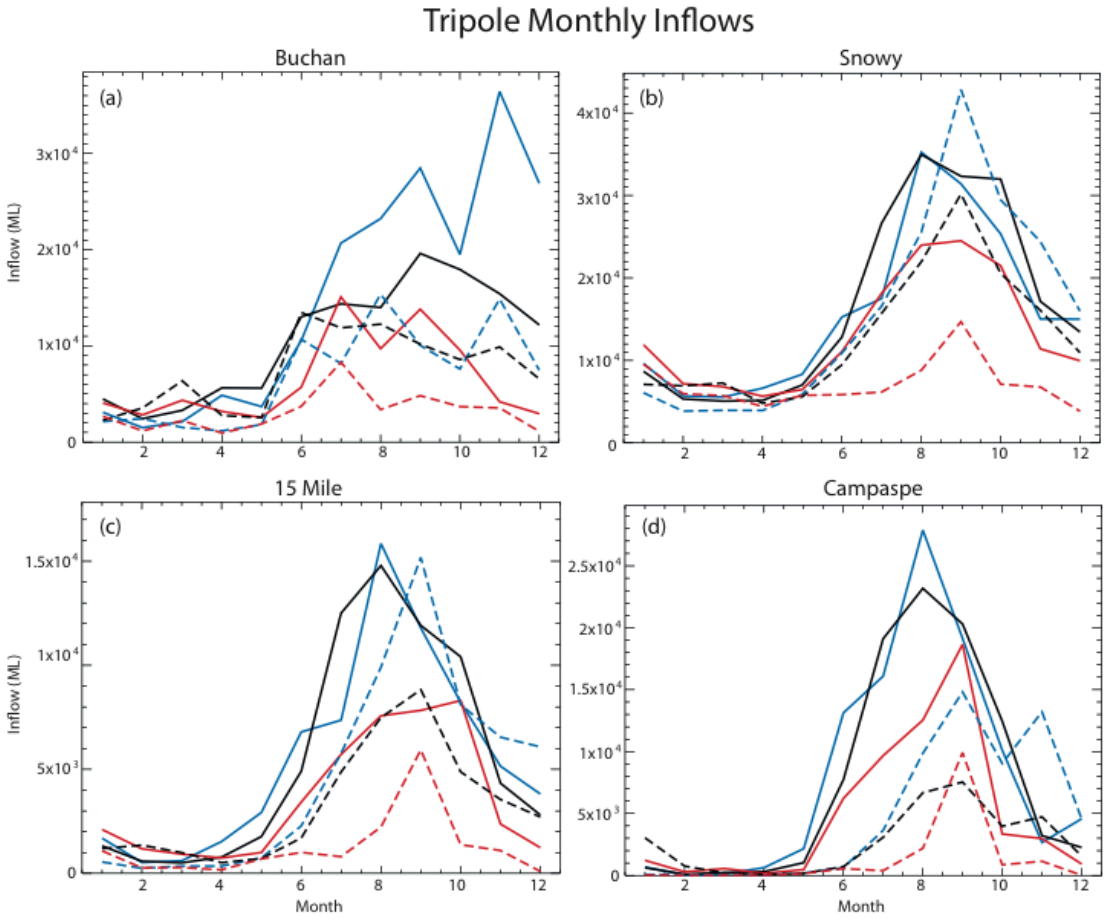

Fig. 5.56 Monthly streamflows for the four chosen catchments during different tripole modes (a) Buchan, (b) Snowy, (c) 15 Mile and (d) Campaspe. Black lines show indicate the overall average of monthly streamflow while blue (red) lines show the average monthly streamflow experienced during years of a positive (negative) tripole. Solid lines represent the period 1977–1996 and dashed lines the period 1997–2012. Note a positive or negative tripole is considered when the tripole is ±0.8 times the standard deviation.

- ***Inter-annual variability and long-term trends***

Rainfall in the MDB during the MD was approximately 12 per cent lower than the 1900–2012 average (CSIRO 2010), and this was found to be predominantly a result of changes in the intensity of the subtropical ridge (Timbal and Drosdowsky 2013). Furthermore, Griffiths et al. (2014) reported that the Melbourne catchments' response to the MD was not able to be explained by modes of tropical variability as have other studies in the past (Kiem and Verdon-Kidd. 2009; Wang et al. 2009). This is supported by catchments in the east, far west and also some of those in the southern end of the alpine region when the streamflow is analysed in terms of the tripole index developed by Timbal and Hendon (2011), which acts as a proxy of tropical SST variability from modes such as the El Niño Southern Oscillation and the Indian Ocean Dipole. The way it is compute, a positive tripole is associated with conditions favouring rainfall across Victoria.

The composite of streamflow during years of positive and negative tripole compared to that of the average for years before and after the commencement of the 1997 drought are shown in Fig. 5.56 and Table 5.8. Fig. 5.56a and Fig. 5.56d, for Buchan and Campaspe (and the subregions east and far west), show that no matter the sign of the tripole, the streamflow for the 1997–2012 period was always less than that of the streamflow prior to this period. These results are in support of the Griffiths et al. (2014) findings.

However, Table 5.8, Fig. 5.56b and Fig. 5.56c show that for the catchments within or close to the GDR, the picture is less clear. Where the monthly streamflow for a positive tripole before or after 1997 tends to be of similar magnitude, the average or negative tripole modes are again less for 1997–2012 than for 1977–1996. This suggests that for catchments within the Alps, tropical modes of variability, when in rain producing mode, still have a large effect on the catchment streamflow and can help, with the aid of orographic enhancement, overcome rainfall deficits caused by other factors such as the subtropical ridge intensity. The increased difference between positive and negative tripole years before and after the mean streamflow reduction in 1996–97 is consistent with the larger elasticity observed during the MD (CSIRO, 2012) and the increase of elasticity with smaller mean inflow (Murphy et al., 2010).

	1977–1996				**1997–2012**			
Catchment	Positive	Negative	All	Difference (%)	Positive	Negative	All	Difference (%)
East	178	62	110	105.9	56	30	68	37.6
Alps	254	203	262	19.2	250	118	216	61.1
West Slopes	223	174	240	20.5	196	60	159	85.7
Far West	99	58	95	42.6	54	17	31	117.1
Melbourne	653	573	689	11.6	534	240	474	62.1
Average	**257**	**197**	**261**	**22.7**	**213**	**87**	**182**	**69.0**

Table 5.8 Average annual streamflow (GL) received for years when the tripole is positive, negative and for all for years over the time periods 1977–1996 and 1997–2012.
The difference of streamflow between the positive and negative tripole years as a percentage of the mean (all years) is also shown.

Furthermore, Table 5.8 shows that the difference between the positive and negative tripole years (compared to that of the mean) is much larger for only the east catchments in the earlier time period, whilst the catchments in the alps and west show much larger differences in the latter period, possibly indicating a shift in the influence the tripole years have over streamflow.

Conclusions

Water catchments across the entire Victorian state have experienced declines in the total streamflow received each year since at least 1977. Interestingly, it is seen that catchments in close proximity to the GDR show much weaker trends in percentage terms than those removed from the GDR's influence on local weather/hydrology. It is unclear what has helped buffer the effect of declining trends in rainfall for the highest elevation catchments; the simple approach relied upon here does not provide insight into the particular hydrology of these catchments which could explain this finding. The magnitude of the MD anomalies experienced by the regional catchments showed a similar pattern, where catchments in the alps showed changes of ~10–30 per cent whilst catchments in the far west and east of the state experienced changes of ~40–90 per cent. When the MD monthly streamflows are analysed in regards to the tropical SST tripole, it is found that the tropical modes of variability were unlikely to have played a major role in causing the MD, which supports results published as part of the SEACI program

and more recently by Griffiths et al. (2014). However, these tropical modes of variability may have mitigated the severity of the MD for catchments in the vicinity of the Alps.

Using the updated statistical model developed by Griffiths et al. (2014) to reconstruct the regional catchments, it has been found that by including the 10 year memory of rainfall in the reconstruction (Rec6), as well as the other rainfall and temperature parameters initially used in Rec4, the model was able to produce improved results, especially in that of capturing the magnitude of the MD. The correlation between streamflow and Rec6 was very strong; however, still, an average of only 80 per cent of the variance was able to be reconstructed. The 1977–2012 decadal trends produced by Rec6 were on average of the correct magnitude and the MD anomalies, whilst still underestimated across most catchments to varying degrees, were in generally an improvement on Rec4.

The updated statistical model is simple to apply and will provide a useful tool to make initial estimates of projected monthly streamflows from rainfall projections which can then be compared with streamflow/runoff projections derived using more sophisticated rainfall–runoff modelling approaches.

Activity 2: Bias-correction techniques for climate change data

Downscaling is commonly used in studies that investigate the impact of climate change on water to bridge the gap between low-resolution Global Climate Model (GCM) simulations and regional-scale climate required by hydrological models. Most studies investigating the impact of climate change on hydrology (including SEACI) rely on a simple empirical scaling—also referred to as 'change factors (CFs)', 'perturbation method', or 'delta-change method'—to derive the future climate projections at catchment scale from GCMs. With the latest advances in Regional Climate Models (RCMs), and the increasing availability of RCM simulations, using RCMs as a downscaling technique is gaining more and more popularity in recent impact studies. However, it is well established that precipitation simulations from RCMs are biased, due to inherited errors from the driving GCM, in addition to those systematic RCM model errors, caused by imperfect conceptualization and parameterizations, inadequate length and quality of reference data sets, or insufficient spatial resolution. The effect of such biases on impact studies is well recognised and various bias-correction methods have been developed in the past decade (Schmidli et al. 2006; Boe et al. 2007; Lenderink et al. 2007; Piani et al. 2010a; Johnson and Sharma 2012).

There have been many studies that compared and evaluated different bias-correction methods (Themeßl et al. 2011; Berg et al. 2012; Teutschbein and Seibert 2012; Teutschbein and Seibert 2013; Gudmundsson et al. 2012; Lafon et al. 2013; Chen et al. 2013; Gutjahr and Helnemann 2013). In general, all of these studies agree that distribution-based bias correction methods give the best performance in terms of reproducing observed climate, whereas mean-based methods, in particular, linear scaling is almost always ranked as the least skilled bias correction method.

Building on the knowledge from previous comparison studies, we assessed the best performing bias-correction technique – distribution mapping was assessed using daily precipitation series simulated by the Weather Research and Forecasting (WRF) model for eight catchments in southeast Australia. The performance of three distribution-based techniques, each with increased degree of dependency on the training data, was evaluated along with their follow-on effects on hydrological impact studies. The effect of bias correction on the relative change in selected precipitation and simulated runoff characteristics was also explored.

Study area and data

The study area was located in the southern Murray–Darling Basin, Australia (Fig. 5.57). This area has experienced a prolonged drought, the so-called Millennium Drought, for 10–15 years since the mid-90s (Chiew et al., 2010). Eight meso-scale catchments from the Loddon, Campaspe and Goulburn River Basins with areas from 250 to 1033 km^2 were selected in this study. The catchments were mainly unimpaired with continuous climate and streamflow measurements available for the assessment period (1985–2000). The period that was not affected by the drought (1985–1992), and the period that was (1993–2000), were chosen as training period and testing period respectively, and then switched over for cross-examination. Compared to the studies that use 'odd-year/even-year' or 'leave-one-out' validation methods, the design of this experiment puts the bias-correction methods to a strict test so that the impact can be scrutinised.

Fig. 5.57 Map showing the eight study catchments, and their locations within the major river basins devised by the Australian Water Resources Council (AWRC).

Observed daily precipitation were derived from 0.05° (~5 km) gridded climate surfaces and averaged over each catchment (Jeffrey et al., 2001). The daily potential evapotranspiration (PET) sequences used in the hydrological modelling were calculated from SILO climate variables using Morton's wet environment algorithms. Measured daily streamflow data were sourced from a previous study and used to calibrate the rainfall–runoff models.

Daily precipitation series for the period 1985–2000 simulated using the Weather Research and Forecasting (WRF) model were obtained from Evans and McCabe (2010). WRF was implemented on a 10 km grid using the lateral boundary conditions from the National Oceanic and Atmospheric Administration's Centers for Environmental Prediction (NCEP)/National Center for Atmospheric Research (NCAR) Reanalysis data. The daily precipitation series for each catchment were aggregated from the WRF simulation by averaging all the grid cells over the catchment.

Method

- **Bias-correction methods**

Daily precipitation was the main variable to be adjusted in this study. Three distribution-based bias-correction methods were assessed and a linear scaling method was also included as a benchmark.

Linear Scaling (LS) finds a linear transformation where a single free parameter subject to calibration is used to match the RCM means to those of the observations. Distribution mapping establishes a relationship so that the distribution of the mapped variable matches the distribution of the observed variable. If the distribution of the variable is known, a probability integral transform can be applied. The transformation can be achieved by using theoretical distributions or empirical distribution. In this study, we assessed three different distributions: 1) the Gamma distribution (DMG); 2) A newly developed double Gamma distribution (DM2G); and 3) the empirical distribution (QM).

- **Hydrological modelling (HM)**

Two lumped conceptual daily rainfall–runoff models: GR4J (Perrin et al., 2003) and Sacramento (Burnash et al., 1973) were used to model runoff. For the application here, the numbers of parameters calibrated were four for GR4J, and 14 for Sacramento. In this study the selection of the hydrological model did not have large impact on the conclusion due to the relatively small uncertainty sourced from hydrological models (Chen et al., 2011; Teng et al., 2012). Therefore only results from GR4J are discussed in this report here after. The models were calibrated against the observations and the optimised parameters were used with WRF precipitation before and after bias correction to estimate impact of bias correction on runoff. The same PET dataset calculated using observed climate variables was used throughout the hydrological modelling.

- **Evaluating performance**

The evaluation of the bias-correction methods was based on a split-sample cross-validation approach. Total of 16 years of data (1985–2000) were split into two periods each with eight years of data (1985–1992 and 1993–2000). The bias-correction methods were trained using one period and tested against the same period ('same') as well as the other period ('cross'), and vice versa. Similarly, the hydrological models were calibrated using one period and the parameters were used in the 'cross' experiments treating the testing period as though we have no other information except RCM runs, as would be the case for a future period.

To investigate the impact of bias-correction methods on precipitation, we compared the RCM precipitation before and after bias correction with the observations using statistical indices: annual and

seasonal means, 99th percentile precipitation as an indicator of high precipitation events, number of dry days (daily precipitation less than 0.1mm) per year as an indicator of low precipitation, and 99th percentile of three-day and five-day cumulative precipitation as indicators of high runoff generating events. The runoff modelled using RCM precipitation before and after bias correction was evaluated against modelled runoff using observed precipitation for the runoff characteristics including annual and seasonal means, 99th percentile runoff as an indicator of high flow events, number of low flow days (daily runoff less than 0.01mm) as an indicator of low flow. We also looked at the effect of bias-correction methods on change signals by comparing the relative difference in precipitation and runoff between the two periods derived from various methods.

Results

Fig. 5.58 shows the percentage differences in raw RCM and bias corrected RCM precipitation relative to observations for annual and seasonal means, 99th percentile precipitation, 99th percentile three-day and five-day cumulative precipitation, and the differences in number of dry days per year. Generally, the raw RCM precipitation exhibits negative errors in annual and seasonal means, with larger negative errors (away from zero) in the drier period (1993–2000). The 99th percentile precipitation is largely overestimated in one period (1985–1992) and underestimated in the other. The raw RCM performs quite well in reproducing 99th percentile three-day and five-day cumulative precipitation but slightly overestimates dry days (precipitation < 0.1mm). The impact of the bias-correction methods is discussed in the following sections.

- **Impact on precipitation**

The calibration results (when testing on the same period as the training period, denoted by '_same'), as expected, show that all of the bias-correction methods are able to improve annual and seasonal means of the precipitation (as shown by LS_same, DMG_same, DM2G_same, and QM_same boxplots in annual and seasonal mean plots in Fig. 5.58). For instance, the median errors in raw RCM annual means are –9.1 per cent and –22.5 per cent for the two periods respectively, LS corrects them to perfect (0 per cent and 0 per cent), followed by DM2G (–0.3 per cent and –0.2 per cent), QM (0.4 per cent and 0.6 per cent), and DMG (–0.7 per cent and –0.7 per cent). Only distribution mapping methods (DMG, DM2G, and QM) are able to reduce the errors in the high and low precipitation characteristics, in particular, QM performs exceptionally well in reproducing 99th percentile precipitation and number of dry days per year. LS is not only unable to reduce the errors in high and low precipitation characteristics, but also increases the errors in some cases as seen in 99th percentile precipitation for 1985–1992 period (period I) and number of dry days per year for 1993–2000 period (period II). This is consistent with the findings from previous studies (Teutschbein and Seibert, 2012; Chen et al., 2013).

However, the cross-validation results (when testing on the period different from the training period, denoted by '_cross') seem to be period dependent with most of the bias-correction methods reducing the raw RCM errors (closer to zero) in period II but increasing the raw RCM errors (away from zero) in period I except for DJF mean precipitation, where all the bias-correction methods increase the errors in both periods. Although DM2G performs better (shown by lower median errors given by DM2G_cross in Fig. 5.58) compared to other bias-correction methods in nearly all precipitation characteristics, the difference between the bias-correction methods is not prominent compared to the overall large overestimation in period I and underestimation in period II. The cause of this 'period dependency' is discussed in the next section. It is worth pointing out that the errors in DJF and MAM mean precipitation are generally larger than other seasons, because the amounts of precipitation in DJF and MAM are smaller in these catchments as they are winter precipitation dominated with more than 60 per cent precipitation coming from JJA and SON.

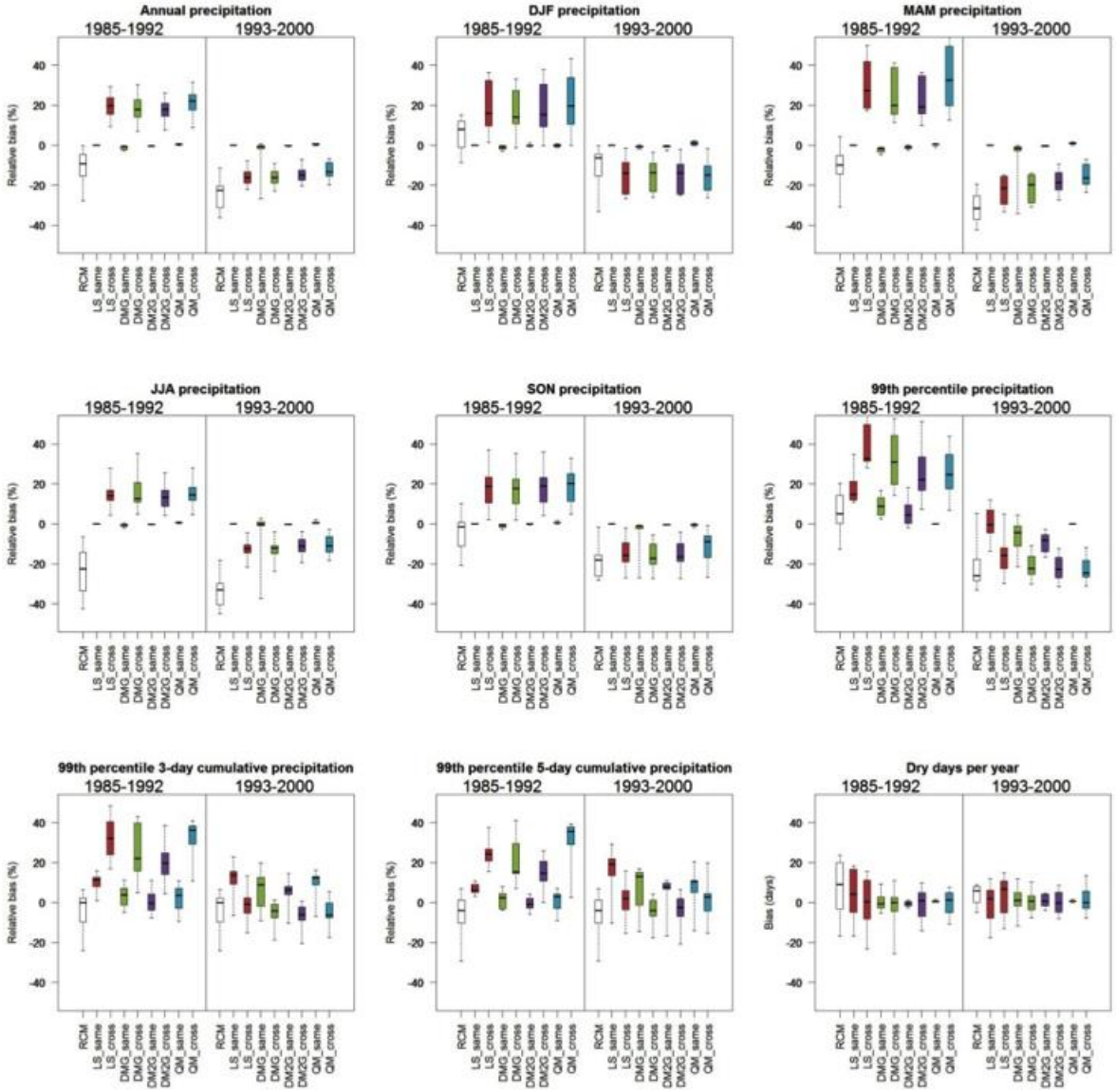

Fig. 5.58 The percentage differences in raw RCM and bias corrected RCM precipitation relative to observations (using bias correction methods LS, DMG, DM2G, and QM) for annual and seasonal means, 99th percentile precipitation, 99th percentile three-day and five-day cumulative precipitation, and the differences in number of dry days per year. Each boxplot is constructed using values from eight catchments, the box represents the interquartile range and the whiskers represent minimum and maximum values (same applies to all boxplot figures below). The two panels in each plot represent the two testing periods. The LS_same, DMG_same, DM2G_same, and QM_same boxplots correspond to the calibration results, whereas the LS_cross, DMG_cross, DM2G_cross, and QM_cross boxplots correspond to the cross-validation results.

- **Impact on runoff**

Fig. 5.59 presents the relative differences in runoff characteristics simulated by GR4J using raw RCM and bias corrected precipitation when compared to those modelled using observed precipitation. The two panels in each plot represent the testing periods, and the boxplots corresponds to the '_same' and '_cross' results in Fig. 5.58. To put the comparison in perspective, the errors sourced from hydrological models are also presented in each plot where 'HM_calib' represents the calibration error (comparing hydrological model simulation driven by observed precipitation with observed streamflow), and 'HM_cross' represents the cross-validation error (comparing hydrological model simulations driven by observed precipitation using parameters calibrated to the same period with those using parameters calibrated to a different period).

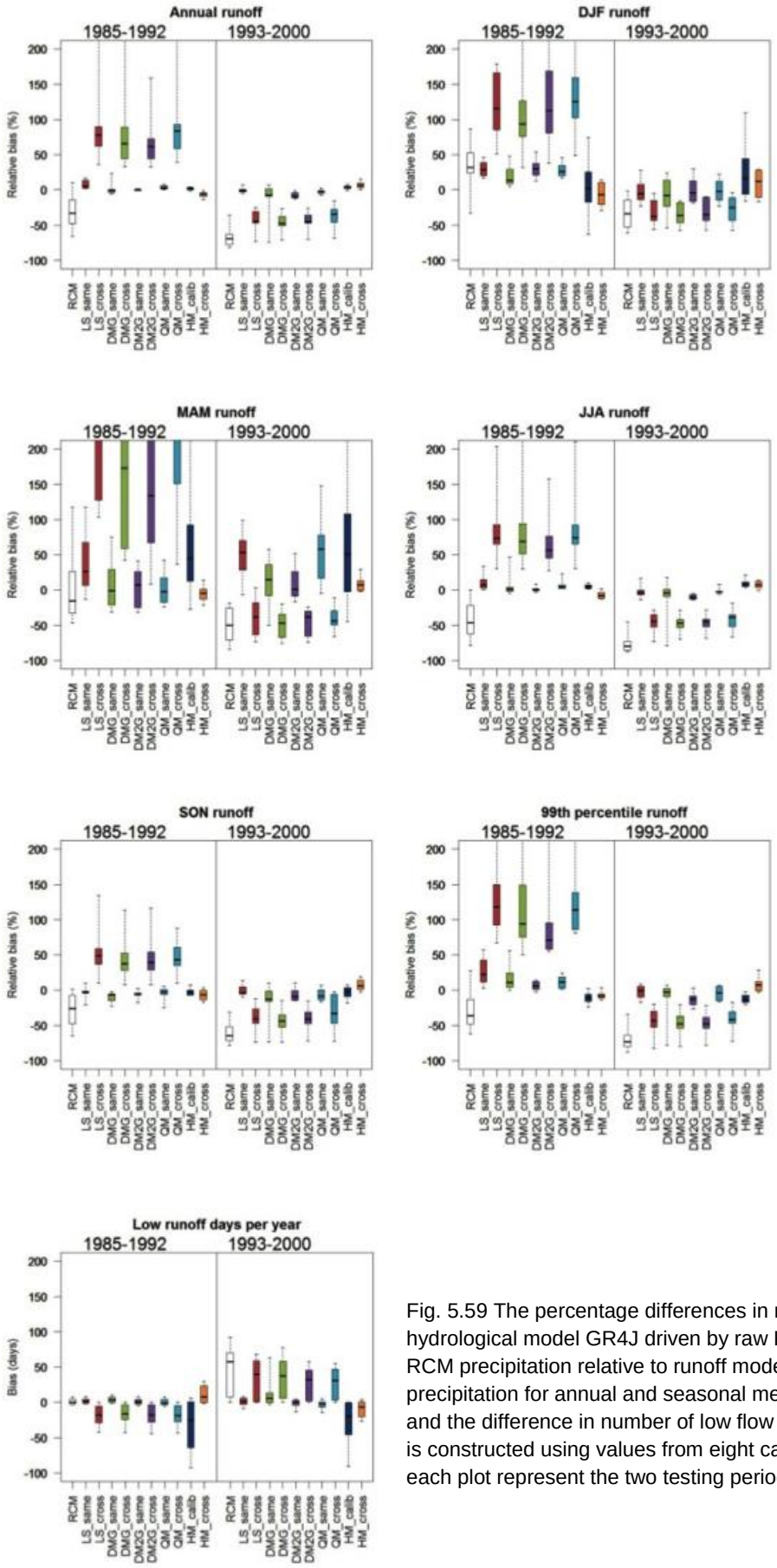

Fig. 5.59 The percentage differences in runoff modelled using hydrological model GR4J driven by raw RCM and bias corrected RCM precipitation relative to runoff modelled using observed precipitation for annual and seasonal means, 99th percentile runoff, and the difference in number of low flow days per year. Each boxplot is constructed using values from eight catchments. The two panels in each plot represent the two testing periods.

The errors in runoff show a similar pattern as those in precipitation, but with an amplified magnitude. For instance the median errors in mean annual runoff simulated using raw RCM precipitation are increased to –33.1 per cent and –69.5 per cent for the two periods respectively. The calibration results show that LS is no longer able to correct the errors in annual and seasonal mean runoff to 0 due to errors in high percentile precipitation (see 99th percentile precipitation plot in Fig. 5.58), and consequently, in high runoff. QM is not performing very well in correcting the high and low runoff characteristics as it does in high and low precipitation characteristics, which may relate to its weakness in reproducing three-day and five-day cumulative precipitation (as shown in Fig. 5.58). This highlights the importance of precipitation sequencing in runoff production.

The cross-validation results show that, after bias correction, the median errors in period I are increased to 61.6 to 83.8 per cent by various bias-correction methods. While the median errors in period II are decreased, a median error of –34.3 to 47.7 per cent is still considered large compared to the conventional hydrological model error of less than 10 per cent as shown by HM_calib and HM_cross.

- **Impact on change signals**

Fig. 5.60 presents the differences in precipitation change signals when comparing raw RCM simulation and bias corrected RCM simulations. Here, the ‘change’ is defined as percentage difference between period II and period I relative to period I. The baseline in Fig. 5.60 is the change derived from raw RCM simulations; the ‘difference’ is between the baseline and the change derived from bias-corrected RCM simulations.

For majority of precipitation characteristics, the bias-correction methods seem to produce similar differences as given by the raw RCM, except for three-day and five-day cumulative precipitation, where the raw RCM does better than bias-corrected simulations. While the bias-correction methods do not alter changes in precipitation means, they do modify changes in high precipitation characteristics as shown with large range of differences given by LS, DMG, DM2G, and QM in 99th percentile precipitation, 99th percentile three-day and five-day cumulative precipitation plots in Fig. 5.60. The follow-on effects on runoff can be seen in Fig. 5.61 that shows differences in runoff corresponding to Fig. 5.60. The differences in runoff changes are much larger compared to precipitation. The bias-correction methods alter changes in every runoff characteristics, especially in high flow indicator (Fig. 5.61).

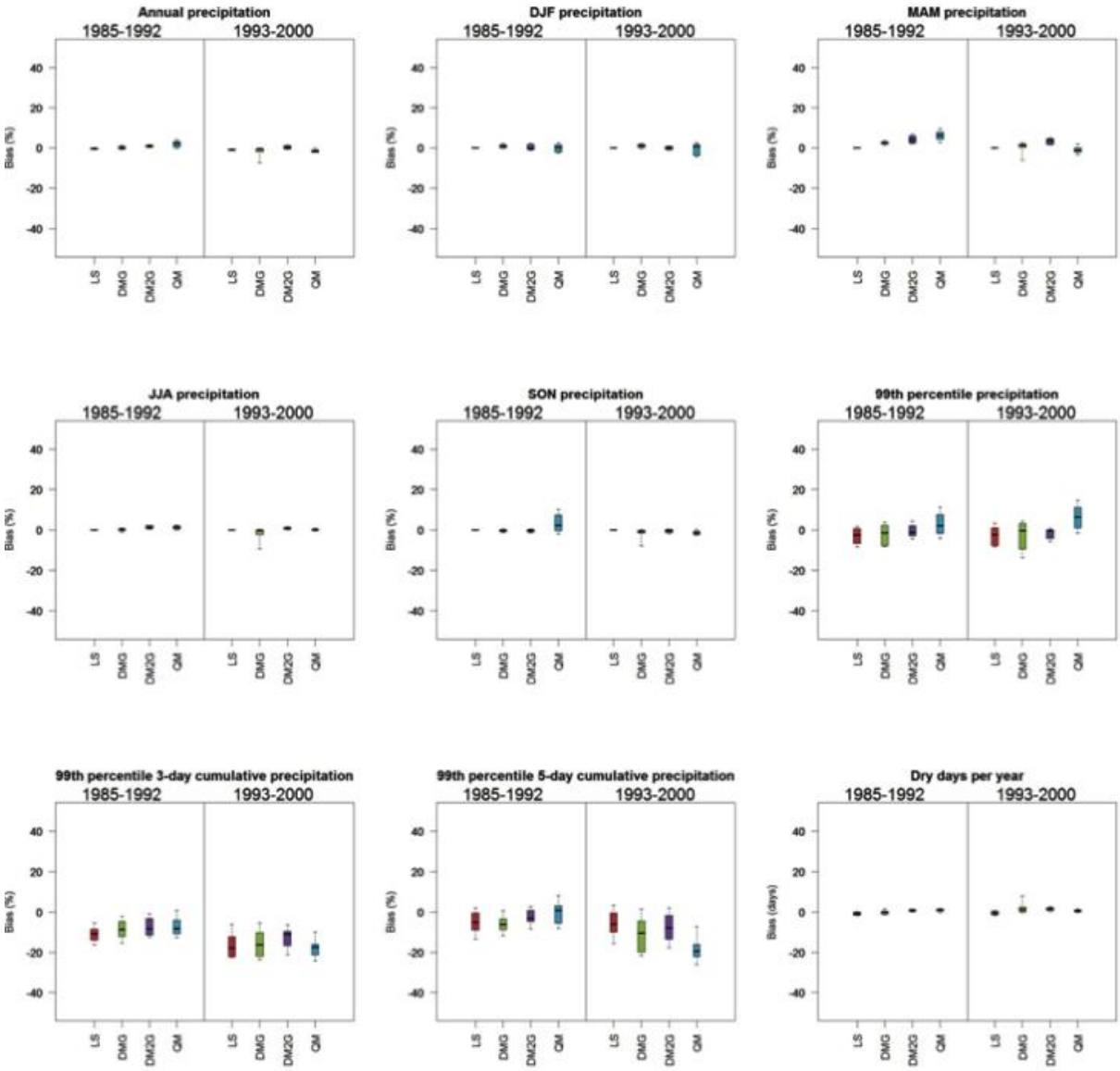

Fig. 5.60 The differences between raw RCM and bias-corrected RCM modelled change in precipitation characteristics between the two periods. The left and right panels indicate the testing periods in each case.

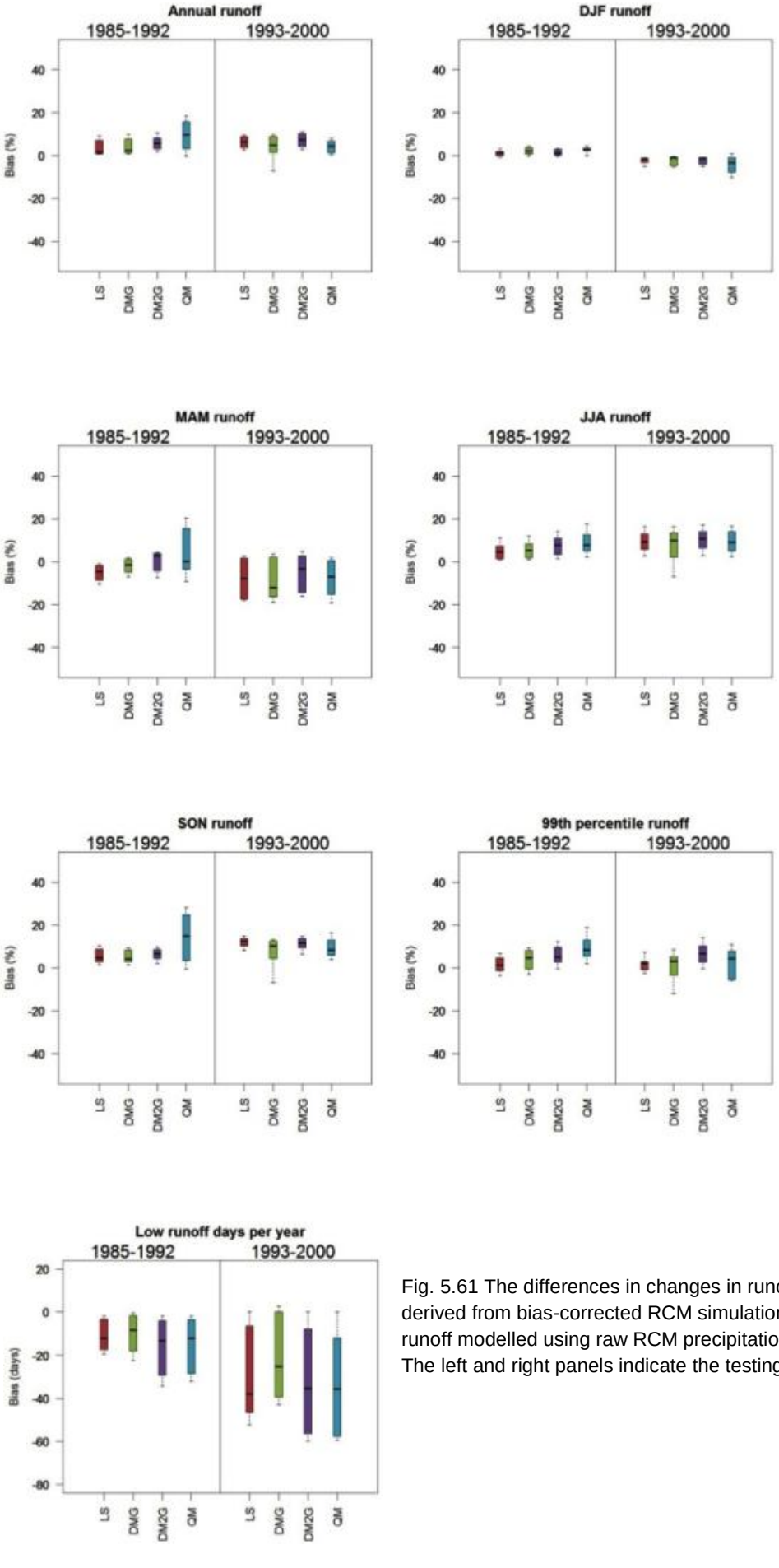

Fig. 5.61 The differences in changes in runoff characteristics derived from bias-corrected RCM simulations when compared to runoff modelled using raw RCM precipitation.
The left and right panels indicate the testing periods in each case.

Discussion

As shown in Fig. 5.58 and Fig. 5.59, the cross-validation results seem to be period dependent with most of the bias-correction methods reducing the raw RCM errors in period II but increasing the raw RCM errors in period I for most of the precipitation and runoff characteristics. The cause of this 'period dependency' could be the inconsistent errors in the raw RCM precipitation between the two periods, which may be a result of not long enough data for robust calibration (Berg et al., 2012), or it could be due to the nonstationarity of bias. The fundamental assumption that bias correction is based on is that the RCM biases are consistent over time (Piani et al., 2010). It is difficult to assess nonstationarity of biases because there are rarely long enough data time series for robust calibration and validation (Maraun, 2012). However, as discussed in Ehret et al. (2012), the possibility of bias nonstationarity is considered high (Christensen et al., 2008; Hagemann et al., 2011; Maraun, 2012). Therefore, the results shown here serve as a good indicator for what could happen if the bias varies over time. When the errors in the training period are larger than, or in a different direction to, the errors in the testing period, all the bias-correction methods overcorrect the errors in the testing period and result in increased errors (e.g. period I in annual precipitation plot, and period II in DJF precipitation plot in Fig. 5.58). When the errors in the training period are smaller than, and in the same direction as the bias in the testing period, although all the bias-correction methods are able to reduce the errors, the undercorrection can still be substantial. As shown in Fig. 5.58 and Fig. 5.59, under the condition of inconsistent errors, although some bias-correction methods perform slightly better than others, none of them can lead to satisfactory results.

Conclusions

We reviewed the recent comparison studies on the popular bias-correction methods applied to RCM simulations. The best-performing bias-correction technique—distribution mapping—was assessed using daily precipitation series simulated by the Weather Research and Forecasting (WRF) model for eight catchments in southeast Australia.

The performance of three distribution mapping techniques—DMG, DM2G and QM, each with increased degree of dependency on the training data—was evaluated including their follow-on effects on hydrological impact studies. A linear scaling method was also included as a benchmark. The effect of bias correction on the relative change in selected precipitation and simulated runoff characteristics was also explored.

The results confirmed the relatively higher skill of distribution-based methods in correcting salient precipitation characteristics, but also revealed their weakness in reproducing runoff characteristics due to low level of coherence in precipitation sequencing between RCM simulation and observations. Although the DM2G method performed relatively better in cross-validation, especially in a wetter period, none of the methods leads to satisfactory results under the condition of inconsistent errors between the training and testing periods. Results further showed that whilst bias correction does not seem to alter the change signals in RCM mean precipitation, it does introduce additional uncertainty to the change signals in high precipitation characteristics, and consequently, in runoff change signals.

Conclusions and future perspectives

This year, two lines of investigation were undertaken with a view to developing improved methodologies for future water availability projections. This work will allow the delivery of a range of water availability projections of varying methodological complexity which will provide a robust understanding of impacts of climate change on water availability across Victoria.

The work in Activity 1 has progressed well and results are promising. A simple statistical method to describe monthly streamflow based on linear regression of rainfall and temperature was applied to 27 catchments across Victoria with most catchments showing satisfactory results but some, mostly located in Gippsland, showed less skill. A paper summarising the findings has been submitted to Climate Research. We are planning to move onto the application of the methodology to catchments across Victoria using data downscaled from GCMs. With the progress in Project 5 (Critical assessment of climate model projections from a rainfall perspective), we look forward to applying this method to CMIP5 downscaled model data for both current and future climates to generate future streamflow projections across the 27 Victorian catchments, and comparing the results from the simple methodology with those from more conventional hydrological modelling approaches.

The work undertaken in Activity 2 produced a paper describing the effect of bias correction for RCM precipitation on hydro-climate projections. The most skilful bias-correction methods, chosen after a thorough literature review was undertaken, include a newly proposed two-state gamma distribution mapping technique, and have been implemented in the R language for future applications. They were assessed using daily precipitation series simulated for eight Victorian catchments. The results confirmed the usefulness of distribution-based methods but also highlighted that when the bias is nonstationary, none of the methods can lead to satisfactory results. We also found that although bias correction does not seem to alter the change signals in RCM precipitation, it does introduce extra uncertainty in the change signals in runoff. The knowledge gained from the thorough review and testing of bias-correction methods will be used in the comparison study that will lead to an improved methodology for the next round of hydro-climate projections.

In the next year, we will be evaluating some commonly used approaches that provide future climate for hydrological modelling—empirical scaling informed by GCMs, empirical scaling informed by RCMs, bias correcting of RCMs simulations, bias correcting of analogue downscaling. And these results will be compared with the results with from Activity 1. We will be aiming to assess each method's strengths and weaknesses and recommending methods for different applications.

Acknowledgements

Victoria catchment streamflows used in Activity 1 were provide by Melbourne Water, the DEPI and the Bureau of Meteorology Extended Hydrological Prediction (EHP) section. Nick Potter, Francis Chiew, Lu Zhang, Biao Wang, Jai Vaze (CSIRO), and Jason Evans (UNSW) are thanked for their valuable inputs into Activity 2.

Appendix 5.2

	Name	Average Elevation (m)	Catchment Size (km²)	Ann Streamflow (ML)	ML/km²	Start Year	End Year	Subregion
1	Genoa River at The Gorge	471.5	844.1	117664	139.4	1973	2013	East
2	Buchan River at Buchan	875.2	850.2	140272	165.0	1951	2013	East
3	Tambo River at Swifts Creek	798.4	899.3	79184.7	88.1	1951	2012	East
4	Wonnangatta River at Crooked River	868.8	1099.5	326705	297.1	1954	2013	Alpine
5	Macalister River at Glencairn	1008.9	570.4	225713	395.7	1968	2013	Alpine
6	Murray River at Biggara	1046.1	1257.3	460903	366.6	1969	2012	Alpine
7	Mitta Mitta River at Hinnomunjie	1080.9	1518.8	437832	288.3	1951	2013	Alpine
8	Snowy Creek at Below Granite Flat	832.5	415.7	194066	466.8	1954	2013	Alpine
9	Nariel Creek at Upper Neriel	1057.8	251.6	132618	527.1	1955	2012	Alpine
10	Big River at Jokers Creek	1234.4	356.8	229159	642.3	1951	2012	Alpine
11	Gibbo River at Gibbo Park	1015	389.8	111667	286.5	1972	2013	Alpine
12	Reedy Creek at Wangaratta North	542.8	5505.8	573588	104.2	1974	2013	West of Alps
13	Fifteen Mile Creek at Greta South	541.8	230.9	57197.9	247.7	1974	2013	West of Alps
14	Buffalo River at Abbeyard	740.8	415	157286	379.0	1966	2012	West of Alps
15	Holland Creek at Kelfeera	482.4	448	81797.4	182.6	1961	2012	West of Alps
16	Howqua River at Glen Esk	825.7	374	162463	434.4	1975	2013	West of Alps
17	Yea River at Devlins Bridge	446	360.6	87832.7	243.6	1976	2013	West of Alps
18	Jamieson River at Gerrang Bridge	844.9	364.2	216071	593.3	1955	2013	West of Alps
19	Goulburn River at Dohertys	751.6	700.2	328891	469.7	1968	2013	West of Alps
20	Pranjip Creek at Moorlim	202	749.4	48391.4	64.6	1975	2013	Far West
21	Big River at Jamieson	726.9	626.9	294266	469.4	1971	2013	West of Alps
22	Campaspe River at Redesdale	508.9	633.8	64145.5	101.2	1977	2013	Far West
23	Loddon River at Newstead	414	1028.5	70812.9	68.9	1976	2013	Far West
24	Avoca River at Coonooer	250.5	2677.3	92331.3	34.5	1967	2011	Far West
25	Eildon (Melbourne Water)	450	3885	1495250	384	1913	2013	Melbourne
26	Yarra (Melbourne Water)	350	559.7	347814	621.4	1913	2013	Melbourne
27	Thomson (Melbourne Water)	494	487.0	245070	503.2	1913	2013	Melbourne

Table 5.9 List of catchment full names, elevation, size, average streamflow, streamflow/size ratio, year data starts and ends and the subregion the catchment belongs to.

References

Adler, R.F., Huffman, G.J., Chang, A., Ferraro, R., Xie, P., Janowiak, J., Rudolf, B., Schneider, U., Curtis, S., Bolvin, D., Gruber, A., Susskind, J. and Arkin, P. 2003. The version 2 Global Precipitation Climatology Project (GPCP) monthly precipitation analysis (1979–present). *J. Hydrometeor*., 4, 1147–1167.

Allen, R.J., Norris, J.R. and Kovilakam, M. 2014. Influence of anthropogenic aerosol and the Pacific Decadal Oscillation on the tropical belt width. *Nature Geoscience*, doi:10.1038/NGEO02091.

Allen, R.J., Sherwood, S.C., Norris, J.R. and Zender, C.S. 2012. Recent Northern hemisphere tropical expansion primarily driven by black carbon and tropospheric ozone. *Nature*, 485, 350–354. doi:10.1038/nature11097.

Arblaster, J.M. and Meehl, G.A. 2006. Contributions of external forcings to southern annular mode trends. *J. Climate,* 19**,** 2896–2905.

Ashok, K., Behera, S., Rao, A.S., Weng, H. and Yamagata, T. 2007. El Niño Modoki and its teleconnection. *J. Geophys. Res.*, 112: C11007. doi:10.1029/2006JC003798.

Balmaseda, M. A., Mogensen, K. and Weaver, A.T. 2013. Evaluation of the ECMWF ocean reanalysis ORAS4, *Q. J. R. Meteorol. Soc.*, doi:10.1002/qj.2063. 0.1029/2007GL030452.

Balmaseda, M., Anderson, D. and Vidard, A. 2007. Impact of Argo on analyses of the global ocean, *Geophys. Res. Lett.*, 34, L16605.

Barnston, A.G., Tripett, M.K., L'Heureux, M.L., Li, S. and DeWitt, D.G. 2012. Skill of real-time seasonal ENSO model predictions during 2002–11: Is our capability increasing? *Bull. Amer. Meteor. Soc.*, 93, 631–651.

Berg, P., Feldmann, H. and Panitz, H.J. 2012. Bias correction of high resolution regional climate model data. *J. Hydrol.*, 448–449(0), 80–92, doi:10.1016/j.jhydrol.2012.04.026.

Bhend, J., Bathols, J.M. and Hennessy, K.J. 2012. *Climate change impacts on snow in Victoria*. CAWCR Research Report. Centre for Australian Weather and Climate Research.

Blanchi, R., Lucas, C., Leonard, J. and Finkele, K. 2010. Meteorological conditions and wildfire-related house loss in Australia. *Int. J. Wildland Fire*, 19, 914–926.

Boe, J., Terray, L., Habets, F. and Martin, E. 2007. Statistical and dynamical downscaling of the Seine basin climate for hydro-meteorological studies. *Int. J. Climatol.*, 27(12), 1643–1655, doi:10.1002/joc.1602.

Burnash, R.J.C., Ferral, R.L. and McGuire, R.A. 1973. *A Generalised Streamflow Simulation System—Conceptual Modelling for Digital Computers*. Joint Federal and State River Forecast Center, Sacramento, Technical Report, 204 pp.

Cai, W. and Cowan, T. 2013. Why is the amplitude of the Indian Ocean Dipole overly large in CMIP3 and CMIP5 climate models? *Geophys. Res. Lett*, 40, 1200–1205.

Cai, W., Borlace, S., Lengaigne, M., van Rensch, P., Collins, M., Vecchi, G., Timmermann, A., Santoso, A., McPhaden, M. J., Wu, L., England, M. H., Wang, G., Guilyardi, E. and Jin, F. 2014. Increasing frequency of extreme El Niño events due to greenhouse warming: *Nature Climate Change*, 4, 111–116.

Chen, F., Manning, K.W., LeMone, M.A., Trier, S.B., Alfieri, J.G., Roberts, R., Tewari, M., Niyogi, D., Horst, T. W., Oncley, S. P., Basara, J. B. and Blanken, P. D. 2007. Description and evaluation of the characteristics of the NCAR high-resolution land data assimilation system. *J. Appl. Meteor. Climatol.* 46.

Chen, G., Lu, J. and Frierson, D.M.W. 2008. Phase speed spectra and the latitude of surface westerlies: Interannual variability and global warming trend. *J. Climate*, 21, 5942–5959.

Chen, J., Brissette, F.P., Chaumont, D. and Braun, M. 2013. Finding appropriate bias correction methods in downscaling precipitation for hydrologic impact studies over North America. *Water Resour. Res.*, 49(7), 4187–4205, doi:10.1002/wrcr.20331.

Chen, J., Brissette, F.P., Poulin, A. and Leconte, R. 2011b. Overall uncertainty study of the hydrological impacts of climate change for a Canadian watershed. *Water Resour. Res.*, 47, W12509, doi:10.1029/2011wr010602.

Chiew, F.H.S. 2006. Estimation of rainfall elasticity of streamflow in Australia. *Hydrol. Sci.*, 51(4), 613–625.
Chiew, F.H.S., Young, W., Cai, W. and Teng, J. 2010. Current drought and future hydroclimate projections in southeast Australia and implications for water resources management. *Stoch. Env. Res. Risk A.*, 1–12, doi:10.1007/s00477-010-0424-x.

Choi, J., An, S-I., DeWitte, B. and Hsieh, W.W. 2009. Interactive feedback between the tropical Pacific Decadal Oscillation and ENSO in a coupled general circulation model. *J. Climate*. 22, 6597–6611

Choi, J., An, S-I., Kug, J-S. and Yeh, S-W. 2011. The role of mean state on changes in El Niño's flavour. *Clim. Dyn.* 37, 1205–1215.

Choi, J., Son, S-W., Lu, J. and Min, S-K. 2014. Further observational evidence of Hadley cell widening in the southern hemisphere, *Geophys. Res. Lett.*, 41, 2590–2597, doi:10.1002/2014GL059426.

Christensen, J.H., Boberg, F., Christensen, O.B. and Lucas-Picher, P. 2008. On the need for bias correction of regional climate change projections of temperature and precipitation. *Geophys. Res. Lett.*, 35(20), L20709, doi:10.1029/2008gl035694.

Chu, P-H., and Li, T. 2013. Interdecadal relationship between the mean state and El Niño types. *J. Climate*, 26, 361–379.

Colman, R., Deschamps, L., Naughton, M., Rikus, L., Sulaiman, A., Puri, K., Roff, G., Sun, Z. and Embery, G. 2005. BMRC Atmospheric Model (BAM) version 3.0: Comparison with mean climatology. *BMRC Research Report No. 108*, Bureau of Meteorology Research Centre, 32 pp (available from www.bom.gov.au/bmrc/pubs/researchreports/researchreports.htm)

CSIRO 2010. *Climate variability and change in south-eastern Australia: A synthesis of findings from Phase 1 of the South Eastern Australian Climate Initiative (SEACI)*. CSIRO, Australia, May 2010, 30 pp.

CSIRO 2012: *Climate and water availability in south-eastern Australia – A synthesis of findings from Phase 2 of the South Eastern Australian Climate Initiative (SEACI)*, CSIRO, Australia, September 2012, 41 pp.

Dee, D. P. et al. 2011. The ERA-Interim reanalysis: configuration and performance of the data assimilation system. *Q. J. R. Meteorol. Soc.*, 137, 553–597. doi:10.1002/qj.828.

Deser, C., Phillips, A.S. and Alexander, M.A. 2010. Twentieth century tropical sea surface temperature trends revisited. *Geophy. Res. Lett.* 37, L10701, doi:10.1029/2010GL043321.

DiNezio, P.N., Kirtman, B.P., Clement, A.C., Lee, S.K., Vecchi, G.A. and Wittenberg, A. 2012. Mean climate controls on the simulated response of ENSO to increasing greenhouse gases. *J. Climate*, 25, 7399–7420.

Ehret, U., Zehe, E., Wulfmeyer, V., Warrach-Sagi, K. and Liebert, J. 2012. HESS Opinions 'Should we apply bias correction to global and regional climate model data?'. *Hydrol. Earth Syst. Sci.*, 16(9), 3391–3404, doi:10.5194/hess-16-3391-2012.

Ekström, M. 2014. *Test of WRF physics schemes for Project 6 of the Victorian Climate Initiative: An outline of selected physical parameterisation schemes and other runtime options*. CSIRO Water for a Healthy Country Flagship, Australia.

Enfield, D.B., Mestas-Nunez, A.M. and Trimble, P.J. 2001. The Atlantic Multidecadal Oscillation and its relationship to rainfall and river flows in the continental U.S. *Geophys. Res. Lett.*, 28, 2077–2080.

England, M.H. et al. 2014. Recent intensification of wind driven circulation in the Pacific and the ongoing warming hiatus. *Nature Clim. Change*. doi:10.101038/NCLIMATE2106.

Evans, J. P., Ekström, M. and Ji, F. 2012. Evaluating the performance of a WRF physics ensemble over South-East Australia. *Clim. Dyn.*, 39,1241–1258.

Evans, J.P. and McCabe, M.F. 2010. Regional climate simulation over Australia's Murray–Darling basin: A multitemporal assessment. *J. Geophys. Res.*, 115, D14114, doi:10.1029/2010jd013816.

Fan, Y. and van den Dool, H. 2008. A global monthly land surface air temperature analysis for 1948–present, *J. Geophys. Res.*, 113, D01103.

Fierro, A.O. and Leslie, L.M. 2013. Relationships between Southeast Australian Temperature Anomalies and Large-Scale Climate Drivers. *J. Climate*, 27, 1395–1412.

Foley, A. M. 2010. Uncertainty in regional climate modelling: A review. *Prog. in Phys. Geogr.*, 34, 647–670.

Folland, C.K., Knight, J., Linderholm, H.W., Fereday, D., Ineson, S., Hurrell, J.W. 2009. The Summer North Atlantic Oscillation: Past, Present, and Future. *J. Climate*, 22, 1082–1103. doi: http://dx.doi.org/10.1175/2008JCLI2459.1.

Fowler, H., Blenkinsop, S. and Tebaldi, C. 2007. Linking climate change modelling to impacts studies: recent advances in downscaling techniques for hydrological modelling. *Int. J. Climatol.*, 27, 1547–1578.

Gent et al. 2011, The Community Climate System Model version 4, *J. Climate*, 24, 4973–4991, doi:10.1175/2011JCLI4083.1.

Gillett, N.P., Fyfe, J.C. and Parker, D.E. 2013. Attribution of observed sea level pressure trends to greenhouse gas, aerosol, and ozone changes, *Geophys. Res. Lett.*, 40, 2302–2306, doi:10.1002/grl.50500.

Grassi, B., Redaelli, G., Canziani, P.O., Visconti, G. 2012. Effects of the PDO Phase on the tropical belt width. *J. Climate*, 25, 3282–3290. doi:10.1175/JCLI-D-11-00244.1.

Griffiths, M., Tan, K.S. and Timbal, B. 2014. Rainfall and streamflows in Greater Melbourne catchment area: variability and recent anomalies. Submitted to *Climate Research,* 10/04/2014.

Gudmundsson, L., Bremnes, J.B., Haugen, J.E. and Engen-Skaugen, T. 2012. Technical Note: Downscaling RCM precipitation to the station scale using statistical transformations – A comparison of methods. *Hydrol. Earth Syst. Sci.*, 16(9), 3383–3390.

Gutjahr, O. and Heinemann, G. 2013. Comparing precipitation bias correction methods for high-resolution regional climate simulations using COSMO-CLM. *Theor Appl Climatol*, 114(3–4), 511–529, doi:10.1007/s00704-013-0834-z.

Haagenson, P. and Shapiro M.A. 1979. *Isentropic trajectories for derivation of objectively analysed meteorological parameters*. NCAR Tech Note NCAR/TN-149+STR, (December 1979), 30 pp.

Hagemann, S., Chen, C., Haerter, J.O., Heinke, J., Gerten, D. and Piani, C. 2011. Impact of a Statistical Bias Correction on the Projected Hydrological Changes Obtained from Three GCMs and Two Hydrology Models. *J. Hydrometeorol.*, 12(4), 556–578, doi:10.1175/2011jhm1336.1.

Ham, Y-G., and Kug, J-S. 2012. How well do current climate models simulate two type of El Niño? *Clim. Dyn.*, doi:10.1007/s00382-011-1157-3.

Hansen et al. 2010. Global surface temperature change. *Rev. Geophys.*, 48, RG4004, doi:10.1029/2010RG000345.

Hendon, H.H., Lim, E-P., Wang, G., Alves, O. and Hudson, D. 2009. Prospects for predicting two flavors of El Niño . *Geophys. Res. Lett.*,36, L19713, doi:10.1029/2009GL040100.

Hendon, H.H., Lim, E-P., Arblaster, J. and Anderson, D.L.T. 2014. Causes and predictability of the record wet east Australian spring, 2010: *Clim. Dyn*. doi:10.1007/s00382-013-1700-5.

Hendon, H.H., Thompson, D.W.J. and Wheeler, M.C. 2007. Australian rainfall and surface temperature variations associated with the southern hemisphere annular mode. *J. Climate*, 20**,** 2452–2467

Hong, S. Y. and Pan, H. L.1996. Nonlocal boundary layer vertical diffusion in a Medium-Range Forecast Model. *Mon. Weath. Rev.*, 124, 2322–2339.

Hong, S.-Y., Noh, Y. and Dudhia, J. 2006. A new vertical diffusion package with an explicit treatment of entrainment processes. *Mon. Weath. Rev.*, 134, 2318–2341.

Hu, Y., Zhou, C. and Liu, J. 2011. Observational evidence for the poleward expansion of the Hadley circulation. *Adv. Atmos. Sci.*, 28, 33–44. doi:10.1007/s00376-010-0032-1.

Hu, Y. and Fu, Q. 2007. Observed poleward expansion of the Hadley circulation since 1979. *Atmos. Chem. Phys.*, 7, 5229–5236. doi:10.5194/acp-7-5229-2007.

Hu, Z-Z., Kumar, A., Ren, H-L., Wang, H., L'Heureux, M. and Jin, F-F. 2013. Weakened interannual variability in the tropical Pacific Ocean since 2000. *J. Climate*, 26, 2601–2613.

Hudson, D., Alves, O., Hendon, H.H. and Wang, G. 2011. The impact of atmospheric initialisation on seasonal prediction of tropical Pacific SST. *Clim. Dyn*. 36, 1155–1171.

Hudson, D., Marshall, A.G., Yin, Y., Alves, O. and Hendon, H.H. 2013. Improving intraseasonal prediction with a new ensemble generation strategy. *Mon. Weath. Rev.* 141, 4429–4449.

Hurrell, J.W. and Deser, C. 2009. North Atlantic Climate Variability: The role of the North Atlantic Oscillation. *J. Marine Sys.*, 79, 231–244. doi:10.1016/j.jmarsys.2009.11.002.

Hurrell, J.W., Hack, J.J., Shea, D., Caron, J.M. and Rosinski, J. 2008. A new sea surface temperature and sea ice boundary data set for the Community Atmosphere Model. *J. Climate*, 21, 5145–5153, doi:10.1175/2008JCLI2292.1.1.

Iacono, M. J., Delamere, J.S., Mlawer, E.J., Shephard, M.W., Clough, S.A. and Collins, W. D. 2008. Radiative forcing by long-lived greenhouse gases: Calculations with the AER radiative transfer models. *J. Geophys. Res. Atmos.*, 113.

Imielska, A. 2011. Seasonal climate summary southern hemisphere (summer 2010–2011): second wettest Australian summer on record and one of the strongest La Niña events on record. *Australian Meteorological and Oceanographic Journal*, 61: 241–251.

IPCC 2014. *Climate Change 2013: The Physical Science Basis. Contribution of Working Group I to the Fifth Assessment Report of the Intergovernmental Panel on Climate Change*. In: Stocker, T. F., D. Qin, G-K. Plattner, M. Tignor, S. K. Allen, J. Boschung, A. Nauels, Y. Xia, V. Bex and P. M. Midgley (ed.).

Janjic, Z. I. 1994. The step-mountain ETA coordinate model—further developments of the convection, viscous sublayer, and turbulence closure schemes. *Mon. Weath. Rev.*, 122, 927–945.

Janjic, Z. I. 2000. Comments on 'Development and evaluation of a convection scheme for use in climate models'. *J. Atmos. Sci.*, 57, 3686–3686.

Jeffrey, S.J., Carter, J.O., Moodie, K.B. and Beswick, A.R. 2001. Using spatial interpolation to construct a comprehensive archive of Australian climate data. *Environ. Modell. Softw.*, 16(4), 309–330.

Johnson, F. and Sharma, A. 2012. A nesting model for bias correction of variability at multiple time scales in general circulation model precipitation simulations. *Water Resour. Res.*, 48, W01504, doi:10.1029/2011wr010464.

Jones, D.A., Wang, W. and Fawcett, R. 2009. High-quality spatial climate data-sets for Australia. *Aust. Met. Oceanogr. J.*, 58, 233–248.

Kalnay, E., Kanamitsu, M. et al. 1996. The NCEP/NCAR 40-year reanalysis project. *Bull. American Met. Soc.*, 77, 437–471.

Kang, S., Polvani, L.M., Fyfe, J.C. and Sigmond, M. 2011. Impact of polar ozone depletion on subtropical precipitation. *Science*, 332, 951–954.

Kendon, E.J., Roberts, N.M., Senior, C.A. and Roberts, M.J. 2012. Realism of Rainfall in a Very High-Resolution Regional Climate Model. *J. Climate*, 25, 5791–5806.

Kent, D.M., Kirono, D.G.C. et al. 2013. Representation of the Australian subtropical ridge in the CMIP3 models. *Int. J. Climatology* 33(1), 48–57.

Kiem, A.S. and Verdon-Kidd, D.C. 2009. Climate drivers of Victorian streamflow: Is ENSO the dominant influence. *Aust. J. of Wat. Res.*, 13(1), 17–29.

Kiem, A.S. and Verdon-Kidd, D.C. 2010. Towards understanding hydroclimatic change in Victoria, Australia—preliminary insight into the 'Big Dry'. *Hydro. Earth. Syst. Sci.*, 14, 433–445.

Kirtman, B. and Schopf, P.S. 1998. Decadal variability in ENSO predictability and prediction. *J. Climate*, 11, 2804–2822.

L'Heureux, M.L., and Thompson, D.W.J. 2006. Observed relationships between the El Niño – Southern Oscillation and the extratropical zonal–mean circulation. *J. Climate*, 19**,** 276–287.

L'Heureux, M.L., Lee, S. and Lyon, B. 2013. Recent multidecadal strengthening of the Walker circulation across the tropical Pacific. *Nature Clim. Change*. 3, 571–576.

Lafon, T. 2013. Bias correction of daily precipitation simulated by a regional climate model: a comparison of methods. *Int. J. Climatol.*, 33(6), 1367–1381, doi:10.1002/joc.3518.

Lanzante, J.R. 2005. A cautionary note on the use of error bars. *J. Climate*, 18, 3699–3703. doi:10.1175/JCLI3499.1.

Laprise, R. 2008. Regional climate modelling. *J.Comput. Phys.*, 227.

Larsen, S. H. and Nicholls, N. 2009. Southern Australian rainfall and the subtropical ridge: Variations, interrelationships, and trends. *Geophys. Res. Lett.* 36, 5.

Leathers, D.J., Yarnal, B., Palecki, M.A., 1991. The Pacific/North American Teleconnection Pattern and United States Climate. Part I: Regional Temperature and Precipitation Associations. *J. Climate*, 4, 517–528. doi: http://dx.doi.org/10.1175/1520–0442(1991)004<0517:TPATPA>2.0.CO;2.

Leblanc, M., Tweed, S., van Dijk, A. and Timbal, B. 2011. A review of historic and future hydrological changes in the Murray–Darling Basin. *Global Planetary Change*, doi:10.1016/j. gloplacha.2011.10.012.

Lenderink, G., Buishand, A. and van Deursen, W. 2007. Estimates of future discharges of the river Rhine using two scenario methodologies: direct versus delta approach. *Hydrol. Earth Syst. Sci.*, 11(3), 1143–1159.

Lim, E-P. and Hendon, H.H. 2014. Understanding and predicting the strong Southern Annular Mode and its impact on the record wet east Australian spring 2010, submitted to *Clim. Dyn*.

Lim, E-P., Hendon, H.H. and Rashid, H.A. 2013. Seasonal predictability of the Southern Annular Mode due to its association with ENSO. *J. Climate*, 26, 8037–8054. http://dx.doi.org/10.1175/JCLI-D-13-00006.1

Lim, K-S.S. and Hong, S-Y. 2010. Development of an Effective Double-Moment Cloud Microphysics Scheme with Prognostic Cloud Condensation Nuclei (CCN) for Weather and Climate Models. *Mon. Weath. Rev.*, 138,1587–1612.

Lucas et al. 2014. The expanding tropics: A critical review of the observational and modelling studies. WIRes *Climate Change*, 5, 89–112. doi:10.1002/wcc.251.

Lucas, C. and Nguyen, H. 2014. Regional characteristics of tropical expansion and the role of teleconnections (in preparation).

Lucas, C., Nguyen, H. and Timbal, B. 2012. An observational analysis of southern hemisphere tropical expansion. *J. Geophys. Res*., 117, D17112, doi:10.1029/2011JD017033.

Lucas, C., Timbal, B. and Nguyen, H. 2014. The expanding tropics: a critical assessment of the observational and modelling studies. WIREs. *Clim. Change*, 5, 89–112. doi:10.1002/wcc.251.

Lund, R. and Reeves, J., 2002. Detection of Undocumented Changepoints: A Revision of the Two-Phase Regression Model. *J. Climate*, 15, 2547–2554.

Mansell, E. R., Ziegler, C.L. and Bruning, E.C. 2010. Simulated Electrification of a Small Thunderstorm with Two-Moment Bulk Microphysics. *J. Atmos. Sci.*, 67,171–194.

Mantua, N.J. and Hare, S.R. 2002. The Pacific decadal oscillation. *J. Oceanography*, 58, 35–44. doi: 10.1023/A:1015820616384.

Maraun, D. 2012. Nonstationarities of regional climate model biases in European seasonal mean temperature and precipitation sums. *Geophys. Res. Lett.*, 39(6), L06706, doi:10.1029/2012gl051210.

Marshall, G.J. 2003. Trends in Southern Annular Mode from observations and reanalyses. *J. Climate*, 16:4134–4143.

McPhaden, M.J. and Zhang, D. 2004. Pacific Ocean circulation rebounds. *Geophys. Res. Lett.* 31, L18301.

McPhaden, M.J., 2012. A 21st century shift in the relationship between ENSO SST and warm water volume. *Geophys. Res. Lett.*, 39, L09706, doi:10.1029/2012GL051826.

McPhaden, M.J., Lee, T. and McClurg, D. 2011. El Niño and its relationship to changing background conditions in the tropical Pacific Ocean. *Geophys. Res. Lett.*, 38, L15709. doi:10.1029/2011GLo48275.

Meehl, G. A., Covey, C. et al. 2007. The WCRP CMIP3 multimodel dataset—A new era in climate change research. *Bull. American Met. Soc.*, 88(9), 1383–1394.

Milbrandt, J. A. and Yau, M. K. 2005. A multimoment bulk microphysics parameterization. Part II: A proposed three-moment closure and scheme description. *J. Atmos. Sci.*, 62, 3065–3081.

Min, S-K., Cai, W. and Whetton, P. 2013. Influence of climate variability on seasonal extremes over Australia. *J. Geophy. Rea.*, 118, 643–654.

Mittermaier, M., Roberts, N. and Thompson, S.A. 2013. A long-term assessment of precipitation forecast skill using the Fractions Skill Score. *Meteorol. Appl.*, 20, 176–186.

Moore, R.W., Martius, O. and Spengler, T. 2010. The modulation of the subtropical and extratropical atmosphere in the Pacific basin in response to the Madden–Julian Oscillation. *Mon. Wea. Rev.*, 138, 2761–2779.

Moss, R., Edmonds, J., Hibbard, K., Manning, M., Rose, S., van Vuuren, D., Carter, T., Emori, S., Kainuma, M., Kram, T., Meehl, G., Mitchell, J., Nakicenovic, N., Riahi, K., Smith, S., Stouffer, R., Thomson, A., Weyant, J. and Wilbanks, T. 2010. The next generation of scenarios for climate change research and assessment. *Nature*, 463, 747–756.

Murphy, R.E., Moran, R., Hill, P.I. and Jusuf, K. 2010. Quantifying the post-1997 climate shift in Victoria. *PRCC conference abstracts*.

Nakanishi, M. and Niino, H. 2006. An improved Mellor-Yamada level-3 model: Its numerical stability and application to a regional prediction of advection fog. *Bound.-Layer Meteor.*, 119, 397–407.

NASA, 7 Sept – 13 October mean ozone hole area, acquired from NASA Ozone Hole Watch website, http://ozonewatch.gsfc.nasa.gov

Nguyen H., Lucas, C. and Timbal, B. 2014. Unprecedented expansion of the southern hemisphere Hadley cell in the 20CR reanalysis (in preparation).

Nguyen, H., Evans, A., Lucas, C., Smith, I. and Timbal B. 2013. The Hadley circulation in reanalyses: climatology, variability and expansion. *J. Climate*, 26, 3357–3376. doi:10.1175/JCLI-D-12-00224.

Nicholls, N. 2009. Local and remote causes of the southern Australian autumn–winter rainfall decline, 1958–2007. *Climate Dyn.*, 34: 835–845.

Nicholls, N. 2011. What caused the eastern Australia heavy rains and floods of 2010/11? *Bull Aust Meteorol Oceanogr Soc.*, *24*, 33–34.

NRM, 2014a: *Technical Report: Southern Slopes*. CSIRO and Bureau of Meteorology.

NRM, 2014b: *Regional Projections Report: Southern Slopes*. CSIRO and Bureau of Meteorology.

NRM, 2014c: *Regional Projections Report: Murray Basin*. CSIRO and Bureau of Meteorology.

Oke, P.R., Schiller, A., Griffin, D.A. and Brassington, G.B. 2005. Ensemble data assimilation for an eddy-resolving ocean model of the Australian region. *Q. J. Roy. Met. Soc.*, 131, 3301–3311.

Oort A. H. and Yienger J. J. 1996. Observed interannual variability in the Hadley circulation and its connection to ENSO. *J. Climate*. 9, 2751–2767.

Pacanowski, R.C. 1996. MOM2. *Documentation, user's guide and reference manual*. Tech. rep. GFDL Ocean Group Tech. Rep. 3.2, 328 pp.

Piani, C., Weedon, G.P., Best, M., Gomes, S.M., Viterbo, P., Hagemann, S. and Haerter, J.O. 2010b. Statistical bias correction of global simulated daily precipitation and temperature for the application of hydrological models. *J. Hydrol.*, 395(3–4), 199–215, doi:10.1016/j.jhydrol.2010.10.024.

Pook, M. J., McIntosh P.C. and Meyers, G.A. 2006. The synoptic decomposition of cool-season rainfall in the southeastern Australian cropping region. *J. Appl. Met. Climatol.*, 45, 1156–1170.

Post, D.A. and Moran, R.J. 2013. Provision of usable projections of future water availability for southeastern Australia: The South Eastern Australian Climate Initiative. Australian Journal of Water Resources, 17.2, 135–142, http://dx.doi.org/10.7158/W13 028.2013.17.2.

Potter N.J., Chiew, F.H.S. and Frost, A.J. 2010. An assessment of the severity of recent reductions in rainfall and runoff in the Murray–Darling Basin, *J. Hydro.*, 381, 52–64.

Potter, N.J. and Chiew, F.H.S. 2011. An investigation into changes in climate characteristics causing the recent very low runoff in the southern Murray–Darling Basin using rainfall–runoff models, *Wat. Res. Res.*, 47, W00G10, doi:10.1029/2010WR010333.

Power, S., Delage, F., Chung, C., Kociuba, G. and Keay, K. 2013. Robust twenty-first century projections of El Niño and related precipitation variability. *Nature*, doi:10.1038/nature12580.

Rikus, L. 2014. A simple climatology of westerly jet streams in global reanalysis datasets. Part 1: mid-latitude upper tropospheric jets. Submitted to *Climate Dynamics*.

Risbey, J., Pook, M., McIntosh, P., Ummenhofer, C. and Meyers, G. 2009. Characteristics and variability of synoptic features associated with cool season rainfall in southeastern Australia. *Int. J. Climatology*, 29, 1595–1613.

Risbey, J.S., McIntosh, P.C. and Pook, M.J. 2012. Synoptic components of rainfall variability and trends in southeast Australia. *Int. J. Climatol.*, doi:10.1002/joc3597.

Risbey, J.S., Pook. M.J., McIntosh, P.C., Wheeler, M.C. and Hendon, H.H. 2009. On the remote drivers of rainfall variability in Australia. *Mon. Wea. Rev.* doi:10.1175/2009MWR2861.1.

Roberts, N. 2008. Assessing the spatial and temporal variation in the skill of precipitation forecasts from an NWP model. *Meteorol. Appl.*, 15, 163–169.

Roberts, N.M. and Lean, H.W. 2008. Scale-selective verification of rainfall accumulations from high-resolution forecasts of convective events. *Mon. Weath. Rev.*, 136, 78–97.

Rodgers, K., Friedrichs, P. and Latif, M. 2004. Tropical Pacific Decadal Variability and its relation to decadal modulations of ENSO. *J. Climate*, 17, 3761–3774.

Sato et al. 1993. Stratospheric aerosol optical depths, 1850–1990. *J. Geophys. Res.*, 98, 22987–22994, doi:10.1029/93JD02553.

Scheff, J. and Frierson, D. 2012. Twenty-first century multimodel subtropical precipitation declines are mostly midlatitude shifts. *J. Climate*, 25, 4330–4347.

Schiller, A., Godfrey, J.S., McIntosh, P.C., Meyers, G., Smith, N.R., Alves, O., Wang, G. and Fiedler, R. 2002. *A New Version of the Australian Community Ocean Model for Seasonal Climate Prediction*. CSIRO Marine Research Report No. 240.

Schmidli, J., Frei, C. and Vidale, P.L. 2006. Downscaling from GCM precipitation: a benchmark for dynamical and statistical downscaling methods. *Int. J. Climatol.*, 26(5), 679–689, doi:10.1002/joc.1287.

Schneider, T. 2006. The general circulation of the atmosphere. *Ann. Rev. Earth Planet. Sci.*, 34, 655–688.

Schneider, T., Smith, K.L., O'Gorman, P.A. and Walker, C.C. 2006. A climatology of tropospheric zonal-mean water vapour fields and fluxes in isentropic coordinates. *J. Climate*, 19, 5918–5933.

Schwendike, J., Govekar, P., Reeder, M.J., Wardle, R., Berry, G.J. and Jakob, C. 2014. Local partitioning of the overturning circulation in the tropics and the connection to the Hadley and Walker circulations, J. *Geophys. Res. (Atmos.)*, 119, 1322–1339, doi:10.1002/2013JD020742.

Seager, R., Naik, N. and Vogel, L. 2012. Does global warming cause intensified interannual hydroclimate variability? *J. Climate*, 25(9), 3355–3372.

Skamarock, W. C. and Klemp, J. B. 2008. A time-split nonhydrostatic atmospheric model for weather research and forecasting applications. *J.Comput. Phys.*, 227, 3465–3485.

Taylor, K.E., Stouffer, R.J. and Meehl, G.A. 2012. An overview of CMIP5 and the experiment design. *Bull. American Met. Soc*., 93.

Teng, J., Vaze, J., Chiew, F.H.S., Wang, B. and Perraud, J-M., 2012b. Estimating the relative uncertainties sourced from GCMs and hydrological models in modeling climate change impact on runoff. *J. Hydrometeorol.*, 13(1), 122–139, doi:10.1175/jhm-d-11-058.1.

Teutschbein, C. and Seibert, J. 2012. Bias correction of regional climate model simulations for hydrological climate change impact studies: Review and evaluation of different methods. *J. Hydrol.*, 456–457(0), 12–29, doi:10.1016/j.jhydrol.2012.05.052.

Teutschbein, C. and Seibert, J. 2013. Is bias correction of regional climate model (RCM) simulations possible for non-stationary conditions? *Hydrol. Earth Syst. Sci.*, 17(12), 5061–5077, doi:10.5194/hess-17-5061-2013.

Themeßl, M.J., Gobiet, A. and Leuprecht, A. 2011. Empirical–statistical downscaling and error correction of daily precipitation from regional climate models. *Int. J. Climatol.*, 31(10), 1530–1544, doi:10.1002/joc.2168.

Thompson, D.W.J. and Wallace, J.M. 1998. The Arctic oscillation signature in the wintertime geopotential height and temperature fields. *Geophys. Res. Lett.*, 25, 1297–1300, doi:10.1029/98GL00950.

Thompson, G., Field, P.R., Rasmussen, R.M. and Hall, W.D. 2008. Explicit Forecasts of Winter Precipitation Using an Improved Bulk Microphysics Scheme. Part II: Implementation of a New Snow Parameterization. *Mon. Weath. Rev.*, 136, 5095–5115.

Timbal, B. 2009. The continuing decline in South-East Australian rainfall – update to May 2009. *CAWCR Research Letter,* 2: 8pp.

Timbal, B. and Drosdowsky, W. 2013. The relationship between the decline of South Eastern Australia rainfall and the strengthening of the subtropical ridge. *Int. J. of Climatol.*, 33, 1021–1034, doi:10.1002/joc.3492.

Timbal, B. and Hendon, H. 2011. The role of tropical modes of variability in the current rainfall deficit across the Murray–Darling basin. *Water Resources Research*, doi:10.1029/2010WR009834.

Townsend, R.D. and Johnson, D.R. 1985. A diagnostic study of isentropic zonally averaged mass circulation during the First GARP Global Experiment. *J. Atmos. Sci.*, 42, 1565–1579.

Valke, S., Terray, L. and Piacentini, A. 2000. *The OASIS coupled user guide version 2.4*, Technical Report TR/ CMGC/00-10, CERFACS.

van Vuuren, D., Edmonds, J. et al. 2011. The representative concentration pathways: an overview. *Climatic Change* 109(1–2): 5–31.

Verdon-Kidd, D.C., Kiem, A.S. and Moran, R. 2014. Links between the Big Dry in Australia and hemispheric multi-decadal climate variability – implications for water resource management, *Hydrol. Earth Syst. Sci.*, 18, 2235–2256, doi:10.5194/hess-18-2235-2014.

Wang, G., Alves, O. and Smith, N. 2005. *BAM3.0 tropical surface flux simulation and its impact on SST drift in a coupled model*. BMRC Research Rep. 107, 30 pp.

Wang, Q.J., Robertson, D.E. and Chiew, F.H.S. 2009. A Bayesian joint probability modelling approach for seasonal forecasting of streamflows at multiple sites. *Water Res. Res.*, 45, doi:10.1029/2008WRR007355.

Whan, K., Timbal, B. et al. 2013. Linear and nonlinear statistical analysis of the impact of subtropical ridge intensity and position on south-east Australian rainfall. *Int. J. Climatology* 34(2): 326–342.

Wilks, D. 2006. *Statistical methods in the atmospheric sciences* (second edition). Elsevier, US.

Wittenberg, A.T., Rosati, A., Delworth, T.L., Vecchi, G.A. and Zeng, F. 2014. ENSO Modulation: Is it decadally predictable?. *J. Climate*, 27, 2667–2681.

Wolter and Timlin 1998. Measuring the strength of ENSO events—how does 1997–98 rank? *Weather*, 53, 315–324.

Xiang, B., Wang, B. and Li, T. 2013. A new paradigm for the predominance of standing Central Pacific Warming after late 1990s. *Clim. Dyn.*, 41, 327–340.

Xie, P. and Arkin, P.A. 1996. Analysis of global monthly precipitation using gauge observations, satellite estimates, and numerical model predictions. *J Climate*, 9, 840–858.

Yin, J. 2005. A consistent poleward shift of the storm tracks in simulations of 21st century climate. *Geophys. Res. Let.*, 32, L18701,doi:10.1029/2005GL023684.

Yin, Y., Alves, O. and Oke, P.R. 2011. An ensemble ocean data assimilation system for seasonal prediction. *Mon. Wea. Rev.*, 139, 786–808.

Zhang, D. and Anthes, R.A. 1982. A high-resolution model of the planetary boundary-layer-sensitivity tests and comparisons with SESAME-79 data. *J. Appl. Met.*, 21, 1594–1609.

Zhao, M., Hendon, H., Alves, O. and Yin, Y. 2014. Impact of improved assimilation of temperature and salinity for coupled model seasonal forecasts. *Clim. Dyn.*, 42, No.9, 2565–2583. doi:10.1007/s00382-014-2081-0.

Zhou Y.P., Xu K-M., Sud, Y.C. and Betts, A.K. 2011. Recent trends of the tropical hydrological cycle inferred from Global Precipitation Climatology Project and International Satellite Cloud Climatology Project data, *J. Geophys. Res.*, 116, D09101, doi:10.1029/2010JD015197.

6. GLOSSARY

Cool season

The seven months from April to October (inclusive).

CMIP3

Refers to the third Coupled Model Intercomparison Project, or more typically, the global climate models involved in this project. They are also the models used in the IPCC Fourth Assessment Report.

CMIP5

Refers to the fifth Coupled Model Intercomparison Project, or more typically, the global climate models involved in this project. They are also the models used in the IPCC Fifth Assessment Report. Note that to make the numbers line up with the IPCC Assessment Reports, there was no CMIP4.

Downscaling

Commonly, so called downscaling methods are used to derive estimates of local scale climate variables from large-scale global climate model outputs. These methods are typically classed as either statistical or dynamical, where the former includes regression or weather pattern based relationships between large and local scale variables and the latter refers to the use of a fine-scale regional climate model.

ENSO

The El Niño – Southern Oscillation. It can be in an El Niño, La Niña or neutral state. El Niño conditions tend to bring drier conditions to south-eastern Australia, while La Niña conditions tend to bring wetter conditions. It is quantified using the southern oscillation index (SOI) which is a measure of the normalised atmospheric pressure difference between Tahiti and Darwin.

Hadley cell

The name given to each of the two cells of the Hadley circulation, typically the southern hemisphere cell as used in this report.

Hadley circulation

The large-scale atmospheric circulation that transports heat from the tropics to the sub-tropics.

IOD

The Indian Ocean Dipole. When the western Indian Ocean is warmer than the eastern part of the ocean, it is termed a positive IOD and it tends to bring drier conditions to south-eastern Australia. The opposite phase is termed a negative IOD and tends to bring wetter conditions to south-eastern Australia. It is quantified using the dipole mode index (DMI) based on the measured difference between sea-surface temperature in the western (50°E to 70°E and 10°S to 10°N) and eastern (90°E to 110°E and 10°S to 0°S) equatorial Indian Ocean.

IPO

The Interecadal Pacific Oscillation, an El Niño-like pattern of sea surface temperature that varies on decadal time scales. The IPO has a positive phase, when temperatures in the equatorial eastern Pacific are above normal and the trade winds are relaxed, that was last active from 1980 to 1999; and a negative phase, when temperatures in the equatorial eastern Pacific are colder than normal and the trade winds are enhanced, that is currently active. The phase modulates the relative frequency of El Niño and La Niña events and their predictability.

Mean meridional circulation

The mean meridional circulation refers to the overall atmospheric circulation of the Earth, transporting heat and moisture from the tropics towards the poles. It includes the Hadley circulation.

NINO3

One measure of the state of the ENSO based on the sea-surface temperature in the central Pacific Ocean and used to indicate whether it is in an El Niño, La Niña, or neutral state.

PDO

The Pacific Decadal Oscillation—related to the IPO but defined based on surface temperatures across the North Pacific region.

Radiosonde

A scientific term for a weather balloon and its instrument package.

Reanalysis dataset

Synthesised assimilation of historical datasets that aim to describe the state of the climate system in a consistent manner.

SAM

The Southern Annular Mode, a measure of the strength of westerly winds across southern Australia based on the difference between the surface pressure at 40 and 65°S. Positive SAM phases typically result in weaker westerly winds and therefore drier conditions across the western part of south-eastern Australia in winter. In summer, the main impact is an increase in easterly winds, leading to wetter conditions across the eastern part of south-eastern Australia.

SOI

The Southern Oscillation Index is based on the surface pressure difference between Tahiti and Darwin and used to indicate if ENSO is in an El Niño, La Niña or neutral state.

Subtropical ridge

The region of high pressure that exists across the mid-latitudes resulting from the descending branch of the Hadley circulation.

Teleconnection

A statistical association between climate variables at widely separated geographical locations. For example, the rainfall pattern associated with El Niño sea surface temperature anomalies in the Pacific.

Warm season

The five months from November to March (inclusive).

Walker circulation

The atmospheric circulation that occurs across the tropical Pacific Ocean with air rising above warmer ocean regions (normally in the west), and descending over the cooler ocean areas (normally in the east). Its strength fluctuates with that of the Southern Oscillation.

Water availability

For the purposes of this report, water availability is synonymous with surface water runoff or streamflow from mid-sized catchments (50–2000 km^2).

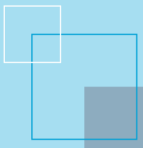

The Centre for Australian Weather and Climate Research is a partnership between CSIRO and the Bureau of Meteorology.